ACTIVATION OF ALUMINUM PARTICLES TO REACT WITH WATER FOR THE PURPOSE OF HYDROGEN GENERATION

A Thesis Submitted to the College of

Graduate Studies and Research

In Partial Fulfillment of the Requirements

For the Degree of Doctor of Philosophy

In the Department of Mechanical Engineering

University of Saskatchewan

Saskatoon

By

Seyed Salman Razavi-Tousi

PERMISSION TO USE

In presenting this thesis in partial fulfilment of the requirements for a postgraduate degree from the University of Saskatchewan, I agree that the Libraries of this University may make it freely available for inspection. I further agree that permission for copying of this thesis in any manner, in whole or in part, for scholarly purposes may be granted by the professors who supervised my thesis work or, in their absence, by the Head of the Department or the Dean of the College in which my thesis work was done. It is understood that any copying or publication or use of this thesis or parts thereof for financial gain shall not be allowed without my written permission. It is also understood that due recognition shall be given to me and to the University of Saskatchewan in any scholarly use which may be made of any material in my thesis.

Requests for permission to copy or to make other use of material in this thesis in whole or part should be addressed to:

Head of the Department of Mechanical Engineering
57 Campus Dr.
University of Saskatchewan
Saskatoon, Saskatchewan (S7N 5A9)

ABSTRACT

Aluminum can react with water and produce hydrogen. Researchers have developed different methods to promote the reaction of aluminum with water for hydrogen generation. Most of these methods considered ball milling of aluminum necessary prior to the reaction. In spite of numerous works on activation of aluminum powder to react with water, the activation process of aluminum powders is not optimized, and there is not enough knowledge on the kinetics and mechanism of the reaction. This research is to fill this gap.

Considering the energy consumption in ball milling, firstly, we optimized the milling time based on the highest rate of hydrogen generation. Then, contributions of milling process to activation of the aluminum powder were evaluated. We found that microstructural refinement has a significant contribution in promoting the reaction. Therefore, we studied the mechanism of grain refinement of aluminum particles during ball milling. We used electrochemical tests to better understand the reaction of aluminum with hot water and effect of addition of water-soluble salts was also studied. The shrinking core model was modified to predict the kinetics of the reaction.

It was found that ball milling promotes the reaction in two ways: a) increasing the instability of the microstructure (by refining the microstructure) and, b) decreasing the particle size of the powders. A considerable increase in amount of the grain boundaries was found as the reason for instability of the microstructure. Deformation banding and subgrain rotation were identified as the mechanisms responsible for introducing new boundaries during milling.

For the pure aluminum, the small size and the laminated structure of particles at the medium stage of milling increased the rate of the reaction, and further milling destroyed the laminated structure and consequently decreased the reaction rate. For the aluminum-salt mixtures, there is no optimum milling time as it was observed for the pure aluminum powder. However, more milling after a certain time does not have any significant influence on the reaction rate of aluminum-salt mixture. The addition of water-soluble salts (potash or salt) considerably increased the hydrogen generation rate. Comparison of different distributions of the salt in the aluminum particles revealed that chemical aspect of the presence of salt is negligible compared to the structural modifications. Finally, considering the changes in thickness and porosity of the hydroxide layer formed on the aluminum particles, the traditional shrinking core model was modified for the reaction of aluminum particles with hot water.

ACKNOWLEDGMENT

I would like to thank my supervisor Prof. Jerzy Szpunar for his leadership and encouragement. This research would not be successful without his support.

I also appreciate the support by department of Mechanical Engineering faculty and staff members, especially the head Prof. Bugg and the graduate chair Prof. Fotouhi. I also appreciate the help by the advisory committee members Prof. Tse, Prof. Wang and Prof. Odeshi. And my sincere thanks to my colleagues in Prof. Szpunar's research team. Finally, I acknowledge NSERC discovery grant and financial support of Canada Research Chair program.

DEDICATION

I DEDICATE THIS THESIS TO MY LOVELY WIFE FOR HER UNCONDITIONAL KINDNESS, AND TO MY BELOVED PARENTS.

TABLE OF CONTENTS

LIST OF TABLES

LIST OF FIGURES

ACRONYMS

DB	deformation band
DRX	dynamic recrystallization
EBSD	electron backscattered diffraction
EDS	energy-dispersive X-ray spectroscopy
FWHM	full-width at half-maximum
GNBs	geometrically necessary boundaries
GoF	goodness of fit
HAGBs	high angle grain boundaries
IDBs	incidental dislocation boundaries
IPF	inverse pole figure
LAGBs	low angle grain boundaries
LEDS	low energy dislocation structure
LMP	low melting point
MAGBs	medium angle grain boundaries
OCP	open corrosion potential
RPM	round per minute
PEM	proton exchange membrane
SCE	saturated calomel electrode
SEM	scanning electron microscope
SCM	shrinking core model

TD	transition bands
TEM	transmission electron microscope
XPS	X-ray photoelectron spectroscopy
XRD	X-ray diffraction

GREEK LETTERS

γ-Al_2O_3	gamma alumina
$K\alpha_1$	main wavelength of XRD
$K\alpha_2$	second wavelength of XRD
λ	wavelength
θ	Braggs angle
η	lattice strain
μm	10^{-6} meter
v	balls speed
ρ	density of the balls
v_{max}	maximum velocity

CHAPTER 1

INTRODUCTION

1.1. Overview of Chapter 1

This chapter briefly introduces the potential of aluminum to react with water and generate hydrogen. Fuel cells, hydrogen sources, ball milling, hydrogen production from reaction of magnesium, zinc and aluminum, and the advantages of the latter will be discussed. Problems and knowledge gaps related to use of aluminum-water reaction for hydrogen production will be addressed. In order to avoid repetition, this chapter does not include the literature review on aluminum-water reaction. A literature review for each part of the study is provided in the introduction section of each manuscript.

1.2. The Necessity of Replacement of Fossil Fuels with Hydrogen

The dependence on fossil fuels as the main energy source and energy carrier results in emission of pollutants and has created serious environmental problems. On the other hand, hydrogen is a carbon-free fuel, which is oxidized by water as a combustion product. Considering the renewable primary energy sources for splitting water, hydrogen is considered as a clean and abundant energy carrier in a carbon-free cycle. Hydrogen can act as a solar storage medium and transform solar energy where and when it is needed. In the future development of new energy options, hydrogen will play an important role.

An important issue regarding using hydrogen as an energy career is its storage. Hydrogen as an energy carrier needs to be stored effectively and safely, particularly for vehicular applications. Hydrogen may be stored as a gas, a liquid, or an atomic "solid", e.g. in a hydride compound [1]. One method for providing hydrogen for use is to generate hydrogen at the same place that it is to be consumed. In this way, hydrogen is not required to be stored because it is almost simultaneously consumed by fuel cells as it is generated from the reactants. Aluminum, zinc and magnesium are among the candidates that can serve to react with water and generate hydrogen. In this chapter, capability of each of the mentioned metals for hydrogen generation is discussed. The focus will be on modification of the reaction of aluminum with water as an onboard source for hydrogen.

1.3. Hydrogen to Electricity by Fuel Cells

Fuel cell is defined as a device used to convert the chemical energy obtained from a fuel into electrical energy by a chemical reaction with oxygen [2]. The fuel can be hydrogen or hydrocarbons, however, because of different issues regarding using hydrocarbons in fuel cells, hydrogen has been mainly considered as the fuel for the chemical reaction. Fig. 1.1 shows a summary of different fuel cell types. One can see that all of them consist of an anode, a cathode and electrolyte. Different ions can be exchanged in the electrolyte, and the working temperature of fuel cells ranges from 70-1000^{o}C.

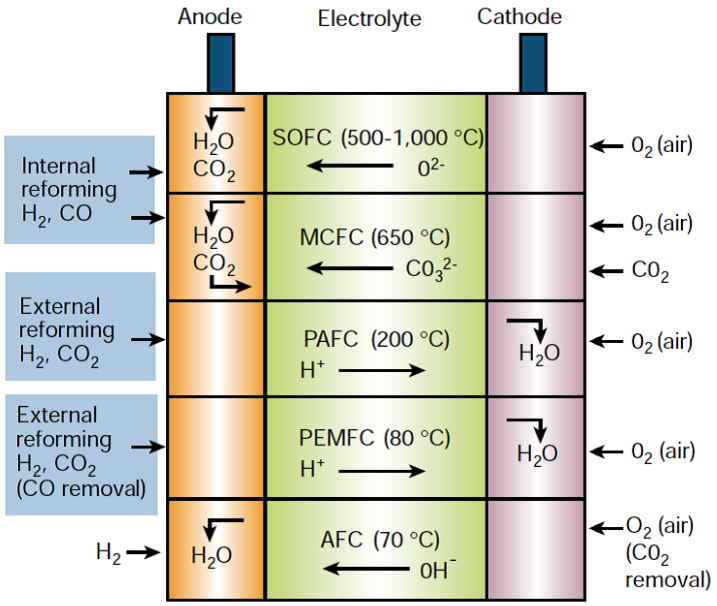

Fig. 1.1 Schematic of different types of fuel cells [3].

Among the different types of fuel cell developed to convert hydrogen to electricity, proton exchange membrane (PEM) fuel cells have been considered as a promising technology [4]. Fig. 1.2 shows the schematic of one single PEM cell. The mechanism of electricity production is as follows: hydrogen is reduced to H^+, the produced electrons pass through a circuit to the other side of the cell, the produced electrons changes oxygen to O^{2-}, H^+ passes through the membrane, H^+ and O^{2-} reacts and form water and the produced current is used as electricity.

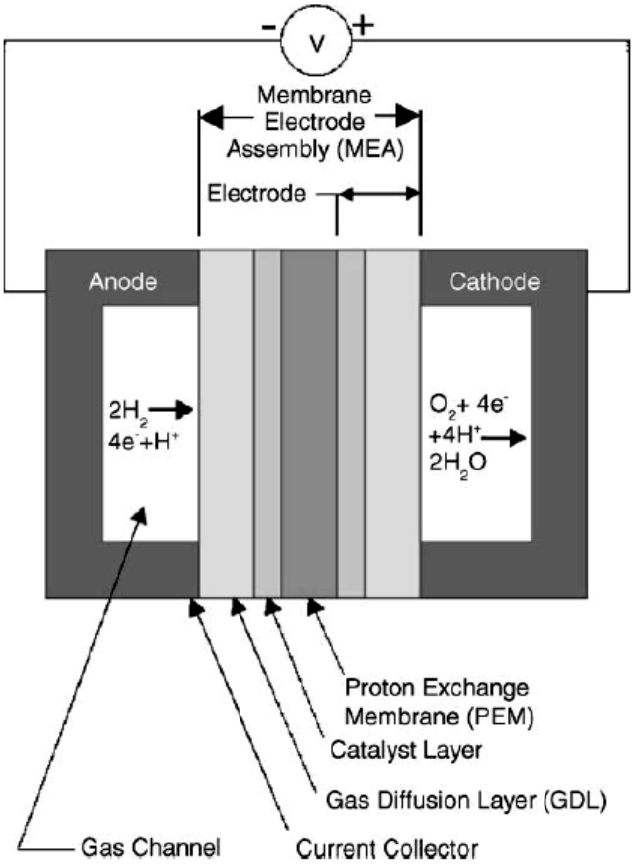

Fig. 1.2 Schematic of one proton exchange membrane (PEM) fuel cell [5].

Theoretically, PEM fuel cells should be charged with pure hydrogen. On an industrial scale, PEM fuel cells use the hydrogen produced by reforming. Reforming process produces hydrogen gas containing 40–75% H_2, 0.5–1% CO, 15–25% CO_2, 15–30% H_2O, and 0–25% N_2 [6]. The content of carbon monoxide is decreased to <50 ppm in a clean-up process. Nevertheless, even small amount of CO can cause a catalyst poisoning, which reduces the efficiency of the PEM fuel cells. The problem of sensitivity of catalyst performance is being studied in current research. The recent developments increased the current density of PEMFC to around 1 Acm^{-2} or higher, while the use of platinum has been reduced by a factor of over 100 [2].

1.4. Different Sources of Hydrogen

Hydrogen can be generated by different methods. However, currently except the steam reforming method (removal of hydrogen from hydrocarbons), the rest of methods are not economically applicable for industries.

- Steam reforming: Fossil fuels are used to produce hydrogen. Hydrocarbons can react with water vapor at high temperatures (700-1100^{o}C):

  $CH_4 + H_2O = CO + 3H_2$ 1.1

  $CO + H_2O = CO_2 + H_2$ 1.2

  Although steam reforming is the dominant source of hydrogen nowadays, this method depends upon consumption of fossil fuels and it generates CO_2 as byproduct. Therefore, the hydrogen produced by this method cannot be considered as a clean source of energy.

- Electrolysis: Applying direct electrical current to water, water molecules can split to hydrogen and oxygen. This method is rather expensive ($3 to $6 per kilogram of hydrogen instead of a little more than $1 for steam reforming method).

- Thermolysis: At temperatures over 2500^{o}C, water decomposes. Obviously, this method is not economically feasible on a large scale.

- Biological hydrogen production: Water can be split by some types of algae in bioreactors. This method is under development to meet targets of Department of Energy (DOE).

- Photocatalytic water splitting: Water can be split to its constituents by photons from solar energy. Different types of catalysts have been developed to promote kinetics of this method. Potentially, this method is one of the most promising ones for mass production of hydrogen without any significant carbon footprint.

- Reaction of metals with water: This method will be discussed in detail in the next section. The advantage of this method is that it can produce hydrogen onboard for vehicular purposes.

1.5. Reaction of Metals with Water to Generate Hydrogen

Reaction of a reactive metal with water can generate hydrogen and oxide/hydroxide of the metal. This reaction is exothermic at room temperature and the produced hydrogen can be used in fuel cells. Zinc, magnesium and aluminum are the metals that their reaction with water for hydrogen generation has been investigated.

There are few studies on reaction of zinc and water for hydrogen generation [7-9]. Zinc-oxide and hydrogen are products of this reaction:

$$Zn + H_2O = ZnO + H_2 \quad 1.3$$

H. H. Funke at al. studied reaction of zinc nanoparticles with water vapour and found that formation of a layer of ZnO hinders the reaction [7]. A. Beman et al. also found that formation of the oxide layer is an important step in determining the kinetics of the reaction [8].

Compared to aluminum or magnesium, zinc a heavier metal; 1 mole of zinc is 65.5 g, while it is 27 g and 24 g for aluminum and magnesium, respectively. One mole of zinc produces one mole of hydrogen, therefore, 1 g of zinc produces 0.03 g of hydrogen. Considering a wholesale price of $2.3 per Kg of zinc, 1 Kg of hydrogen produced by reaction of zinc with water would cost at least $75.3.

Reaction of magnesium and water has received more attention compared to that of zinc. The stoichiometry of reaction of magnesium is the same as zinc:

$$Mg + H_2O = MgO + H_2 \quad 1.4$$

Magnesium has a much higher reactivity compared to zinc. Nevertheless, the reaction results in formation of a protective layer of magnesium oxide or hydroxide on the surface of metal, which slows down the kinetics of the reaction. M. H. Grosjean et al. investigated the effect of ball milling on corrosion mechanism and hydrogen production of magnesium [10-12]. They found that ball milling shifts the corrosion potential to less negative potentials [12]. On the other hand, they found that there is an optimum milling time after which further milling has a negative impact on hydrogen production [10]. In another study, they found that the optimum milling time corresponds to the highest specific surface area. Therefore, the maximum hydrogen production rate depends on the surface area of the particles [13]. They also found that addition of water

soluble salts can have a significant effect on hydrogen production rate, which also depends on the type of the salt [14].

Magnesium scrap also can be used as a source for hydrogen [15]. S. H. Yu et al. studied effects of concentrations of salt and acids on hydrogen production from magnesium metal scraps [16]. They found that concentration of citric acid has a larger effect compared to the effect of salt.

In addition to magnesium, reaction of MgH_2 with water also has been studied for hydrogen production [17]. Effect of different parameters such as pH, type and concentration of the acid used in the solution and temperature has been studied [18-19]. S. H. Hong et al. studied effect of ball milling and addition of magnesium oxide to MgH_2 and found that both parameters have positive effect on hydrogen generation rate [20].

Compared to zinc, magnesium a light metal; 1 mole of magnesium is 24 g, which makes it one of the lightest metals. One mole of magnesium produces one mole of hydrogen, therefore, 1 g of magnesium produces 0.083 g of hydrogen. Considering a wholesale price of $2.5 per Kg of magnesium, 1 Kg of hydrogen produced by reaction of magnesium with water would cost $30. Compared to the price of the hydrogen produced by zinc ($75 per 1 Kg hydrogen), magnesium is more affordable, which explains the higher numbers of studies on hydrogen generation from magnesium compared to zinc.

In spite of high affinity of magnesium to react with water, and the rather affordable produced hydrogen compared to zinc, magnesium is highly flammable when it is powder or ball milled. This drawback introduces some safety precautions that must be addressed if magnesium is to be used largely for hydrogen generation.

1.6. Reaction of Aluminum with Water

Aluminum has a high affinity to react with water. Aluminum reacts with water; hydrogen is released and aluminum changes to more stable oxide or hydroxide forms. The reaction consumes aluminum and water, and produces hydrogen and aluminum oxide/hydroxide. The reaction can happen in three general ways (see reactions 1.5, 1.6 and 1.7). For a given amount of aluminum, the amount of produced hydrogen is fixed; 1 g of aluminum produces 0.11 g (1270 ml) of

hydrogen. However, the amount of the water consumed and the byproduct depends on the temperature and pH of the reaction:

$Al + 3H_2O = ½(Al_2O_3.3H_2O) + 1.5H_2$ -427.98 kJ/mol, (1.5)

$Al + 2H_2O = ½(Al_2O_3.H_2O) + 1.5H_2$ -415.24 kJ/mol, (1.6)

$Al + 1.5H_2O = ½(Al_2O_3) + 1.5H_2$ -407.7 kJ/mole. (1.7)

The number next to each reaction represents enthalpy changes [21]. The produced $Al_2O_3.3H_2O$ or $Al(OH)_3$ phase (alumina hydrate) can be in the form of bayerite or gibbsite. The $Al_2O_3.H_2O$ phase (aluminum oxyhydroxide) can be in the form boehmite or diaspore, and theAl_2O_3 phase (aluminum oxide) can be alpha or gamma alumina.

It is experimentally proved that the reaction byproduct is generally bayerite around room temperature, boehmite with boiling water and alumina at supercritical conditions. All the reactions are exothermic at room temperature and produce considerable amount of heat, however, from reaction 1.5 to 1.7, the produced heat decreases.

Similar to magnesium, aluminum also is a light metal. 1 mole of aluminum is 27 g; after magnesium, aluminum is the lightest industrial metal. One mole of aluminum produces one and half mole of hydrogen. 9 Kg of aluminum is needed to produce 1 Kg of hydrogen. Considering a wholesale price of $2 per Kg of aluminum, 1 Kg of hydrogen produced by reaction of aluminum with water would cost $18. Compared to the price of hydrogen produced by zinc and magnesium ($75 and $30 per 1 Kg hydrogen, respectively), aluminum is much more affordable. The rather affordable price of hydrogen produced by aluminum explains the higher numbers of studies on hydrogen generation of aluminum compared to magnesium. Moreover, aluminum does not have the safety issues regarding catching fire, which is the case for magnesium.

In 2008, (DOE), released a reports regarding the pros and cones of hydrogen generation by reaction aluminum with water. Moreover, they reported on cost, efficiency and applicability of the method. Some of the facts are summarized as fallow [22]:

- Volumetric Hydrogen Capacity: 46 g H_2/lit.
- Gravimetric Hydrogen Capacity: 3.7 wt%.
- 15.5 KWh Energy is needed for production of 1 Kg of aluminum (140 KWh for 9 Kg).

- 33.6 KWh per 1 Kg of hydrogen => Efficiency = 25%.
- Given the DOE target of flow of 1.6 g H_2/sec for vehicular purposes=> ~ 8 Kg aluminum is needed to satisfy 80 KW of energy to run an intermediate car.
- 8 Kg Al (3 Lit) + 10 Kg H_2O (10 Lit) = 18 Kg (13 Lit) is the weight and volume of the needed aluminum and water to run an intermediate car.

1.7. Aluminum- as Anode in Aluminum-Air Batteries

Aluminum can also be used as a source of energy in aluminum-air batteries. Here, instead of reaction with water, aluminum reacts with the oxygen in air and generates electricity.

The anode half-reaction is:

$$Al + 3OH^- = Al(OH)_3 + 3e^-. \quad (1.8)$$

The cathode half-reaction is:

$$3/4O_2 + 3/2H_2O + 3e^- = 3OH^-. \quad (1.9)$$

The total reaction is:

$$Al + 3/4O_2 + 3/2H_2O = Al(OH)_3. \quad (1.10)$$

These batteries have one of the highest energy densities among different batteries. However, their widespread use has been limited because of issues regarding the high price of anodes and removal of byproduct after consumption of anodes. The aluminum used is anode turns to aluminum hydroxide. The produced aluminum hydroxide can be recycled to aluminum for further use as anode (Fig. 1.3). S. Yang et al. calculated a total efficiency of 15% for aluminum-air batteries and concluded [23]:

"From our design analysis, it can be seen that the cost of aluminum as an anode can be as low as US$ 1.1/kg as long as the reaction product is recycled. The total fuel efficiency during the cycle process in Al/air electric vehicles (EVs) can be 15% (present stage) or 20% (projected) comparable to that of internal combustion engine vehicles (ICEs) (13%). The design battery energy density is 1300 Wh/kg (present) or 2000 Wh/kg (projected). The cost of battery system chosen to evaluate is US$ 30/kW (present) or US$ 29/kW (projected). "

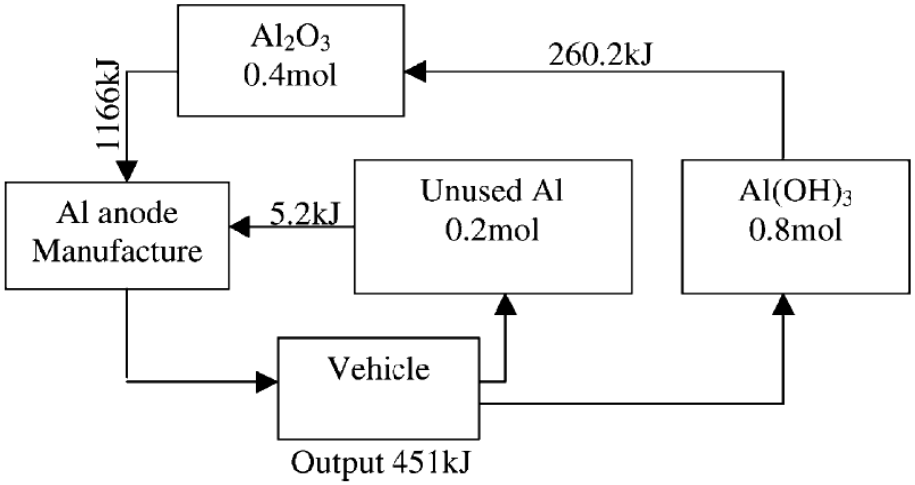

Fig. 1.3 Fuel cycle of aluminum-air batteries [23].

The electrolyte used for these batteries is water based, which made the aluminum anode prone to corrosion. This issue is also known as problem of hydrogen generation in aluminum-air batteries [24]. Presence of iron contamination in pure aluminum can significantly increase its corrosion rate. One of the approaches to address this issue is to use a high purity aluminum [25]. However, ultra high purity aluminum anodes are too expensive. Another approach is to alloy aluminum with zinc [26] or gallium [27], which can considerably prevent corrosion of aluminum anode by water based electrolyte. Indeed, reaction of aluminum with water is to be prevented in aluminum-air batteries, while this reaction is promoted as a hydrogen generation method in the present study.

1.8. Improving Aluminum-Water Reaction Rate

The reaction of aluminum and water has been studied vastly with regards to prohibition of the corrosion of aluminum parts in aqueous media. During past 10 years, more attention has been paid to the capability of aluminum to generate hydrogen from reaction with water [28-30]. The rate of hydrogen production from the reaction slows down as the byproducts form on the aluminum surface. All of the above mentioned byproduct phases (section 1.6) have a good adherence to the aluminum substrate, which makes the formed layer acting like a protective film.

The produced film is thermodynamically stable, and is not water soluble; therefore, the aluminum substrate is protected against the reaction with water even at high temperatures.

The investigations on promoting the aluminum-water reaction for hydrogen production can be categorized into three methods [22, 31]:

1. Increasing the pH of water (toward more alkaline solutions) so that the aluminum hydroxide becomes soluble and the bare aluminum surface is exposed to water molecules.
2. Alloying aluminum with low melting point metals (LMPs) like Ga, In, Hg, etc., which makes the barrier layer destroyed and water can reach the aluminum surface.
3. Addition of water soluble salt or ceramic particles to the aluminum matrix. The mechanism for improving the reaction will be discussed in chapter 7.

Another method for improving the reaction is ball milling of aluminum particles. The activation process by ball milling was not categorized as a separate method because ball milling is used parallel to any of the above mentioned methods rather than a standalone activation process.

1.9. High Energy Ball Milling

High energy ball milling was initially introduced by John Benjamin as a method for production of oxide dispersion strengthened (ODS) alloys [32-33]. This method has been extensively used for production of nanocomposites, nanostructured materials, metal matrix composites and synthesis of new materials [34]. There are different types of mills for high energy milling such as planetary ball mill, SPEX, Attritor, etc. Planetary ball mill is the most popular mill for laboratory researches. Fig. 1.4 shows the schematic of motion of balls and particles in a vial in a planetary ball mill.

The main difference between high energy milling by planetary ball mill, Spex, Attritor mill, etc. and conventional milling is that the former applies much larger doses of energy to particles over time [34]. This large input energy makes high energy mills capable of producing materials with special properties that could be synthesized by conventional mills. On the other hand, the large amount of energy consumed by high energy mills is potentially a burden in industrial

application of this method. That is because the electrical energy spent for production of the powders by high energy mills is added to the final price of the products.

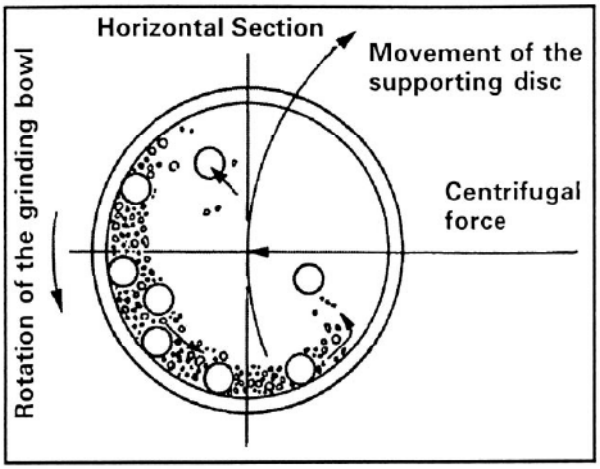

Fig. 1.4 Schematic showing the balls and particles motion in a vial of a planetary ball mill [34].

Researchers have adopted two ways to decrease the energy needed for production of powder products by high energy mills. The first is to find the minimum time needed to produce the desired products. For the products that are synthesized by a reaction, whether the reaction occurs gradually or suddenly during milling, the minimum milling time can easily be determined by the time that is required for whole amount of reactants to be transformed/reacted to form the desired products [35-38]. However, for production of nano-crystalline powders by severe plastic deformation where no reaction is involved, or for activating a powder product for a reaction, it is not straightforward to determine the needed minimum milling time. Accordingly, researchers introduced the "steady state time", which is defined as the milling time after which further milling has negligible effects on the powder products [33-34, 39-42]. Changes in size and shape of particles, preferred orientation and presence of lattice imperfections (e.g. grain boundaries, dislocations etc.) can be used as the criteria for determination of the steady state.

The second way of decreasing the energy consumed by high energy mills is to make the milling more efficient in a way that the system reaches the steady state in a shorter period of time. Changes in ratio of rotation of vials compared to disk [43-44], balls size [36, 45-48], mill speed [43-45, 47, 49-53], filling ratio of vials [36, 45, 48-51, 54] and charge ratio [36, 38, 55-56]

have been studied to optimize the milling process. Although there is no agreement in literature on the effect of most of the mentioned variables, the unanimous conclusion is that a higher speed and a larger charge ratio result in a faster formation of final products. However, a higher speed of a mill requires higher energy inputs. A larger charge ratio also means that for a given amount of feed (balls + powder), a less amount of powder is produced. Therefore, although an increase in either mill speed or charge ratio decreases the steady state time, it still may increase the price of final products.

Changes in microstructure of ductile metals (such as aluminum) during ball milling can be explained by two mechanisms; cold welding and fracture. At the beginning of ball milling where particles are ductile, impacts produce hard aggregates of particles by cold welding [39-41, 57]. As milling continues and deformation causes work hardening in microstructure of particles, fracture mechanism activates. For ball milling of a single phase ductile metal, steady state milling time is defined as the milling duration after which fracture and cold welding of particles reach equilibrium. Particle size of the powder does not change after steady state, although fracture and cold welding of particles continue. Fig. 1.5 schematically shows the fracture and cold welding during collisions. As it will be discussed in chapter. 2, ball milling of aluminum powder for the purpose of hydrogen production can be stopped at a time much shorter than the steady state time.

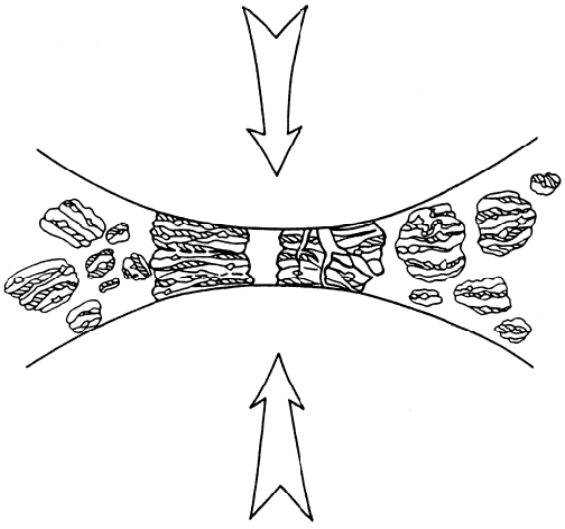

Fig. 1.5 Schematic shows the fracture and cold welding of particles during collisions [34].

1.10. Objectives of the Project

This research aims to understand and optimize the activation process of aluminum powder to react with water and generate hydrogen. There are six objectives to be achieved in this project:

1.10.1. Optimizing the Milling Time

Ball milling has been widely used as an activation process for aluminum powder. However, not enough attention had been paid to the fact that the high energy ball milling is an energy consuming process that can markedly add to the final price of the produced hydrogen. Therefore, milling time should be optimized for the minimum energy consumption. Moreover, prolonged ball milling can have a deleterious effect on the efficiency of the reaction. Therefore, chapter 2 (manuscript #1) was prepared to understand the effect of milling time and optimize the milling duration.

1.10.2. Contribution of Milling in the Activation Process

Ball milling has been known as an effective method to mix the second phase with aluminum particles. Nevertheless, other contributions of ball milling to modification of the reaction had remained obscure. Chapter 3 (manuscript #2) identifies and explains different effects of ball milling on improving aluminum-water reaction.

1.10.3. Mechanism of the Reaction

In spite of numerous works on the reaction of aluminum with hot water to generate hydrogen, a thorough evaluation of the reaction mechanism needed further investigation. No electrochemical experiments had been performed in the literature to understand the mechanism of the reaction in correlation to hydrogen generation results. This gap in knowledge motivated us to perform electrochemical tests to explain the reaction mechanism. The obtained results are discussed in chapter 4 (manuscript #3).

1.10.4. Mechanism of Grain Refinement during Ball milling

As will be discussed in chapter 3 and chapter 4, microstructural refinement of aluminum has a significant effect on kinetics of the reaction. This refinement occurs through formation of new low and high angle grain boundaries. There had been no thorough investigation on effect of severe plastic deformation during ball milling on grain subdivision mechanism in aluminum.

Chapter 5 (manuscript #4) explains deformation mechanism and microstructural evolution of aluminum powder during ball milling.

1.10.5. Modeling the Reaction

The previous works have not proposed realistic model of hydrogen generation, or have used the simple core-shell model. Because some of the conditions of the traditional core-shell model are distinctly different from that of the reaction of aluminum particles in hot water, a considerable difference has been observed in literature between the theoretical and experimental data. Therefore, we modified the core-shell model to make it more appropriate for the type of observed reactions. An explanation of the assumptions of the traditional core-shell model and the changes that were made are provided in chapter 6 (manuscript #5).

1.10.6. Effect of Addition of Water-Soluble Salts on the Reaction

Among the mentioned methods in section 1.3, the first two were not included in the scope of this research as they are not promising to be applied in the clean sustainable industries:

- The first method is applicable when the pH is higher than 11. The use of high pH solutions for the reaction with aluminum involves dealing with corrosive/irritant materials, which are often not environmentally friendly.
- Although LMPs can effectively improve the reaction, they are expensive. The use of LMPs to improve reaction of water with alloyed aluminum significantly increases the price of the produced hydrogen (for example, the whole sale price for aluminum and gallium is $2-3 and $800, respectively). Moreover, LMPs are mostly toxic, which makes their use limited.

Considering these problems, the present project is focused on the last method because water-soluble salts or ceramic particles are not expensive, not toxic and not corrosive. Since water-soluble salts (such as NaCl or KCl) are cheaper and more abundant compared to the ceramics that can be used for promoting the reaction (such as Al_2O_3, SiC, MgO, AlOOH, etc.), this project specifically focused on activation of aluminum particles by the addition of water-soluble salts. Chapter 7 (manuscript #6) provides results and discussion regarding the effect of addition of salt (NaCl) or refined potash (KCl) to the aluminum matrix on the hydrogen generation rate.

CHAPTER 2

EFFECT OF STRUCTURAL EVOLUTION OF ALUMINUM POWDER DURING BALL MILLING ON HYDROGEN GENERATION IN ALUMINUM-WATER REACTION

2.1. Overview of Chapter 2

Ball milling is an energy consuming process and needs to be optimized to reduce the cost of the produced hydrogen. The effect of milling time on the kinetics of the reaction of aluminum and water will be explained in this chapter. The main factor that determines the optimized milling time is the hydrogen generation rate. Therefore, the shortest milling duration that results in the highest hydrogen generation rate is considered as the optimum milling time. The microstructural evolution of aluminum particles during milling is evaluated by examining the morphology, cross section, surface and size of the ball milled particles. Using the results from investigation of the microstructural evolution, the changes in hydrogen generation rate are correlated to the milling time.

This chapter is presented as manuscript #1 (Effect of Structural Evolution of Aluminum Powder during Ball Milling on Hydrogen Generation in Aluminum-Water reaction). The PhD candidate's contributions to the manuscript are: a) Ball milling the powder. b) Preparation of the experimental set-up to measure hydrogen production accurately. c) Hydrogen measurement tests

and study of the particles before and after the reaction. d) Analyzing the data, reviewing the relevant literature and preparing the manuscript.

The manuscript was published in 2013 in International Journal of Hydrogen Energy:

- S.S. Razavi-Tousi, J.A. Szpunar, Effect of structural evolution of aluminum powder during ball milling on hydrogen generation in aluminum–water reaction, Int J Hydrogen Energ, 38 (2013) 795-806.

http://dx.doi.org/10.1016/j.ijhydene.2012.10.106

The manuscript presented here is different from that of published in two parts:

- The first three figures in the present manuscript are extra to figures of the published paper. They are added to clarify the hydrogen measurement procedure.
- The graph of the particle size vs. milling time was slightly changed compared to that of the published paper.

The copyright permission to use the manuscript in the thesis was obtained and provided in the Appendix section. The references for this chapter along with references from other chapters are provided at the end of the thesis.

Effect of Structural Evolution of Aluminum Powder during Ball Milling on Hydrogen Generation in Aluminum-Water reaction

S.S. Razavi-Tousi, J.A. Szpunar

Department of Mechanical Engineering, University of Saskatchewan, S7N 5A9 Saskatoon, Saskatchewan, Canada

2.2. Abstract

Effect of milling time on structure of pure aluminum powder and consequently on efficiency of aluminum-water reaction and hydrogen production is studied. The concept of steady state milling time is examined to determine the optimum milling time for the best hydrogen yield. Dimensions of particles before and after the reaction are measured to establish a role of size and shape of particles on kinetics of the reaction. It is demonstrated that the formation of interlayer spaces within the investigated aluminum particles effectively increases hydrogen yield. Moreover, prolonged ball milling eliminates the interlayer spaces and decreases the rate of reaction of water with the powders.

Keywords: *Hydrogen Generation, Ball Milling, Steady State Time, Microstructure, Reaction Mechanism*

2.3. Introduction

During the past 10 years many researchers have considered reaction of aluminum powder with water to generate hydrogen [58-59]. The major difficulty for this reaction is the passivation of aluminum powder surface by a protective oxide/hydroxide layer that slows the reaction and may stop it. This problem can be overcome using alkaline solutions that dissolve the protective layer on surface of aluminum [28, 60-64]. Moreover the reaction of aluminum powder with supercritical water [65-66] or reaction of aluminum nano-powder with water [67-68] to produce hydrogen have been examined and were successful.

High energy ball milling (also called mechanical alloying or mechanical activation) of aluminum powder with or without additives has been considered as an alternative. The role of ball milling is to activate aluminum particles by increasing their surface area and mixing them with additives. So far reaction of water with aluminum powder milled with low melting point metals like Ga, In, Bi, Hg and Zn [69-74], water soluble salts like NaCl and KCl [73-78] and ceramic powders like $Al_2O_3(\alpha)$, $Al_2O_3(\gamma)$, TiO_2, C, SiO_2 and aluminum$(OH)_3$[78-86] have been reported. In many cases the reaction rate was fast and aluminum powder was consumed completely to generate hydrogen.

Although high energy ball milling of aluminum powder is capable of promoting aluminum-water reaction, less attention has been paid to the amount of energy needed to activate aluminum powder. Ball mills usually consume a lot of electrical energy during the milling process. This electrical energy should be considered while calculating the final price of the hydrogen generated by this method. Moreover prolonged milling time increases unwanted impurities in the milled powders because of balls/vial abrasion [87]. Therefore it is necessary to optimize milling time for lower energy consumption and a higher hydrogen yield.

Steady state time is a milling duration after which further ball milling has negligible effects on the powders [34]. Steady state milling time is therefore a parameter that characterizes maximum recommended energy consumption; this value should not be exceeded in the milling process. Researchers studied the steady state milling time of aluminum powders for high energy ball milling and often recorded morphological changes, particle size distribution, average particle size, accumulated strain energy in aluminum lattice and orientation of crystallites. Such structural characteristics determine steady state time for milling of aluminum powder [40-41, 88-95].

To the best knowledge of the authors, no research has examined the steady state milling concept for reaction of milled aluminum powders with water. However, there are studies that concluded that ball milling after a certain time does not have significant effect on hydrogen yield [74-75].

Also extended milling after some particular time can decrease hydrogen yield. A. N. Streletskii et al. found also that hydrogen yield decreases as energy supplied to activate aluminum powders exceeds a particular value [84]. They justify this decrease to oxidation of the

aluminum powder during milling and supported that explanation with chromatographic analysis. E. Czech et al. milled aluminum powder in air and recorded an optimum milling time for the highest hydrogen production [78]. They also explained decrease of hydrogen production by oxidation of aluminum powder during milling. M. Q. Fan et al. ascribed the decrease of hydrogen production to a higher reactivity of milled aluminum-Hg-NaCl powder with air [71]. In another work the observed decrease is related to a change in crystallite size of In in aluminum-In-Zn-NaCl powders [73]. H. W. Wang et al. observed a deleterious effect of a heavy ball milling on hydrogen production of aluminum powder mixed with nano-TiO_2 [85]. They relate this effect to migration of TiO_2 nanoparticles away from surface of the aluminum particles in the heavily milled samples.

This two-fold effect was also observed for reaction of ball milled Mg with water. M. S. Grosjean et al. observed a similar trend of change in hydrogen generation for ball milled Mg and MgH_2 powders [10, 13]. They found that ball milling can increase hydrogen yield as long as it increases the surface area of the powder, otherwise it has a negative effect on hydrogen yield [12]. In spite of the fact that milling time is an effective parameter, no study rationalized the correlation between efficiency of the reaction and microstructural evolution of aluminum powder during milling. This rationalization could help researchers to find a proper milling time for the lowest energy consumption during milling and the highest hydrogen yield during reaction with water.

In this paper, we investigate steady state time for ball milling of a monolithic pure aluminum powder. The hydrogen production efficiency of the aluminum powders milled for different times is correlated to microstructural changes during milling process. In order to investigate the effect of aluminum microstructure on efficiency of the reaction, ball milling was done in argon atmosphere to prevent the effect of oxidation of the aluminum powder during ball milling on hydrogen yield. Moreover additives like salts, ceramics or metals were not added to the aluminum powder. Therefore the hydrogen generation rate is low in the absence of any promoting additive but, it directly shows how kinetics of the reaction depends on microstructure of the aluminum powder.

2.4. Experimental Procedure

2.4.1. Ball Milling

Aluminum powder of 99.8% purity (MFCD00134029, the 0.02% impurity was not determined by vendor) was provided by Alfa Aeasar Company. Stearic acid (97% purity, Fisher Scientific-AC17449-0010) was used as process control agent (PCA) and 3 wt% of it was mixed with the aluminum powder prior to milling. High energy ball milling was done in a planetary ball mill (Torrey Hills- ND2L) with stainless steel cups (285 ml capacity) and balls (28 of 16 mm and 6 of 18 mm diameter) in an argon atmosphere (99% purity). Ball to powder weight ratio was 30:1 and mill speed was maintained at 200 RPM for durations of 0.25, 0.5, 1, 2, 4, 7, 11 and 19 hours.

2.4.2. X-ray Analyses of Powders

Microstructure of the powders was characterized by a Bruker D8 Discover X ray diffractometer with a chromium target. In order to obtain improved peak parameters, X-ray diffraction (XRD) peaks were analyzed as follows:

$K\alpha_2$ stripping was done applying the Rachinger method [96], considering $K\alpha_1 = 2.289760$ and $K\alpha_2 = 2.293663$. It was assumed that the $K\alpha_1$ and $K\alpha_2$ line profiles are identical in shape and not necessarily symmetrical, and that the α_2 peak is half of the intensity of the α_1 peak, and is shifted from it toward larger angles by

$$\Delta 2\theta = 2\tan\theta\left(\frac{\Delta\lambda}{\lambda}\right) \tag{2.1}$$

where $\Delta\lambda$ is the dispersion separation $\lambda(\alpha_2) - \lambda(\alpha_1)$ in angstroms.

Pseudo-Voigt profile fitting was used to decompose a complicated powder diffraction pattern, assuming it can be represented by the weighted mean between a Lorentz and a Gauss function:

$$G_{ik} = \gamma\frac{C_o^{0.5}}{H_k\pi}[1 + C_o X_{ik}^2] + (1-\gamma)\frac{C_1^{0.5}}{H_k\pi^{0.5}}\exp[-C_1 X_{ik}^2] \tag{2.2}$$

where $C_0 = 4$, $C_1 = 4\times\ln 2$, H_k is the full-width at half-maximum (FWHM), $X_{ik} = (2\theta_i - 2\theta_k)/H_k$.$\gamma$ is a refinable "mixing" parameter describing the amount of Gaussian profile versus the amount of Lorentzian profile; and thus describing the overall profile shape.

Crystallite size of the samples was calculated using the Williamson-Hall method for at least three peaks [97]:

$$B_s^2 = B_t^2 - B_i^2 \quad (2.3)$$

$$B\cos\theta = 0.9\lambda / D + 2\eta\sin\theta \quad (2.4)$$

Where B_s is FWHM for structural broadening, B_t is FWHM for combination of structural and instrumental broadening, B_i is FWHM for instrumental broadening, λ is the wave length, θ is peak position, D is crystallite size and η is lattice strain.

2.4.3. Hydrogen Measurement

The hydrogen measurement setup is illustrated in Fig. 2.1. Aluminum powder (amount of 2 gr) was added into an Erlenmeyer flask containing 200 ml distilled water at temperature of 80°C with a constant stirring rate of 120 rpm. The produced hydrogen gas was passed through a desiccant ($CaCl_2$) to absorb moisture, and then an ADM2000 flowmeter measured its flow with an accuracy of 0.1 ml/min. The flowmeter was connected to the computer and an ADM Trend software acquired data. The flow was measured for the first 1.5 h of the reaction for each sample and then normalized for 1 gr aluminum powder.

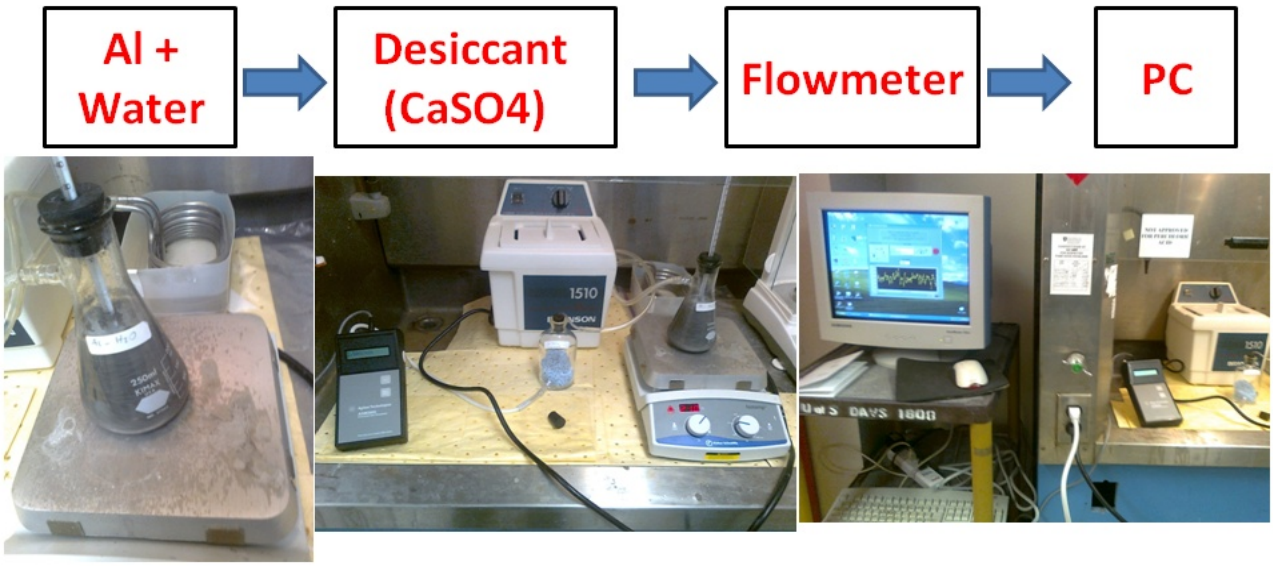

Fig. 2.1The set up and flowchart of hydrogen measurement experiment.

A hydrogen yield curve vs. time was obtained by integrating the flow data over time. Some measurements were repeated to make sure that the experiment is capable of giving reproducible results. We did not continue measuring hydrogen flow after 90 min of the reaction because the

obtained data was enough to investigate effect of microstructure on the rate of aluminum-water reaction. For our results, the term "hydrogen yield" refers to hydrogen generated in the first 1.5 h of the reaction.

To make sure that water moisture or expansion of air in the flask during heating were not measured as the hydrogen flow, a baseline curve was subtracted from the flow obtained from the reactions. This baseline curve was obtained by measuring and averaging the flow from 200 ml distilled water at temperature of 80^{o}C with a constant stirring rate of 120 rpm with no aluminum powder added for 3 times. Fig. 2.2 shows the baseline and Fig. 2.3 shows a typical raw data curve obtained from the 7 h milled samples.

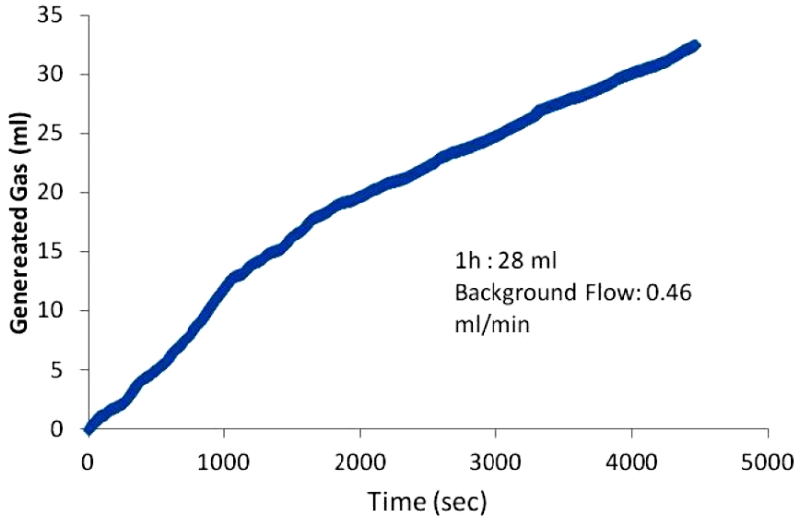

Fig. 2.2 The obtained baseline, which is mainly due to water vapor.

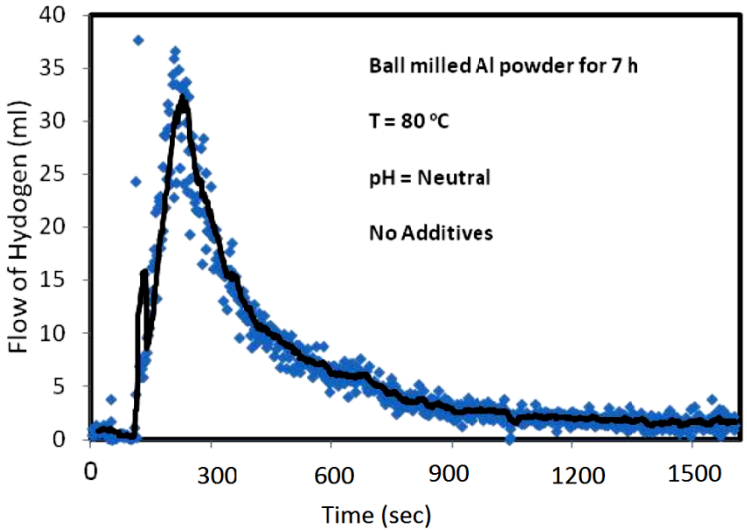

Fig. 2.3 A typical obtained flow vs. time after corrections in neutral pH (6-7).

2.4.4. Scanning Electron Microscope (SEM)

Morphology and cross section of the powders after ball milling and after the reaction were examined with a Hitachi SU6600 SEM. In order to study effect of the reaction on morphology of the aluminum powders, reaction was stopped before the aluminum powders reacted completely with water. The by-product powder was washed with cold water and dried at room temperature.

To study cross section of the particles, a small amount of the powder was added to a conductive carbon resin powder, mixed and mounted. The mounted samples were polished with abrasive grinding papers from 600 to 1600 grit followed with additional grinding with diamond pastes. Finally to get a high quality surface, samples were polished using Buehler VibroMet for few hours.

2.4.5. Particles Size Measurement

The particle size distribution of the powders was measured by a Laser Particle Size Analyzer (Mastersizer Particle Size Analyzer, Malvern Instruments Ltd.). Samples were deagglomerated in 99.9% ethyl alcohol prior to measurement and their D_{50} is presented as the median particle size.

2.5. Results and Discussion

2.5.1. Steady State Milling Time

Fig. 2.4 shows the morphology of the aluminum powder milled for different times. One can see an increase in particle size to about 500 μm, followed by a decrease to less than 50 μm. The morphological changes during ball milling of ductile powders can be explained by assuming that there is a competition between two mechanisms: fracture and cold welding [40-41, 98]. During the first 30 min of milling, the aluminum particles are ductile and tend to deform and cold weld. Impacts of balls flatten the as received aluminum particles (Fig. 2.4(a) & (b)), and they cold weld to form bigger disc-shape particles (Fig. 2.4(c)). The plastic deformation makes particles hard and brittle, therefore fracture mechanism activates after 1 h milling. Accordingly the big plate-like particles fracture to form smaller flake-like particles (Fig. 2.4(d) & (e)). Fracture mechanism is dominant over cold welding between 4 h to 11 h where flake-like particles change to equiaxed ones and particle size of the powder decreases (Fig. 2.4(f), (g) & (h)).

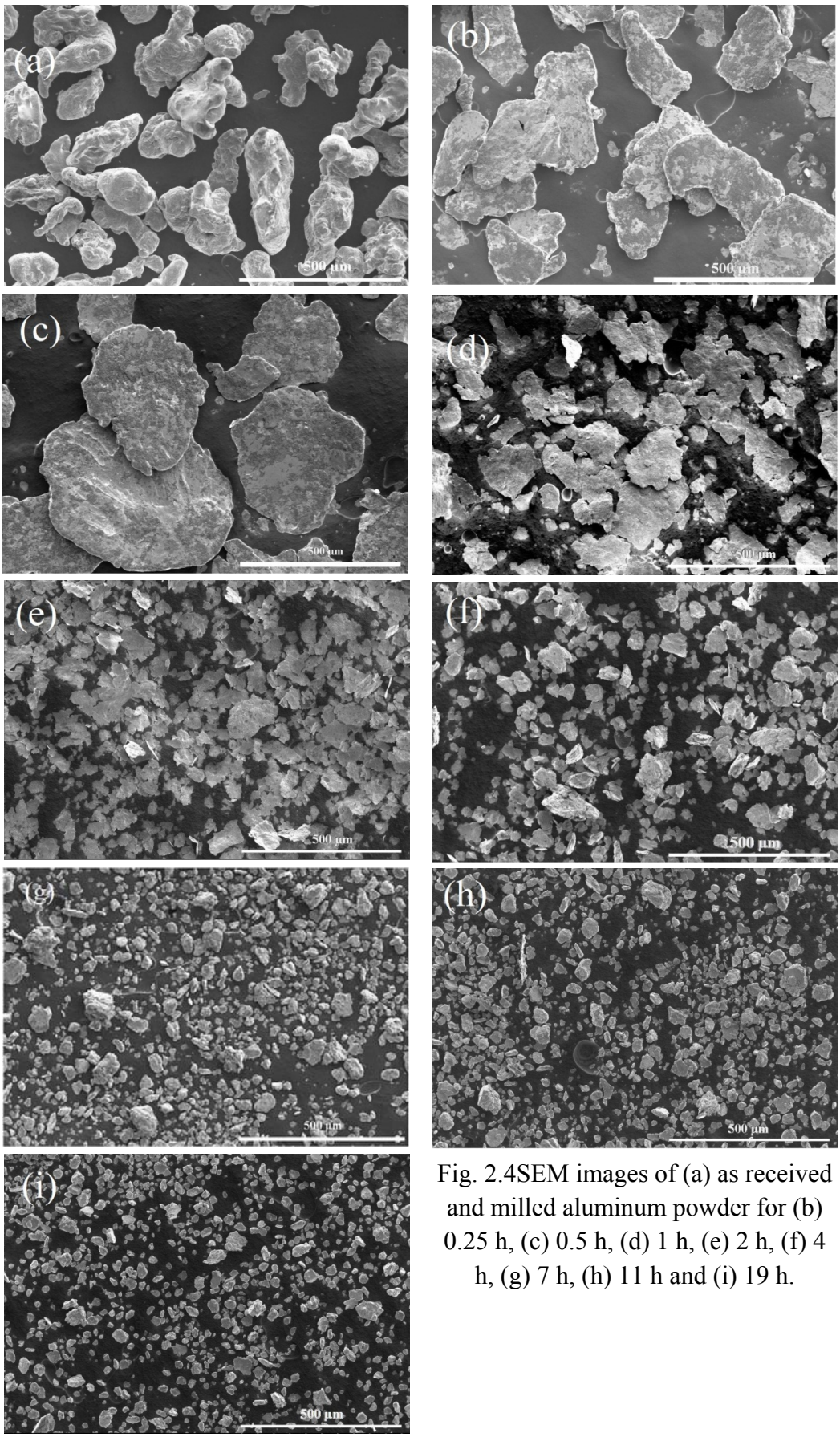

Fig. 2.4SEM images of (a) as received and milled aluminum powder for (b) 0.25 h, (c) 0.5 h, (d) 1 h, (e) 2 h, (f) 4 h, (g) 7 h, (h) 11 h and (i) 19 h.

One can consider 7-11 h as steady state milling time because further milling up to 19 h has only negligible effect on morphology and size of the particles. Nonetheless, it is important to note that after stabilization of particles size, microstructural refinement can still take place and terminate at a later time[99].

Fig. 2.5 shows effect of ball milling time on the average particle size of the aluminum powder. It clearly shows that ball milling up to 7-11 h results in marked changes, but further milling after 11 h has no significant effect.

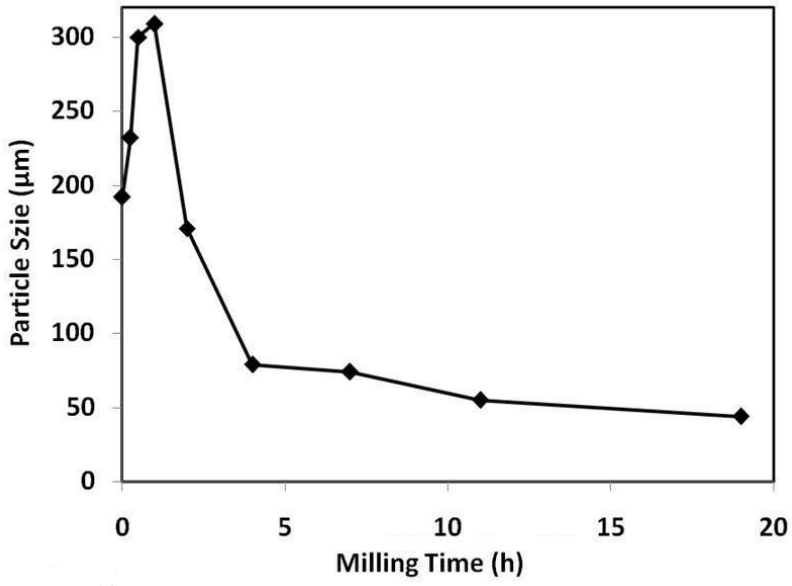

Fig. 2.5 Effect of milling time on average particle size of the aluminum powders.

We used XRD to study the accumulated strain energy in the aluminum lattice and orientation of crystallites as criteria for steady state time. Fig. 2.6(a) shows effect of milling time on FWHM of (111) peak of the powders. The FWHM increases after 1 h milling and becomes stagnant after 11 h milling. The severe plastic deformation during ball milling creates lot of imperfections (grain boundaries, dislocations, stacking faults, etc.) in lattice of the milled powders. The presence of imperfections results in peak broadening and an increase in FWHM. The increase of FWHM vs. milling time stops after 11 h of milling which implies that the aluminum lattice is saturated with imperfections.

Another criterion for steady state that can be extracted from XRD profiles is orientation of crystallites in ductile materials. This factor can be used to determine steady state milling time because preferred orientation of crystallites changes during milling time. A remarkable preferred orientation shows up when particles are flattened and it disappears when particles shape changes to equiaxed at the end of milling [39, 41-42].

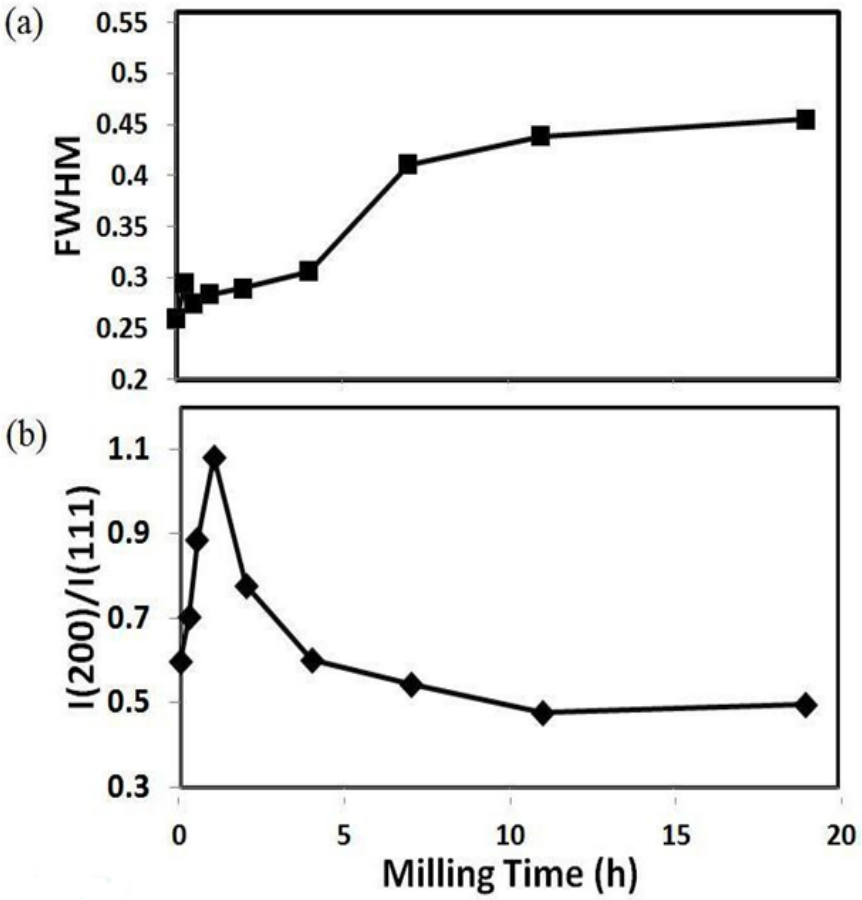

Fig. 2.6 Effect of milling time on (a) FWHM of (111) reflection and (b) ratio of intensity of (200)/(111) reflection.

Fig. 2.6(b) shows effect of milling time on ratio of intensity of (200) to (111) reflection. The ratio increases rapidly up to 1 h milling and then decreases gradually. This phenomenon can be explained by the fact that some orientations can be readily deformed while some are resistance to deformation [42]. One can see that the preferred orientation effect disappears as milling continues and a milling time longer than 11 h has a negligible effect on the ratio of intensity of

(200) to (111) reflection. This result is consistent with that presented in Fig. 2.5& 2.4 confirming that it takes 7-11 h for the aluminum powder to reach its steady state during ball milling.

2.5.2. Effect of Microstructure on Hydrogen Yield

Fig. 2.7 shows hydrogen generation vs. time for reaction of water with the aluminum powders milled for different times. We did not detect any reaction for the as received aluminum powder and also the powder milled for 0.25 h, 0.5 h and 1 h, therefore they are not reported in Fig. 2.7. One can see that the hydrogen yield increases as milling time increases up to 7 h, but after 7 h milling hydrogen yield decreases. A negative effect of milling for more than 7 h on the reaction rate cannot be explained by a change in particle size and morphology because they do not change markedly.

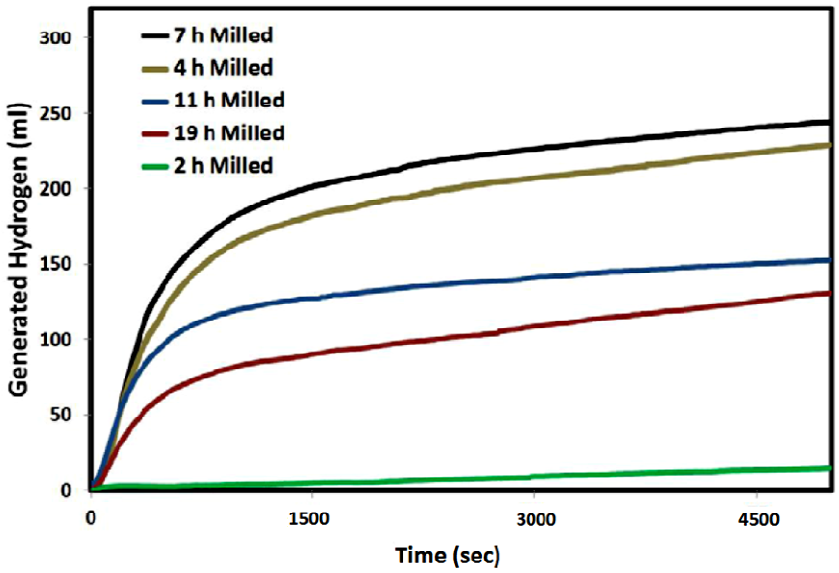

Fig. 2.7 Experimental data on hydrogen generation vs. time for reaction of water with the aluminum powders milled for different durations.

High magnification SEM images from particles before and after the reaction illustrate whether the reaction causes any substantial changes in shape and size of particles that explain the trend illustrated in Fig. 2.7. Many SEM images were taken to examine particles and Fig.2.8 demonstrates few examples of them. Fig. 2.8 shows SEM images of 4, 7, 11 and 19 h milled powders before the reaction with water. One can see that the surfaces of the milled aluminum particles are smooth, with some cracks caused by cold welding and fracture.

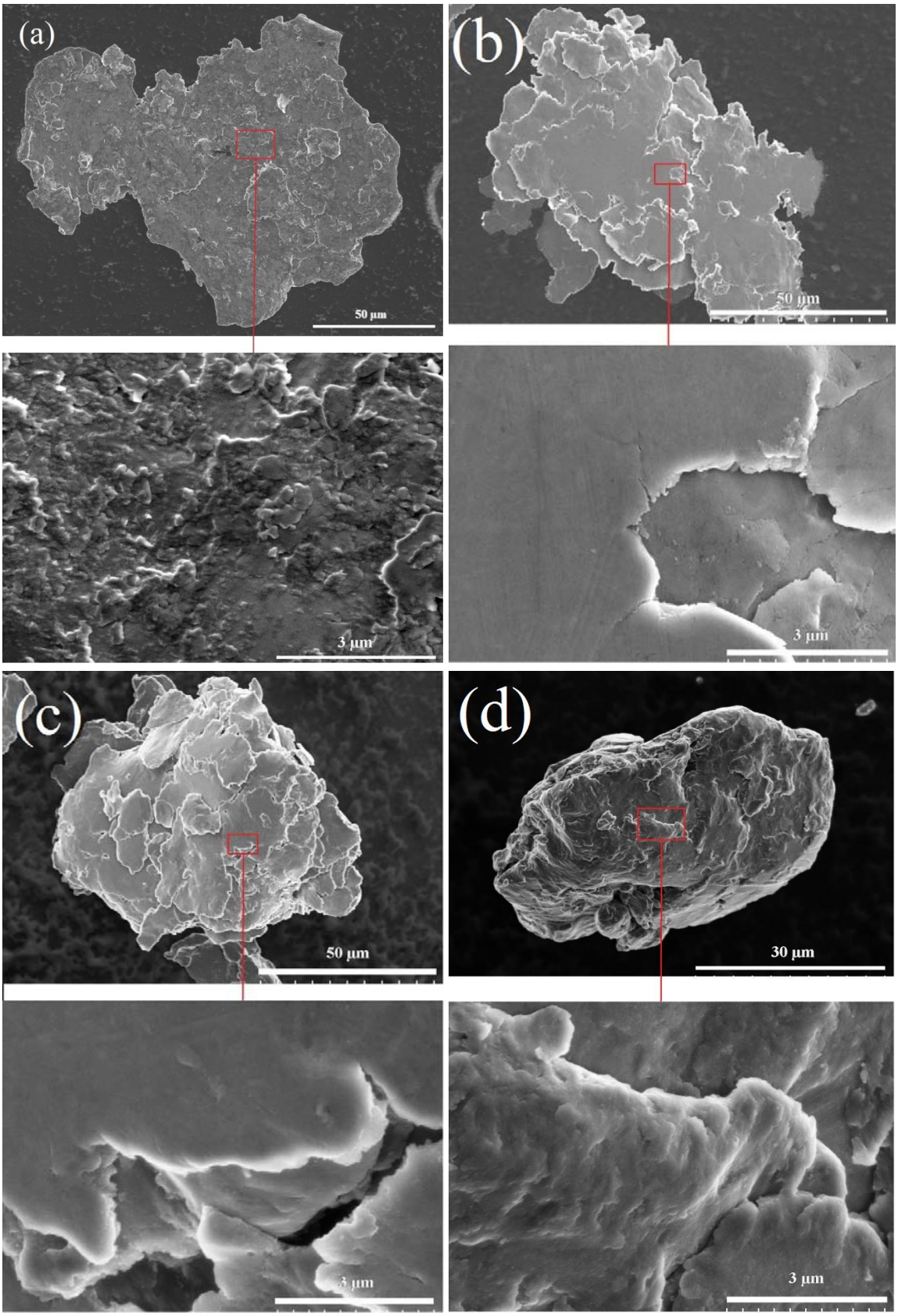

Fig. 2.8 SEM images of the particles milled for (a) 4 h, (b) 7 h, (c) 11 h and (d) 19 h.

Fig. 2.9 shows SEM images of 4, 7, 11 and 19 h milled powders after 2 h of the reaction. One can see that the morphology of the particles have not changed after the reaction. Moreover, a layer of aluminum hydroxide covers the surface of particles.

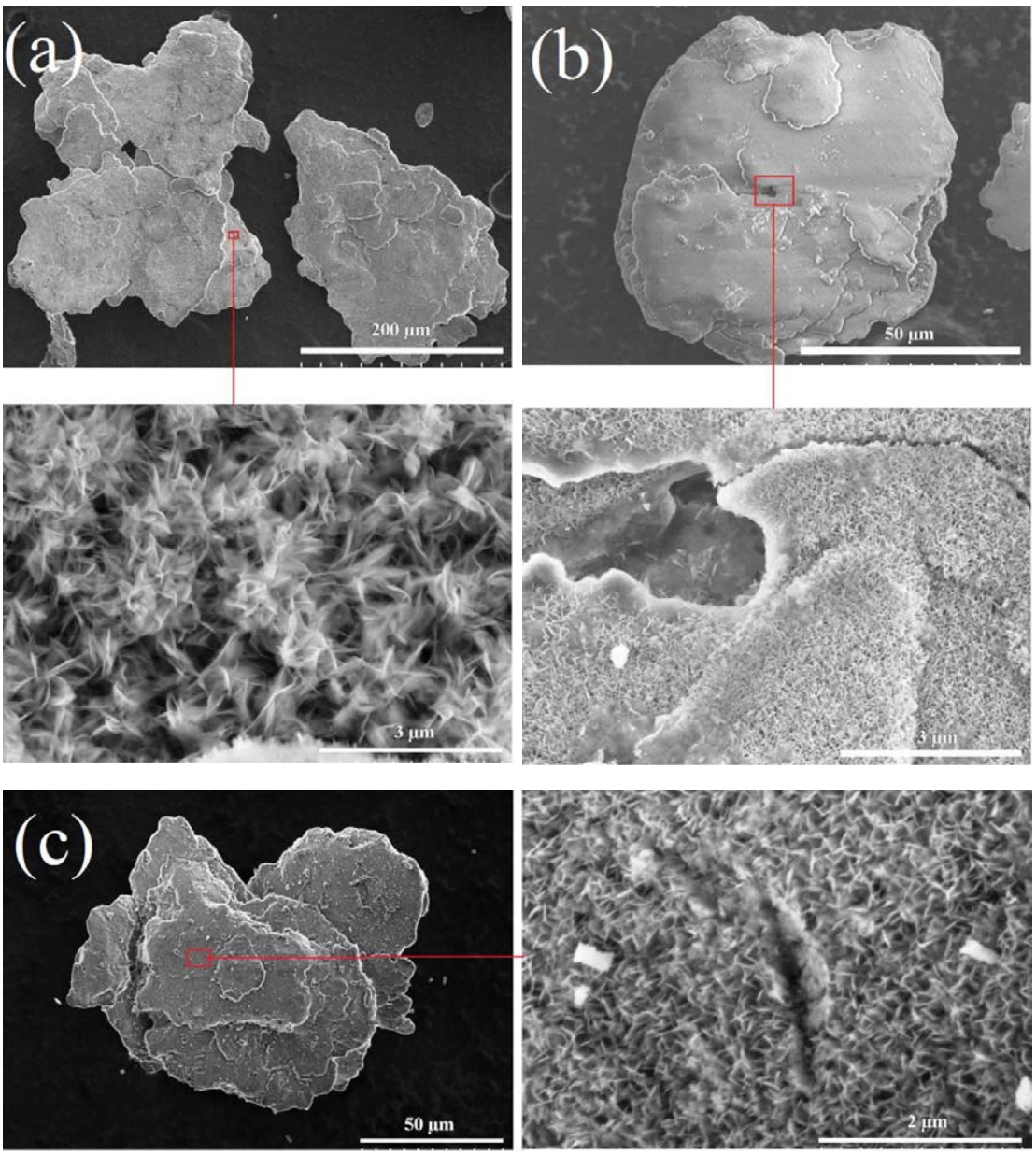

Fig. 2.9 SEM images of the particles milled for (a) 4 h, (b) 7 h and (c) 11 h after 2 h reaction with water.

Fig. 2.9 shows that morphology of the hydroxide layer for all the samples is the same as that of so called fibrillar boehmite [100-102]. The boehmite structure is rather coarse for 4 h milled sample compared to that of 7 and 11 h samples. Moreover only a few hexagonal shape particles

are observed in the 11 h milled sample, which can be classified as the gibbsite phase based on their morphology [103-107]. Considering Fig. 2.8 & 2.9, one can conclude that the aluminum particles were not fragmented during reaction with water. Also the produced hydroxide layer is almost the same for all the samples and it cannot be the reason for the difference in hydrogen yield observed in Fig. 2.7.

As the next step, cross sections of the particles were examined to check if microstructure of the particles can explain the difference in hydrogen yield. Fig. 2.10 shows SEM images of cross section of the particles milled for 1, 4, 7, 11 and 19 h.

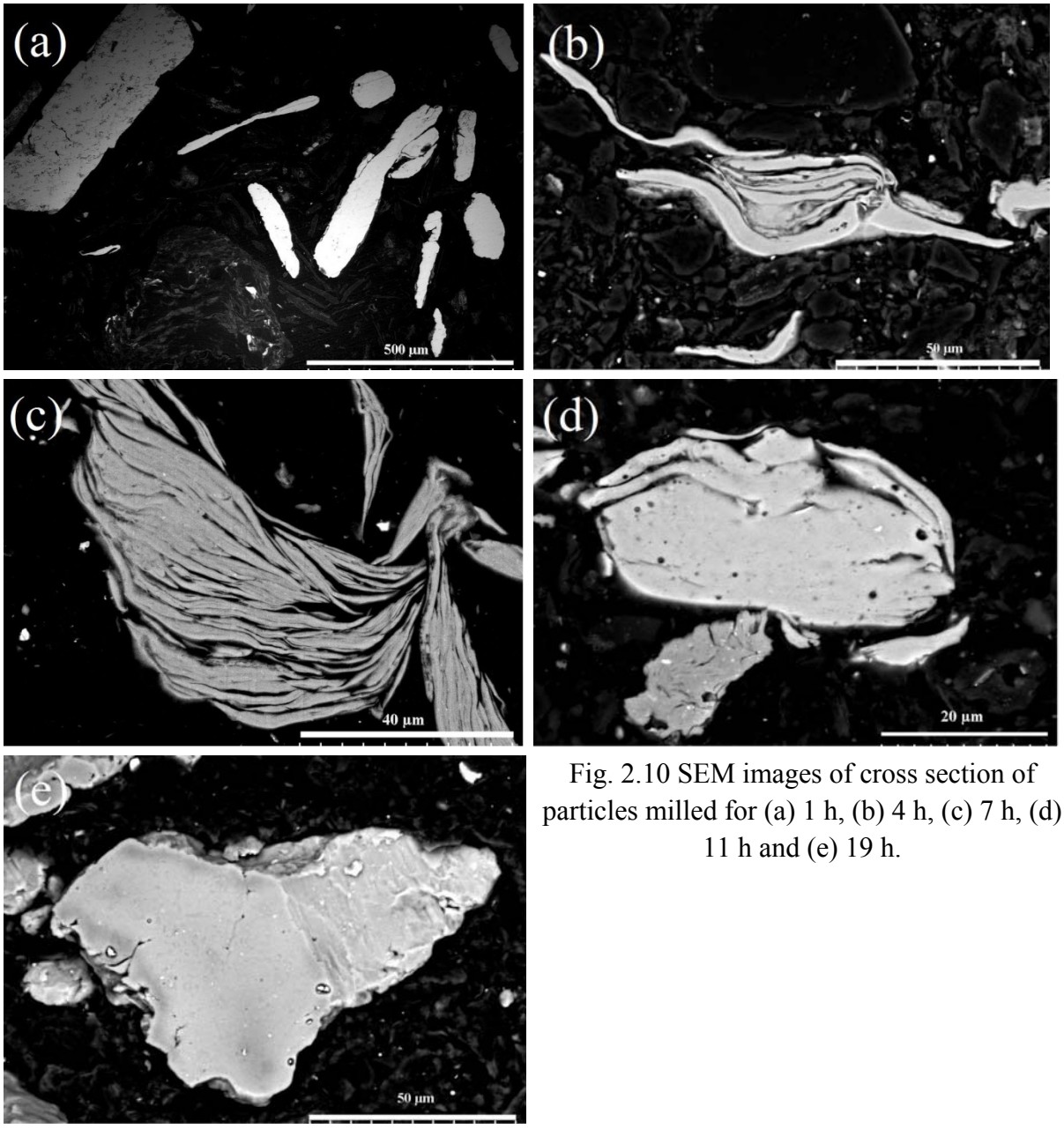

Fig. 2.10 SEM images of cross section of particles milled for (a) 1 h, (b) 4 h, (c) 7 h, (d) 11 h and (e) 19 h.

It can be seen that the particles after one hour milling are not affected by fracture and cold welding but only flattened by deformation (Fig. 2.10(a)). 4 h milled particles are formed by cold welding of a few flattened particles (Fig. 2.10(b)), which produces a laminated structure with layers of 1 to 10 μm thickness. Microstructure of 7 h milled particles is similar to that of 4 h milled sample, but has more layers with smaller thicknesses (between 1μm to 5 μm) that are cold welded to form these particles (Fig. 2.10(c)). Fig. 2.10(d) shows that the laminated structure no longer exists after 11 h milling. More impacts during milling for up to 19 h can compress the particles so they have a more uniform matrix without pores or interlayer spaces (Fig. 2.10(e)). Indeed, by further milling after 7 h, the laminated structure is pressed by balls and the space between layers is eliminated by cold welding of layers. These sequences were also observed by other research for ball milling of aluminum or others ductile powders [40, 98, 108].

Fig. 2.10 suggests that most probably the 4 h or 7 h milled powders have a higher specific surface area than that of 19 h milled powder, albeit the particles size of 19 h milled powder is smaller. Surface area of particles is an important parameter that can determine how fast a reaction occurs. For example, a large surface area of nano-particles explains the spontaneous reaction of aluminum nano powders with water [31, 67].

To understand whether the interlayer space of the laminated particles contributes in the reaction, we studied cross section of the milled particles after the reaction with water. Fig. 2.11 shows the backscatter electron (BSE) SEM images of cross section of 7 and 19 h milled particles after 2 h of the reaction. One can observe that the laminated structure of 7 h milled particle has two phases (Fig. 2.11(a)); a white core which is surrounded by a gray shell (the black matrix is the carbon resin). The core represents the aluminum phase and the shell is ascribed to the boehmite phase. This core-shell microstructure is seen at all the layers in the laminated particle. The presence of the boehmite shell on the internal layers in the particle implies that water penetrated to the interlayer spaces during the reaction. As Fig. 2.10(c) shows, the interlayer space in the 7 h milled particle is within 1-4 μm. This range is enough wide for a liquid with low viscosity (such as water) to penetrate into the interlayer space and react with aluminum surface.

The core-shell microstructure is seen also in 19 h milled sample (Fig. 2.11(b)). A small portion of the boehmite phase is seen inside the particle, which means there was not much space for water to penetrate inside the particle during the reaction.

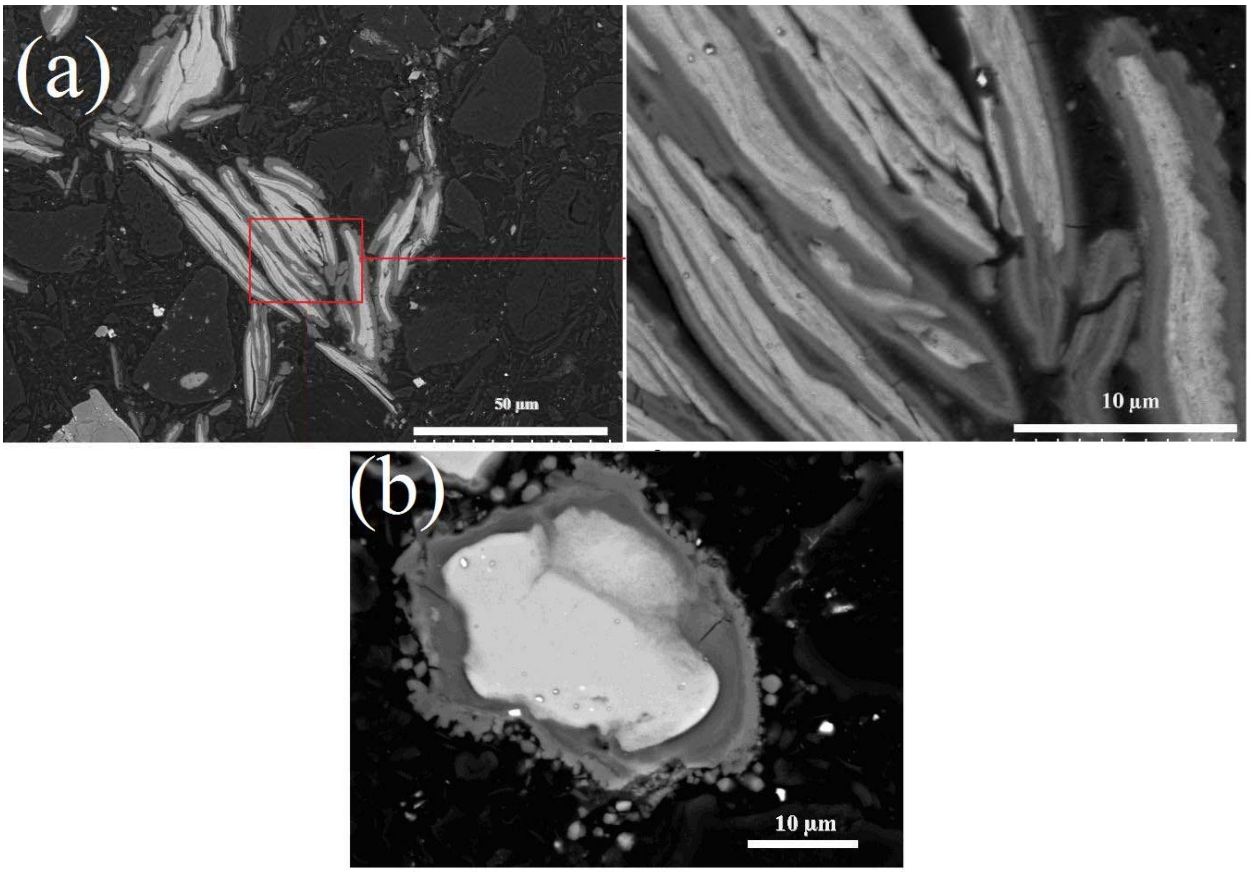

Fig. 2.11BSE SEM images of cross section of particles milled for (a) 7 h and (b) 19 h after 2 h reaction with water.

Fig. 2.12(a) & (b) show SEM image of a 7 h milled particle after the reaction and Fig. 2.12(c), (d) & (e) depict its energy-dispersive X-ray spectroscopy (EDS) elemental map for C, aluminum and O respectively. The orange color represents the carbon resin that surrounds the particle. The red color represents aluminum atoms; one can see that the aluminum content is higher in the core compared to the surrounding shell. Oxygen (green) is present in the shell while the core is almost free of oxygen. The presence of oxygen in the shell results from the boehmite phase.

Fig. 2.13(a) & (b) show SEM image of an 11 h milled particle after the reaction and Fig. 2.13(c), (d) & (e) depict its EDS elemental map for C, aluminum and O respectively. Fig. 2.13(a) shows that the particle is not laminated, but some of the laminate layers still exist after 11 h milling. In spite of the presence of interlayer spaces in the particle in Fig. 2.13(b), Fig. 2.13(e) shows that no oxygen is present at the aluminum layers beneath surface of the particle. This means water could not reach this area and produce hydroxide phase. Accordingly one can

assume that, in the case of the particles milled for 11 h, there may be some interlayer spaces that are not interconnected and therefore have no significant role in increasing rate of the reaction.

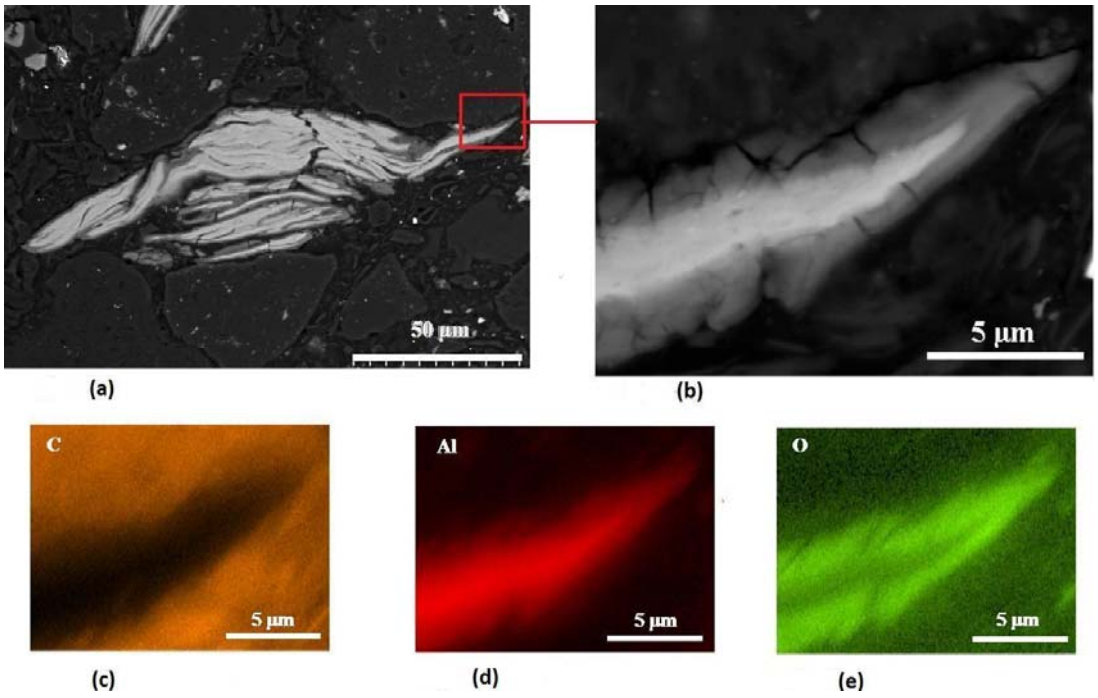

Fig. 2.12 (a) & (b) SEM image of cross section of a particle milled for 7 h, and the corresponding elemental map for (c) C, (d) aluminum and (e) O.

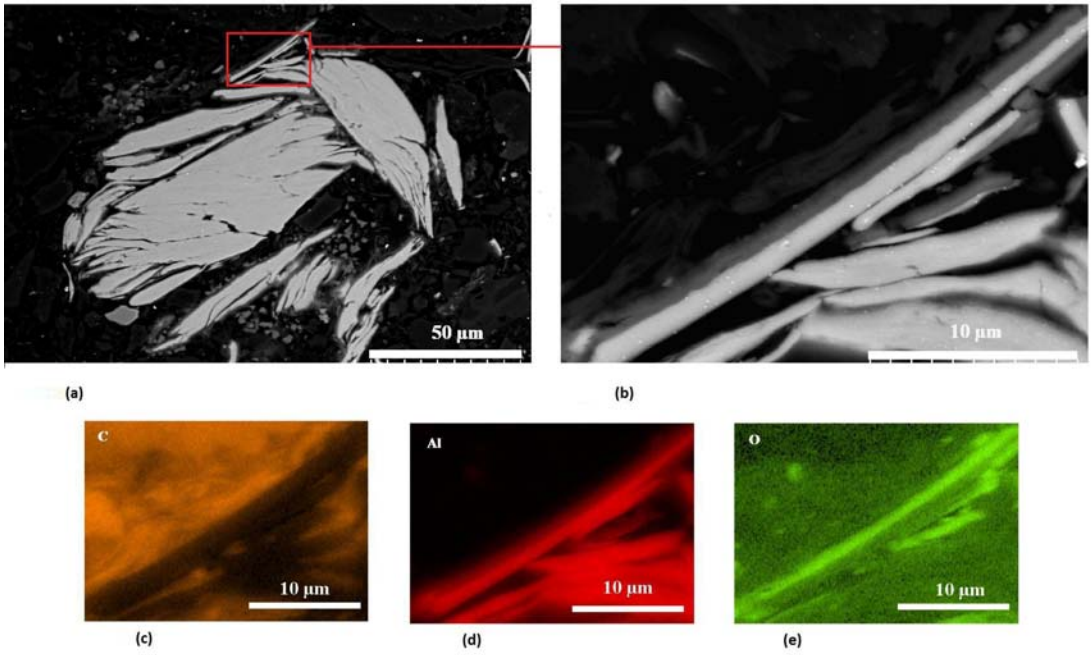

Fig. 2.13 (a) & (b) SEM image of cross section of a particle milled for 11 h, and the corresponding elemental map for (c) C, (d) aluminum and (e) O.

Fig. 2.14 shows the EDS of the particle presented in Fig. 2.11(b). It can be seen that the water hardly penetrated into the particle and the hydroxide phase mostly has formed on the surface of the particle. Moreover a presence of Fe atoms also was detected by the EDS detector (Fig. 2.14(d)). Presence of Fe in the milled powder is ascribed to the abrasion of stainless steel balls and vial that introduces Fe. The abrasion can be always present but there is more Fe in 19 h sample because of the higher hardness of aluminum particles and the longer period of milling [87].

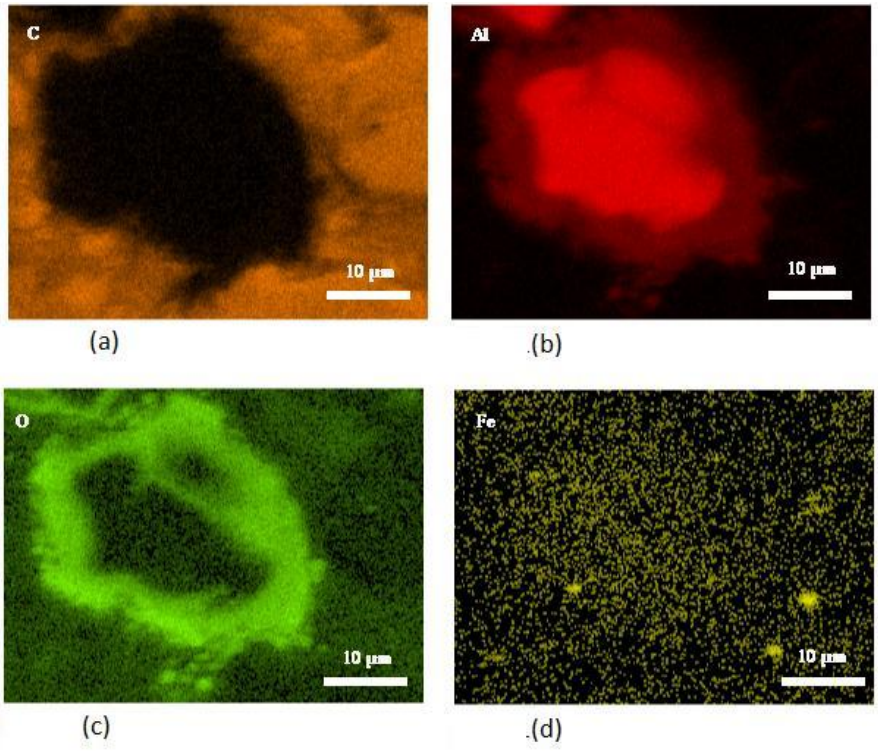

Fig. 2.14 The corresponding elemental map for the particle showed in Fig. 2.11(b). (a) C, (b) Al, (c) O and (d) Fe.

One can explain different reaction rates illustrated in Fig. 2.7 considering the differences in microstructures illustrated in Fig. 2.10 to Fig. 2.14. The particle sizes of the as received powder and the powders milled for 0.25, 0.5 and 1 h are big (Fig. 2.5) and their microstructure have not enough imperfections (Fig. 2.6(a)), therefore they do not start reacting with water. Milling up to 7 h results in a decrease in the particle size, an increase in the lattice imperfections (grain boundaries, dislocations, stacking faults, etc.) and a change in the microstructure to a laminated one (Fig. 2.10(b) & (c)). The interlayer spaces in the laminated microstructure supposedly increase the surface area that is in contact with water (Fig. 2.11(a)). Accordingly there is a

remarkable increase in the hydrogen production by increasing milling time to 7 h. Increasing milling time from 7 h up to 19 h results in a small increase in lattice imperfections, also the change in particle size is negligible. Moreover the laminated microstructure with interlayer spaces that were accessible for water no longer exists for samples milled more than 7 h. Consequently increasing milling time from 7 h to 19 h causes a decrease in hydrogen yield.

One should note that beside a change in the surface area (based on particle size and laminated structure observations), a change in lattice imperfections also affects the rate of the reaction. Generally, nanocrystalline materials show higher reactivity compared to large grained materials [34-35, 109-110]. In the case of aluminum-water reaction, W. Wang et al. found that rate of reaction of aluminum with water increases as grain size decreases [111]. H. Leth-Olsen et al. found that a nano crystalline layer formed on surface of a rolled aluminum sheet is the preferred place for corrosion attack [112]. W. Vedder et al explained that during reaction of aluminum with water, electrons are removed faster at grain boundaries. Therefore hydroxyl ion concentration increases at grain boundaries which results in a rapid attack on the protective layer [113].

A grain size of 20 μm was measured by SEM for the as received aluminum powder. Using Williamson-Hall method, a lattice microstrain of more than 0.2% and crystallite sizes of 59 and 54 nm were calculated for 11 and 19 h milled samples respectively. This significant decrease in grain size during ball milling can increase the affinity of the aluminum powder to react with water. However a higher hydrogen yield for 4 and 7 h milled samples compared to 11h and 19 h samples implies that influence of surface area on kinetics of the reaction is stronger than the presence of imperfections.

2.6. Conclusion

Hydrogen generation of aluminum-water reaction was correlated to structural evolution of aluminum powder during high energy ball milling. Milling progress was demonstrated based on changes in morphology, particles size and X-ray characteristics of the powders. SEM observations from the hydroxide layer formed on the surface of particles suggest that milling duration has no significant influence on the morphology of the aluminum hydroxide phase formed as by-product of the reaction. Examination of cross section of the particles revealed that beside a decrease in particle size, milling can introduce new surfaces inside particles. The interlayer spaces inside particles are blocked and then eliminated for milling durations more than an optimum time. Longer milling after the optimum milling time is not recommended because it consumes electrical energy, decreases hydrogen yield and increases iron contamination of the powders.

CHAPTER 3

ROLE OF BALL MILLING OF ALUMINUM POWDERS IN PROMOTION OF ALUMINUM-WATER REACTION TO GENERATE HYDROGEN

3.1. Overview of Chapter 3

In the previous chapter, the effect of milling time on the structural evolution of aluminum particles and consequently the hydrogen generation rate was explained. It was noted that ball milling can change the morphology, internal structure and crystallite size of the particles. This chapter aims to categorize different effects of milling process on hydrogen generation capability of the activated particles. Different contributions of milling are categorized as: a) morphological changes, b) introduction of crystallographic imperfections to the lattice, and d) removal of the native oxide film. The morphological changes (particles size, shape and internal structure) were discussed in the previous chapter, thus, are just briefly explained in this chapter as one class of the contributions of ball milling. Afterward, this chapter mainly focuses on the two latter contributions.

This chapter is presented as manuscript #2 (Role of Ball Milling of Aluminum Powders in Promotion of Aluminum-Water Reaction to Generate Hydrogen). The PhD candidate's contributions to the manuscript are: a) Ball milling the powder and aging the ball milled powders in air and argon. b) XRD and SEM examination of the powders and analysing the data. c) Reviewing the relevant literature and preparing the manuscript.

The XPS test and its relevant data analyses were performed in ACSES centre in University of Alberta. Apart from that, all of the experiments were performed in U of S and by the PhD candidate.

The manuscript was published in Metallurgical and Materials Transactions E: Materials for Energy Systems (METTRANS E).

DOI: 10.1007/s40553-014-0024-7

The manuscript presented here is different from that of published in two parts:

- In order to avoid repetition in content, some parts of the experimental section were deleted and referenced to chapter 2.
- Fig. 1 in the manuscript was deleted as it contained the same message as Fig. 2.5 in chapter 2.

The copyright permission to use the manuscript in the thesis was obtained and is provided in the Appendix section. The references for this chapter along with references from other chapters are provided at the end of the thesis.

Role of Ball Milling of Aluminum Powders in Promotion of Aluminum-Water Reaction to Generate Hydrogen

S.S. Razavi-Tousi, J.A. Szpunar

Department of Mechanical Engineering, University of Saskatchewan, S7N 5A9 Saskatoon, Saskatchewan, Canada

3.2. Abstract

Effect of ball milling of an aluminum powder on hydrogen generation through a reaction with hot water was investigated. Ball milling deceased particle size and thus increased surface area of the aluminum particles, increased crystalline imperfections (grain boundaries and dislocations) in the aluminum lattice, and removed the native oxide film on surface of the particles. The effect of crystalline imperfections was studied by room temperature recovery and high temperature annealing of the ball milled particles. The effect of the native oxide film and its thickness was studied by exposing ball milled aluminum particles to air for different durations. Hydrogen production capability of different aluminum powders after each of the above mentioned treatments was tested and correlated to microstructural changes.

Keywords: *Hydrogen, Ball Mill, Aluminum, Deformation*

3.3. Introduction

Numerous studies have been performed to promote the reaction of aluminum with water for hydrogen generation. Ball milling of monolithic aluminum powders [114-117] or aluminum powders with low melting point (LMP) metals such as Ga, In, Bi, Hg and Zn [69-74], water soluble salts such as NaCl and KCl [73-78, 118] and ceramic powders such as $Al_2O_3(\alpha)$, $Al_2O_3(\gamma)$, TiO_2, C, SiO_2 and aluminum$(OH)_3$[78-86, 119] have been considered to activate aluminum reaction with water.

Each type of the second phase particles can promote the reaction of aluminum with water in distinctive ways. A presence of LMP metals can promote the reaction by different mechanisms:

destruction of aluminum intercrystalline contacts [29, 69], diffusion of aluminum nano-particles through LMP metals to the reaction sites[111], formation of micro-galvanic cells [70, 72-74], destruction of the native alumina film and diffusion of aluminum through a LMP metal layer to reach water [30, 69, 72, 120-121] and also shifting the operating potential of aluminum to more negative values [120]. In the case of ceramic particles, Z.Y. Deng et al. explained that a dispersion of oxide particles in the aluminum matrix can modify the protective layer and make it less strong [80-81]. P. Dupiano et al. claimed that the dispersions of a ceramic phase can introduce new diffusion paths for OH^- ions [79]. A presence of water soluble salt particles in the aluminum matrix promotes the reaction by increasing the specific surface area of aluminum particles. Water dissolves the salt particles in the aluminum matrix, and thus fresh surfaces of aluminum are introduced for the reaction [76, 122]. Moreover, dissolution of the salts introduces Cl^- ions, which can diffuse into the hydroxide layer and induce a localized dissolution of aluminum at the metal/oxide interface [74, 118, 123-124].

Most of the above mentioned works have explained the mechanism and progress of the reaction focusing on the role of the second phase particles. In spite of variety of the works on activation of aluminum through ball milling with the second phase particles, the role of ball milling in modification of the reaction has remained obscure. Regardless of the role of ball milling in embedding the second phase particles in the aluminum matrix, ball milling can contribute to the activation of aluminum particles in three ways. First of all, ball milling increases the specific surface area of an aluminum powder by decreasing its particle size or/and introducing cracks and interlayer spaces inside the aluminum structure [117]. Secondly, ball milling, as a severe plastic deformation method, increases lattice imperfections (grain boundaries, dislocations, etc.), which consequently increases affinity of the milled powder for the reaction [35]. Thirdly, ball milling breaks the native oxide film on the surface of the particles and exposes fresh surfaces for the reaction [34, 116]. Although the effects of ball milling on activation of aluminum powders are generally known, it is not clear how and to what extent each of the ball milling activation mechanisms can contribute to the modification of aluminum-water reaction.

The present work attempts to analyze different functions of ball milling in modification of aluminum-water reaction. We set the temperature of the reaction at 80^oC because this is the

optimum temperature for operating PEM (proton exchange membrane) and many other types of fuel cells. In order to purely study the effects of ball milling, we did not add any second phase powder to promote the kinetics of the reaction.

3.4. Experimental Procedure

3.4.1. Ball Milling

The detail of ball milling procedure is similar to the manuscript #1. It is not repeated here in order to keep the thesis concise.

3.4.2. Aging and Annealing Process

In order to study effects of the native oxide film and room temperature aging on hydrogen production of the milled powders, we exposed a portion of the milled powder to air and stored the rest of the powder in an argon atmosphere (99.9% purity). During hydrogen measurement tests, we added the powders that were kept in argon to water in an inert atmosphere. Therefore, considering the argon atmosphere of the ball milling process, these powders did not form an oxide film prior to the reaction with water.

In order to study effect of lattice imperfections of the milled aluminum powders on hydrogen production rate, we used a tube furnace with an argon atmosphere to anneal the milled aluminum powders. The heating rate of the furnace was 10^{o}C/min and the annealing temperature was 550±2^{o}C. We annealed the powders for 1, 40 and 360 min and turned off the furnace till it reached to the room temperature, then we took the samples out of the argon atmosphere. Considering the argon atmosphere in the furnace, the annealing process did not change the oxide layer but just increased grain size and released lattice strain of the samples.

3.4.3. X-ray Analyses

A Bruker D8 Discover X ray diffractometer with a copper target characterized microstructure of the powders. We treated the diffraction patterns with the Rietveld refinement method, using the MAUD program, to calculate crystallite size and micro-strain of the powders. The as received aluminum powder annealed for 3 h at 550^{o}C was used as the standard sample to evaluate instrumental parameters. To estimate the quality of fittings, we evaluated the refinement of each

pattern using the weighted pattern factor (R_{wp}), the expected pattern factor (R_{exp}) and the goodness of fit (GoF) values [125].

$$R_{wp} = \left(\frac{\sum w_i (I_{io} - I_{ic})^2}{\sum w_i I_{io}^2}\right)^{1/2} \quad (3.1)$$

$$GoF = \frac{R_{wp}}{R_{exp}} \quad (3.2)$$

$$R_{exp} = \left(\frac{N-p}{\sum w_i I_{io}^2}\right) \quad (3.3)$$

where I_{iO} and I_{iC} are the observed and calculated intensities at the i^{th} step, $w_i = (1/I_{iO})$ is the weight factor, N is the number of observations and P is the number of adjusted parameters. We obtained acceptable fittings with R_{wp}<15% and GoF<2 for all the Rietveld refinements.

3.4.4. Hydrogen Measurement

The detail of hydrogen measurement procedure is similar to the manuscript #1.

3.4.5. Scanning Electron Microscopy

The detail of scanning electron microscope (SEM) procedure is similar to the manuscript #1.

3.4.6. X-ray Photoelectron Spectroscopy (XPS)

An AXIS 165 spectrometer (Kratos Analytical) performed XPS tests with a monochromatic aluminum K_α source (hν = 1486.6 eV) used at a power of 140 W. The base pressure in the analytical chamber was lower than 5×10^{-8} Pa. The analysis spot was 400×700 μm and the take-off angle was 90^o. The survey scans were collected for binding energy spanning from 1100 eV to 0 with analyzer pass energy (PE) of 160 eV and a step of 0.4 eV and high-resolution spectra with PE = 20 eV and step of 0.1 eV. Charge compensation was not required. Aluminum oxide thickness was evaluated using the method suggested by Strohmeier [126]. Instrument software Vision2 performed the component analysis of high-resolution spectra of Al2p and calculation of the areas of oxide and metallic peaks.

3.5. Results and Discussion

3.5.1 Ball Milling Effect: Morphological Changes

Fig. 3.1 shows the cross section of an as received aluminum particle and aluminum particles milled for 1 h, 4 h, 7 h, 11 h and 19 h. Apart from changes in shape and size of the particles resulted from ball milling, one can notice that the 7 h and 4 h milled particles have a laminated structure. Cold welding of flattened aluminum particles produces this laminated structure [40]. The presence of interlayer spaces between the layers of the 4 h and 7 h milled particles is assumed to increase their specific surface area.

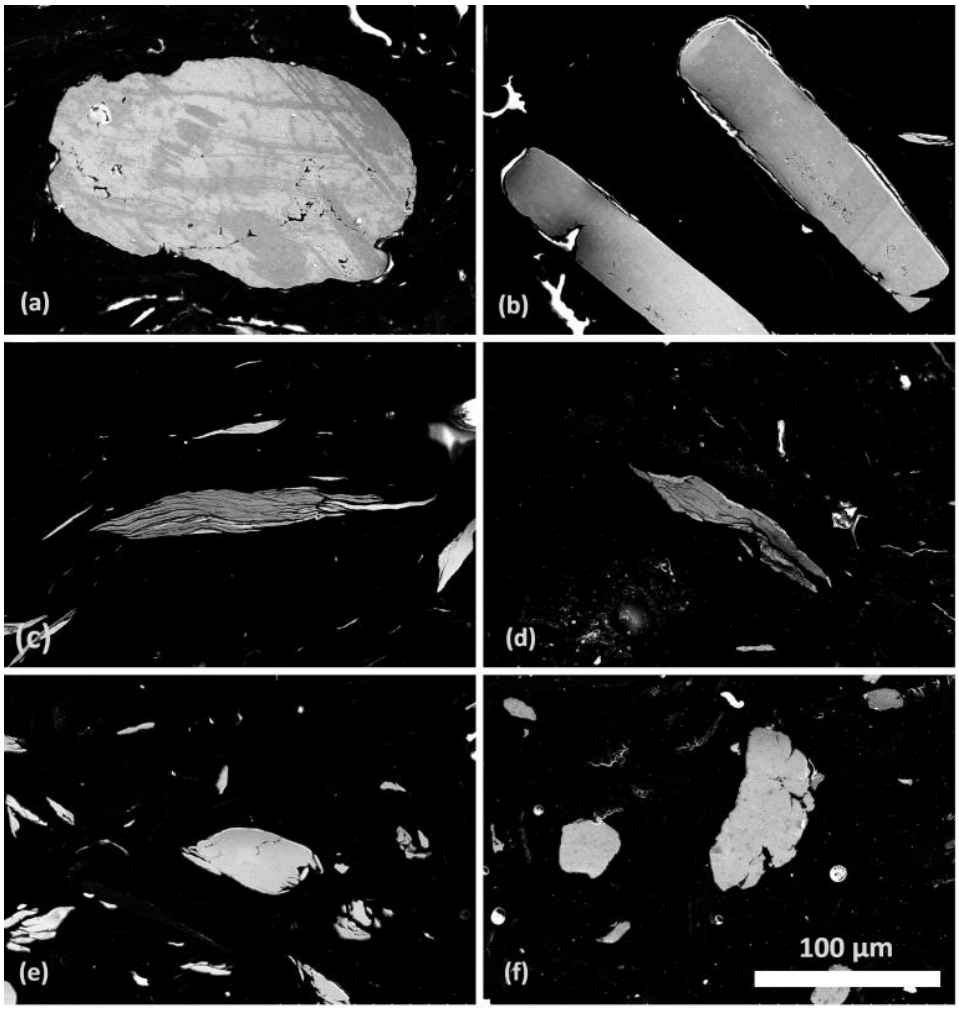

Fig. 3.1 SEM images of cross section of (a) the as received aluminum particle and the aluminum particles milled for (b) 1 h, (c) 4 h, (d) 7 h, (e) 11 h and (f) 19 h.

Fig. 3.2 shows hydrogen flow vs. time for the reaction of water with the aluminum powders milled for different times. One can see that the hydrogen flow increases as milling time increases

up to 7 h, but after 7h milling it decreases. The higher hydrogen production rate of 4 h and 7 h milled samples is because of the presence of internal surfaces due to the laminated structure of these samples. Further milling up to 11 h or 19 h eliminated the internal surfaces. Therefore, the reaction happens just on the outer surface of 11 h and 19 h milled samples and hydrogen production rate decreases.

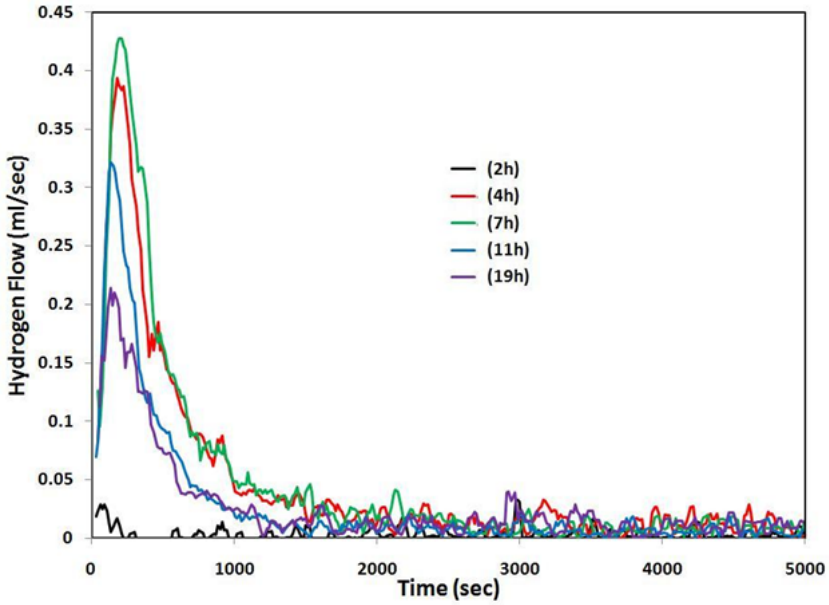

Fig. 3.2 Hydrogen generation flow vs. time for the reaction of water with the aluminum powders milled for different durations.

Considering Fig. 3.1 & Fig. 3.2, one realizes that ball milling increases the specific surface area of the aluminum powders in two ways: firstly by reducing the particle size that presumably correlates inversely by specific surface area, secondly by generating interlayer spaces inside the particles. Since the reaction of aluminum and water initiates on and continues through the surfaces (either on or in particles), ball milling improves kinetics of the reaction by providing more aluminum sites reachable for water.

Several studies have reported that ball milling improves reaction of aluminum powders with water by modifying the size or specific surface area of aluminum particles [71, 73, 75-76, 78, 84-85, 114, 117-118, 127]. Among the mentioned studies, some reported that although ball milling activates aluminum powders, extended milling after a particular time can decrease the hydrogen yield [71, 73, 78, 84-85, 117, 127]. The two-fold effect of ball milling time remained unexplained in most of the mentioned studies. Some researchers ascribed this effect to oxidation

of aluminum particles during ball milling [71, 78, 84]. However, they did not perform cross sectional examination of the aluminum particles to investigate the role of internal surfaces on the reaction rate. In the present work, we performed milling in an argon atmosphere, thus, no oxidation happened during milling. In the absence of oxidation, Fig. 3.1 & Fig. 3.2 allow to establish that a prolonged ball milling can reduce the hydrogen generation rate by eliminating internal surfaces inside aluminum particles produced during early stages of milling.

3.5.2. Ball Milling Effect: Deformation

Ball milling, as a severe plastic deformation technique, introduces lattice imperfections such as grain boundaries and dislocations to microstructure of milled particles. Fig. 3.3 shows electron backscatter diffraction(EBSD) patterns of an as received and an aluminum particle milled for 11 h. Different colors represent different orientations and the white and black lines represent grain boundaries with misorientation of 5^{o}-15^{o} and over 15^{o}, respectively. The average grain size (misorientation cut-off: 15^{o}) of the aluminum particles was about 100 µm before milling which changed to 0.33 µm after 11 h milling. The proportion of atoms that lie at inter-crystalline regions as a total of surface area becomes significant as the grain size decreases. A decrease of 2 orders of magnitude in the grain size introduces many grain boundaries to the aluminum lattice.

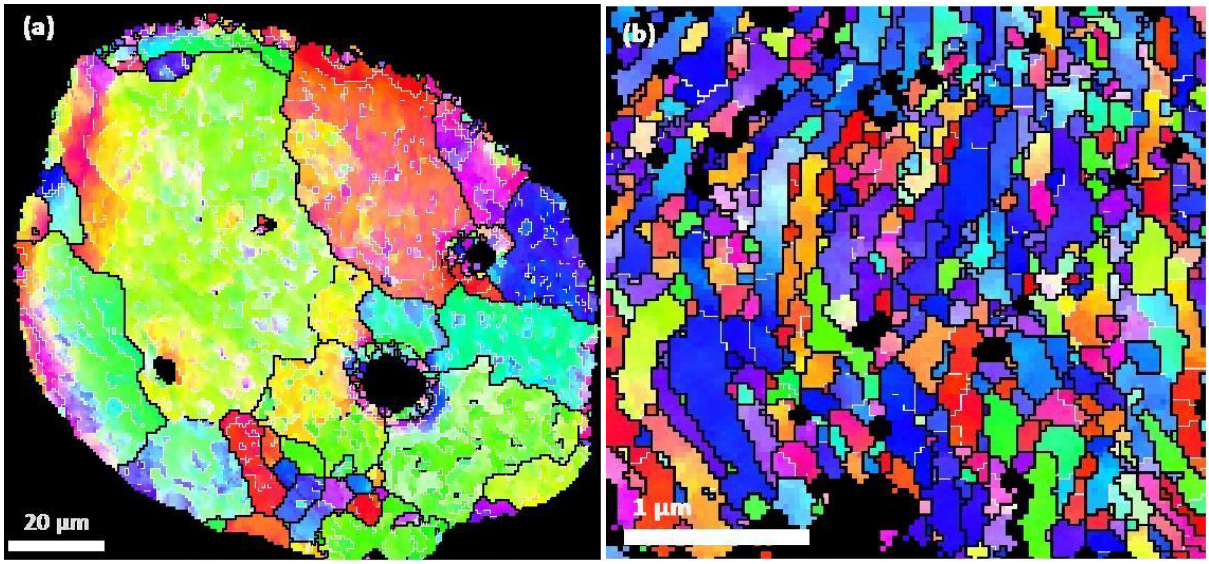

Fig. 3.3 EBSD patterns of the as received aluminum particle (step size: 0.65 µm) and the particle milled for 11 h (step size: 0.03 µm), note the difference in the scale bars.

To knowledge of the authors, effect of aluminum grain size on the hydrogen generation rate has not been studied so far. However, effect of aluminum lattice imperfections, mainly as a reaction promoting driving force, has been noted in few studies. E. David et al., Z. Zhao et al and H. Luo et al. discussed that deformation of aluminum particles by ball milling promotes the hydrogen production rate, but they did not perform experiments to prove that [75, 114, 118]. W. Wang et al. observed that a finer grain aluminum has a higher hydrogen generation rate [111]. They ascribed that to a presence of a LMP metal layer on grain boundaries, which facilitates reaction of aluminum with water. W. Veddar et al. and R. K. Hart also noticed that the reaction of aluminum and hot water mainly occurs at grain boundaries [113, 128].W. Veddar et al. ascribed the higher corrosion that occurs at grain boundaries as a result of intense removal of electrons from grain boundaries, which increases hydroxyl ion concentration and results in more rapid destruction of the protective film. They found that the hydroxyl attack on the grain boundaries is 4 times as fast as on the surface grains [113]. P. Dupiano et al. aged ball milled aluminum powder for 1200 h at 40^{o}C in air and found a significant decrease in hydrogen generation rate [79]. However, no further investigation was performed to explain the aging effect. E. Czech et al. Ball milled a mixture of aluminum-NaCl powder and annealed the produced powder at 550^{o}C for 1 h [78]. They measured hydrogen generation rate before and after annealing and found no significant difference. However, the effect of ball milling and annealing on the lattice imperfections has not been reported.

3.5.2.1.Recovery Effect

In order to study effect of lattice imperfections on kinetics of the reaction, we treated the milled powders with room temperature aging and high temperature annealing. Fig. 3.4 shows hydrogen generation of the 7 h milled samples kept in argon atmosphere at room temperature for 2.5, 8 and 16 days. One observes a lower hydrogen generation rate for the samples aged for the longer times. Since the samples were not exposed to oxygen prior to the reaction, the only explanation for the different reaction rates is room temperature recovery and possibly grain growth. In order to explain the effect of aging time on the reaction rate, we performed Rietveld refinement on XRD patterns of the 7 h milled samples aged for 1, 2, 5, 9 and 18 days. We found that crystallite size of the samples did not change significantly with aging time, although micro-strain decreased with time. Fig. 3.5 shows changes in micro-strain of 7 h milled powder vs. aging time. The micro-strain decreases by over 30% between 1-18 days of aging. Room temperature

instability (recovery, recrystallization or grain growth)is a well-known phenomenon for ultrafine grained or nanocrystalline metals [129-132]. As the crystallite size of the 7 h Ball milled aluminum powders was rather stagnant (95-105 nm), one can gather that just recovery and dislocation rearrangement happened during the aging time. Accordingly, the change in microstructure of the deformed aluminum particles toward a more stable state is the reason for the lower hydrogen generation rate of the aged samples.

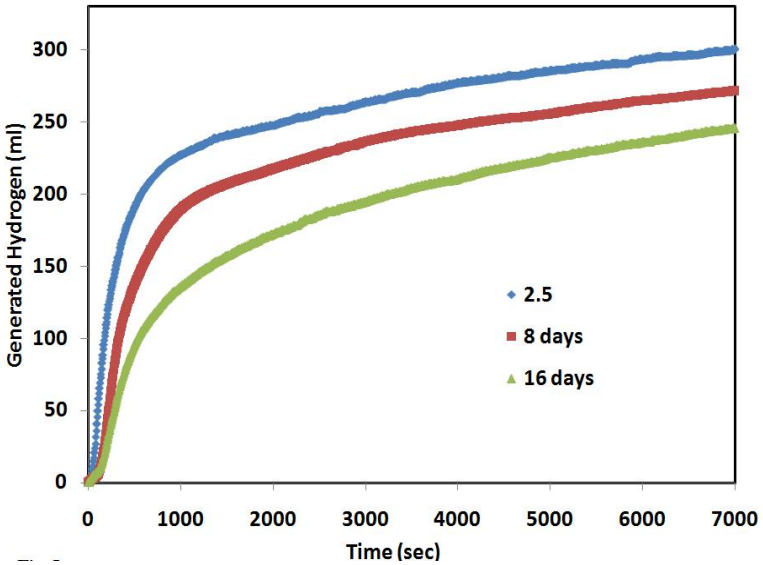

Fig. 3.4 Hydrogen generation of the 7 h milled samples aged at room temperature in argon atmosphere for 2.5, 7 and 16 days.

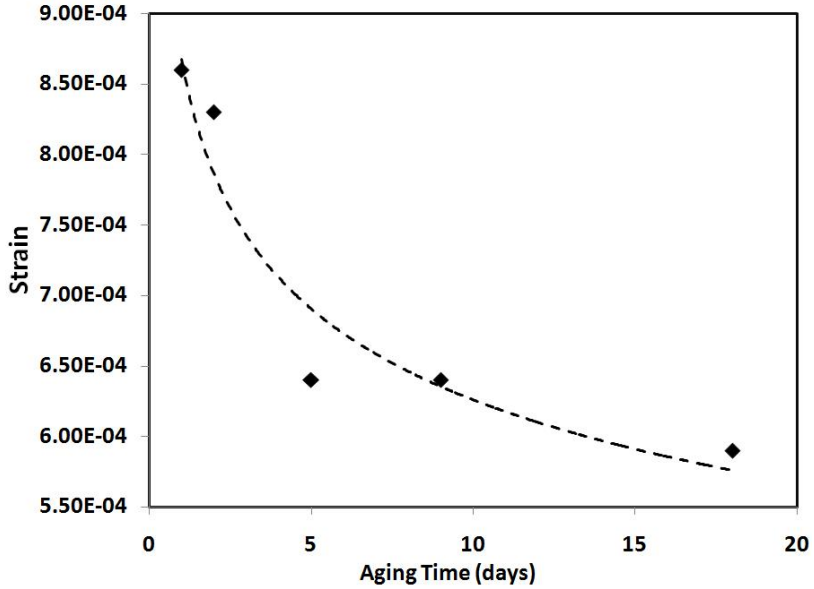

Fig. 3.5 Effect of aging time on micro-strain of the7 h milled powder.

3.5.2.2. Annealing Effect

Fig. 3.6 shows hydrogen generation of the 19 h milled sample and the 19 h milled samples annealed at 550°C for 1, 40 and 180 min at an argon atmosphere. One observes that annealing for 1 or 40 min results in remarkable changes in hydrogen generation rate. However, further annealing after 40 min up to 180 min does not significantly affect the reaction rate. The results of Rietveld refinement of XRD of the annealed samples are shown in Fig. 3.7(a) & (b). The crystallite size increased and micro-strain in the samples decreased with annealing time.

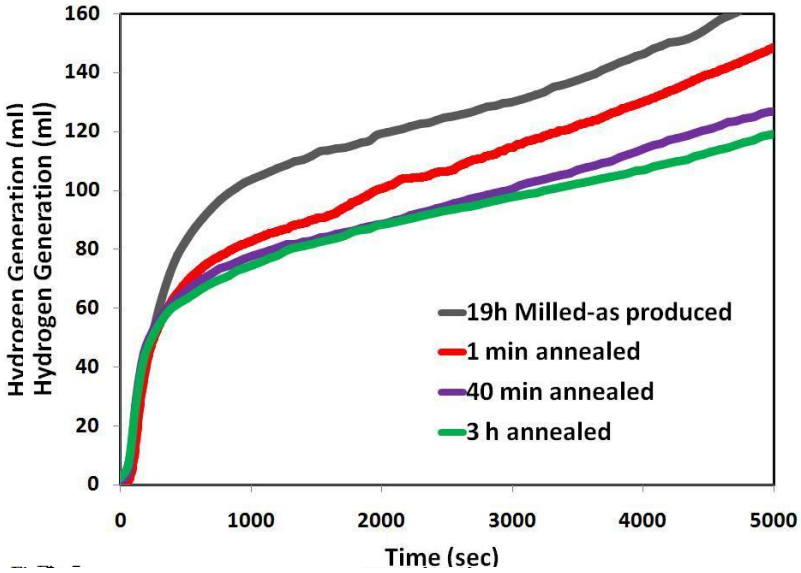

Fig. 3.6 Hydrogen generation of the as produced 19 h milled sample and the 19 h milled sample annealed at 550°C for 1, 40 and 180 min at argon atmosphere.

Thermodynamically, a presence of a high amount of grain boundaries increases microstructural instability and thus, fine grains in deformed metals have a higher affinity for reactions than coarse grains in recrystallized metals. However, a higher affinity of the fine grain metals for reactions does not necessarily lead to a higher corrosion rate. An obvious contradiction exists among results of different works reporting effect of grain size/residual stress on corrosion resistance of different metals [133]. The disagreement has been reported for corrosion resistance of different alloys of the same metal. For example in the case of aluminum alloys, it was reported that grain size reduction and deformation result in a better corrosion resistance [134-138], while other papers results show the opposite [112, 139-140]. One can however explain the existing contradiction assuming different corrosion mechanisms. For example, a decrease in grain size results in an increase in corrosion rate of a metal with primary

intergranular corrosion mechanism, while an opposite effect would be expected for a metal with a pitting corrosion mechanism. K.D. Ralston et al. discussed that a finer grain size increases corrosion resistance of a metal that forms a protective layer [141]. The finer grain size increases reactivity and thus, a uniform protective film forms faster and protects the metal from further corrosion. On the other hand, the deformed state of a metal can make it more susceptible to corrosion if protective film on the metal is not formed.

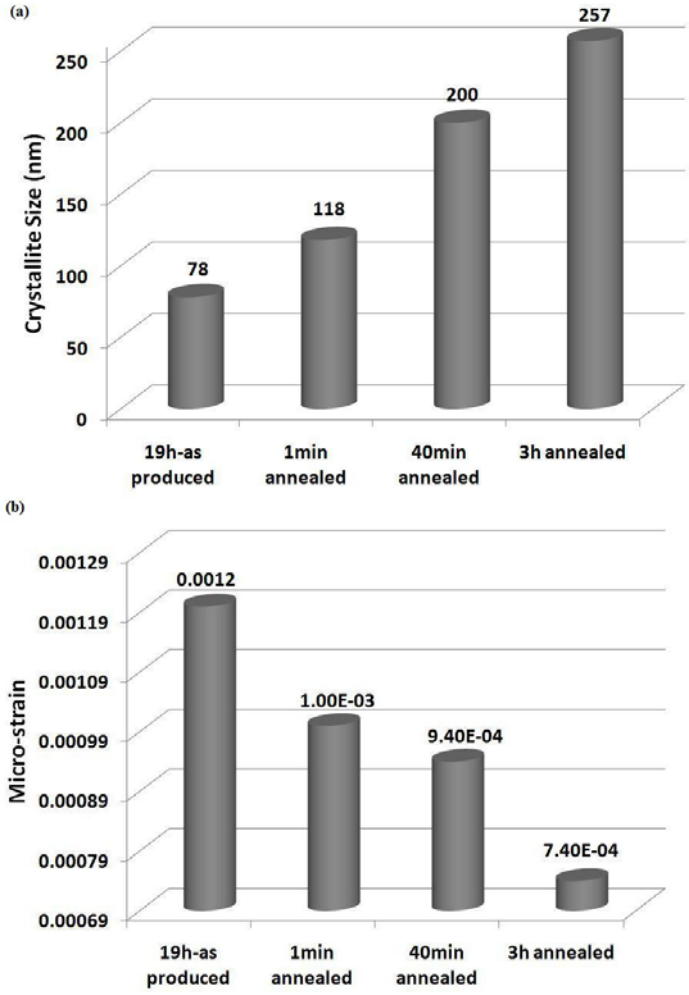

Fig. 3.7 Effect of duration of the annealing process at 550^{o}C on (a) crystallite size and (b) micro-strain of the 19 h milled powder.

The protective nature of the oxide film on aluminum surface varies in different oxidizing media and at different temperatures. Regarding the reaction of aluminum with hot water at neutral pHs, the oxide film on surface of aluminum gradually transforms to a hydroxide film, this film is less protective than the oxide layer [142]. After the oxide film is hydrated, ion species

can diffuse through the film and reach and oxidize the aluminum substrate [143]. Higher temperatures increase diffusivity of the ion species, which makes the hydrated layer less protective. Considering the semi-protective nature of the hydroxide film on the surface of the aluminum immersed in hot water, a finer grain size and deformed aluminum substrate cannot reduce the corrosion by a fast and uniform formation of the protective layer. But the deformed state of the microstructure promotes the corrosion by increasing the affinity of water to react with the aluminum substrate. Consequently, as Fig. 3.4 & 3.6 show, the rate of the reaction between the deformed aluminum particles and hot water decreases as the microstructure is stabilized by either room temperature aging or high temperature annealing. There is a negligible difference between hydrogen generation rate of 40 and 180 min annealed samples (Fig. 3.6), while the difference is considerable for different crystallite size and micro-strain of the mentioned samples (Fig. 3.7 (a) & (b)). Hence, it is concluded that a significant change in the stored deformation energy in the aluminum lattice does not necessarily lead to a significant change in hydrogen production rate, but it depends on the range in which the crystallite size and micro-strain change.

3.5.3. Ball Milling Effect: Removal of the Native Oxide Film

Reviewing the literature on activation of aluminum by ball milling, one can realize that breaking and removal of the native oxide film on the surface of aluminum particles is the most known effect of this process. Although elimination of the native oxide film by ball milling is well established, one must note that this role of ball milling is effective as long as milled aluminum particles are not exposed to air before the reaction. A new native oxide film forms upon exposing the milled aluminum powder to air. In order to study effect of the native oxide film, we exposed part of the Ball milled powders to air and kept part of it in an argon atmosphere and then performed the hydrogen generation test on these powders.

Fig. 3.8 shows hydrogen generation from the 7 h milled aluminum powders kept for 8 days in argon or air after ball milling. The overall shape of the curves for the powder kept in air or argon is quite the same, but for the 7 h milled aluminum powder kept in argon the reaction initiates faster than the one kept in air. The delay in starting the reaction for the air kept powder is so called “induction period” or “incubation time”. There are two explanations for presence of an incubation time before aluminum reaction with water starts. The first explanation is that the time

is needed for hydration of the native aluminum oxide film by water. When the hydration front reaches the aluminum substrate, hydrogen generation starts [142, 144]. The second explanation is dissolution of the native oxide film in water and precipitation of the dissolved ions (in pH of 3-10) as aluminum oxide hydroxide on the surface of aluminum substrate [145-147]. Regardless of what explanation is closer to reality, the outcome of the both is that before hydrogen generation starts, aluminum-O bonds in the oxide film should be broken and replaced by aluminum-hydroxide bonds. The time needed for substitution of the aluminum-O bonds in the film with aluminum-hydroxide bonds delays hydrogen generation of the air kept sample compared to the one kept in argon.

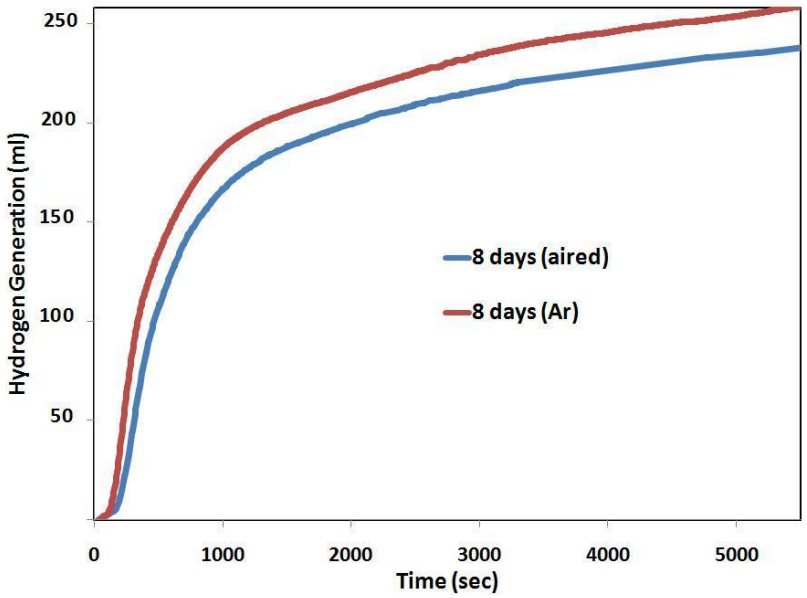

Fig. 3.8 Hydrogen generation of the 7 h milled aluminum powders kept for 8 days in argon or air.

One may notice that even the sample that was kept in argon does not initiate hydrogen production instantly. We attribute the delay in hydrogen generation of the sample kept in argon to agglomeration of the aluminum particles when they are immersed in water. We observed that the 7 h milled aluminum particles tend to form clusters as they meet water and it takes some time until the stirring dissolve this agglomeration. The time needed for the surface of aluminum particles to be covered entirely by water explains the delay in hydrogen generation from particles kept in argon.

There are few studies that considered effect of air storage of activated aluminum powders on incubation time with contradictory results. A.V. Ilyukhina et al. found that air storage of 3 min milled aluminum particles with LMP metals does not affect incubation time [69]. P. Dupiano et al. also found no change in incubation time after 40^{o}C aging of a milled aluminum powder [79]. On the other hand, Z. Zhao et al., A. N. Streletskii et al. and A. V. Parmuzina et al. noticed significant changes in incubation time as storage in the air was extended [72, 84, 118]. We tend to agree more with the result of the latter authors, because if the activation process of aluminum powders removed the oxide film, an exposure to air should form the film on the surface and a longer aging time should slow down the hydrogen generation. Dupiano et al. collected data points using big time intervals [79], and the incubation period, even if it existed, could not be identified. A.V. Ilyukhina et al. ball milled the aluminum powder for 3 min [69]; such a short milling time could only partially remove the oxide film, thus they did not observe any change in the incubation time even after 63 days of air storage.

In order to verify the effect of duration of air storage on incubation time, we kept the 7 h milled powders in air for different durations up to 23 days. Fig. 3.9 shows hydrogen generation of the 7 h milled aluminum powders kept for different times in air. The hydrogen generation rate decreases dramatically as the powder was kept for longer periods in air.

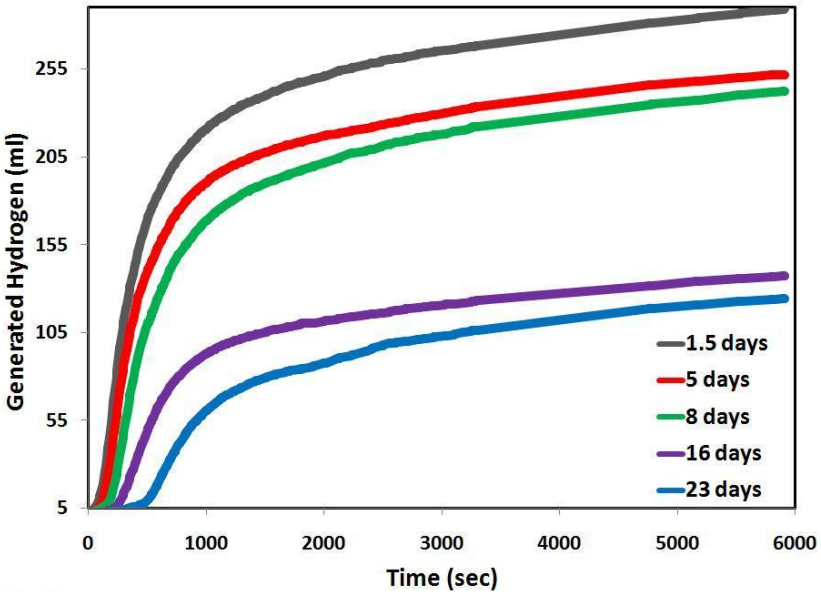

Fig. 3.9 Effect of duration of the room temperature aging in air on hydrogen generation of the 7 h milled aluminum powders.

This decrease can be justified by two phenomena. The first phenomenon is the effect of room temperature aging on the native oxide film on the surface of the powder particles. A change in the oxide film can be inferred from the increasing incubation time as the powder was kept longer in air. The oxide film can grow thicker as the powder is exposed longer to air. The second phenomenon can be inferred from hydrogen production rate. Even when the reaction starts after the delay due to the incubation time, the amount of hydrogen generated from the longer aged powders was smaller than that from particles aged for shorter time. As explained in section 3.5.2.1, the second phenomenon is because of a room temperature recovery of the deformed aluminum powder, which diminishes aluminum affinity to react with water.

In order to study the effect of room temperature aging in air on the incubation time, we extracted the delay time by a linear slope fitting of the curves in Fig. 3.9. We also measured the thickness of the oxide film on surface of the milled powder by XPS to find a correlation between aging time, oxide thickness and incubation time. Fig. 3.10 shows effect of number of days of aging on the incubation time. The incubation time increases linearly as the aging time increases. Fig. 3.11 shows effect of aging time on the thickness of the native oxide film. The oxide film thickness also increases linearly with the aging time. The insets in Fig. 3.10 & 3.11 show the equations and their R square obtained by a linear fitting to the curves.

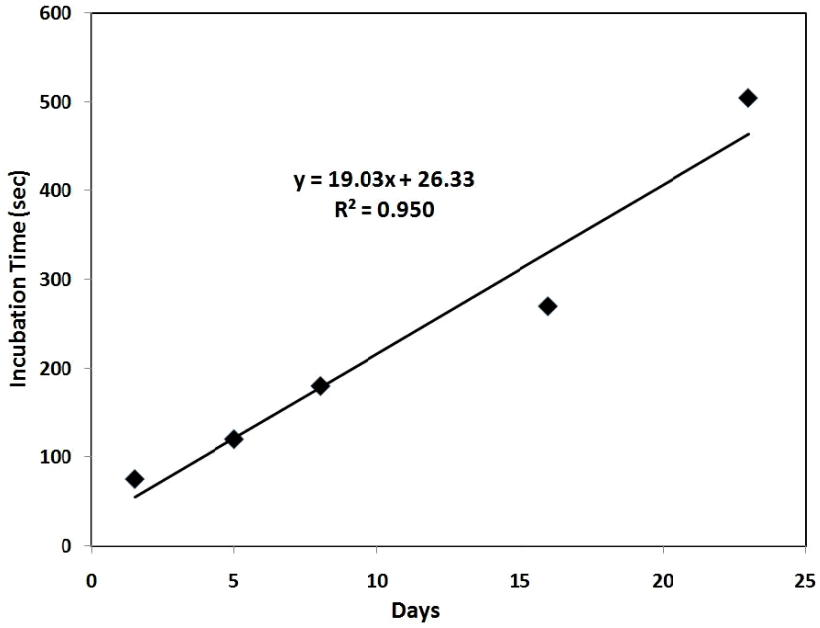

Fig. 3.10 Effect of aging time on the incubation time of the hydrogen generation reaction.

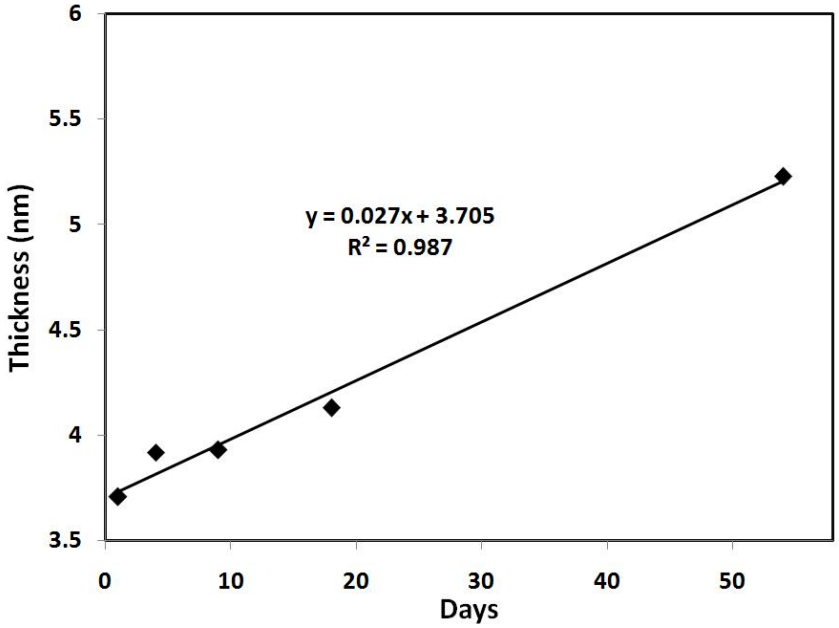

Fig. 3.11 Effect of aging time on thickness of the native oxide film measured by XPS.

Considering Fig. 3.10&3.11, one realizes that the aging at room temperature causes an increase in thickness of the oxide film, and accordingly, the incubation time increases. Extrapolating the incubation time to 0 day, we obtained that it takes about 26 sec for the fresh 7 h milled powder to start hydrogen generation. This 26 sec represents the time approximately needed for the aluminum particles to break their agglomerates by being stirred in water. An oxide thickness of 3.7 nm is calculated by extrapolating the oxide thickness to 0 day. The value of 3.7 nm roughly represents the thickness of the oxide film at its first day of formation. The oxide film linearly grew with aging throughout our measurements span. However, considering previous researches, we assume that the formation and growth of the oxide film was much faster at the initial seconds and hours of exposure to air. An initial fast growth of the oxide film on aluminum followed by a slow [148-149] and linear growth [150-151] has been reported in the literature. In the time span of our measurements, the film thickness increases at the rate of 0.027 nm/day and this results in an increase rate of 19 sec/day for the incubation time. Assuming that progress in hydration of oxide film toward the aluminum metal sub-layer explains the incubation time [142, 144], and based on the derived equations from Fig. 3.10 & 3.11, we calculated that the hydration front moves with an average speed of 1.4×10^{-3} nm/sec.

3.6. Conclusion

In addition to the role of ball milling in incorporating additives to aluminum powders to promote hydrogen generation during the reaction of aluminum with water, ball milling contributes in the production of hydrogen in three distinct ways:

1. Ball milling increases surface of the particles by decreasing the particles size (as specific surface area is correlated reversely to particle size) and introducing a laminated structure inside the particles. The role of inter-layer spaces inside the particles is significant.

2. Ball milling introduces crystallographic imperfections (grain boundaries and dislocations) into lattice of the aluminum particles, which increases affinity of the particles for the reaction. A partial annihilation of the crystallographic imperfections by either the room temperature recovery (decrease in the lattice micro-strain) or the high temperature annealing (decrease in the lattice micro-strain and increase in the crystallite size)markedly decreased the hydrogen generation rate.

3. Ball milling removes the native oxide film formed on the surface of the aluminum particles. The absence of the protective film makes the reaction to start without the delay resulted from a hydration of the oxide film. However, the protective film forms on the fresh surfaces as the particles are exposed to air. The film grew in a linear trend in the span of our measurements (1-56 days), resulting in a linear increase in the incubation time of the reaction. Considering the slope of changes in the incubation time vs. the film thickness, we calculated that the hydration front proceeds toward aluminum substrate with the speed of 1.4×10^{-3} nm/sec.

In spite of the common attention to the oxide removal by ball milling, the present results established that the role of ball milling in introducing crystallographic defects and new surfaces to the aluminum particles is more substantial for hydrogen generation. The presence of the native oxide film affects the start of the reaction, while the latter effects can substantially change the overall rate of hydrogen generation.

CHAPTER 4

MECHANISM OF REACTION OF ACTIVATED ALUMINUM PARTICLES WITH HOT WATER

4.1. Overview of Chapter 4

In the previous chapter, the different contributions of ball milling to hydrogen production of aluminum-water reaction were discussed. This chapter explains the mechanism and electrochemistry of the reaction. This explanation focuses on two questions:

- How the two main contributions of milling (microstructural refinement and the increase in the specific surface area) take part in the reaction from an electrochemical point of view?
- How the reaction of aluminum with hot water is explained from an electrochemical point of view?

Electrochemical tests together with investigation of the produced hydroxide layer on the surface of aluminum particles during the reaction are considered to answer those questions. Not only this chapter correlates the hydrogen production to the characteristics of the milled aluminum particles, but also elucidates the electrochemistry of reaction of aluminum with hot water, which had been a knowledge gap considering the limited studies on corrosion of aluminum particles in hot aqueous media.

This chapter is presented as manuscript #3 (Mechanism of Reaction of Activated Aluminum Particles with Hot Water). The PhD candidate's contributions to the manuscript are: a) Open circuit potential and Tafel tests. b) Cross sectional and surface examination of the particles after reaction. c) Reviewing the relevant literature and preparing the manuscript.

We got help from Dr. S.A. Lajevardi for preparation of the samples for Tafel tests and analyzing the Tafel and open circuit potential results. Therefore, his help was appreciated in the acknowledgment of the published paper. Moreover, Dr. R. Evitts was acknowledged because of his tips in answering the reviewers' comments. We also received some additional comments from Prof. V. Birss after publication of the manuscript. The comments were applied in the thesis and she is acknowledged here.

The manuscript was published in the journal of Electrochemica Acta:

S.S. Razavi-Tousi, J.A. Szpunar, Electrochim Acta, 127 (2014) 95-105.

http://dx.doi.org/10.1016/j.electacta.2014.02.024

The manuscript presented here is different from that of published in few sections:

- The decrease in OCP was explained based on pH changes in the published manuscript. According to Prof. V. Birss's suggestion, this part was revised in the thesis and changes in cathodic and anodic lines in Evans diagram were used to explain OCP changes.
- The cross sectional and EBSD studies are explained rather briefly here compared to the published work. It is because the microstructural changes were fully explained in chapter 2 and chapter 3.

The copyright permission to use the manuscript in the thesis was obtained and provided in the Appendix section. The references for this chapter along with references from other chapters are provided at the end of the thesis.

Mechanism of Reaction of Activated Aluminum Particles with Hot Water

S.S. Razavi-Tousi, J.A. Szpunar

Department of Mechanical Engineering, University of Saskatchewan, S7N 5A9 Saskatoon, Saskatchewan, Canada

4.2. Abstract

Mechanism of reaction of aluminum particles with hot water for hydrogen generation is evaluated. The aluminum powder was activated by ball milling for different durations, which modified size and microstructure of the particles. Open circuit potential and Tafel tests were carried out to explain the effect of ball milling and growth of hydroxide layer on corrosion of the particles. Surface, cross section and thickness of the grown hydroxide on the aluminum particles were studied in a scanning electron microscope. The changes in corrosion potential of the aluminum powders are explained by cathodic and anodic lines in Evans diagram, which depend on microstructure and morphology of the aluminum particles, porosity, defects and thickness of the hydroxide layer, iron contamination on aluminum surface and pH of the solution. The hydrogen production test showed that a deformed microstructure and smaller particle size accelerates the corrosion rate of aluminum by hot water, the effect of the deformed microstructure being more significant at the beginning of the reaction. Effect of growth of the hydroxide layer on corrosion mechanism is discussed.

Keywords: *Hydrogen production; deformation; native oxide film; core-shell; passivation*

4.3. Introduction

The corrosion behavior of aluminum at room temperature has been studied extensively in the past, however, less attention has been paid to understanding the reaction mechanism of aluminum in hot water. In addition to hydrogen generation, there have been few aspects for which the reaction of aluminum and hot water has been a subject of interest. Corrosion of aluminum alloys used in fuel cladding in reactors was studied using hot water treatment [152-157]. On the other hand, the corrosion of aluminum with hot water was also studied as a method

to improve adhesion strength of polymer coatings to aluminum surface [158-160]. The corrosion of aluminum by hot water forms a porous hydroxide layer on the surface of aluminum, which remarkably increases strength of the bonding between aluminum and polymer coatings. The reaction of aluminum with hot water was also investigated to manipulate the oxide/hydroxide layer on the surface of aluminum components used in electronic industries [161].

The above mentioned applications led scientists to gain a good insight into the mechanism of the reaction of bulk aluminum with hot water. R.S. Alwitt [146], W. J. Bernard et al. [144], W. Vedder et al. [113] and B. R. Baker et al [162] conducted methodical investigations dedicated to understand corrosion behaviour of aluminum samples by use of hot water.

On the other hand, in spite of the numerous studies on hydrogen generation through the reaction of ball milled aluminum particles with water, a thorough evaluation of the mechanism is yet to be understood. The main focus of the previous studies on hydrogen generation from Al-water reaction was to activate aluminum in a way to generate higher amount of hydrogen in a short time period. To knowledge of the authors, no electrochemical route has been performed till date to understand the reaction between aluminum particles and hot water and how ball milling promotes the reaction.

This study aims to fill the gap between the remarkable interest in production of hydrogen from reaction of ball milled aluminum particles with hot water and a deeper understanding on the mechanism of the reaction. We conducted the reaction at 80^{o}C. Because this temperature is the optimum temperature for operating PEM (proton exchange membrane) and many other types of fuel cells. We neither manipulated pH of the water nor added any second phase powder to promote the kinetics of the reaction. Thus, the study purely considers the reaction mechanism of aluminum with hot water and effect of ball milling on the reaction kinetics. We examined four different powders (as received, 1 h, 7 h and 19 h milled), however, we focus on comparison of the as received and 19 h milled powders. That is because both as received and 19 h milled particles show equiaxed morphology and a non-laminated structurally. Thus, without interference of other variables, we can investigate effect of particle size and deformed microstructure on electrochemistry of the reaction and hydrogen generation.

4.4. Experimental

4.4.1. Ball Milling

The detail of ball milling procedure is similar to the manuscript #1. It is not repeated here in order to keep the thesis concise.

4.4.2. Hydrogen Measurement

The detail of hydrogen measurement procedure is similar to the manuscript #1.

4.4.3. Scanning Electron Microscopy

The detail of scanning electron microcopy (SEM) is mostly similar to the manuscript #1. On the case of the thickness of the produced hydroxide layer, the Microstructure Measurement software calculated thickness of the hydroxide layer on the surface of the particles by analyses of SEM images from cross section of the particles. The thickness data point for each sample was obtained by arithmetic averaging of 30-70 measurements. An Oxford Instruments Nordlys Nano detector was used as an integral part of the microscope to collect the electron backscattered diffraction (EBSD) patterns generated from the samples tilted at an angle of 70^{o} relative to the microscope stage. The SEM for the EBSD characterization was operated at an acceleration voltage of 10-30 kV, depending on the grain size of the sample. Applying a misorientation cut-off of 15^{o}, the grain size of the samples was determined by a post processing module Channel 5-Oxford Instruments.

4.4.4. Open Circuit Potential and Tafel Measurements

A Gamry potentiostat (interface 1030) obtained the open corrosion potential (OCP) of the powders vs. saturated calomel electrode (SCE) with a step size of 1 sec. We pasted the aluminum powders to microscope slides using conductive carbon paint (LEIT-C™) and applied a 0.95 cm^2 area by PortHoles electrochemical sample masks (Gamry3M Model 470). We used a solution of 2.84 g sodium sulphate in 200 ml distilled water (equivalent of 0.1 mol/lit) as the electrolyte, which was conductive and neutral. For the Tafel tests, the potential was swept in the positive direction from a cathodic potential of -250 mV_{ocp} to an anodic potential of 250 mV_{ocp} with a step size of 1 sec. The situation for the OCP and Tafel experiments was similar to that of the

hydrogen measurement tests (stirring rate: 120 rpm, temperature: 80^{o}C and distilled water volume: 200 ml).

4.5. Results and Discussion

4.5.1. Microstructure of Particles and Hydrogen Generation

The evolution of particle size and microstructure by ball milling was investigated in chapter 2 and chapter 3. It was found that ball milling decreases the particle size and increases crystallographic defects (grain boundaries, dislocations, etc.). Fig. 4.1 shows an electron backscattered diffraction (EBSD) pattern of an as received aluminum particle. The white and black lines represent boundaries with misorientation of (5-15)^{o} (subgrain boundaries) and over 15^{o} (high angle boundaries), respectively. One can see that in the as received particle, grains are equiaxed and most of grains are between 50-100 μm.

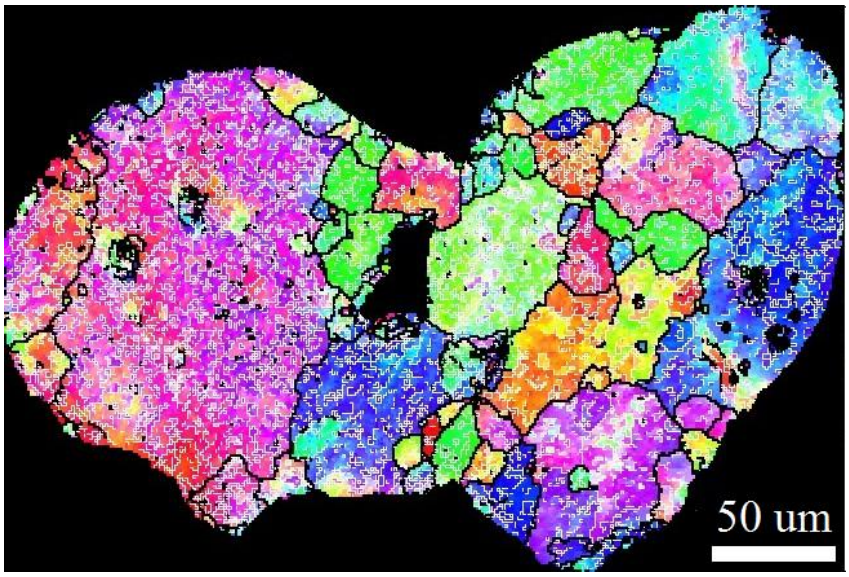

Fig. 4.1 EBSD patterns of an as received aluminum particle

Because of the large strain induced as a result of heavy deformation in the 19 h milled particles, we could not obtain any EBSD pattern for the particular sample. However, we performed refinement by MAUD software on X-ray diffraction of the particles milled for 19 h. Fig. 4.2 shows the X ray diffraction pattern and the corresponding refinement result by Rietveld method. Using the Rietveld method [125], a crystallite size of 78 nm was calculated for the 19 h milled sample. Considering Fig. 4.1 and the result obtained from Fig. 4.2, we conclude that ball milling results in a significant decrease in grain size of the aluminum powder.

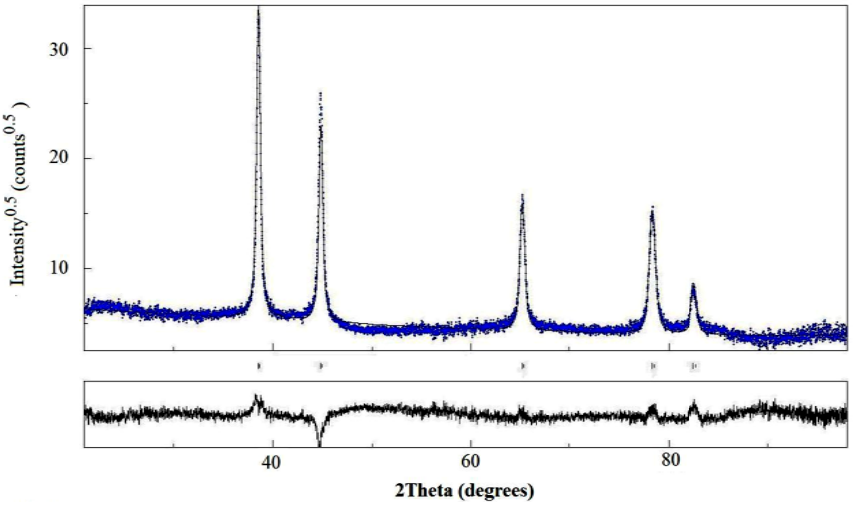

Fig. 4.2 The XRD pattern of the 19 h milled sample and the correspondent Rietveld refinement. A crystallite size of 78 nm was obtained from the refinement.

Fig. 4.3 shows the plot for hydrogen generation as a function of time for the reaction of water with the aluminum powders milled for 7 h and 19 h. The reaction of the as received and 1 h milled aluminum powders with water was very slow and no significant flow of hydrogen could be detected by the flowmeter; therefore their results have not been reported. The ball milling for 7 h or 19 h makes the aluminum powder active for the reaction with water and leads to generation of considerable amount of hydrogen.

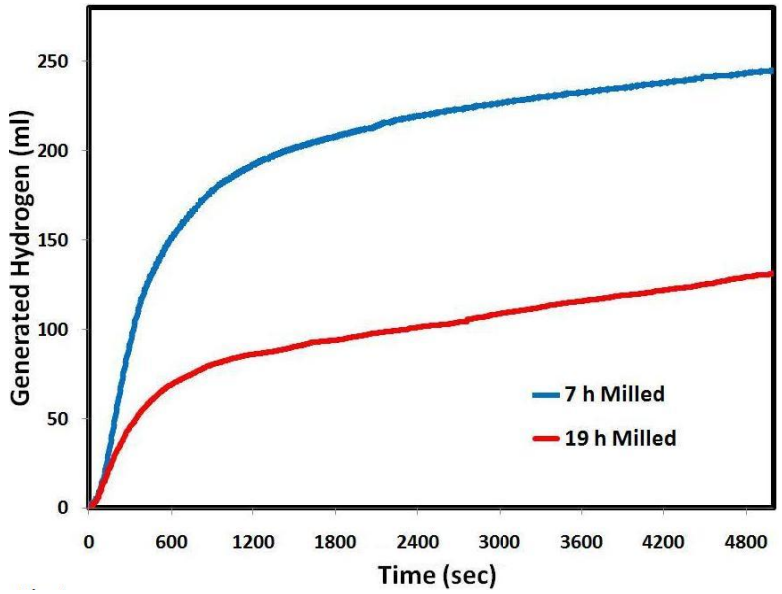

Fig. 4.3 Hydrogen generation of the aluminum powders milled for 7 h and 19 h.

We observed that there was a short delay of 10-30 seconds before hydrogen generation started for the 7 h and 19 h milled samples. This delay is so called "induction period" or "incubation time" and is usually observed before hydrogen starts forming [142]. One can see that although ball milling for 7 h has a noticeable effect on hydrogen yield, further milling up to 19 h decreases hydrogen yield. As explained in Chapter 3 and Chapter 4, the higher hydrogen production rate of the 7 h milled particles can be ascribed to the presence of internal surfaces due to the laminated structure. Fig. 4.1 to Fig. 4.3 are provided and briefly explained in this manuscript to help elucidating the mechanism of the reaction that will be discussed in the rest of the manuscript.

4.5.2. The Reaction Mechanism

The mechanism of the reaction between aluminum and hot water strongly depends on the pH. The oxide or hydrated-oxide film on the surface of aluminum is soluble in solutions with pH higher than 11 or lower than 2 [113, 147]. At intermediate pHs, the solubility of aluminum ions in the solution is limited. Therefore, the aluminum ions dissolved by an anodic reaction precipitate on the surface of aluminum [113]. The precipitation forms a layer of $Al(OH)_3$ at temperatures lower than 70^oC or AlOOH at temperatures higher than 70^oC [128]. After formation of the hydroxide layer, the reaction continues by penetration/diffusion of the water/ion species through the layer from water to aluminum sub-layer and vice versa. Aluminum ions diffuse outward as Al^{3+} in acidic solutions, $Al(OH)^{2+}$/$Al(OH)_2^+$ in neutral pHs or as $Al(OH)_4^-$ in basic solutions [64, 143, 146, 163-165]. The inward flow of ion species includes H_2O molecules, H^+ or OH^-, depending on porosity of the hydroxide layer and pH of the solution. This should be noted here that the hydroxide layer has a porous structure. Supposedly, the pores are filled with water, which makes the diffusion of ion species possible.

Fig. 4.4 shows the schematic of sequences of corrosion aluminum with hot water. The first stage is hydration of the native oxide film on the surface of aluminum. B. C. Bunker et al. argued that because of thermodynamic instability of aluminum hydroxide next to aluminum, an oxide layer always exists between the aluminum hydroxide and aluminum [142]. As the hydration front reaches to aluminum surface (and at the presence of thin oxide layer), ion species diffuses through the oxide layer and reacts with aluminum. The generated hydrogen gas forms bubbles beneath the oxide layer. Ion species that contain aluminum ion (Al^{3+}) diffuse outward, however, as solubility of aluminum is limited in water, aluminum hydroxide (AlOOH or $Al(OH)_3$

depending on pH or temperature) deposits on the surface of particles. When the pressure of hydrogen gas reaches a critical value, it breaks the layer and gas is released [80, 142]. In the case of aluminum particles, dissolution of metallic aluminum atoms at the interface of the metal and the hydrated oxide on one hand, and diffusion of the produced aluminum ions toward solution and precipitation on the layer on the other hand, result in formation of a core-shell structure (Fig. 2.14). The core is the remained metallic aluminum and the shell is the precipitated AlOOH or $Al(OH)_3$ [117].

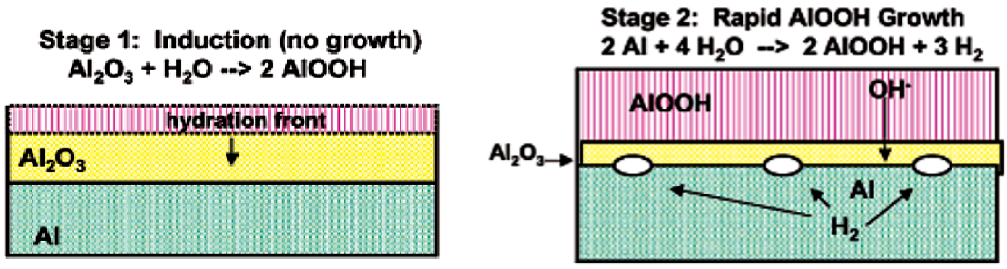

Fig. 4.4 The schematic illustration of mechanism of corrosion of aluminum by hot water [142]

Fig. 4.5 shows the changes in corrosion potential vs. time for the as received and 1 h, 7 h and 19 h milled aluminum powders. The potential of the 7 h and 19 h milled particles initially sharply decreases and reaches a minimum, and then gradually increases toward a steady state. The decrease in the potential of the as received and 1 h milled samples is not very sharp and the potential does not reach to a minimum during the first hour of immersion.

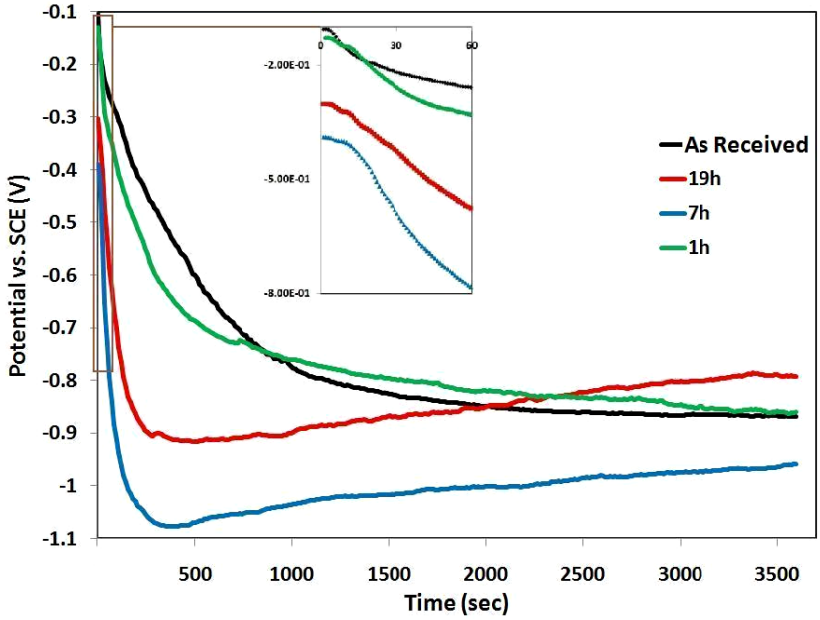

Fig. 4.5 Corrosion potential vs. time for the as received and 1 h, 7 h and 19 h milled aluminum powders. The inset magnifies corrosion potential during the first 60 sec after the immersion.

4.5.2.1. Changes in Corrosion Potential

Potential of a reaction can be written in terms of Nernst equation [166]:

$$E = E_o - \frac{RT}{nf} lnQ \qquad 4.1$$

where E^o is the standard reaction constant, R is the universal gas constant, T the Kelvin temperature, n the number of electrons in the balanced chemical equation for the half cell, and f is the Faraday constant. Q represents the ratio between activities of substances in two sides of the reaction. For a reaction that occurs at a constant temperature, the potential can change by changes in activity of reactants and products.

Reaction of aluminum and water can be algebraically divided into separate oxidation and reduction reactions. The E-I relation of each half reaction can be written in terms of Butler-Volmer equation. On the Evans diagram, the corrosion potential can be determined from interception of the anodic and cathodic lines. Fig. 4.6 (a) shows the Evans diagram for reaction of aluminum and water. The corrosion potential and corrosion current can be determined from the intercept of the cathodic ($3H^+ + 3e = 3/2H_2$) and anodic ($Al = Al^{3+} + 3e$) lines. Any change in slope or position of the cathodic or anodic lines results in a change in corrosion potential and corrosion current of the overall reaction. For example, Fig. 4.6 (b) shows the effect of shifting the anodic line to more negative potentials on the potential and current of the reaction.

Accordingly, the significant change in corrosion potential in Fig. 4.5 can be explained by the changes in cathodic and anodic lines in the Evans diagram. The sharp decrease in corrosion potential means that either or both cathodic and anodic lines shifted toward more negative potentials during the reaction. This shift can be explained by hydration of the oxide film, change in concentration of aluminum ions in the solution, developing cracks in the oxide film and change in pH toward more alkaline solution.

One can see that for the 19 h and 7 h milled sample, the corrosion potential increases slightly after 300-400 sec of reaction. This increase also can be explained by shifting the anodic and/or cathodic lines in Evans diagram toward more noble potentials. The cathodic line ($3H^+ + 3e = 3/2H_2$) can move upward when iron contamination (caused during milling, see Fig. 2.14) deposits on the surface aluminum. On the other hand, the anodic line ($Al = Al^{3+} + 3e$) can move

toward noble potentials when the hydroxide layer thickens or densified (i.e. when the pores are closed in the hydroxide layer).

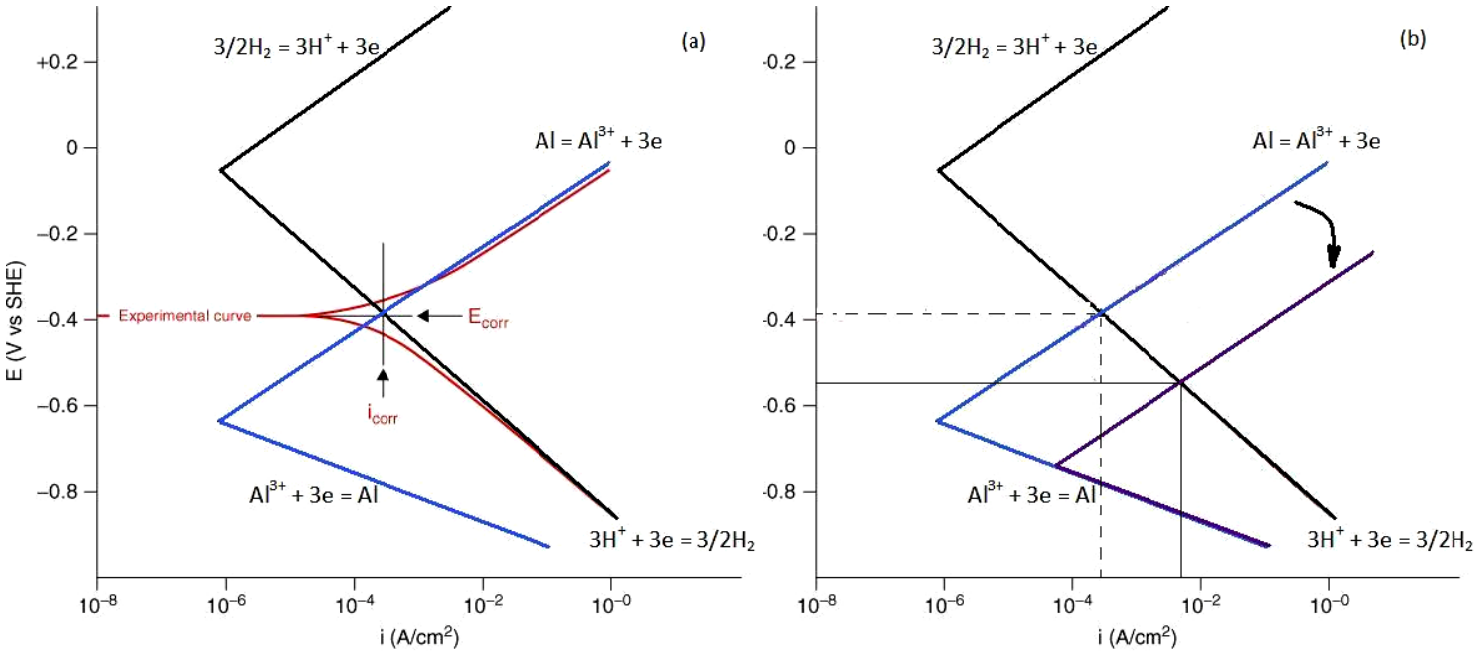

Fig. 4.6 (a) Schematic of Evans diagram for corrosion of aluminum by hot water, (b) effect of a change in position of anodic line on potential and current of corrosion.

Another parameter affecting the reaction potential is the ratio between surface of cathodic and anodic sites [167]. The Q parameter in Nernst equation (Eq. 4.1) depends upon ratio of surface of cathodic to anodic sites; a larger cathodic surface sites increases Q and accordingly potential of reaction increases. W. Vedder et al. argued that grain boundaries act as cathodic sites during corrosion of aluminum by hot water [113], and that grain boundaries are corroded faster than the grain interior. As reaction continues and grain boundaries are corroded, the ratio between the anodic and cathodic sites changes, and accordingly, the corrosion potential changes because of the change in Q in Nernest equitation.

4.5.2.2. Formation of a Passivating Hydroxide Layer

Fig. 4.5 shows that for the 7 h and 19 h milled samples, the potential increases gradually after passing the minimum. However, the potential of the as received and 1 h milled samples decreases gradually and does not reach a minimum in the first hour of the immersion. In order to

determine why the trend of the OCP curves of the highly deformed powders (19 h and 7 h milled) is different from that of the as received and lightly deformed (1 h milled) powders, we repeated the OCP test of the as received powder, but for a longer period of time. Fig. 4.7 shows the OCP curve of the as received powder during a 3 h immersion period. The inset in Fig. 4.7 magnifies the first minute of the curve. The minimum that was observed for the OCP curves of the 7 h and 19 h milled powders occurs at a later time for the as received powder. The minimum occurs after about 400 sec for the 7 h and 19 h milled samples, while it occurs after about 3000 sec for the as received sample. Considering Fig. 4.5 and Fig. 4.7, we conclude that ball milling does not change the corrosion mechanism of the aluminum powder, but it causes the sequences of the reaction to take place at a shorter period of time.

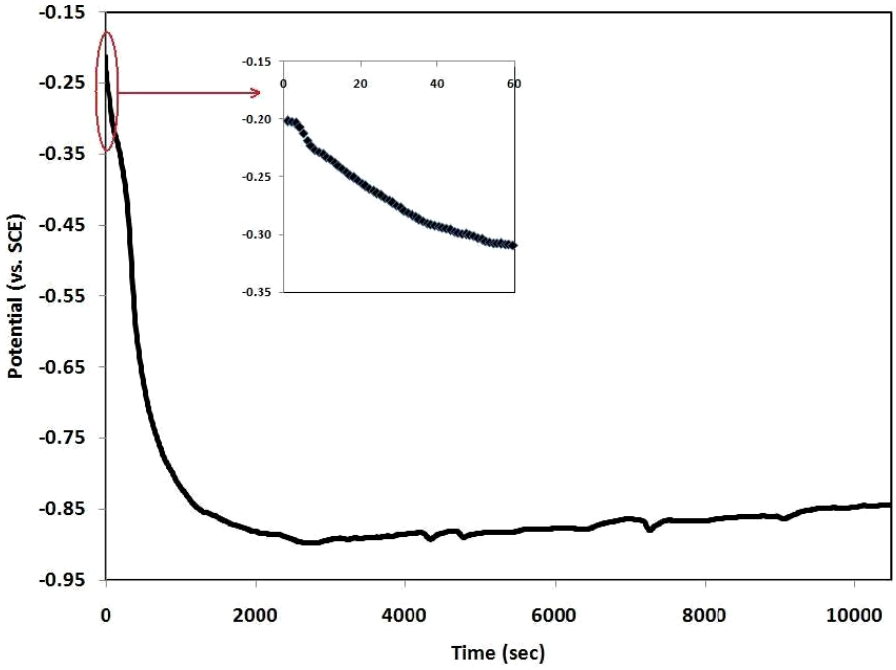

Fig. 4.7 Corrosion potential vs. time for the as received aluminum powder during first 3 h of immersion. The inset magnifies corrosion potential during the first 60 sec after the immersion.

4.5.3. Effect of Ball Milling on the Reaction

4.5.3.1. Effect of particle Size

Ball milling modifies the aluminum particles in two ways. First and foremost, ball milling decreases the particle size and thus, increases the specific surface area of the powders. Assuming spherical particles, a decrease in particle size from 192μm (as received) to 44 μm (19 h milled) is

equivalent of an increase of 19 times in the specific surface area. Since the reaction can just occur on the surface of aluminum, hydrogen production should increase linearly with the increase in surface. Considering production of about 100 ml hydrogen after 60 min reaction of 19 h milled sample, the as received powder should produce about 5 ml hydrogen during the same period. However, the hydrogen production of the as received aluminum powder was negligible. The almost zero hydrogen production of the as received powder implies that the decrease in particle size is not the only effect of ball milling on the reaction, otherwise, the hydrogen production should have changed linearly with the square of size of non-laminated spherical particles.

4.5.3.2. Effect of Deformation

The second effect of ball milling is introducing crystalline imperfections such as grain boundaries and dislocations. Under thermodynamic viewpoint, grain boundaries increase microstructural instability and thus, fine grained and deformed metals have a higher affinity for reactions than coarse grained and recrystallized metals. However, corrosion rate of fine grained metals is not necessarily higher than coarse grained metals. Contradictory results have been reported for the effect of grain size and deformation on the corrosion behaviour [112, 134-140]. K.D. Ralston et al. explained that formation of a protective layer on the surface of a metal determines the effect of grain size on the corrosion [141]. A finer grain size increases corrosion resistance of metals that form a protective film. The finer grain size increases reactivity and thus, a uniform protective layer forms at a faster rate and protects the metal from further corrosion. Conversely, deforming a metal can increase the corrosion rate if a film on the metal is not formed or formed in a non-protective way.

The protectiveness of the oxide/hydroxide film on aluminum surface depends on oxidizing media and temperature. In the case corrosion of aluminum using hot water, the oxide film on the surface of aluminum gradually transforms to a hydroxide film, which the latter is less protective compared to the former [142]. As temperature increases, diffusivity of the ion species increases and the hydrated layer becomes less protective. Therefore, the hydroxide film on the surface of the aluminum immersed in hot water has semi-protective properties. Accordingly, the deformed aluminum substrate does not reduce the corrosion by a fast and uniform formation of the

protective layer, but promotes the corrosion by increasing the affinity of water to react with the aluminum substrate. This rationalization is in accordance with the observations made by W. Veddar et al. and R. K. Hart; they noticed that reaction of aluminum and hot water mainly occurs at grain boundaries [113, 128].E. David et al., Z. Zhao et al and H. Luo et al. also noted that deformation of aluminum particles by ball milling promotes the hydrogen production rate [75, 114, 118], which confirms semi-protectivity of the hydroxide layer on the surface of aluminum.

Based on the above discussion, the deformed state of aluminum particles promotes the reaction and effect of microstructure should be considered while comparing hydrogen generation of the as received and highly deformed powders. The negligible hydrogen production of the as received sample compared to the highly deformed powders is because not only ball milling decreases the particle size of the powder, but also introduces crystalline imperfection to aluminum lattice, which increases the affinity of aluminum to react with water.

4.5.3.3. Effect of Microstructure on the Hydroxide Layer

We examined surface and cross section of the particles after different periods of reaction with water to study the effect of microstructure on the reaction. We observed that there is not much difference between the outside morphology of the hydroxide layer grown on the as received and 19 h milled particles. The evolution of morphology of the hydroxide layer by emersion time was very similar to what observed by P.R. Underhill et al. and A. C. Geiculescu et al. [159, 168-169]. Fig. 4.8 provides the SEM images of surface of the as received and 19 h milled particles after 1 h immersion in hot water. The hydroxide layer is formed by stacking of 10-20 nm thickness flakes. These flakes are aligned almost perpendicular to the particle surface but oriented randomly, which results in formation of a porous microstructure.

Fig. 4.9 shows effect of immersion time on the thickness of the hydroxide layer grown on the surface of the particles. Error bars represent the standard deviation of the thickness measurements. We observed a wide range of the hydroxide thicknesses for different particles of the same powder, which resulted in big standard deviations of the measurements especially for longer immersion times. The growth of the layers is fast at the beginning of the reaction and then becomes gradual; the trend is similar to that of hydrogen generation (Fig. 4.3).

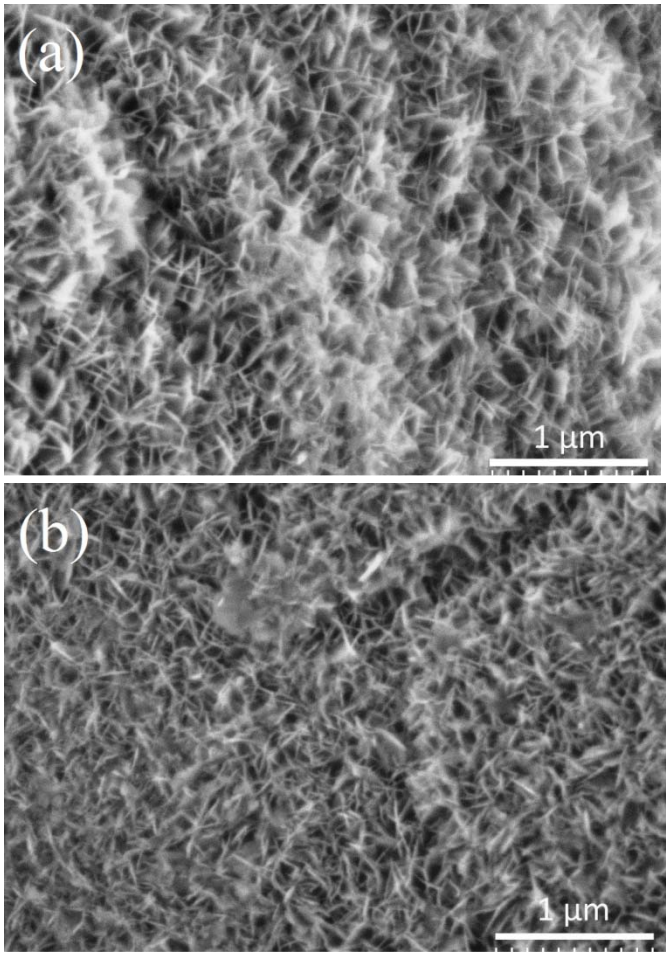

Fig. 4.8 SEM images of surface of the hydroxide layer formed on (a) the as received and (b) 19 h milled particles after 1 h immersion in hot water.

Considering the effect of a deformed microstructure on the reaction, we expected a thicker hydroxide layer on the 19 h milled particles compared to the as received one. However, it is brought out in Fig. 4.9 that the difference between the hydroxide thickness of the as received and 19 h milled particles is negligible. The similar thickness of the hydroxide layer on the particles with different microstructures does not mean the particles have had the same progress of the reaction.

Fig. 4.10 shows SEM images of cross section of the hydroxide layer grown on the as received and 19 h milled particles. The hydroxide formed on the 19 h particle comprises two layers; a dark one that is next to the aluminum surface and a white one that forms the outer surface of the hydroxide layer. We did not detect any distinct double layer on the surface of as received

particles reacted for up to 1 h with hot water and only a white layer covers the particles. We examined many as received and 19 h milled particles and observed this difference for almost all of them.

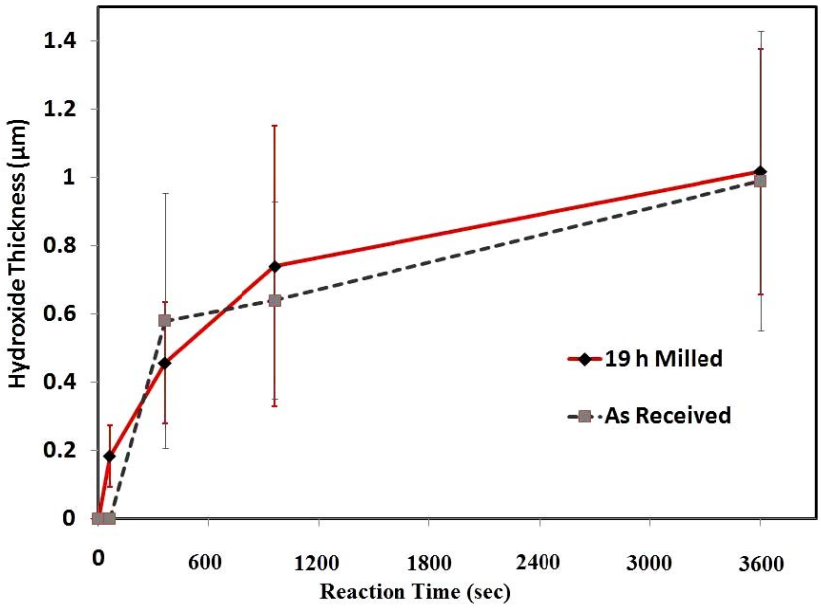

Fig. 4.9 Effect of immersion time on the thickness of the hydroxide layer grown on the as received and 19 h milled particles. Error bars represent standard deviation in measurements.

R. S. Alwitt thoroughly studied formation of hydroxide layers on the surface of aluminum during reaction with hot water and explained presence of separate hydroxide layers on the surface of aluminum [146]. Some other researchers also noted that the grown hydroxide layer is not uniform along its thickness [156-158, 162]. At the beginning of the reaction, the hydroxide phase forms a porous layer that is permeable and grows fast on the surface of aluminum. As reaction continues, the inner side of the hydroxide layer next to the aluminum surface densifies; pores become disconnected and then filled, thus, water no longer can penetrate through the layer. Formation of the inner layer imposes a change in the reaction mechanism; permeation of water through the layer is replaced by permeation through the outer porous layer and diffusion of ion species through the inner densified layer [145]. A change in the mechanism of the reaction because of the growth of a dense layer has been identified by a sudden change in the rate of weight gain [144, 146, 162] or thickening of the layer [170].

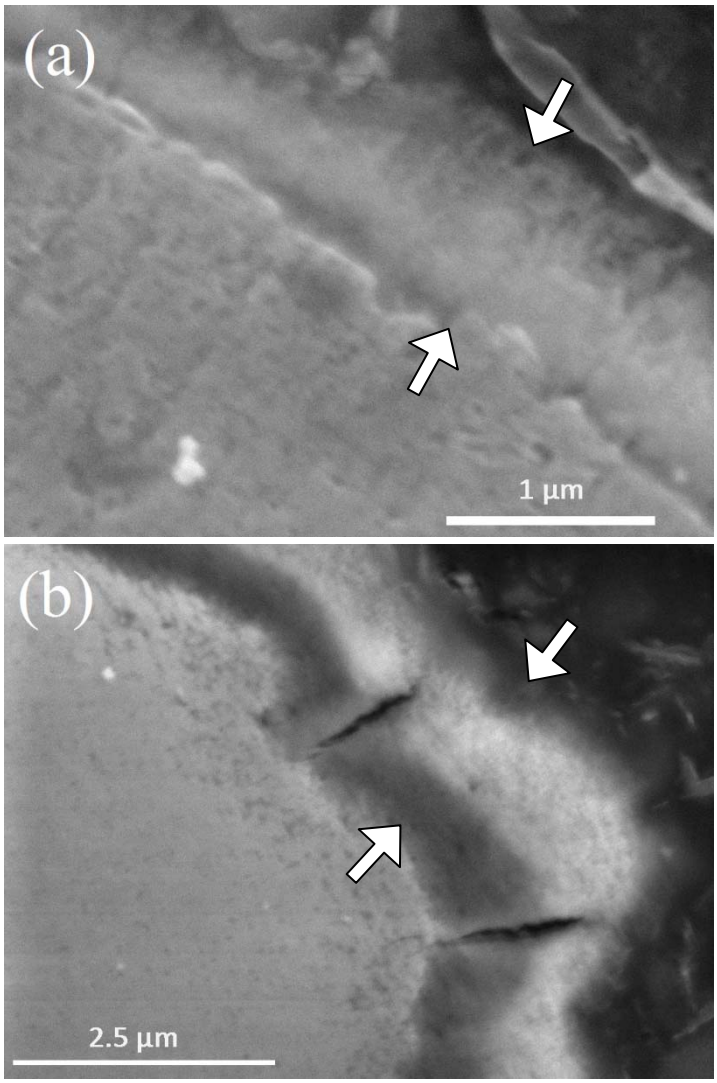

Fig. 4.10 SEM images of cross section of the hydroxide layer grown on (a) the as received and (b) 19 h milled particles. Note the difference in the scale bar. Arrows mark the thickness of the oxide.

While all of the above mentioned studies considered time as the parameter that determines formation of the inner layer, our observation establishes that in addition to the time, the microstructure of aluminum also affects formation of the inner layer. In other words, time is the influential factor because it determines the extent of the reaction. This means in the same period of time, the non-porous layer forms faster on an aluminum microstructure that thermodynamically has a higher affinity to react with water, compared to a more stable aluminum microstructure.

In spite of equal thicknesses, the hydroxide layer on the 19 h milled sample is denser than that of the as received one, implying that more hydroxide phase was deposited on the 19 h milled particle. Therefore, the presence of the double layer hydroxide suggests that for a unit of surface area, the 19 h milled particle reacted more than the as received particle.

The difference between hydroxide layers clarifies why the minimum in corrosion potential of the 19 h milled happened sooner than that of the as received particles (Fig. 4.5). As the 19 h milled particles react faster with water, more hydroxide phase precipitates on their surface and formation of a densified inner layer happens at a shorter time. Densification of the hydroxide layer on the surface of aluminum moves the anodic line to more noble potentials. Accordingly, the OCP increases as the interception of the cathodic and anodic lines moves up in the Evans diagram. Fig. 4.11 shows high magnification SEM of cross section of the hydroxide layer on the 19 h milled particle after 540 sec of the reaction. The white part on the left is aluminum and the grey part on the right is the hydroxide layer.

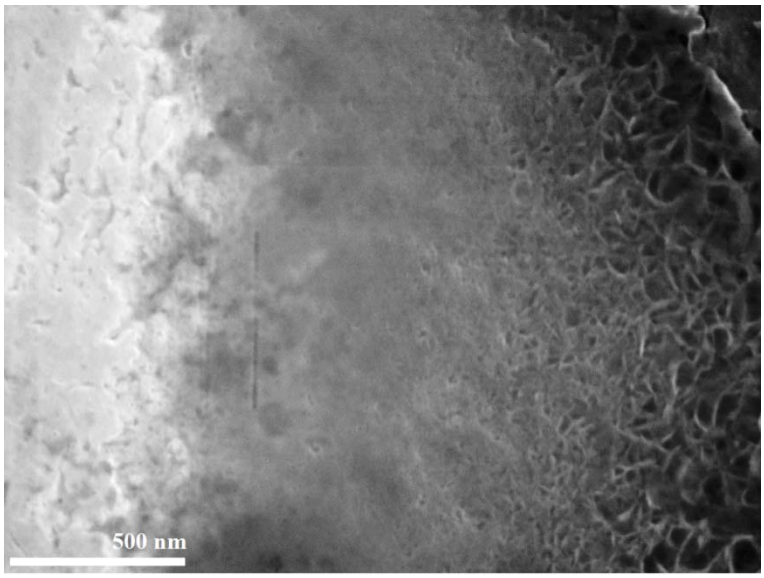

Fig. 4.11 SEM image of cross section of the hydroxide layer on the 19 h milled particle after 540 sec of the reaction.

There is a noticeable gradient between volume of pores in the external surface of the layer and inner part of the layer next to the aluminum substrate. The outer surface of the layer is porous while the inner part is almost free of pores. On the other hand, because of a lower extent of the

reaction, the layer formed on the surface of the as received particles is not dense enough to cause passivation.

4.5.4. Effect of Reaction Time on Corrosion Current

Fig. 4.12 shows the Tafel curves of the 19 h milled sample after 10 sec (curve A), 30 min (curve B) and 60 min (curve C) of the start of the reaction. The potential was swept in the positive direction from -250 mV to +250 mV compared to the OCP after 10 sec, 30 min and 60 min of the reaction. Because of the sharp decrease in the potential at first few minutes, the cathodic polarization branch of the curve A is extremely short and almost the whole 500 mV was swept on the anodic branch. On the other hand, the corrosion potential of the 19 h milled powder is increasing after 30 and 60 min of the reaction (Fig. 4.5), therefore, the anodic polarization branch is shorter than the cathodic one for curve B and C.

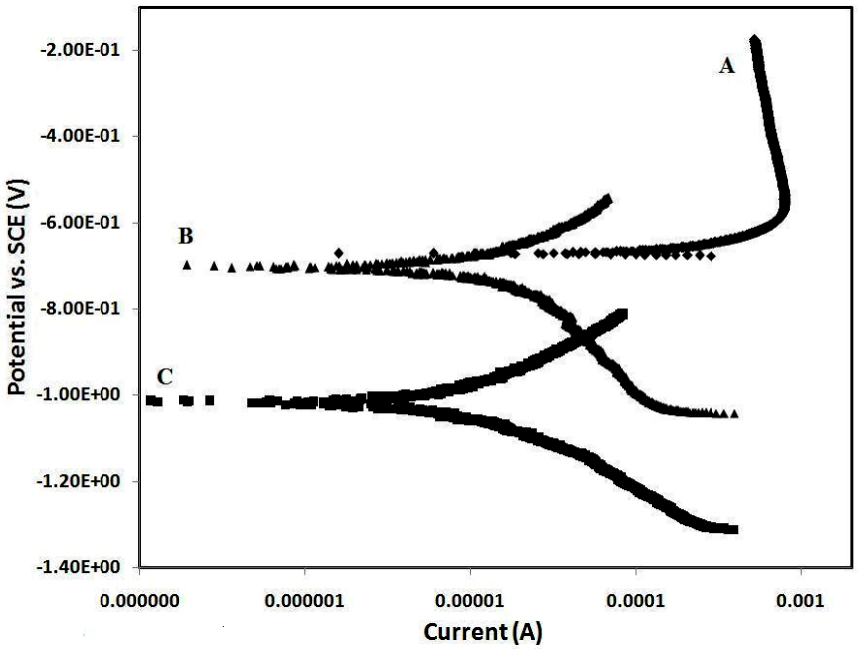

Fig. 4.12 Tafel curves of the 19 h milled sample after 10 sec (curve A), 30 min (curve B) and 60 min (curve C) of the start of the reaction.

Applying an anodic polarization results in a passivation of the powder reacted for 10 sec (curve A), however, the passivation current (~800 μA) is much higher than the corrosion current of curve B or C (~10-20 μA). While there is a big difference in polarization currents of curve A compared to curve B or C, the difference between curve B and curve C is negligible. Therefore,

one can conclude that growth of the hydroxide film in the first 30 min of the reaction has a remarkable effect on prohibition of corrosion of the particles, whereas in the next 30 min the growth of hydroxide layer has a negligible effect.

4.5.5 Effect of the Ball Milling on Corrosion Current

Fig. 4.13 shows effect of ball milling on Tafel curves of the aluminum particles after 1 min of start of the reaction. The number next to each curve corresponds to the corrosion current of the sample. The cathodic branch of the curves is shorter than the anodic one, which is because the corrosion potential was decreasing during Tafel test. Activation of the aluminum powders by ball milling shifts the Tafel curves to higher currents. Ball milling does not change the overall shape of the Tafel curves. However, slope of the anodic polarization branch of the 7 h and 19 h milled samples is higher than that of the as received and 1 h milled sample. The higher slope of the anodic branch of the 7 h and 19 h milled particles indicates that during anodic polarization, their surface tends to passivate faster compared to the as received and 1 h milled particles. The higher tendency of highly deformed particles (7 h and 19 h milled) for passivation compared to the as received sample is explained by formation of a densified hydroxide layer on surface of the highly deformed particles (Fig. 4.10).

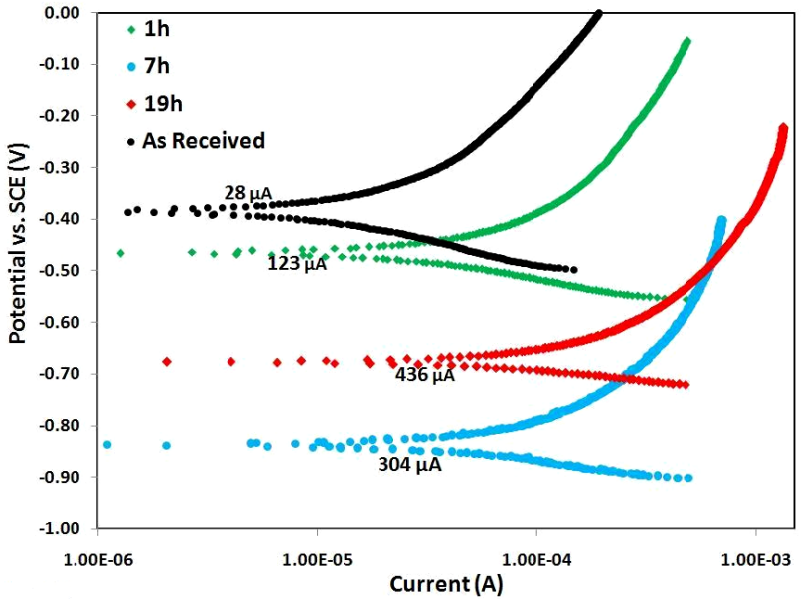

Fig. 4.13 Tafel curves of the as received and 1 h, 7 h and 19 h milled aluminum powders. The potential was swept from -250 to +250 vs. OCP after 1 min of the reaction. The number next to each curve is the corrosion current of the sample.

The potential of the 19 h milled sample is less negative compared to 7 h milled sample. This can be explained by the introduction of iron contamination because of erosion of the balls and vial during ball milling. Our EDS analysis did not detect any significant iron peak in the 7 h milled particles or particles milled for shorter periods of time, though it confirmed presence of iron contamination in the 19 h milled particles [117]. R. Ambat et al. investigated effect of iron contamination on OCP of aluminum and found that even small amount of iron contamination shifts corrosion potential of aluminum to less negative values [171]. This can be explained by the effect of presence of iron on the surface of the particles, which shifts the cathodic line ($3H^+ + 3e = 3/2H_2$) to less negative potentials in Evans diagram. Therefore, the less negative corrosion potential of the 19 h milled compared to the 7 h milled sample is ascribed to the presence of iron contamination in the former one.

Fig. 4.14 shows effect of ball milling on Tafel curves of the aluminum particles after 60 min of start of the reaction. The difference between the different samples is relatively small for both corrosion potential and corrosion current.

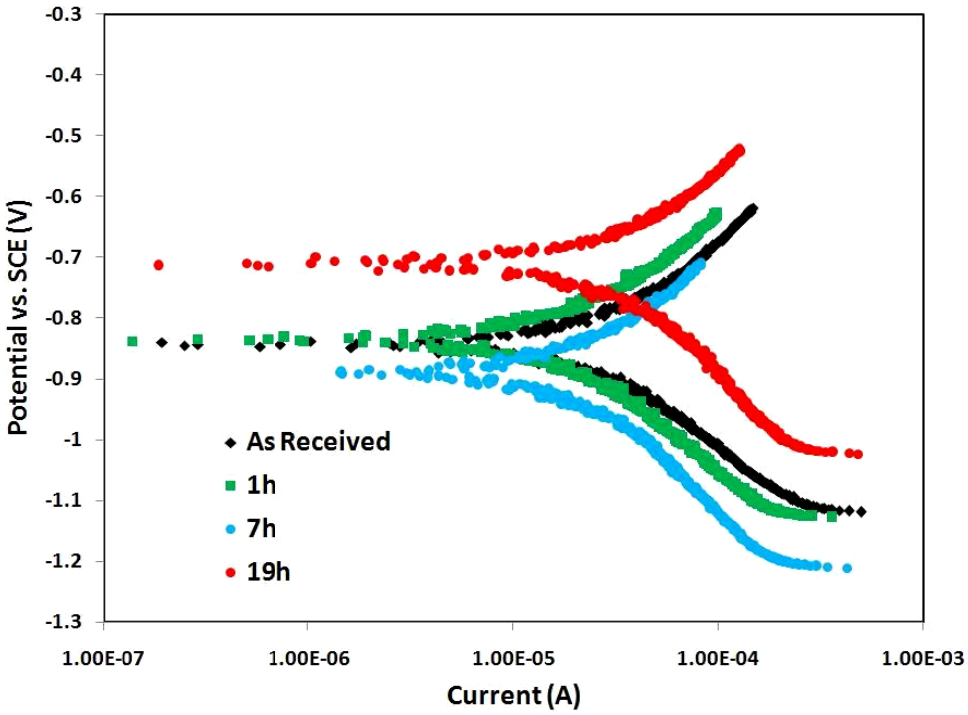

Fig. 4.14 Tafel curves of the as received and 1 h, 7 h and 19 h milled aluminum powders. The potential was swept from -250 to +250 vs. OCP after 60 min of the reaction.

Comparing Fig. 4.13 and Fig. 4.14, one observes that immersion in hot water for 60 min causes Tafel curves of different samples to converge together. The same trend can be seen in Fig. 4.5; at first few minutes of the immersion the corrosion potential is very different for the different samples, however, corrosion potentials converge to similar values after 60 min of the immersion. Therefore, the longer the immersion time, the less difference between corrosion properties of the different samples is observed. The microstructure of the particles does not change during the test; the only change is growth of the hydroxide layer on surface of the particles. Accordingly, we conclude that the passivating effect of growth of the hydroxide layer on the particles prevails over the difference in microstructures.

At the beginning of the reaction where the hydroxide layer is thin and mostly porous, highly deformed particles corrode faster at relatively more active potentials. As the reaction continues, the hydroxide layer becomes thick and dense and water cannot anymore penetrate through hydroxide layer. Then, the controlling step is diffusion of ion species through the non-porous part of the hydroxide layer. The dependence of the reaction on diffusion of ion species (the kinetics effect) prevails over the higher affinity of the highly deformed structure for the reaction (the thermodynamic effect), thus after 60 min of the reaction, particles with different microstructures show the similar corrosion behavior.

4.6. Summary

1. As aluminum particles are exposed to hot water, water molecules attack the native oxide film on the surface of particles. The oxide film is hydrated by hot water, which facilitates diffusion of ion species. Besides, formation of cracks and defects in the hydroxide layer, change in concentration of aluminum ions in the electrolyte and change in pH can promote the anodic dissolution of aluminum. As reaction continues, the hydroxide layer thickens and densifies, which slows down the kinetics of the reaction.
2. In spite of similar thickness and external morphology of the hydroxide layer grown on the as received and highly deformed particles, cross sectional examination of the particles suggested that hydroxide layer formed on the highly deformed particles is denser than that of the as received particles.
3. The passivating effect of the hydroxide layer depends on impermeability of the layer than its thickness. For the highly deformed particles, the reaction occurs faster and

more hydroxide deposits on the surface of aluminum, thus formation of a dense impermeable layer occurs at a shorter period of time compared to the as received particles.

4. The effect of a deformed microstructure on the reaction behavior is significant at the beginning of the reaction where the hydroxide layer is thin and porous. Highly deformed particles react at more active potentials with higher corrosion currents compared to the as received particles. As the hydroxide layer gradually thickens and densifies, the passivating effect of the hydroxide layer neutralizes the high affinity of the deformed particles for the reaction.

CHAPTER 5

MICROSTRUCTURAL EVOLUTION AND GRAIN SUBDIVISION MECHANISMS DURING SEVERE PLASTIC DEFORMATION OF ALUMINUM PARTICLES BY BALL MILLING

5.1. Overview of Chapter 5

Chapter 3 explained different contributions of ball milling on the reaction of aluminum with water, and revealed that grain refinement of aluminum particles has a significant contribution in the rate of hydrogen generation. Chapter 4 explained the effect of grain refinement of aluminum particles on the electrochemistry of the reaction. It was concluded that the particles of smaller grain size have a more active corrosion potential in water and react faster. However, it was not defined how grain refinement occurs.

Ball milling is the method used in this research and many other research to refine microstructure of particles. Compared to the extensive amount of studies on deformation of bulk metals by severe plastic deformation methods, the knowledge of mechanism of deformation of metallic particles during ball milling can hardly be considered satisfactory. This is in spite of thousands of publications in the literature on production of advanced metallic powders by this method. For the very first time, we used EBSD technique to thoroughly investigate grain refinement and deformation mechanism of aluminum particles during ball milling.

This chapter is presented as manuscript #4 (Microstructural Evolution and Grain Subdivision Mechanisms during Severe Plastic Deformation of Aluminum Particles by Ball Milling). The PhD candidate's contributions to the manuscript are: a) Powders preparation. b) EBSD investigation of the cross section of the particles. c) Post processing and analyses of the EBSD results. d) Reviewing the relevant literature and preparing the manuscript.

Because of the importance of the details of EBSD patterns presented in Fig. 1(a-f) and Fig. 2(a-f) in this chapter, these figures could not be reduced in size to fit one page, and are presented in rather large size.

The manuscript was submitted to the journal of Acta Materialia. Its current status is under review.

The copyright permission to use the manuscript in the thesis was obtained and provided in the Appendix section. The references for this chapter along with references from other chapters are provided at the end of the thesis.

Microstructural Evolution and Grain Subdivision Mechanisms during Severe Plastic Deformation of Aluminum Particles by Ball Milling

S.S. Razavi-Tousi, J.A. Szpunar

Department of Mechanical Engineering, University of Saskatchewan, S7N 5A9 Saskatoon, Saskatchewan, Canada

5.2. Abstract

Electron backscattered diffraction (EBSD) technique was used to investigate the microstructure of aluminum particles deformed by high energy ball milling. The length of different types of boundaries was calculated for different samples. The results showed that deformation mechanism as well as the rate of grain subdivision considerably change as milling time increased. At the beginning of the milling, deformation banding subdivided grains, and dynamic recovery formed a cellular structure of low angle boundaries. By further milling, particles were flattened; an increase in aspect ratio of the grains was clearly observed and cold welding of the particles contributed to formation of high angle grain boundaries. Lattice rotation progressively increased the misorientation between grains and high angle grain boundaries (HAGBs) were formed, which resulted in formation of new small equiaxed grains by continuous dynamic recrystallization (DRX). Subgrains rotation was found as the main mechanism of formation of new high angle grain boundaries.

Keywords: *Mechanical Milling, Impacts, Geometrical and Incidental Dislocation Boundaries, Orientation, Grain Refinement*

5.3. Introduction

During last two decades, researchers paid extensive attention to the high energy ball milling of metallic powders to produce various products with superior properties. This milling method is named depending on the type and purpose of the processing such as mechanical milling [172], mechanical alloying [34], mechanically induced self-propagating reaction [35] and cryomilling

[173]. In spite of some differences, the shared concept among all the mentioned methods is that cold welding and fracture mechanisms determine the morphology, and severe plastic deformation determines the microstructure of the milled particles.

The experimental and theoretical studies have established mechanisms of morphological changes of metallic particles during ball milling. The changes in size, shape and internal structure of ductile particles during milling time can be summarized as following [33, 40-41, 117, 174-175]: particles are deformed, flattened, cold welded, laminated, work hardened and fractured. The final shape of the milled particles is equiaxed after steady state, and the final size is determined by surface properties and hardenability of the particles, which consequently determine the equilibrium between fracture and cold welding mechanisms.

On the other hand, the current understanding of deformation and grain refinement mechanisms during milling is not established. A lack of comprehensive understanding is partially related to many complexities of the milling method that makes it considerably different from other severe plastic deformation methods that deal with bulk materials. For example; the deformation mode and stress direction acting on each particle continuously change during milling, no texture is developed by deformation, some impurities may be dispersed in the particles, the deformation happens through impacts and the strain rate is high, also some local increases in temperature may exist, and new surfaces are continuously formed during milling.

There have been various studies aimed to evaluate the deformation and grain refinement mechanisms induced by ball milling. The most accepted model was proposed by H. J. Fecht [176-177], who considered that grain refinement during milling follows three steps: a) localization of deformation in shear bands with high density of dislocations, b) annihilation and recombination of dislocations, which result in formation of a nanostructure network of subgrain boundaries, and c) grain boundary sliding that forms nano grains that are randomly oriented.

Most of the studies on the formation of nanostructures by ball milling confirm that at the very end stages of deformation, subgrain rotation or/and boundary sliding explain formation of nano grains that were formed from the subgrains. But, there is no agreement as to the role of shear bands in the grain refinement during ball milling. Referring to H. J. Fecht's model, some researchers ascribed the initial grain refinement during ball milling to the formation of shear

bands [178-181]. On the other hand, there are studies reporting that grain refinement occurs during ball milling without presence of shear bands [175, 182-185]. Moreover, even in the presence of shear bands, other deformation mechanisms like slip and twining also occur [186].

In comparison with deformation of bulk metals and/or based on other observations, different deformation and refinement mechanisms have been considered for the early to mid stages of ball milling: shear banding [176-177], twining [185], shear banding and slip/twining [186], slip and twining [175],slip and grain subdivision similar to bulk materials [183, 187], and fracture and cold welding induced refinement[178, 181]. Apart from the comparisons to the deformation of bulk materials, all of the observations made by transmission electron microscope (TEM) were in the nano regime [175, 178-183, 185-187], namely between ten and few hundred nanometres. On the other hand, the results that were based on analyses of broadening of X ray diffraction (XRD) peaks [176-177, 181, 184, 188] were also limited to nano range, because the calculation of crystallite size and microstrain by XRD is not reliable if the crystallite size exceeds the submicron range.

Accordingly, although the mechanism of deformation/grain refinement at the very end of milling (grain/crystallite size of 10-500 nm) is fairly established, there is a significant lack of knowledge on grain refinement mechanism during early and mid stages of milling, which was the motivation for this study. In order to investigate the deformation mechanism during ball milling, we used electron backscattered diffraction (EBSD) method rather than XRD or TEM that were used in the previous works. EBSD can examine bigger areas than TEM, which increases statistical reliability of data. Moreover, in contrast to analyses of broadening of XRD peaks, EBSD provides direct observation of boundaries, which is not limited to very small crystallite sizes.

In spite of the extensive use of EBSD for evaluation of microstructure of bulk materials, the use of this method for powders has been very limited. There are just four studies that used EBSD to characterize surface [189-190] or cross section [191-192] of particles. One can consider two reasons for such a limited use. Firstly, contrary to bulk materials, particles do not have a frame of reference for analyzing the orientation, thus the texture measurement becomes useless. Secondly, preparation of the EBSD samples from small particles is much more difficult than that of bulk materials.

Nevertheless, the present study shows that high quality EBSD patterns can be obtained from deformed aluminum particles, and novel data can be extracted that elucidate deformation and grain refinement mechanisms during the early to mid stages of ball milling. Our work does not extend to TEM study of the deformed particles at the end stages of milling, because that part is already extensively investigated in the literature.

5.4. Experimental Procedure

5.4.1. Powder Preparation

The detail of ball milling procedure is similar to the manuscript #1. It is not repeated here in order to keep the thesis concise.

5.4.2. Sample Preparation for EBSD

To study cross section of the particles, a small amount of the powders was separately added to a conductive carbon resin powder (SPI ConductoBed™ Carbon Black Filled Conductive Epoxy), mixed and cold mounted. The mounted samples were polished with abrasive grinding papers from 600 to 1600 grit followed with additional grinding by 3 and 0.04 μm diamond pastes. The 30 min, 1 h, 2 h and 4 h milled samples then were polished using a Buehler VibroMet for less than one hour. However, Vibromet polishing for the not deformed samples (the as received and 15 min milled particles) caused corrosion pitting on the surface, thus this stage of polishing was not applied for them. Finally, all samples were ion milled for 2 min at a voltage of 2 kV by a Hitachi IM4000 argon ion milling system.

5.4.3. EBSD Measurements

A Hitachi SU6600 field emission scanning electron microscope (SEM) equipped with a NordlysNano Oxford detector with an angular resolution of $0.1^{o}$was used to collect EBSD patterns from cross section of the particles. Channel 5-Oxford Instruments software was used for the post processing of the obtained patterns. The SEM for the EBSD characterisation was operated at acceleration voltages between 10-30 kV; the smaller grain size, the lower acceleration voltage was used for the samples. There was a remarkable change in the shape,

particle size and grain size of the powders induced by milling. The grain size and particle size changed from ~110 μm and ~200 μm for the as received sample to ~2 μm and 75 μm for the 4 h milled sample, respectively. Accordingly, we could not maintain either a similar step size or a similar scan area for different samples. Whenever it was possible, a rectangular scan was collected, otherwise, the particles shape dictated the shape of the EBSD scans.

We found that because of the particulate nature of the system under investigation, different particles in the same powder can have rather different microstructures. In other words, different particles in a powder milled for a particular time may have experienced different extent and mode of deformation. Therefore, in order to increase the reliability of the data, we obtained EBSD of at least five particles for each sample. Each single graph/pattern in this study is either a typical one among or an average obtained from few patterns.

5.5. Results and Discussion

5.5.1. Microstructural Evolution of the Particles

Fig. 5.1 shows the inverse pole figure (IPF) map in the Z direction (normal to the cross section of the particle) for the as received sample and the 15 min, 30 min, 1 h, 2 h and 4 h milled particles. Fig. 5.2 shows the band contrast of the patterns presented in Fig. 1, which is superimposed with grain boundaries with misorientation of 1-5^{o} (red), 5-15^{o} (blue) and 15-62^{o} (black). In this work, we name the 1-5^{o}, 5-15^{o} and 15-62^{o} grain boundaries as low angle grain boundaries (LAGBs), medium angle grain boundaries (MAGBs) and high angle grain boundaries (HAGBs), respectively.

The processing method (air atomization) used for the production of the as received powder determines their microstructure. The particle (Fig. 5.1(a) and Fig. 5.2(a)) includes few big grains (the average grain size: ~110 μm) with a small amount of HAGBs and MAGBs inside, but contains significant amount of LAGBs that are irregularly distributed in the grains. The presence of few large grains inside the particle implies that there were just few nuclei in the molten droplet that initiated the solidification in different orientations. However, the undercooled

condition made the solidification fast in a way that grains were left with a chaotic distribution of LAGBs inside.

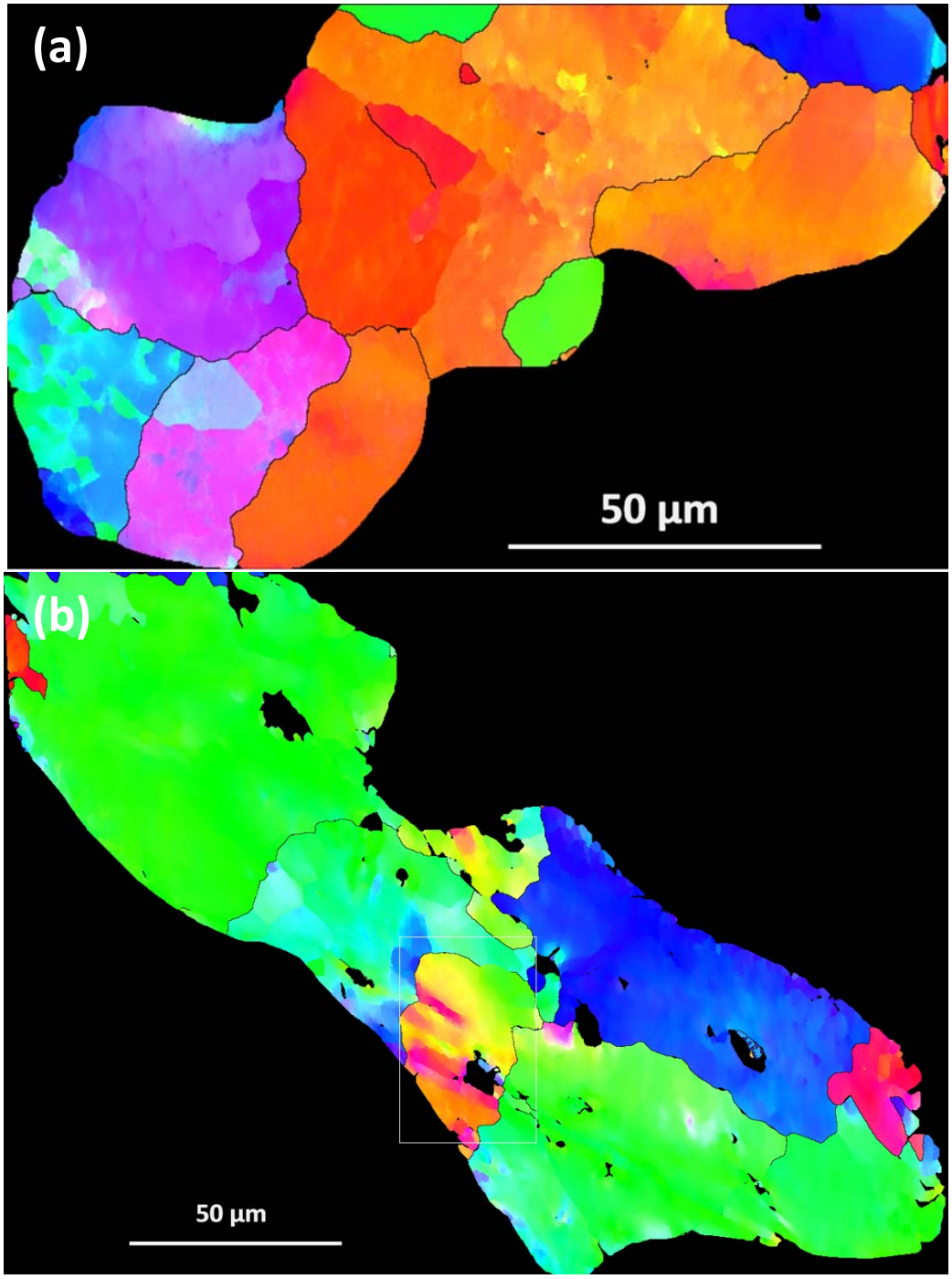

Fig. 5.1 IPF patterns of cross section of (a) an as received particle and (b) 15 min milled sample. Colors and black lines represent orientations (normal to the cross section) and HAGBs, respectively. See to the text for explanation of the arrows and signs.

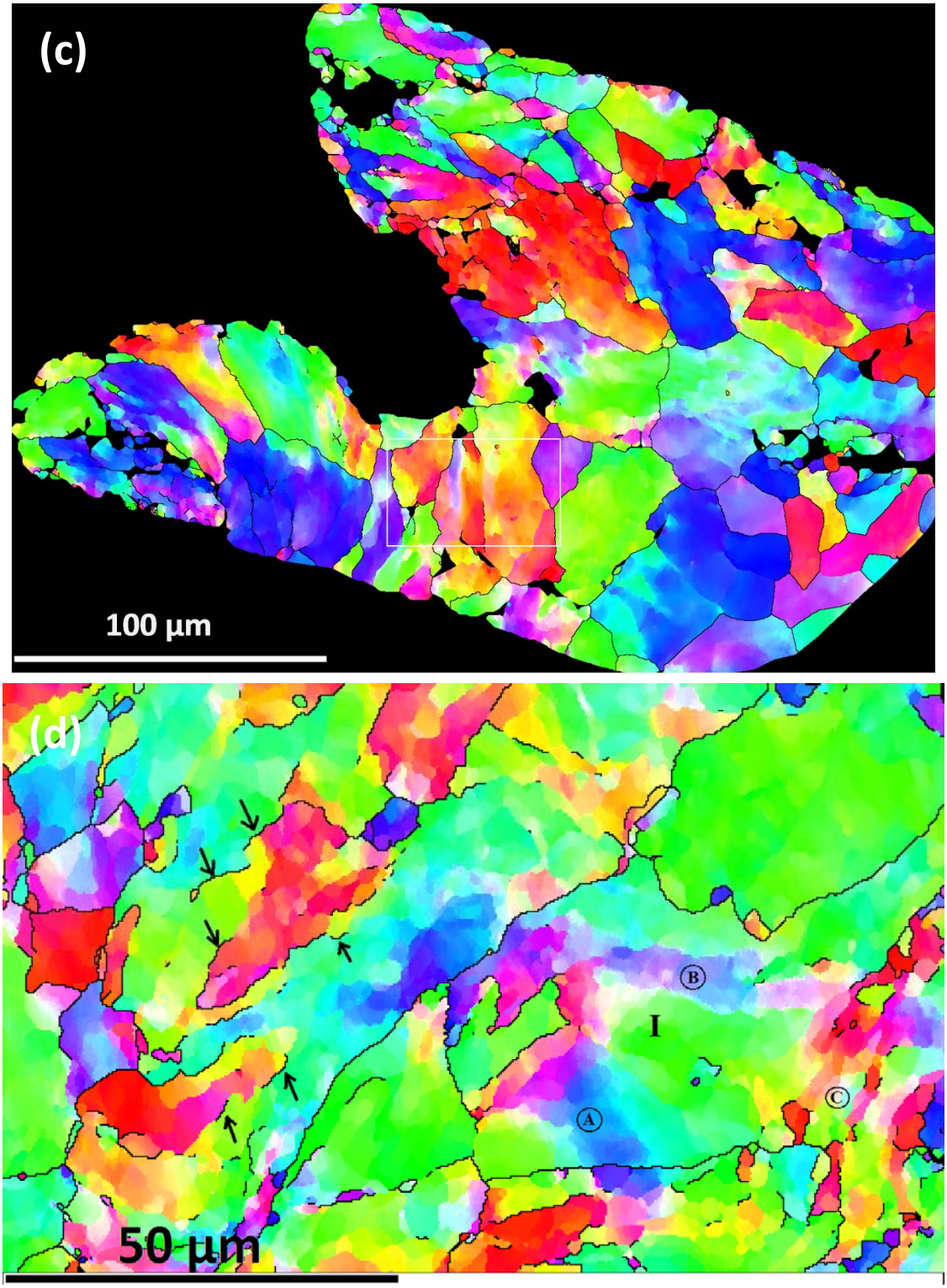

Fig. 5.1 Continued: IPF patterns of cross section of (c) 30 min and (d) 1 h milled samples. Colors and black lines represent orientations (normal to the cross section) and HAGBs, respectively. See to the text for explanation of the arrows and signs.

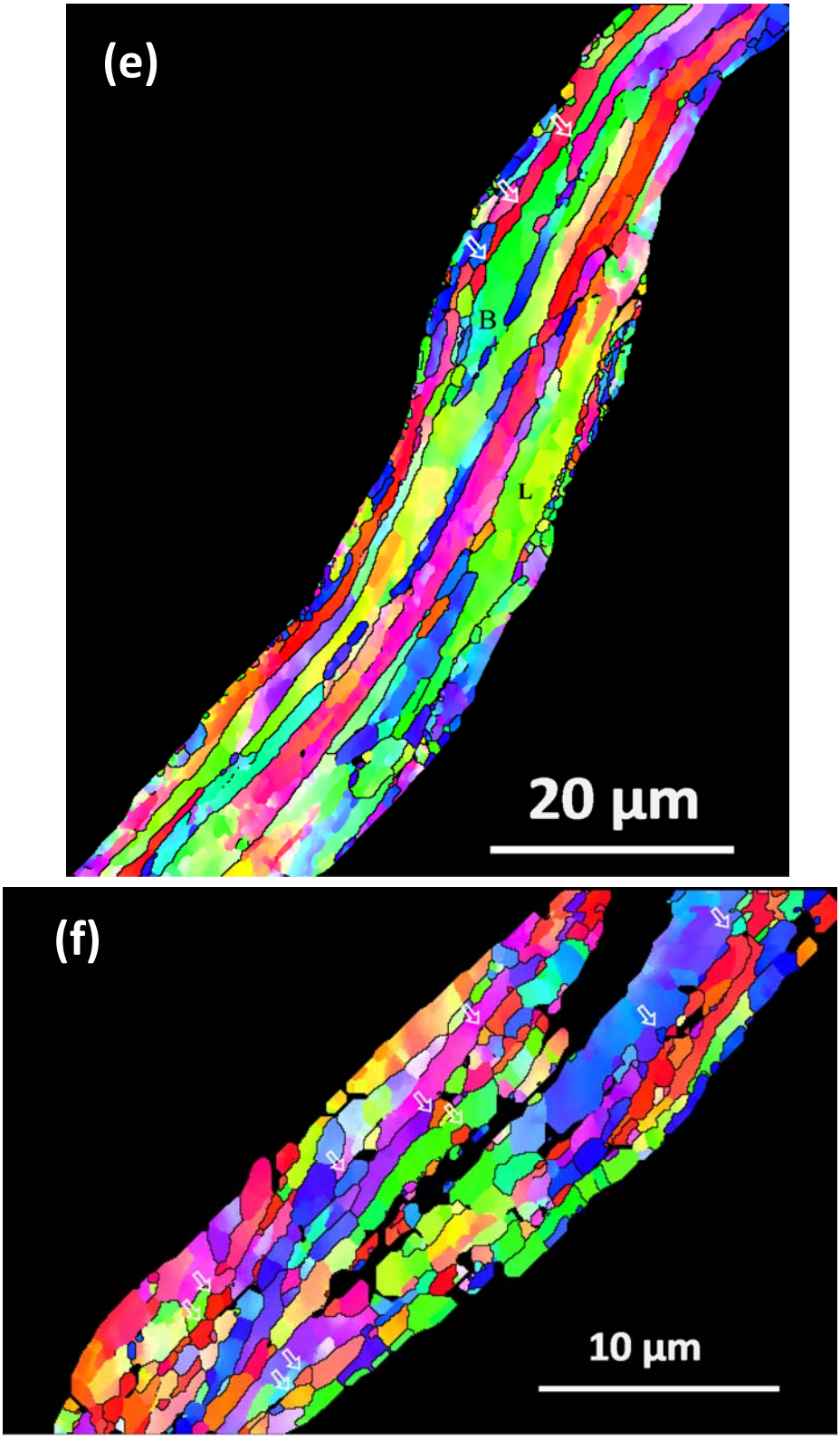

Fig. 5.1 Continued: IPF patterns of cross section of (e) 2 h and (f) 4 h milled samples. Colors and black lines represent orientations (normal to the cross section) and HAGBs, respectively. See to the text for explanation of the arrows and signs.

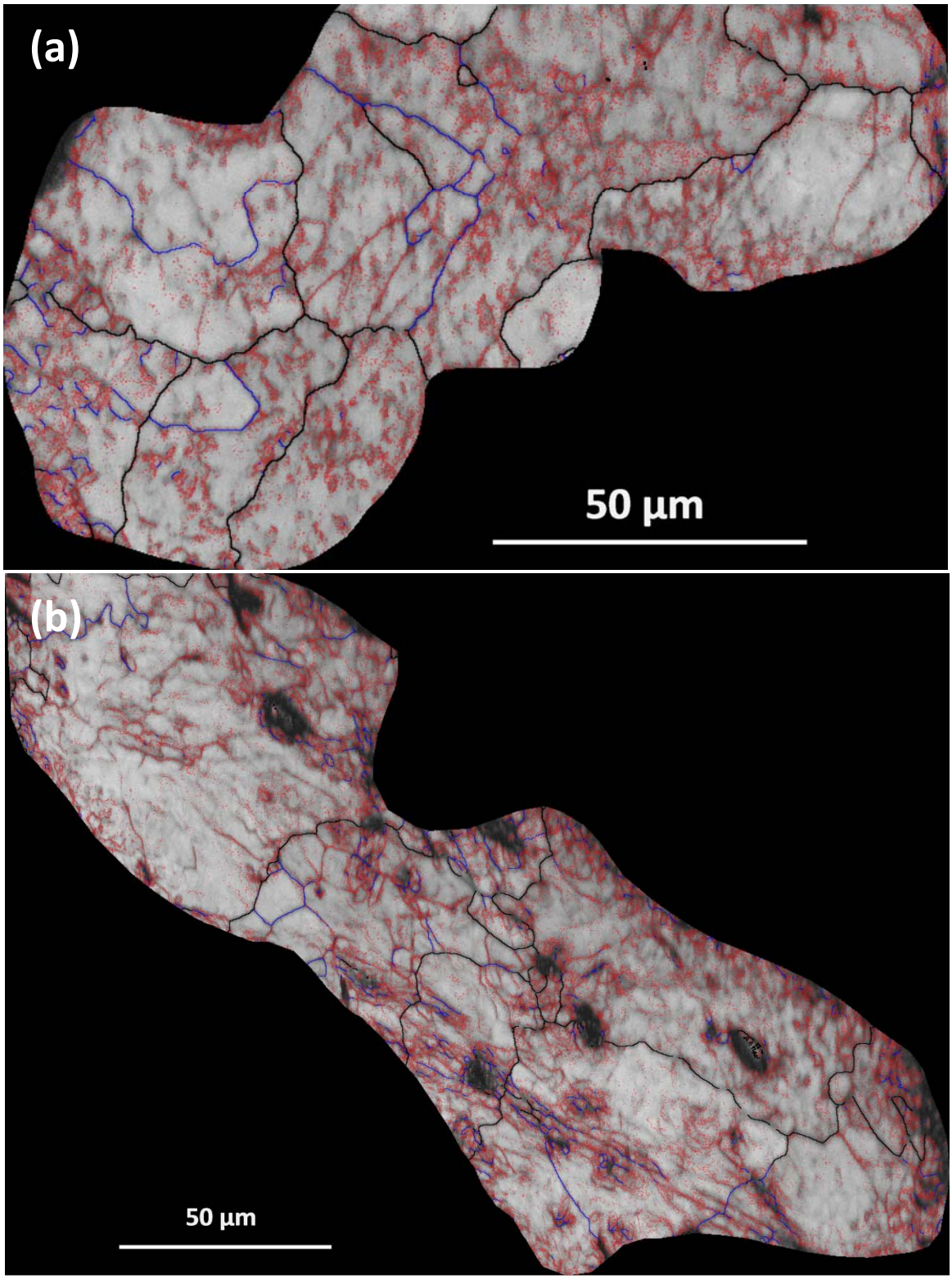

Fig. 5.2 Grain boundaries superimposed on band contrast patterns of cross section of (a) the as received particle and (b) the particle milled for 15 min, which their IPF pattern were shown in Fig. 5.1. Boundaries with misorientations of 1-5^{o}, 5-15^{o} and 15-62^{o} are presented by red, blue and black, respectively.

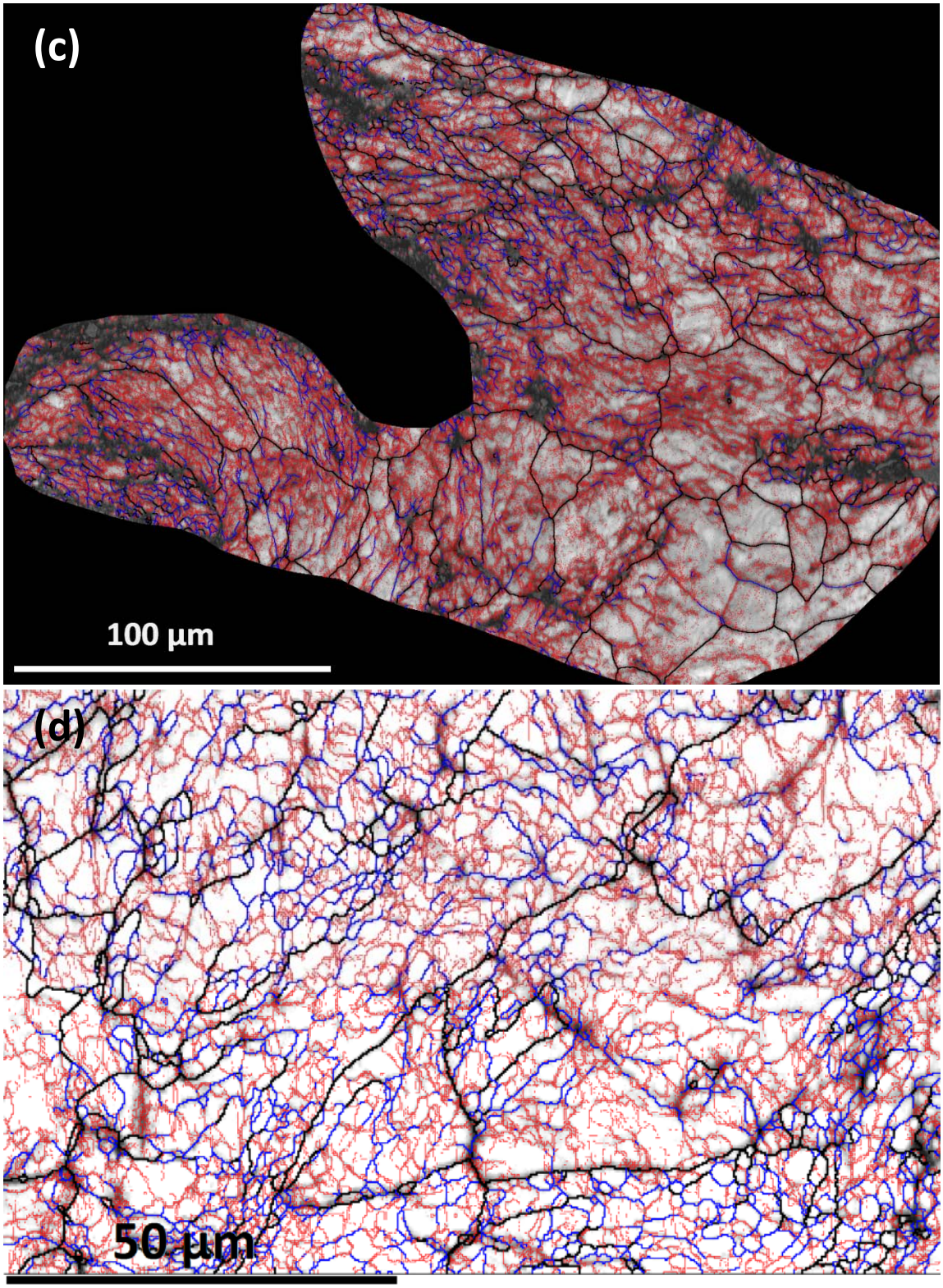

Fig. 5.2 Continued: Grain boundaries superimposed on band contrast patterns of cross section of (c) 30 min and (d) 1h milled particles, which their IPF pattern were shown in Fig. 5.1. Boundaries with misorientations of 1-5^{o}, 5-15^{o} and 15-62^{o} are presented by red, blue and black, respectively.

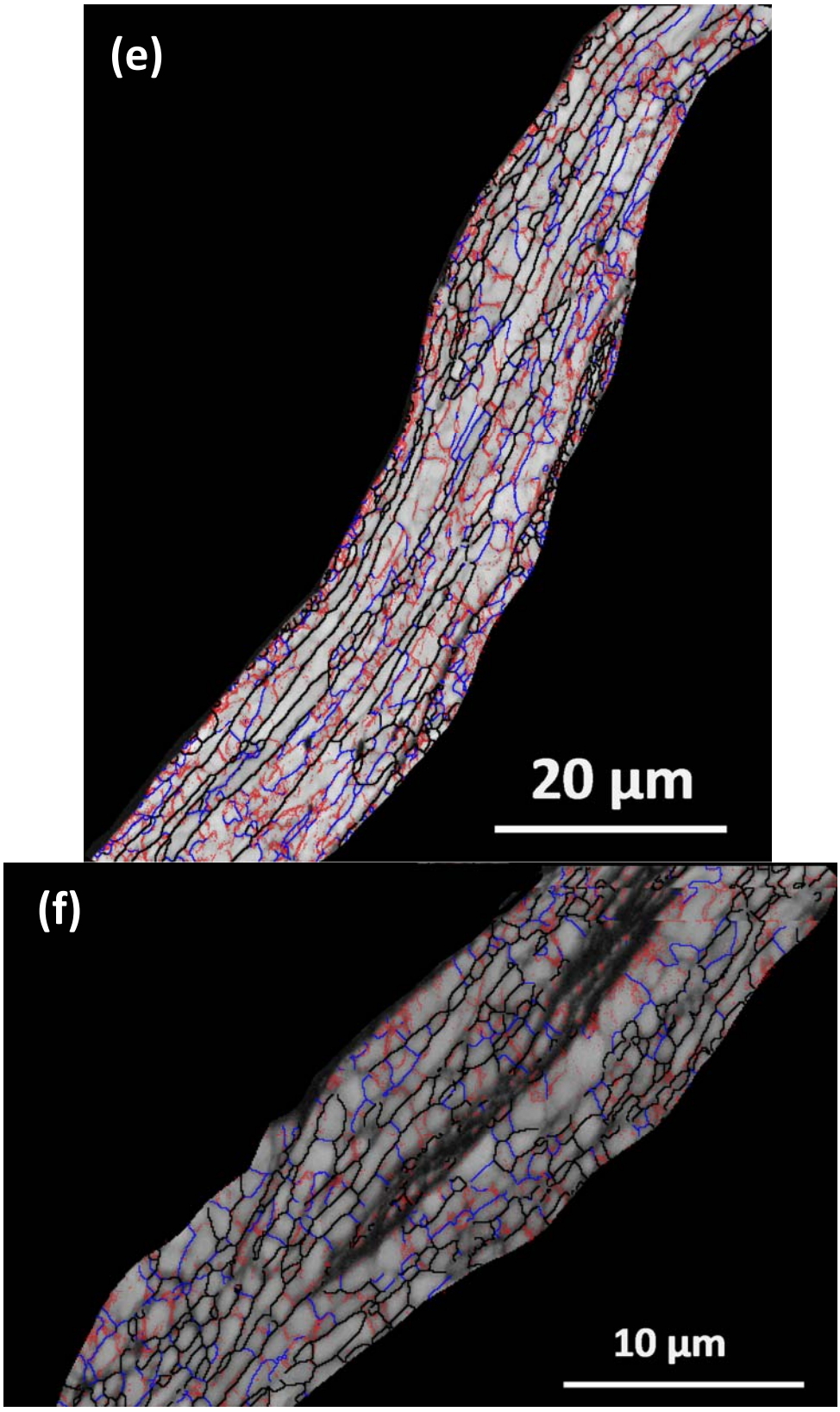

Fig. 5.2 Continued: Grain boundaries superimposed on the contrast patterns of cross section of (e) 2 h and (f) 4 h milled particles, which their IPF patterns were shown in Fig. 5.1. Boundaries with misorientations of 1-5^{o}, 5-15^{o} and 15-62^{o} are presented by red, blue and black, respectively.

Fig. 5.1(b) and Fig. 5.2(b) show the microstructure of a particle milled for 15 min. The average grain size obtained for 15 h milled particles showed a negligible decrease compared to that of the as received one. One can see that in the middle of the particle, deformation caused fragmentation of few grains by inducing LAGBs and MAGBs. Nevertheless, other grains are rather intact after deformation. We observed such a non-uniform deformation in all of the 15 min milled particles. The different deformation response of different grains can be explained by the so called "stable or unstable" crystallographic orientations [193] in relation to the stress direction (that is known just at the time of the impact for a shapeless particle). However, the localization of the deformation at the middle of the particle is more likely because of a considerably inhomogeneous stress applied to the particles during impacts.

A distinct difference between the deformation of particles by ball milling (particles are trapped in collisions of ball-ball or ball-vial) and other deformation methods is that particles are very less constrained compared to a bulk metal deformed by rolling, equal-channel angular pressing (ECAP), extrusion, etc. A typical deformation situation for ball milling can be described as: an equiaxed particle that is compressed between two flat surfaces (two heads-on colliding balls or a ball colliding wall of the vial); the particle is just constrained at two contact points. Such a deformation results in the highest strain at the centre of the particle and less deformation at the free surfaces. There is no simulation in the literature on strain distribution in a metallic compressed particle. However, M. Kazeminezhad et al. simulated flattening of a wire with a circular cross section by a compressive force, and found that the strain at the centre of the section can be up to eight times more than the outer parts. Therefore, not only different particles in the same powder can be deformed to different extents [33, 194], but also different points in one particle may be deformed differently [186]. The different history of deformation of different particles, the non-uniform distribution of strain in a particle, and the presence of the stable and unstable crystallographic orientations explain the significant inhomogeneity that we observed in and among deformed particles in the 15 min milled particles. We observed that this inhomogeneity decreased as the powder was milled for longer durations.

Fig. 5.1(c) and Fig. 5.2(c) show the microstructure of a particle milled for 30 min. Most of the grains are affected by deformation, which resulted in presence of domains of different orientations inside grains. Most of the original grain boundaries are still distinguishable,

however, grain subdivision resulted in a decrease in the average grain size to 68 μm. The presence of misorientations of 1-5^{o} is higher in the 30 min milled particle in a way that in some grains LAGBs exist in all around the grain interior.

Fig. 5.1(d) and Fig. 5.2(d) show the microstructure of a particle milled for 1 h. Each grain includes several domains of different orientations. The misorientation between the domains inside the grains ranges between that of LAGBs to HAGBs. There is a considerable amount of HAGBs inside grains that is not continued to form a circle as a new grain, but made the grains interior banded to regions of different orientations. The boundaries and orientation of the original grains are hardly distinguishable because of the formation of new HAGBs, distortion of the grains shape and formation of various new orientation areas inside the original grains.

Although the reduction in grain size is not considerable (the average grain size measured for the 1 h milled particles is 60 μm), the rearrangement of LAGBs after 1 h milling is noticeable. Contrary to the 15 min and 30 min milled samples where deformation resulted in production and chaotic distribution of LAGBs, Fig. 5.2(d) shows formation of a cellular network of LAGBs for the 1 h milled particle. In addition to LAGBs, some MAGBs and a few HAGBs also contributed to formation of the cellular structure inside grains. Apart from the cell walls that are mostly made from LAGBs, the area inside the cells is almost free of any boundary with a misorientation of bigger than 1^{o}. In other words, the misorientation induced by deformation inside the grains is tidily accommodated by formation and rearrangement of LAGB and MAGB rather than a cluttered presence of LAGBs.

Prolonging the milling time to 2 h completely changes the microstructure of the powder (Fig. 5.1(e) and Fig. 5.2(e)). There is a significant microstructural refinement and the average grain size of the particles reduces to 6 μm after 2 h milling, which is one order of magnitude smaller than that of 1 h milled particles. The majority of the grains are elongated and are sectioned by transverse LAGBS and MAGBs (Fig. 5.1(e)). Such a lamellar structure (or so call “bamboo”, “ribbon” or “pancake” structure) was observed for all of the 2 h milled particles that we analyzed.

Fig. 5.1(f) and Fig. 5.2(f) show the microstructure of a particle after 4 h of milling. The microstructure consists of both lamellar and equiaxed grains. Compared to the 2 h milled sample,

the diameter along the longitudinal and transverse directions of the lamellar grains decreased. Similar to the 2 h milled sample (Fig. 5.2(e)), LAGBs and MAGBs are mostly aligned with the transverse direction of the high aspect ratio grains. However, contrary to the 2 h milled sample, HAGBs also section the high aspect ratio grains, which results in a decrease in the aspect ratio and grain size of the 4 h milled sample. An average grain size of 2.3 μm was measured for the 4 h milled particles.

5.5.2. Formation of the Lamellar Structure

During ball milling particles were continuously impacted in random directions. However, the formation of a lamellar structure (Fig. 5.1(e) & (f)) implies that at some point the strain was accumulated in a particular direction. Our SEM observation showed that most of the particles started flattening after 30 min and changed to thin flakes after 2-4 h of milling [117]. T. H. Courtney formulated the amount of strain that a metallic particle undergoes by one impact [174]:

$$\varepsilon = -ln\left\{1 - \frac{vR}{h}\left(\frac{\rho}{H_v}\right)^{1/2}\right\} \quad (5.1)$$

where ε is the strain, v is the balls speed (m/s), ρ is the density of the balls (7.8 gr/cm^3), h = 2D where D is the particle diameter (for the as received powder: 192 μm), H_v is the hardness (0.226 GPa) and R is the ball radius (17 mm).

The average velocity of balls was formulated by Y. Lin et al [195]:

$$v = 0.5\pi Fd \quad (5.2)$$

where d is radius of the vial (0.037 m) and F is the rotational frequency (3.3 sec^{-1}), thus, an average velocity of 0.195 m/s is calculated for the balls. Putting the average velocity in Eq. 5.1, an average strain of 0.05 is obtained. For deformation of an equiaxed particle, strain can roughly be obtained by $\ln(D/D_f)$ [196], where D_f is the diameter of the particle after deformation induced by one impact. Thus, a strain of 0.05 changes the initial particle size of 192 μm to 182 μm. Such a change is very smaller than the enough strain to make an equiaxed particle flattened with elongated grains as seen in Fig. 5.1(e) and Fig. 5.1(f). Considering an average strain of 0.05, we calculated the particle size after the impact and put it in Eq. 5.1, which gives a new amount of strain for the next impact with the same velocity. The new amount of strain was used to obtain

the particle diameter after the second impact, and we continued this calculation to understand approximately how many impacts are needed to reduce the diameter of the particle to half. The result of this calculation is presented in Table. 5.1; one can see that at least ten impacts (cumulative strain: 0.71) with the average velocity are needed to make an equiaxed as received particle to a semi-disk shape one. We considered that the hardening of the particle is negligible, otherwise even more impacts are needed. On the other hand, impacts during milling are randomly oriented toward an equiaxed particle and it is highly improbable that a particle receives ten successive impacts in the same direction. Therefore, flattening of the particles and formation of a lamellar structure cannot be explained by accumulation of small strains.

Table. 5.1 Effect of the average velocity impacts on the applied strain and consequent change in diameter of a particle, calculated by Eq. 5.1 and Eq. 5.2.

	As Received	Impact 1	Impact 2	Impact 3	Impact 4	Impact 5	Impact 6	Impact 7	Impact 8	Impact 9	Impact 10
strain	0	0.052	0.054	0.058	0.061	0.066	0.070	0.076	0.082	0.090	0.099
Particle Diameter (μm)	192	182	172.2	162.5	152.7	142.9	133.2	123.4	113.6	103.8	94

Considering the distribution of balls velocities instead of applying the average velocity, the flattening of the particles can be explained. Simulation of ball motion in vials showed that although an average velocity can be determined for the balls, the distribution of velocities ranges between 0 to a maximum velocity (v_{max}) [54, 197]. Y. Lin et al. calculated v_{max} [195]:

$$v_m = 2\pi FR \tag{5.3}$$

A v_{max} of 2.1 m/s is calculated and a maximum strain of 0.79 is obtained by Eq. 5.1, which means an as received particle can be compressed to 87 μm by one maximum velocity impact. After a particle is partially flattened by a maximum velocity impact, the strain induced by lower velocity impacts also can contribute in further flattening. That is because a flattened particle is more likely to be impacted in a direction almost perpendicular to the disk surface rather than parallel to that. Accordingly, although the smaller impacts can deform the particles, at least one impact with a velocity about the maximum is needed to initiate the flattening. We observed the lamellar structure for all of the 2 h and 4 h milled particles. Therefore, we conclude that

deformation of particles occurred by at least one big impact followed by smaller strains built up upon the initial flattening strain.

This should be noted that although the compressive impact is known as the main deformation mode during ball milling [44, 198], particles may also be deformed by a shear force between balls or a combination of shear and compression [55, 195]. Nevertheless, in all different possible modes of deformation of particles, a disk shape particle is more likely deformed along the disk surface. Therefore, after receiving one big impact that makes the particle flattened, smaller impacts mostly accumulate in the same direction and the particle is more flattened and grains are more elongated. These disk shape particles are fractured to smaller flakes by further milling [41, 117].

5.5.3. Calculation of the Length of Boundaries

Researchers have widely used misorientation distributions obtained by EBSD to evaluate microstructural evolution during deformation. This evaluation is usually based on comparison of the relative (or normalized) misorientation distribution [199-204]. This distribution simply shows how the ratio of different misorientations changes by deformation, which can be generated by most post processing software. However, this method of evaluation has limitations; it does not give the actual length of grain boundaries with different misorientations. Moreover, the comparison of relative frequencies of misorientations can be misleading. For example, let consider the following situations for a sample during a processing: a) Length of HAGBs increases while length of LAGBs is constant. b) Length of LAGBs decreases while length of HAGBs is constant. c) Length of LAGBs increases and length of HAGBs increases by a higher extent. In all of the three assumed situations, the relative frequency of misorientation distribution shows that HAGBs increases compared to LAGBs, but without capability to distinguish which situation occurred.

D. Synder et al. also noted this insufficiency of comparisons between the relative misorientation distributions [205]. L. Sun et al. used the actual value (occurrence) of the misorientations by reporting frequency per area [206]. However, even reporting the occurrence of each misorientation range does not provide the actual length of different boundaries.

Moreover, the comparison between frequency of misorientations per area for different samples must be limited to EBSD patterns of the same area and the same step size (pixel size).

In this work, in order to have the actual length of different boundaries per area, we performed a simple processing on the misorientations data. Firstly, one needs to understand the algorithm by which the software obtain misorientation distribution: 1) the misorientation of every pixel is measured compared to its neighbours, 2) the cumulative frequency (occurrence) within every misorientation interval (or the binning, for example 1-2^o, 2-3^o, 3-4^o, …, which is user defined) is calculated, 3) the cumulative frequency in each interval is divided to the occurrence of all misorientations and the result is plotted as the relative frequency distribution.

In order to calculate the actual length of different boundaries per area, firstly, the frequency of counted pixels in each misorientation interval should be multiplied by the pixel length (step size), which gives the length of the boundary with that particular misorientation. Then the total number of pixels in the pattern should be multiplied by one pixel area (square of the step size), which gives the total area of the pattern. The total area of the pattern should be multiplied by the ratio of number of indexed (solved) pixels to the total number of pixels so that the area of the pixels that are not solved is excluded from the calculation. Finally, the length of the boundary obtained in the first step should be divided to the area obtained in the last step. The method is summarized as Eq. 5.4:

$$D_{A_i} = \frac{N_i \times d_s}{N_T \times {d_s}^2 \times R_s} = \frac{N_i}{N_T \times d_s \times R_s} \tag{5.4}$$

where D_{Ai} is the total length of boundaries with misorientation i per area, N_i the frequency of counted pixels with misorientation i, d_s the step size, N_T the total number of pixels in the pattern and R_s is the ratio of the indexed pixels to the total number of pixels. This method can calculate and compare the boundary length per area for EBSD patterns with different area, step size and hit rate.

5.5.4. Evolution of Boundaries by Milling

We used Eq. 5.4 to calculate length of different boundaries per area, and added up the length of boundaries within the range of 1-5^o, 5-15^o and 15-62^o as the overall length of LAGBs, MAGBs and HAGBs, respectively. EBSD patterns of at least three particles from each powder

were used to calculate the average length per area. Fig. 5.3 shows the effect of milling time on the overall length of LAGBs, MAGBs and HAGBs per area. The error bars represent the standard deviation of the measurements.

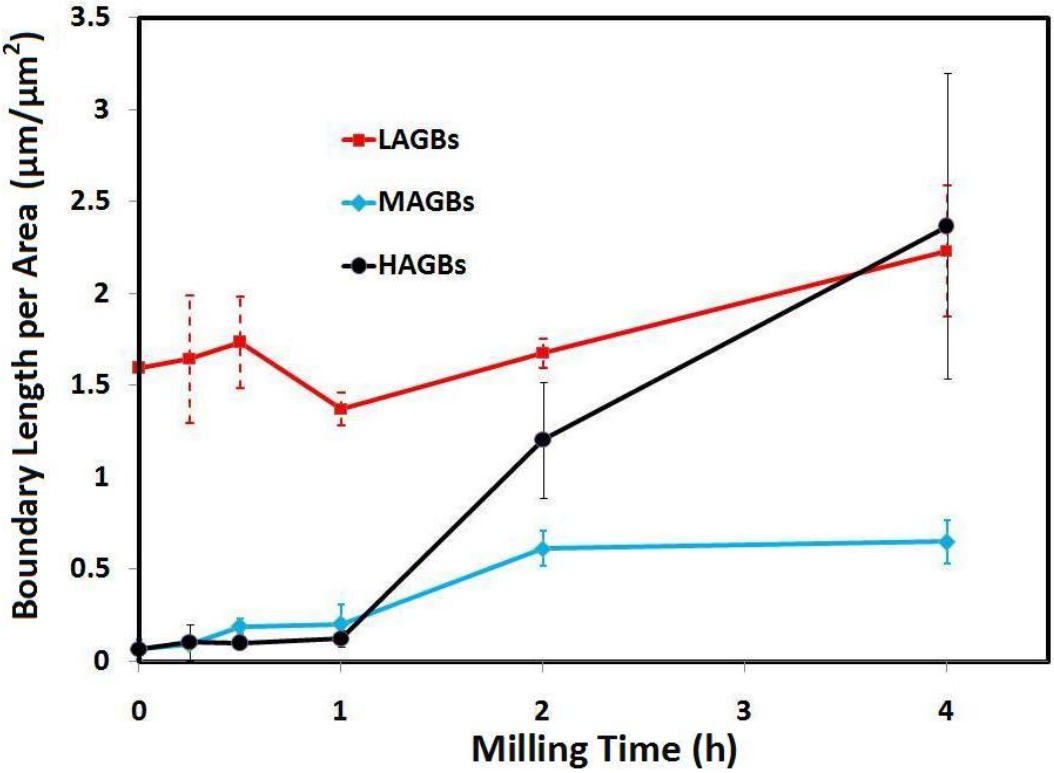

Fig. 5.3 Effect of milling time on the overall length of LAGBs (1-5°), MAGBs (5-15°) and HAGBs (15-62°) per area calculated by Eq. 5.4. The error bars represent the standard deviation of the measurements.

During the first 30 min of the milling, LAGBs increases slightly (from 1.6 μm/μm^2 to 1.7 μm/μm^2), which can be regarded as insignificant considering the error bars. Prolonging milling up to 1 h results in a decrease in length of LAGBs to 1.37 μm/μm^2. The length of HAGBs is very small in the as received sample (0.066 μm/μm^2) and is almost doubled by 1 h milling (0.12 μm/μm^2). The length of MAGBs is tripled by 1 h milling and increases to 0.2 μm/μm^2. Further milling up to 4 h results in a significant increase in length of LAGBs, MAGBs and HAGBs.

5.5.4.1. Deformation and Dynamic Recovery at Early Stages of Milling

The slight increase in the length of LAGBs during the first 30 min of milling (Fig. 5.3) is ascribed to the effect of deformation on production of dislocations, which consequently produces dislocation walls that are distinguished in EBSD patterns as boundaries with small

misorientations. Fig. 5.4 (a) & (b) show the higher magnification patterns of the areas marked with rectangles in Fig. 5.1(a) and 1(b). One observes a presence of noticeable length of LAGBs at the regions that because of deformation are oriented rather differently compared to their surrounding area.

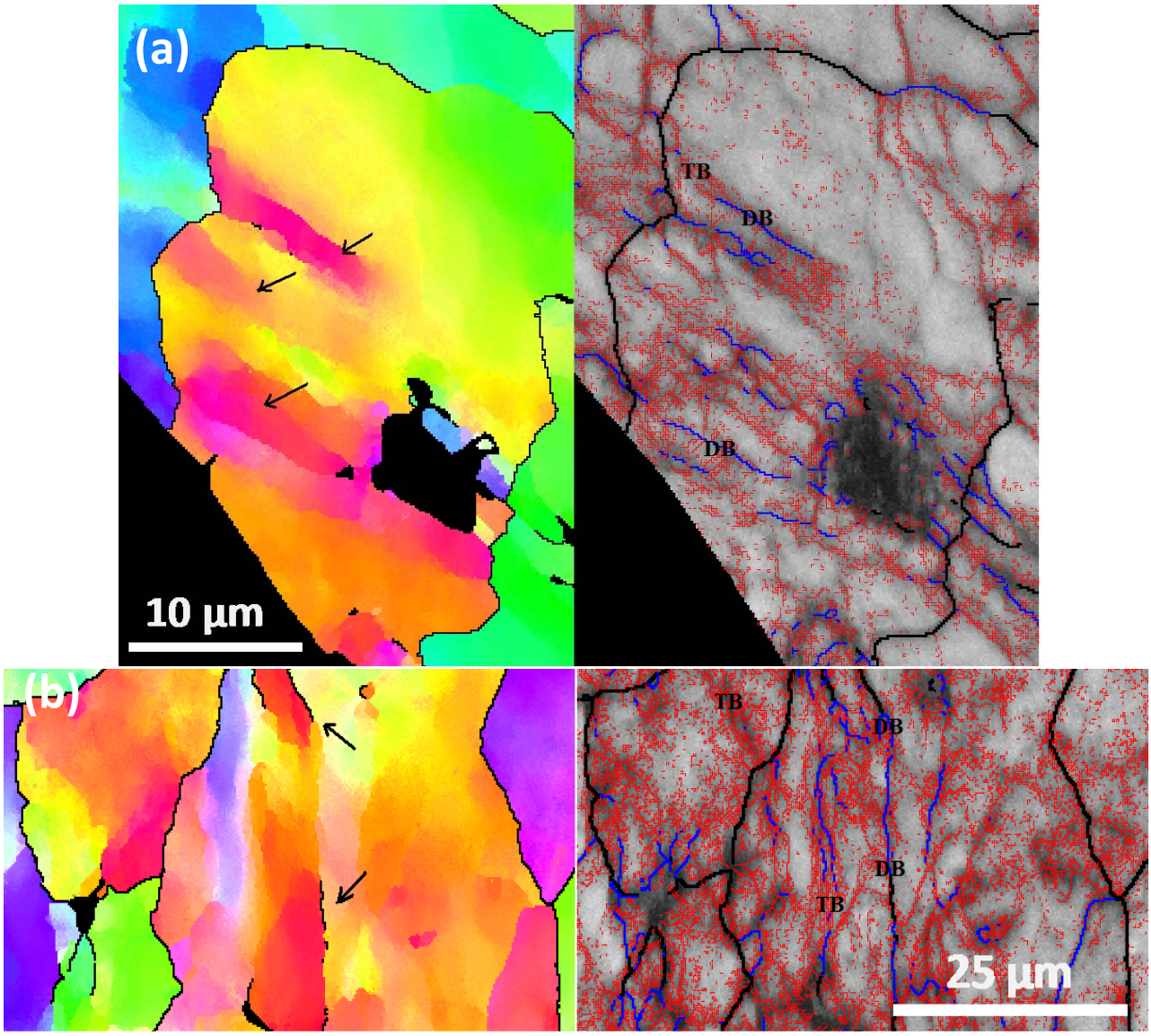

Fig. 5.4 High magnification IPF and band contract patterns of the areas marked with rectangles in Fig. 5.1(a) and 1(b). The arrows mark deformation bands. "DB" represents deformation band induced boundaries, and "TD" represents transition bands.

It has been established that deformation of an FCC metal with high stacking fault energy (such as aluminum) occurs through slip. Slip occurs through dislocations glide, i.e. in each grain

that deforms dislocations are generated from sources (e.g. grain boundaries), and glide inside the grain to accommodate the applied strain. This mechanism increases the amount of dislocations inside grains, which consequently increases instability of the microstructure. For the medium and high stacking fault energy metals, dislocations can cross slip and climb, which help them to decrease the instability by rearranging themselves as a low energy dislocation structure (LEDS) [207-209]. This rearrangement of gliding dislocation to dislocation boundaries results in formation of a cellular structure, which the cell walls are dislocation boundaries and there are no much dislocations in the cells interior [183, 210]. These boundaries that formed by mutual trapping of gliding dislocations are so called incidental dislocation boundaries (IDBs) [211]. Further deformation adds more dislocations to the cell walls, which can increase their misorientation and change them to LAGBs.

Fig. 5.4 shows that ball milling for 15 and 30 min resulted in introducing new LAGBs cluttered at the deformed regions of the particles. Further milling up to 1 h results in rearrangement of LAGBs to a tidy cellular structure (Fig. 5.2(c)). This rearrangement includes annihilation of LAGBs in the interior of cells, which as Fig. 5.3 shows, consequently results in a decrease in the length of LAGBs for the particles milled for 1 h. Accordingly, we conclude that dynamic recovery occurred during 30 min to 1 h of milling that resulted in a decrease of 20% in the length of LAGBs.

5.5.4.2. Grain Subdivision by Deformation Banding

Formation of IDBs by deformation is non-crystallographic, i.e. they are not aligned to any particular direction and their formation is not to accommodate any texture dictated by deformation. Because of their small misorientation, IDBs are categorized as LAGBs, however, it does not mean that all the LAGBs observed in Fig. 5.2 are IDBs. Deformation banding can also generate boundaries that, contrary to IDBs, are to accommodate the strain and depend on the orientation and rotation of grains. Basically, deformation banding occurs in large grains that are unstable due to their crystallographic orientation [201]. For such a grain, it is energetically easier to split to regions (bands) that deform with fewer than five independent slip systems, but those regions collectively accommodate the applied strain over the constrained grain [200, 212]. Fig. 5.4 shows that deformation banding (marked with arrows) occurs in the 15 min and 30 min milled particles. The change in the orientation can be sharp, which results in deformation band

induced grain boundaries. The MAGBs and HAGBs marked by DB in Fig. 5.4 illustrate formation of boundaries by deformation banding. If the change in orientation occurs gradually with a cumulative misorientation from one side of the band to the other side, it is named transition band [212]. Example of transition bands are marked by TB in Fig. 5.4. Therefore, in addition to formation of the LAGBs that are IDBs and have no textural preferences, boundaries of low to high misorientations can be formed to accommodate emergence of different orientations inside grains. Because of contribution of the latter group of the boundaries in accommodating the strain, they are called geometrically necessary boundaries (GNBs) [211].

The microstructure of the 15 min, 30 min and 1 h milled particles has similarities and differences compared to the typical microstructure of bulk aluminum alloys deformed to low or moderate strains. They are similar because grain subdivision by GNBs and formation of IDBs occur in the milled aluminum particles. However, contrary to the previous works, we did not detect formation of cell blocks containing IDBs that neatly fragment large grains by cell block boundaries (GNBs) aligned in a particular direction [207-208, 212]. For example, in the grain named "I" in Fig. 5.1(d), one observes formation of three banded areas (A, B and C) that are aligned to different directions and appear to have experienced different extent of deformation. Formation of such a microstructure can be explained by the fact that during ball milling, a particle may be repeatedly strained in different directions with an inhomogeneous distribution of the strain in the particle.

5.5.4.3. Low Angle Grain Boundaries in the Highly Strained Particles

Fig. 5.3 shows that after the minimum at 1 h, the length of LAGBs increases by further milling up to 2 h and 4 h. This means after the dynamic recovery that annihilated some LAGBs, further deformation induced formation of more LAGBs. The increase in the LAGBs length in a highly strained microstructure sounds contrary to the previous works that observed a significant decrease in relative frequency of LAGBs after deformation to large strains [200-202, 204]. Apart from the differences between deformation of bulk materials and deformation of particles by ball milling, this contradiction can be explained by the difference in the methods for presentation of the misorientation distribution. As explained in section 5.5.3, we used the actual value of grain boundaries in this work instead of the relative misorientation distribution that is usually used in the literature. For the sake of comparison, the data on relative frequency of misorientations is

also presented. Fig. 5.5 shows the effect of milling time on the relative frequency of misorientations of 1-5°, 5-15° and 15-62°. One observes that unlike the trend in Fig. 5.3, Fig. 5.5 shows that the relative frequency of misorientations of 1-5° continuously decreases by milling, which is similar to what presented by the previous works. However, comparing Fig. 5.3 and Fig. 5.5, one realizes that the decrease in the relative frequency of misorientations of 1-5° is not because of a decrease in the length of LAGBs, but because the length of HAGBs increases by a higher extent compared to the increase in LAGBs. This comparison clarifies that drawing a conclusion based on changes in relative frequency of misorientations can be misleading.

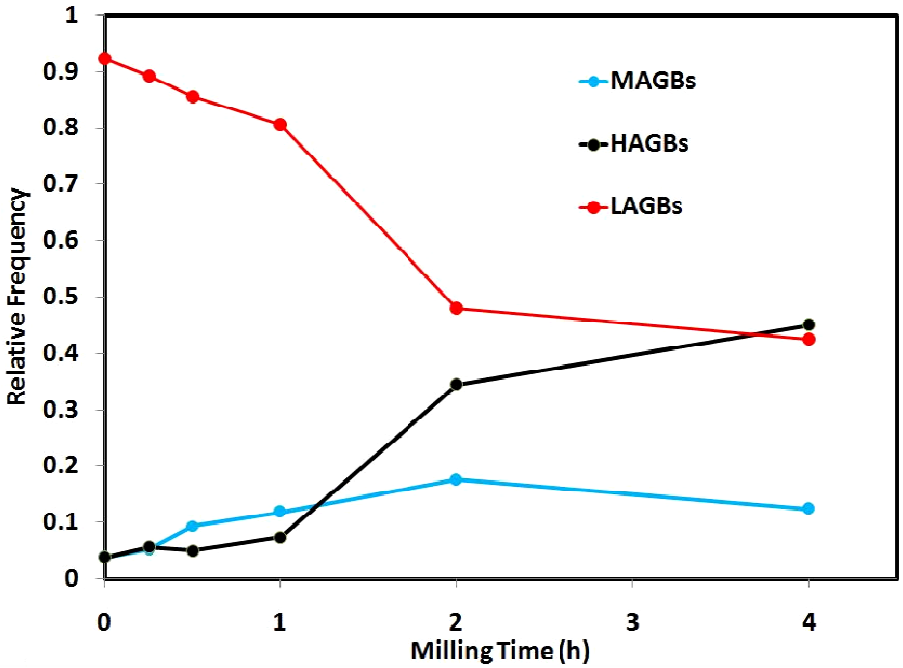

Fig. 5.5 Effect of milling time on the relative frequency of LAGBs (1-5°), MAGBs (5-15°) and HAGBs (15-62°).

Fig. 5.2(e) and 5.2(f) show that the microstructure of the 2 h and 4 h milled particles includes a cellular network of LAGBs, MAGBs and HAGBs, and is not cluttered by presence of unorganized LAGBs similar to the 15 min and 30 min milled samples. This implies that although deformation primarily is supposed to generate dislocations and consequently dislocation boundaries and LAGBs in the 2 h and 4 h milled particles, dynamic recovery annihilates and reorganizes the produced extra LAGBs so that the internal energy of the microstructure decreases. Therefore, the increase in the length of LAGBs during ball milling up to 2 h and 4 h

cannot be explained by the same explanation used for the increase in the length of LAGBs for the 15 min and 30 min particles.

The increase in the length of LAGBs can be explained by the large changes in orientation inside the lamellar grains. As Fig. 5.1(e) and Fig. 5.1(f) show, the orientation inside the lamellar grains can considerably change from one end to another end of the ribbon like grains. Fig. 5.6 (a) shows higher magnification patterns of the grain marked as "L" in Fig. 1(e). Fig. 5.6(b) shows the change in orientation along the line drawn from point "A" to "B" compared to the point "A". The graph shows that misorientation increasingly changes up to 35^{o} along a length of 45 μm in the longitudinal direction of the grain.

Depending on the stacking fault energy of dislocations, a grain can accommodate a noticeable amount of change in orientation in two ways. For materials with low stacking fault energy, dislocations can be arranged in a diffuse geometric pattern along the slip planes that defines a so-called "Taylor lattice" [207, 211-212]. For high stacking fault energy materials, the easier mobility of dislocations promotes the boundary formation. Therefore, a change in orientation can be satisfied by formation of cell/subgrain boundaries, which misorientation of each boundary is to fulfil a fraction of the overall misorientation. This concept of boundary formation is very similar to that of deformation banding. However, deformation banding, by definition, is fragmentation of a large grain to a banded structure on a coarse scale [212], which is not obviously the case for the rather small ribbon like grains observed in Fig. 5.1(e) and Fig. 5.1(f).

Whether or not the formation of LAGBs/MAGBs in the ribbon like grains can be named as a small-scale deformation banding, these boundaries are to accommodate the misorientation along the longitudinal direction of the grain and thus, they are geometrically necessary for the microstructure. Considering these boundaries as GNBs is contrary to the model proposed by D. A. Hughes and N. Hansen that considered that in the bamboo like structures in highly strained metals "IDBs are sandwiched between long GNBs" [208]. The type of boundaries (GNB or IDB) sandwiched between in the ribbon grains can be distinguished by the overall change in the orientation inside grains. The subgrain boundaries formed between HAGBs can be considered IDBs if there is no significant change in the orientation of a ribbon like grain along its length.

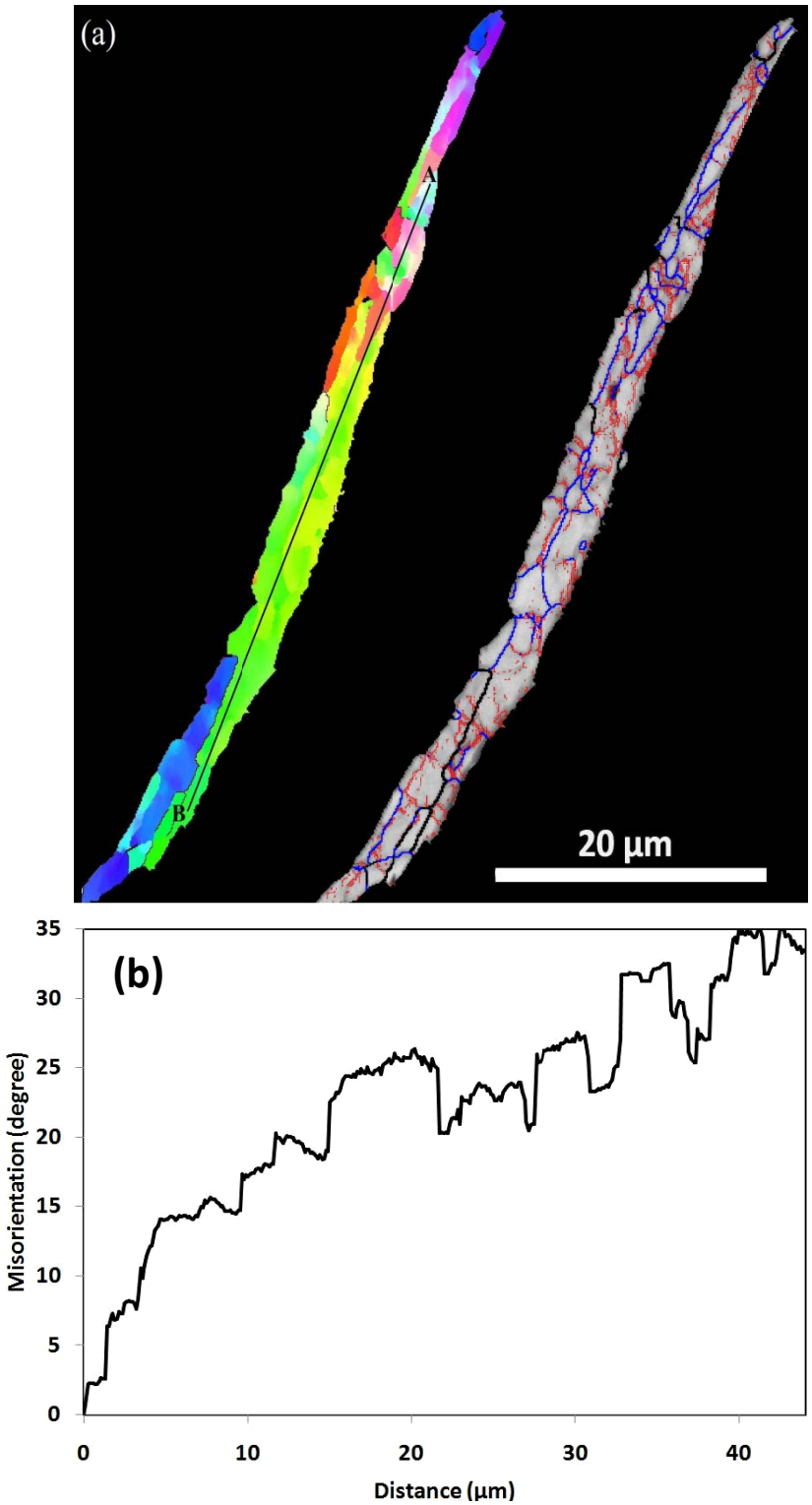

Fig. 5.6 (a) High magnification patterns of the grain marked "L" in Fig. 5.1(e). (b) Misorientation change vs. distance compared to point "A" along the A-B line in the grain.

Such a case was observed by Y. Huang et al. [213] and P.J. Apps et al. [201]; the ribbon like grains are subdivided by subgrain boundaries where there is no significant change in orientations along the longitudinal direction of the grains. Those subgrain boundaries can be considered as IDBs formed by mutual trapping of dislocations to decrease the instability of the microstructure. On the other hand, the MAGBs and LAGBs observed in Fig. 5.6(a) contributed in the big change in the orientation of the grain. This contribution is presented as accumulating steps in Fig. 5.6(b) toward an end orientation, which each step represents a LAGB or MAGB. Therefore, the increase in the length of LAGBs (Fig. 5.3) in the 2 h and 4 h milled particles is explained by the formation of GNBs that mostly interconnect the ribbon like grains along their transverse direction.

5.5.4.4. Evolution of Medium and High Angle Grain Boundaries during Milling

While the maximum change in the length of LAGBs during milling is limited to 40% of their length in the as received particles, the length of MAGBs and HAGBs changes up to 10 and 36 times compared to their length in the as received particles, respectively. It is known that misorientation of cell boundaries (IDBs) can gradually increase because of addition of more dislocations to the boundaries. However, the rate of increase in misorientation of IDBs is very smaller than that of GNBs [206, 214-215], and a critical increase in misorientation of IDBs has been rejected [211, 216-217]. Therefore, considering the transient nature of IDBs [202, 212], an increase in their misorientation by addition of more incidental dislocations is not considered as mechanism for formation of HAGBs. We consider four mechanisms that contribute in formation of MAGBs and HAGBs: deformation banding, increase in aspect ratio of grains, cold welding of the particles and rotation of subgrains. The first three mechanisms are explained in this section, and rotation of subgrains together with dynamic recrystallization will be addressed in the next section.

Deformation Banding

As explained in section 5.5.4.2, deformation banding introduces HAGBs and MAGBs by subdividing large grains. Fig. 5.4 shows that although deformation banding can form HAGBs, most of the boundaries formed by this mechanism are LAGBs formed in transition bands or MAGBs. One cannot ascribe the increase in the length of HAGBs and MAGBs after 2h and 4 h

of milling to deformation banding because the grain size of those samples (D_{2h} : 6μm, D_{4h} : 2.6 μm) are too small for deformation banding. The HAGBs in the banded areas (for example marked by arrows in Fig. 5.1(d)) may be directly formed by deformation banding, or may be evolved through rotation of a previously deformation banded area (with a medium or low misorientation compared to the original grain) to a higher misorientation, which produces HAGBs. Even if all the MAGBs and HAGBs added to the microstructure by 1 h milling (a sum of 0.32μm/μm^2) are considered as the result of deformation banding, the contribution of deformation banding in the overall length of produced HAGBs and MAGBs by 4 h of milling (3.1 μm/μm^2) is not significant.

Increase in Aspect Ratio of Grains

Elongation of the original grains increases the length of HAGBs in the microstructure. J.Y. Chae et al. [218] and P.S. Bate et al. [219] modeled the effect of strain on increase in the surface area of spherical and tetrakaidecahedronal grains, respectively. Y. Huang et al. [213] and H. Jazaeri et al. [202] also analysed their EBSD observation to separate the "geometry" and "grain subdivision" contributions in the increase of HAGBs during deformation. The above mentioned modeling and experimental analyses on the effect of deformation geometry on length of HAGBs are based on the amount of strain, which is not applicable for elongation of grains in the ball milled particles because the value of strain is not known. Therefore, in order to have an approximate estimate, we simply calculate the geometry effect of deformation on the increase in length of HAGBs through a 2D rectangular model. Let consider a square of length L that is deformed to a rectangular of L×R in L/R (Fig. 5.7(a)). The area is constant while the circumference increases because of the increase in the aspect ratio (R). The increase in the circumference because of the geometry effect (G) can be calculated by Eq. 5.5:

$$G = \frac{\boldsymbol{CircumferenceafterDeformation}}{\boldsymbol{OriginalCircumference}} = \frac{1+R}{2\sqrt{R}} \qquad \text{Eq. 5.5}$$

Using the HKL software, we measured the average aspect ratio of the grains with high angle boundaries; the average increases by milling up to a maximum of R = 4.3 for the 2 h milled particles and then decreases by further milling. Using Eq. 5.5, the maximum increase in the HAGBs length because of the increase in the aspect ratio is 1.3 times. Although this value reflects the effect of increase in aspect ratio on geometrical increase in grain boundaries, the

aspect ratio itself does not necessarily reflect the effect of strain. That is because some high aspect ratio grains can be divided to smaller segments by shear banding or pinch-off mechanism. We did not observe shear banding in the deformed particles, but the pinch-off mechanism occurs in the 2 h and 4 h samples. Considering that the pinch-off mechanism reduces the aspect ratio of the ribbon grain, the 1.3 times, at the very least, is the increase in length of HAGBs because of the geometry effect of straining.

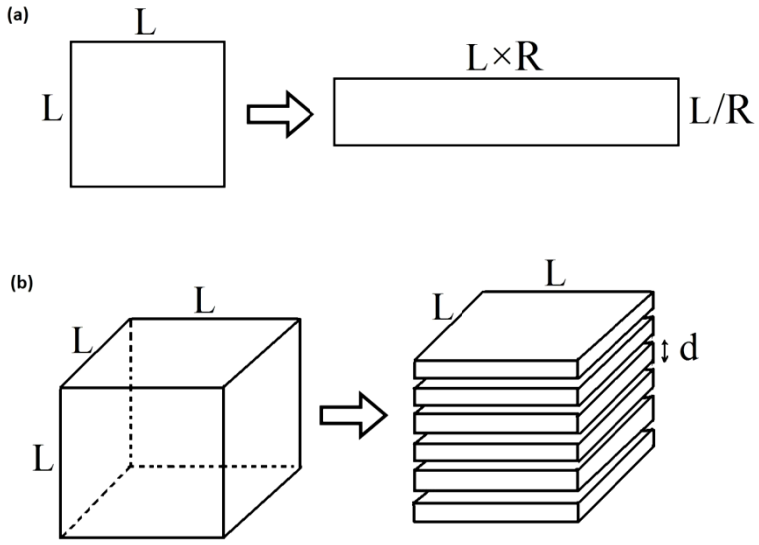

Fig. 5.7 Schematics on (a) effect of increase in aspect ratio, and (b) effect of formation of a laminated structure on increase in the length of boundaries.

Cold Welding of the Particles

At the beginning of the milling, particles are only deformed by impacts (the 15 min, 30 min and 1 h milled samples). Further milling up to 2 h and 4 h results in fracture and cold welding of the particles in addition to deformation. That means each particle in the 2 h or 4h milled powders is formed by cold welding of many fragments from the previously deformed particles. This process is somewhat similar to accumulative roll bonding (ARB), in which the final sample is formed by cold welding of deformed layers during rolling. Fig. 5.8 (a) shows the SEM image of the cross section of a 4h milled particle. One observes presence of cold welded layers that are mostly aligned in a particular direction. To illustrate the width and abundance of layers, we highlighted boundaries of the layers with black lines for a small area of the particle.

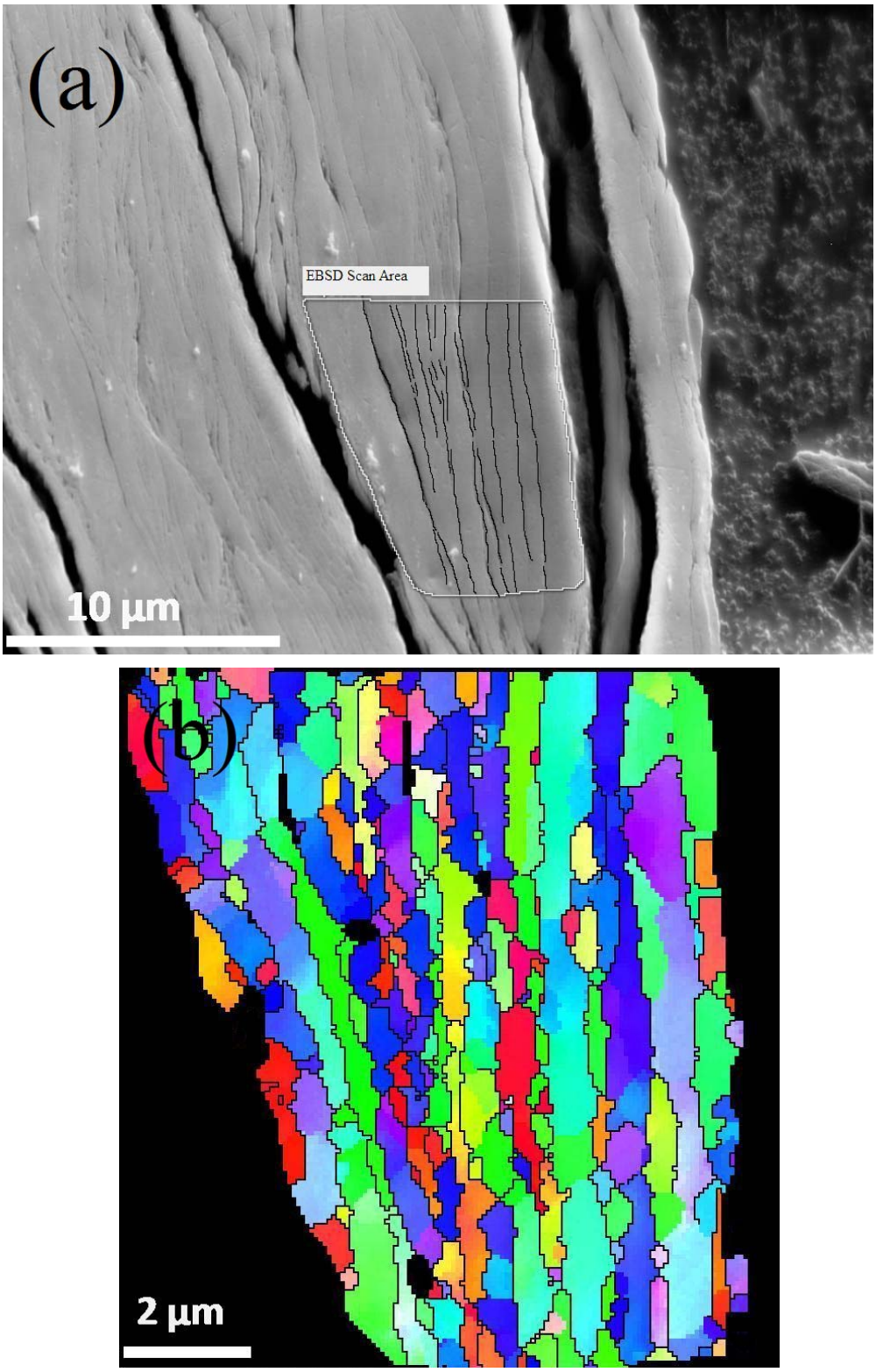

Fig. 5.8 (a) SEM image of cross section of a 4 h milled laminated particle. The lines in the highlighted area represent the boundaries between the cold welded layers. (b) IPF pattern of the highlighted area.

Cold welding of randomly selected particles most probably results in formation of boundaries between them. In order to estimate the extent of the produced boundaries by cold welding of the layers, we compare a non-laminated cube shape particle with a laminated one formed by layers with a thickness of d (the schematic in Fig. 5.7(b)). This schematic represents a ball milled laminated particle by a laminated cube that all of its layers have the same thickness. Although the assumptions partially deviate from the reality of the particles (milled particles are shapeless and the thickness is not the same for all the layers), the model still approximately represents the length of boundaries produced by cold welding. Presuming that all the layers form boundaries (low to high misorientations) by cold welding, the length of boundaries added to the cube (D_L) because of the laminated structure is obtained by:

$$D_L = \frac{\frac{L}{d}}{L^3} \times L^2 = \frac{1}{d} \qquad \text{Eq. 5.6}$$

Using the *Microstructure Measurement* software, we measured thickness of over one hundred layers in the different 4 h milled particles and obtained an average of 1.1 μm. Applying the average thickness in Eq. 5.6, a value of 0.9 μm/μm^2 is approximated for the length of boundaries added to the microstructure because of cold welding.

Although the produced boundaries may have small, medium or high misorientations, formation of HAGBs is more likely. Fig. 5.8(b) shows the EBSD of the selected area in Fig. 5.8(a), which demonstrates the effect of cold welding of the layers on formation of boundaries. The pattern shows that cold welding of the layers forms boundaries that are mostly HAGBs. Considering the estimated value of 0.9 μm/μm^2 for the contribution of cold welding in boundary formation, and comparing with 2.37 μm/μm^2 (length of HAGBs in the 4 h milled sample), we conclude that cold welding contributes significantly to formation of new HAGBs.

5.5.5. Lattice Rotation and Evolution of Boundaries

Deformation of a grain fragmented by LAGBs and MAGBs to subgrains is different from that of a grain that is not subdivided. For the former where the grain contains regions of rather different crystal orientations, the misorientation difference can be enough high to trigger activation of different slip systems for different regions [211]. Accordingly, depending on their locations in the orientation space, different fragments of a subdivided grain can rotate in different

directions [193]. Rotation of subgrains inside a grain to different end orientations can be promoted by three factors, which take place in deformation of the particles by ball milling:

1) Inhomogeneity in amount and direction of applied strain to a subdivided grain assist rotation of different segments to different end orientation, even if the misorientation between subgrains of a subdivided grain is not big.

2) X. Wu et al. argued that for an equivalent increase in strain, a high strain rate results in a higher flow stress compared to a low strain rate [216]. Therefore, rotation is promoted at high strain rates, which is supported by simulation results [220].

3) Presence of large amounts of change in orientation along the ribbon like grains (the 2 h and 4 h milled samples) significantly promotes rotation of the subgrains. For example, considering 35^{o} change in orientation from one end to another end for the grain presented in Fig. 6, it is almost inevitable for the subgrains at two ends of the grain to rotate differently, even if the direction and amount of applied stress is the same from one end to another end of the grain.

Deformation can induce the subgrains with MAGBs to rotate and increase their misorientation by forming an incomplete or full circle of HAGBs. As an example, Fig. 5.9(a) shows the higher magnification of a part of the grain named “B” in Fig. 5.1(e). It shows formation of a region of 111 orientation inside the grain that has mainly an orientation close to 101 (the orientations are referenced to the normal (z direction) to the cross section of the particle). Fig. 5.9(b) shows the presence of HAGBs and their misorientations superimposed on the band contrast pattern of the grain presented in Fig. 5.9(a). One observes that the misorientation between the newly formed 111 region and the original grain ranges between $14\text{-}35^{o}$, which is a rather low misorientation range for HAGBs and implies that HAGBs that separate two regions were newly formed by rotation.

5.5.6. Dynamic Recrystallization (DRX)

We found two mechanisms that break the high aspect ratio grains to smaller segments. The first mechanism is the pinch-off effect in the lamellar structure: the surface tension from transverse LAGBs causes a capillary effect that results in necking followed by pinch-off of lamellar HAGBs, which consequently subdivides a lamellar structure to shorter segments. This

mechanism is so called “geometric dynamic recrystallization” or GDRX [221-222]. Some evidences of the pinch-off effect are marked by arrows in Fig. 5.1(e).

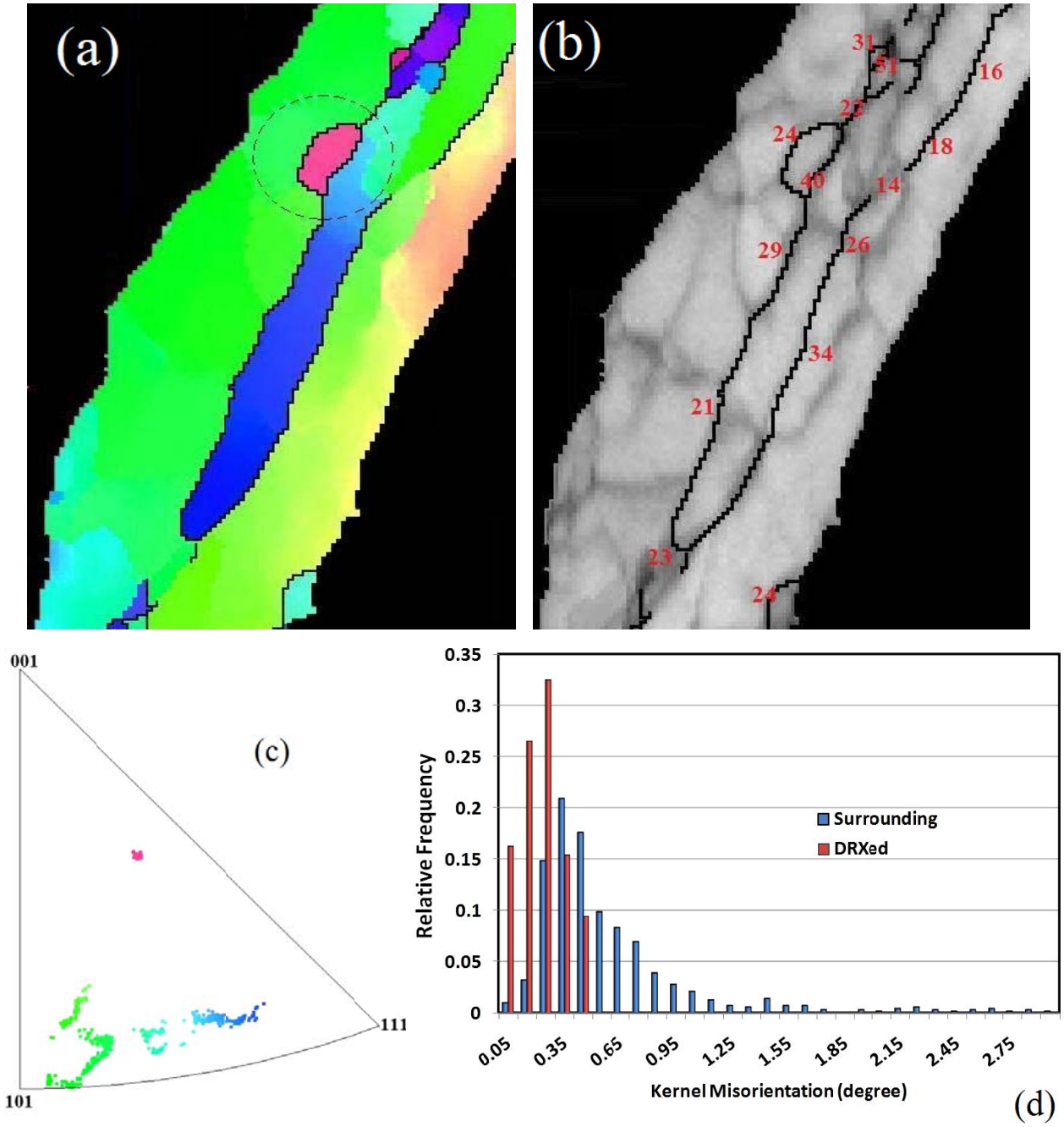

Fig. 5.9 (a) The higher magnification IPF pattern of the grain marked (B) in Fig. 5.1(e). (b) The band contrast pattern of the grain superimposed by HAGBs, numbers show the misorientation of the boundaries. (c) IPF orientation distribution triangle of the area marked by circle in the grain. (d) The Kernel misorientation distribution of the small equiaxed grain compared to that of its surrounding in the marked circle.

The second mechanism for formation of small equiaxed grains out of big lamellar ones is rotation of subgrains, which is so called "continuous dynamic recrystallization" or continuous DRX. It is named dynamic because it occurs during deformation, and it is named continuous because formation of a new equiaxed grain occurs by a gradual increase in misorientation of the subgrain compared to its neighbours rather than nucleation and growth mechanism. The grains formed by this mechanism are considered recrystallized because they are formed by HAGBs, they are not fragmented, and amount of misorientation (dislocations) is low inside them. Fig. 5.1(f) shows presence of many equiaxed small recrystallized grains (some of them are marked by arrows) that their formation is ascribed to DRX.

This should be noted here that lattice rotation does not necessarily result in recrystallized grains. This can be understood by comparison of the small equiaxed grain (Fig. 5.9(a)) with its surrounding matrix. Fig. 5.9 (c) shows the inverse pole figure (IPF) of the area in the circle that covers the small grain and its surrounding as marked in Fig. 5.9(a). Although the area of the small grain is not very different from that of the selected surrounding (the circle in Fig. 5.9(a)), the IPF shows that the orientation of the small grain is focused while that of the surrounding is widely distributed. The continuous spread of orientation (form 111 to 101) confirms that the HAGB formed between the two regions is most probably just formed by rotation. On the other hand, orientation of the small grain is focused and isolated from the matrix orientation. This implies that either mechanisms of recrystallization (GDRX or rotation induced DRX) created a new equiaxed recrystallized grain that is no longer correlated to its matrix.

The difference between a recrystallized grain and a deformed or partially recrystallized one can also be understood by Kernel misorientation distribution. The Kernel misorientation is calculated based on an algorithm that disregards the boundaries in EBSD patterns, but takes into account the misorientation between pixels inside grains. Therefore, the higher amount of dislocations inside the lattice, the bigger Kernel misorientation is obtained for the matrix. Fig. 5.9(d) shows the relative frequency of the Kernel misorientation distribution of the equiaxed grain and its surrounding matrix as marked in Fig. 5.9(a). The graph shows that the Kernel misorientation distribution is extended up to 3^{o} for the surrounding matrix, while it is limited to less than 0.5^{o} for the equiaxed grain.

We examined some other small equiaxed grains from the EBSD patterns of the 2 h and 4 h milled particles; we found that for all of them, the Kernel misorientation is significantly lower than their surrounding matrix, which indicates contribution of DRX in formation of the small grains. Another evidence for occurrence of DRX during milling is that the size and shape of the newly formed small grains are similar to that of the subgrains in the fragmented grains (Fig. 5.2(e) and Fig. 5.2(f)). Accordingly, we conclude that the lattice rotation induced DRX is an effective mechanism in formation of HAGBs and transforming subdivided grains to new smaller recrystallized ones.

Lattice rotation not only can evolve new HAGBs out of former MAGBs and LAGBs, but also can increase the misorientation of newly formed HAGBs. Fig. 5.10 shows the relative frequency of misorientation distribution of HAGBs for the samples milled for different times. Each of the data point in Fig. 5.10 was obtained averaging data from different EBSD patterns of each sample. For the sake of comparison, the distribution of misorientation of HAGBs for a theoretically random textured sample (Mackenzie distribution) is also provided.

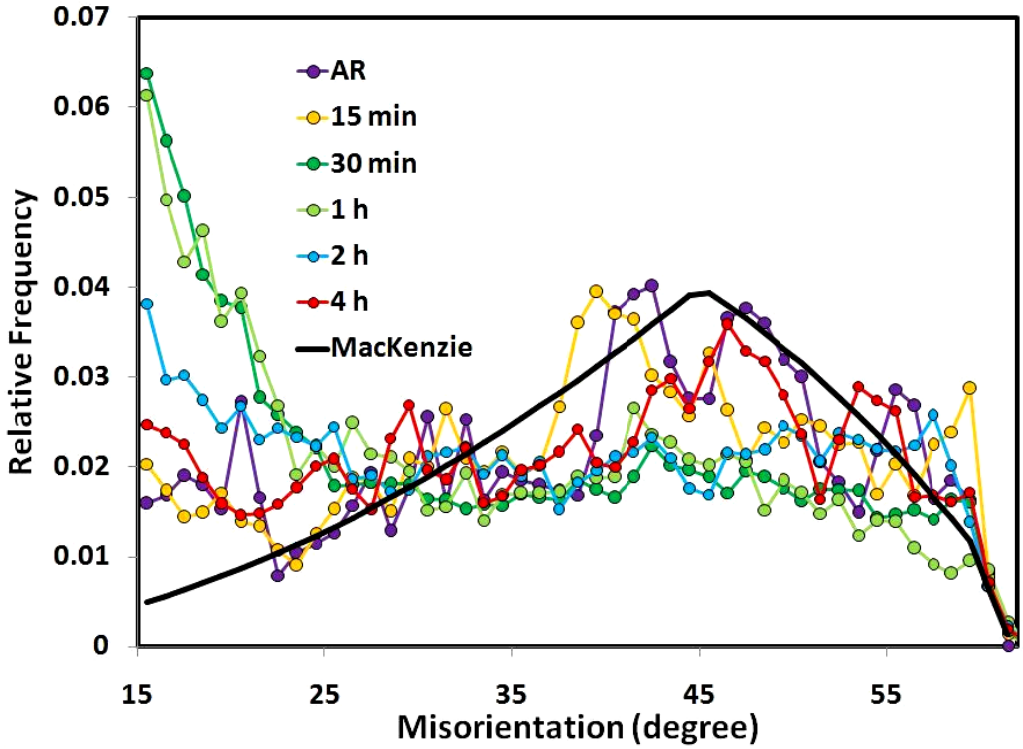

Fig. 5.10 Relative frequency of misorientation of HAGBs for the as received and milled samples. The black solid line represents the Mackenzie misorientation distribution for a theoretically randomly oriented sample.

The graph shows that for the as received particles, the misorientation of the HAGBs is most frequently distributed between 35-55^{o}. Ball milling for 15 min does not change the distribution, which is because the length of produced HAGBs is negligible compared to the original ones (Fig. 5.3). Further milling up to 30 min and 1 h results in a noticeable change in the distribution; there is a rise in the relative frequency of HAGBs with misorientations of 15-25^{o}. This increase is explained by formation of new HAGBs by deformation banding and rotation mechanisms. Since both mechanisms generate new HAGBs of rather modest misorientations, the relative frequency shifts toward lower misorientations because of the formation of new HAGBs. Ball milling up to 2 h and 4 h results in decrease in the relative frequency of HAGBs with misorientation of 15-25^{o}, in a way that the distribution of the 4 h milled sample is similar to that of the as received sample. This change can be explained by formation of new HAGBs because of cold welding of the particles, and rotation of previously formed HAGBs toward higher misorientations compared to their neighbours. Comparing with the theoretically random textured sample (Mackenzie distribution), one observed that the 4 h milled sample still has relatively a higher length of HAGBs of 15-35^{o} and a lower length of HAGBs of 35-62^{o}. This difference can be understood considering the continuous formation of new HAGBs of rather modest misorientations in the 4 h sample, which shifts the distribution toward a relatively higher length of HAGBs of 15-35^{o}.

5.6. Conclusion

Deformation mechanism of aluminum particles during the first 4 h of high energy ball milling was investigated. Since the direction of impacts was random, a significant inhomogeneity in microstructure of the particles milled for short periods of time (15 min, 30 min and 1 h milled samples) was observed. A lamellar structure was recorded for all of the highly strained particles (milled up to 2 h and 4 h), indicating that impacts accumulated the strain in a particular direction. The calculation of the average and maximum amount of strain caused by impacts suggested that at least one impact with highest speed is needed to flatten a particle. Only after the big impact, smaller impacts can contribute to deformation in a particular direction and the microstructure becomes lamellar.

Contrary to some previous works that considered shear banding as the most important mechanism in grain refinement during ball milling, our observation of over 50 deformed particles did not confirm any presence of the shear bands. Instead, slip, lattice rotation and deformation banding were confirmed as being responsible for mechanisms in deformation induced by milling. Deformation resulted in an increase of fraction of LAGBs, which was followed by dynamic recovery that arranged IDBs as a cellular structure. Deformation banding had a major contribution in accommodating the applied strain at the beginning of the milling where the grains were big. As further deformation decreased the grain size to less than 10 μm, rotation of subgrains had an important role in accommodating the strain.

Ball milling for 4 h increased the length of HAGBs by 36 times compared to their length in the as received particles. We distinguished four mechanisms contributing to the increase of length of HAGBs during ball milling: 1) Deformation banding. 2) Geometry effect of the increase in aspect ratio of the grains. 3) Cold welding of the particles. 4) Rotation of subgrains. Among these mechanisms, the first two have rather modest effects while the last two have significant contributions. A gradual increase in misorientation of subgrain boundaries resulted in formation of small equiaxed grains separated by HAGBs from their surrounding matrix. Comparing the shape, size, Kernel misorientation inside the grain and boundary misorientation of the newly formed grains with those of their surrounding matrix, it was established that DRX resulted in formation of the fine equiaxed grains in the extremely strained particles.

CHAPTER 6

MODIFYING THE SHRINKING-CORE MODEL TO EVALUATE THE KINETICS OF THE REACTION BETWEEN ALUMINUM PARTICLES AND HOT WATER

6.1. Overview of Chapter 6

Chapter 2-5 explained the effect ball milling on the microstructure of the particles, effect of microstructure of the particles on the mechanism and electrochemistry of the reaction, and consequently on the hydrogen production rate. Chapter 4 explicitly elucidated that deformation makes the particles active, therefore, particles react with water in faster rate. However, it was also shown that a higher affinity for the reaction does not necessarily promotes the hydrogen generation rate. That is because formation of the hydroxide layer on the particles that can significantly prevent the progress of the reaction. In other words, hydrogen production depends on both thermodynamic and kinetics of the reaction. Investigation of the kinetics of the reaction is essential, because it deals with some factors that basically are not considered in thermodynamic of the reaction (for example effect of diffusion of ion species or growth of hydroxide layer on reaction rate), and can effectively determine the hydrogen production rate.

This chapter, with a focus on diffusion of ion species through the produced hydroxide layer, is to address the kinetics of the reaction. The shrinking-core model is used and modified to predict the effect of reaction time on hydrogen generation.

This chapter is presented as manuscript #4 (Modifying the shrinking-core model to evaluate the kinetics of the reaction between aluminum particles and hot water). The PhD candidate's contributions to the manuscript are: a) Powder preparation and hydrogen measurement tests. b) Developing the model and fitting to the experimental results. c) Reviewing the relevant literature and preparing the manuscript.

The manuscript is to be submitted to the journal of American Ceramic Society.

The references for this chapter along with references from other chapters are provided at the end of the thesis.

Modifying the Shrinking-Core Model to Evaluate the Kinetics of the Reaction between Aluminum Particles and Hot Water

S.S. Razavi-Tousi, J.A. Szpunar

Department of Mechanical Engineering, University of Saskatchewan, S7N 5A9 Saskatoon, Saskatchewan, Canada

6.2. Abstract

The traditional shrinking-core model is modified to fit the situation applicable to the reaction of a deformed aluminum particle with hot water. Two main assumptions are changed compared to the original model. Firstly, it is considered that the thickness of the produced shell is bigger than thickness of the consumed core. Secondly, the diffusion coefficient of the shell is considered to change as the reaction progresses. The modified model is fitted to the experimental data and the result is compared to that of the original model. Finally, the diffusion coefficient obtained from the model is used to calculate the flux of water in the produced shell.

Keywords*: Shrinking-core model, aluminum hydroxide, hydrogen, diffusion*

6.3. Introduction

Due to the applications of reaction of aluminum particles with hot water, researchers have attempted to formulate the kinetics of this reaction. The studies on formulating the kinetics of the reaction can be categorized into two groups. The first group of studies described the reaction through either/both traditional shrinking core or/and diminishing sphere model [62, 84, 223-224]. Although the assumptions considered in the mentioned models are partially similar to the condition of the reaction of aluminum particles with hot water, a mismatch between the experimental data and theoretical fitting was observed [62, 84, 223-224]. The second group of studies described kinetics of the reaction of metallic particle with water based on empirical or diffusion models. The empirical models can result in a good fitting to the experimental data [7, 111, 225]. However, the empirical models do not provide any insight to the mechanism of the reaction. The diffusion model was developed by A. I. Ratko et al. [226], and later was used by H. Nie et al. [227]. Although this model was developed considering the mechanism of the reaction,

H. Nie et al. concluded that the diffusion coefficient changes with the time of the reaction, which indicated “inadequacy of the simplified model” [227].

The approach considered in this study is closer to the first group of studies: the kinetics of the reaction is formulated based on a shrinking-core mechanism of the reaction, which was concluded from observation of the reacted particles. However, there are two main differences between the assumptions of the traditional shrinking-core model and that of the core-shell structure. The first difference is that the diffusion coefficient of the shell (hydroxide layer) formed on the core (aluminum) changes with time. Some researchers found that the grown hydroxide layer is not uniform along its thickness [156-158, 162], which was explained by the change in the density of the formed hydroxide during the reaction time. As the reaction starts, the shell is formed from a hydroxide phase permeable to water. As reaction continues, the hydroxide densifies and pores become filled, therefore, water cannot penetrate anymore through the shell. This change in the porosity of the shell results in a change in the reaction rate, which has to be incorporated into the formulating of the kinetics of the reaction.

The second difference between the assumptions of the traditional shrinking-core model and that of the reaction of aluminum particles with water is about the thickness of the shell. The traditional shrinking-core model was developed based on the leaching process [228], in which the thickness of the shell is the same as that of the consumed core. However, considering the difference between the density of the produced hydroxide layer and the consumed aluminum core, the thickness of the hydroxide layer is bigger than that of the consumed core.

Considering the above mentioned differences, this work modifies the traditional shrinking-core model for the reaction of aluminum particles with hot water.

6.4. Experimental

6.4.1. Ball Milling

The detail of ball milling procedure is similar to the manuscript #1. It is not repeated here in order to keep the thesis concise.

6.4.2. Hydrogen Measurement

The detail of hydrogen measurement procedure is similar to the manuscript #1.

6.5. Development of the Model

The development of the reaction rate equation is based on the assumptions made in the literature for development of the shrinking core model [228]. The model developed here is not a basically new one, but is modified based on the differences in the situation of the reaction of aluminum with hot water compared to that known as the shrinking core reactions.

The assumptions in the traditional shrinking core model are:

1. The reaction occurs between a solid particle and a fluid reactant.
2. The reaction between the particle and the fluid results in formation and growth of a product around the particles.
3. After formation of the shell, the reaction continues through diffusion of fluid (or ion species) through the shell.
4. Diffusion of the fluid (or ion species) through the shell is the controlling step for the reaction.
5. There is no composition/structure change in the shell during the reaction.
6. The thickness of the shell equals to the diameter of the unreacted core subtracted from the diameter of the original particle.
7. The shape of the particle is spherical.
8. For a powder, all particles are the same size and react in the same way.
9. There is no temperature gradient along the shell thickness.
10. The thickness of the shell is the same for different particles.

Among the above mentioned assumptions, #5 and #6 are significantly different from the situation of the reaction of aluminum particles with hot water. Assumption #5 is not applicable to the reaction of aluminum particles with hot water because our observations and literature [145-146] established that porosity of the shell decreases over time. Assumption #6 is not applicable because the volume of the produced hydroxide on the aluminum core is bigger than the volume of the consumed aluminum. Therefore, an equation should be developed to calculate the thickness of the produced hydroxide.

The steady state of the reaction is considered as the time after the so called "incubation time". Incubation time is the time needed for the native oxide film on the surface of the particles to be hydrated by hot water. No hydrogen is generated during the incubation time, but this step is a prerequisite for the hydrogen generation (steady state) step.

The schematic used for the model is presented in Fig. 6.1. The particle on the right represents the situation before the reaction, and the particle on the left shows how the reaction results in formation of a core-shell structure. One can see that in spite of the traditional model that the overall size of the particle is unchanged during the reaction, here it is assumed that the size of the particle grows and the radius of the particle changes from R_o to R.

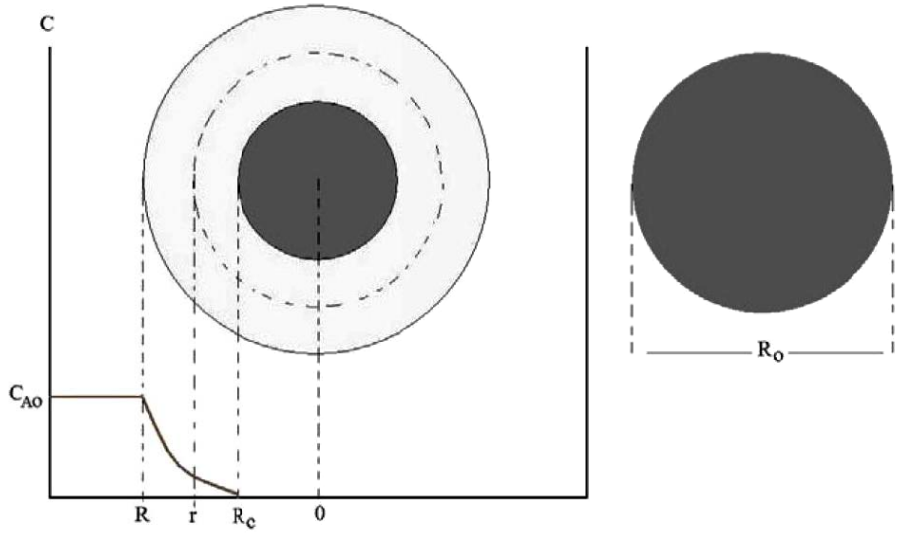

Fig. 6.1 The schematic of the model; the unreacted particle is shown on right and the particle during the reaction is shown on left.

Water molecules are considered as the fluid that reaches to the core and reacts with aluminum. The mass transfer equation at a hypothetical diameter within the hydroxide layer can be written as:

$$\{H_2O_{\text{towards the core}}\} - \{H_2O_{\text{consumed by reaction}}\} + \{H_2O_{\text{generated by reaction}}\} = \{H_2O_{\text{accumulated}}\} \quad (6.1)$$

$$H_2O_{\text{generated by reaction}} = H_2O_{\text{accumulated}} = 0 \quad (6.2)$$

Eq. 6.2 means that no water is generated/accumulated by aluminum-water reaction, therefore;

$$H_2O_{\text{towards the core}} = H_2O_{\text{consumed by reaction}} \quad (6.3)$$

Eq. 6.3 means that the amount of water that diffuses toward the core should be the same as the amount of water consumed by the reaction to generate hydrogen. This equation relates the rate of consumption of aluminum core to the diffusion equation of water in the shell. The correlation between the rate of consumption of aluminum core and diffusion of water will be formulized in Eq. 6.17 to explain the reaction rate based on the diffusion of water.

The first steps of developing the model is borrowed from the literature [228]. The reaction can be written in terms of Eq. 6.4:

$$A(fluid) + bB(solid) = C(solid) + dD(fluid) \quad (6.4)$$

The rate at which A atoms (water atoms) react is determined by the flux of A atoms to the core. Flux by definition is the number of moles (or amount of mass) that passes an area (S) over time (t). At any hypothetical radius (Fig. 6.1) during the steady state, the flux of water toward core can be written as:

$$Q = \frac{dN}{S \times dt} \quad (6.5)$$

where N, Q, and S are the number of moles, flux and the surface area, respectively.

Considering the spherical shape of the particle, S can be replaced by $4\pi r^2$.Moreover, based on Eq. 6.3, the flux of water toward core is equal to the consumption (consumption gives the negative sign) of water by the reaction [228], therefore:

$$-\frac{dN_A}{dt} = 4\pi r^2 Q_A = 4\pi R^2 Q_{As} = 4\pi {R_c}^2 Q_{Ac} \quad = \text{constant} \quad (6.6)$$

where Q_{AS} and Q_{AC} are the flux at the surface of the particle and the boundary of the core, respectively. That means whatever amount of water that enters the shell is consumed at the core-

shell boundary by the reaction with the aluminum core. The flux of fluid atoms can be written by Fick's law:

$$Q_A = D_A \frac{dC_A}{dr} \tag{6.7}$$

where $C_A$is the concentration of A atoms. Putting Eq. 6.7 in Eq. 6.6 yields:

$$-\frac{dN_A}{dt} = 4\pi r^2 D_A \frac{dC_A}{dr} \tag{6.8}$$

Integrating Eq. 6.8 over the thickness of the shell and concentration of A atoms from the surface of the particle to the core gives:

$$-\frac{dN_A}{dt}\left(\frac{1}{R_c} - \frac{1}{R}\right) = 4\pi D_A C_{AO} \tag{6.9}$$

where C_{AO} is the concentration of A at the surface of the particle.

In this step, the first modification to the model will be applied. We need to calculate how the overall thickness of a particle changes with the reaction. The overall volume of the particle (shell + core) can be written as:

$$V_R = V_{Rc} + V_x \tag{6.10}$$

where V_R, V_{RC} and V_x are the overall volume of the particle, volume of the remained core and volume of the produced shell on the core, respectively.

If "n" is the ratio of volume of the produced shell to volume of consumed core, one can write:

$$V_x = n(V_{Ro} - V_{Rc}) \tag{6.11}$$

where V_{RO} is the volume the original particle.

Therefore, considering Eq. 6.10&6.11 one can write:

$$V_R = V_{Rc}(1 - n) + nV_{R0} \tag{6.12}$$

Eq. 6.12 can be written as:

$$\frac{4}{3}\pi R^3 = \frac{4}{3}\pi R_c^3(1 - n) + n \times \frac{4}{3}\pi R_o^3 \tag{6.13}$$

Therefore:

$$R = [(1 - n)R_c^3 + nR_o^3]^{1/3} \tag{6.14}$$

Eq. 6.14 predicts the overall radius of a particle with an initial radius of R_O, which after the reaction the radius of the core reduced to R_C.

Now that the equation for the changes in overall radius of the particle is developed, Eq. 6.9 can be modified by replacing the R value from Eq. 6.14:

$$-\frac{dN_A}{dt}\left(\frac{1}{R_c}-\frac{1}{[(1-n)R_c^3+nR_o^3]^{1/3}}\right)=4\pi D_A C_{AO} \tag{6.15}$$

Number of B moles in the core material (N_B) is related to the density of B atoms (ρ_B: number of B moles in the unit volume of the core material) through Eq. 6.16:

$$N_B=\rho_B V_c \tag{6.16}$$

Considering Eq. 6.3, the amount of water that diffuses toward the aluminum core should be the same as the amount of water that is consumed by the reaction. The amount of water consumed by the reaction is related to the amount of consumed aluminum by Eq. 6.4. Therefore, the consumption rate of B atoms (atoms from aluminum core) can be written as:

$$-dN_B=-bdN_A=-\rho_B dV_c=-\rho_B d\left(\frac{4\pi {R_c}^3}{3}\right)=-4\rho_B\pi {R_c}^2 dR_c \tag{6.17}$$

Therefore:

$$dN_A=\frac{4\rho_B\pi {R_c}^2 dR_c}{b} \tag{6.18}$$

Replacing Eq. 6.18 in Eq. 6.15 gives:

$$-\frac{4\rho_B\pi {R_c}^2 dR_c}{b}\left(\frac{1}{R_c}-\frac{1}{[(1-n)R_c^3+nR_o^3]^{1/3}}\right)=4\pi D_A C_{AO}dt \tag{6.19}$$

In this step the next modification in the model is applied. Since the porosity of the hydroxide layer decreases over time, the diffusion coefficient should be a variable by time rather a constant value. We consider that D_A changes by a hyperbolic function of time (Eq. 6.20). In this equation, D_o is the diffusion coefficient at the time=0, k is a constant that determines the extent of effect of time on the diffusion coefficient and +1 is required to avoid an infinite D_A at the beginning of the reaction:

$$\mathrm{D_A}=\frac{\mathrm{D_o}}{\mathrm{kt+1}} \tag{6.20}$$

and Eq. 6.19 turns to:

$$\left[\frac{R_c^2}{2} - \frac{[(1-n)R_c^3+nR_o^3]^{2/3}}{2(1-n)}\right]_{R_o}^{R_c} = -\frac{bD_oC_{AO}}{k\rho_B}\ln(t+1) \quad (6.21)$$

Defining X_B as the fractional conversion:

$$1-\left(\frac{R_c}{R_o}\right)^3 = X_B \quad (6.22)$$

Eq. 6.21 can be re-written as:

$$n+(1-n)(1-X_B)^{2/3} - [n+(1-n)(1-X_B)]^{2/3} = -\frac{2bD_oC_{Ao}(1-n)}{k\rho R_o^2}\ln(kt+1) \quad (6.23)$$

Eq. 6.23 was mostly developed based on the assumptions made in the literature for the shrinking core model. However, because of the modifications according to the changes in assumption #5 and #6, the final equation is completely different from that of the literature [228].

6.6. Results and Discussion

6.6.1. Fitting the Model

Eq. 6.23 was fitted to the experimental data using the Origin software. The result of the fitting is presented in Fig. 6.2. Moreover, the fitting of the traditional shrinking core model (SCM) to the experimental data is provided.

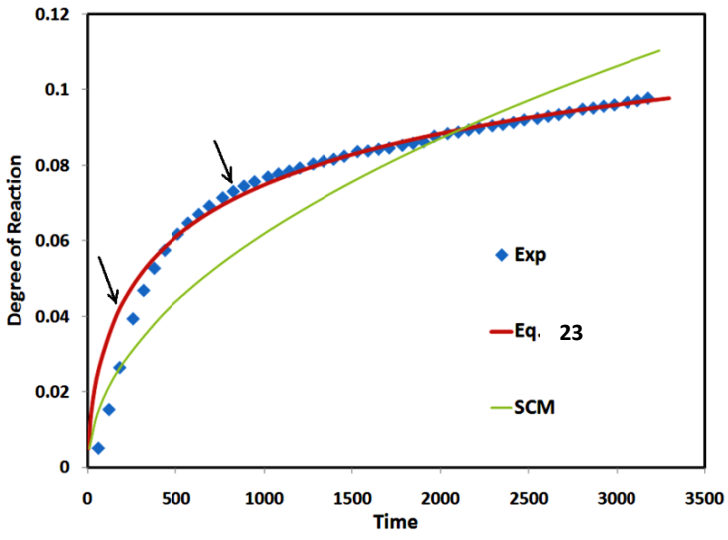

Fig. 6.2 The results of fitting of the traditional shrinking core model (SCM) and Eq. 6.23 on the experimental hydrogen production data.

One can see that modification of the shrinking core model based on changing two assumptions particularly applicable for the reaction of aluminum particles with hot water resulted in a better fitting compared to the original model. However, even the modified model deviates from the experimental data as indicated by arrows. The deviation of the modified model from the experimental data can be ascribed to the following reasons:

1. The model assumes that all particles are perfectly spherical. This is not the case for the 19 h milled particles that are equiaxed, but the shape of the particles is not spherical. Fig. 6.3 shows a high magnification SEM image of one typical particle from the 19 h milled sample before the reaction. One can see that since the particle was formed because of the fracture/cold welding mechanisms during ball milling [41], the surface is rough with many bumps and holes, which makes the shape of the particle rather different from a sphere. This can be the reason behind the second mismatch marked by arrow.

2. The model assumes that for a powder, the size of all particles is the same. However, this assumption also deviates from the situation of the powder used for the experiments. Fig. 6.4 shows the results of size distribution of the 19 h milled particles measured by a laser particle size analyzer. One can see that the distribution is slightly bimodal, and for each peak the distribution is broadened over a range of size.

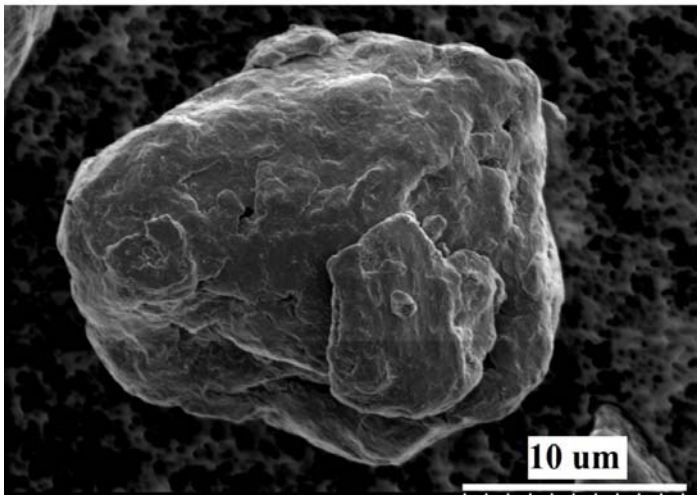

Fig. 6.3 High magnification SEM image of a typical 19 h milled particle before the reaction.

3. The model assumes that there is no gradient in temperature along the hydroxide layer (shell). However, considering the exothermic nature of the reaction and that the reaction occurs at the boundary of the core (aluminum) and shell (hydroxide layer), one

can consider a declining gradient of temperature from the core-shell boundary toward the shell surface. This can be the reason behind the second mismatch marked by arrow.

4. The model assumes that the thickness of the shell (hydroxide layer) is the same in different points of the same particle. However, our observations showed that the shell thickness can be different for different points of the same particle, and from one particle to another one.

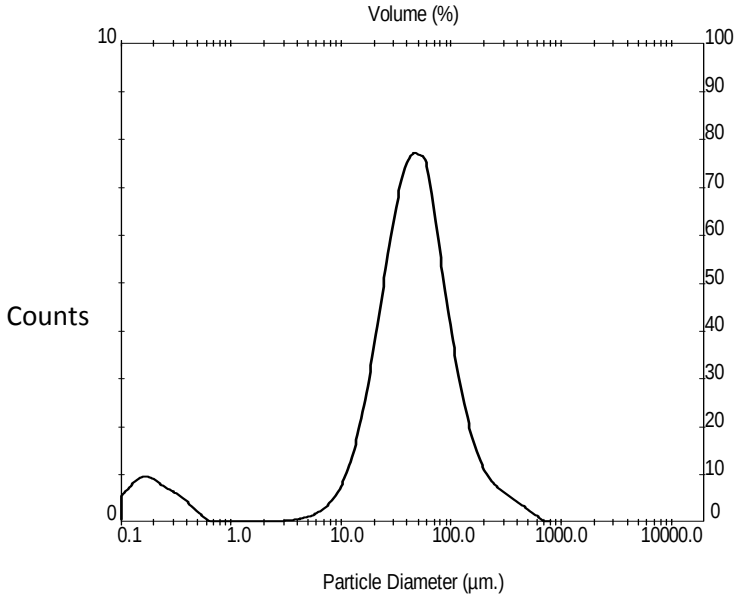

Fig. 6.4 Particle size distribution of the 19 h milled powder before the reaction. The D_{50} of the powder is 44 µm.

Therefore, the deviation between the model fitting and the experimental data can be explained by the above mentioned discrepancies between the modified model assumptions and the experiment situation.

6.6.2. Theoretical Comparison of the Modified Model with SCM and Reaction Control Model

Fig. 6.5 shows the comparison of the normalized result of modified model (Eq. 6.23), traditional SCM and the reaction control model [228]. The X axis is t/τ, which t is time and τ is complete conversion time. The Y axis is the fraction of conversion. For the sake of comparison, the diffusion coefficient of modified model is considered constant. However, different "n" values (different ratio of volume of produced shell divided to volume of consumed core based on the density of the produced shell) from 0.25 to 4 were applied. One can see that at the beginning of

the reaction, the rate of the reaction control model is slower compared to the traditional SCM and modified model. However, as the reaction continues, the reaction rate of SCM and modified model slows down faster compared to the reaction control model. This change in the reaction rate is because at the end of the reaction, SCM and the modified model consider that the core particle is covered by a thick shell that slows down the reaction rate. Comparison of SCM and the modified model reveals that the rate of the reaction for a particle with a shell depends on the ratio of volume of the produced shell compared to the consumed core (n). Depending on "n", the modified model predicts faster or slower reaction rate compared to SCM. At n=1, both SCM and modified model predicts the same reaction rate.

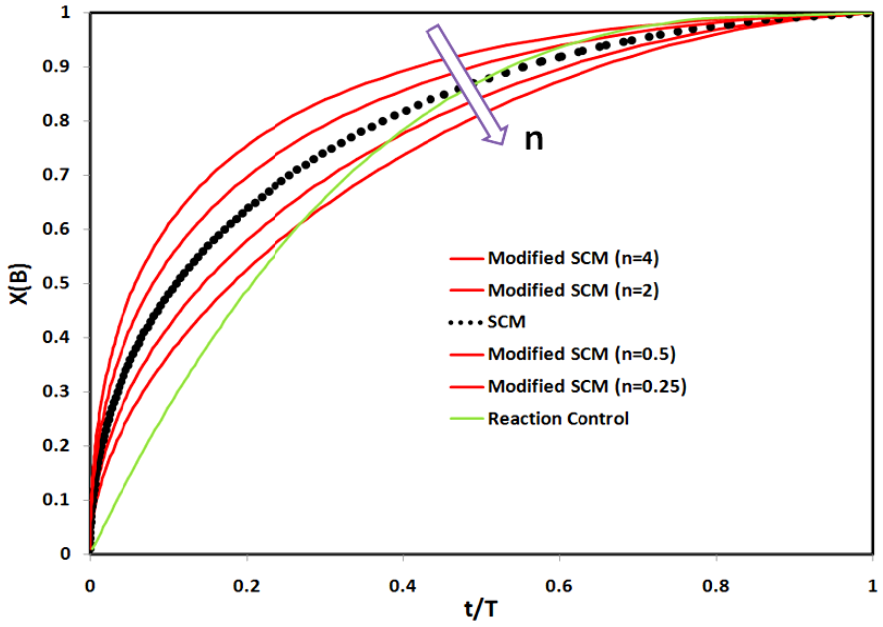

Fig. 6.5 Comparison of traditional SCM, reaction control and modified SCM (Eq. 6.23) based on the density of the produced shell.

6.6.3. Calculation of the Rate of Mass Transfer

The main advantage of the developed model compared to the traditional one is that one can obtain rate of mass transfer (flow rate) of ion species from the modified model. Eq. 6.23 can be rewritten as:

$$t = \frac{exp\left[\frac{n+(1-n)(1-X_B)^{\frac{2}{3}}-[n+(1-n)(1-X_B)]^{\frac{2}{3}}}{A}\right]-1}{k} \qquad (6.24)$$

A and k are obtained from the fitting, and therefore from Eq. 6.20 one can calculate changes in the diffusion coefficient with time. From the Fick's law:

$$J = -D\frac{\partial C}{\partial x} = -D_t\frac{C_x - C_0}{x_t - 0} \tag{6.25}$$

where x_t is the distance for diffusion:

$$x_t = R - r_c \tag{6.26}$$

The relation between the core radius and fractional conversion can be written as:

$$r_c = R_o(1 - X_B)^{1/3} \tag{6.27}$$

$$x_t = \left[nR^3 + {R_o}^3(1 - X_B)(1 - n)\right]^{1/3} - R_o(1 - X_B)^{1/3} \tag{6.28}$$

Putting Eq. 6.28 and Eq. 6.20 in Eq. 6.25, the diffusion flux of ion species (J), which is considered water molecules in this case, can be obtained. In order to understand how J depends on time and microstructure of the sample, the hydrogen production of a fresh 19 h milled sample and those annealed for 1 min and 3 h were obtained. Fig. 6.6 shows the hydrogen production data used for the fitting with Eq. 6.24.

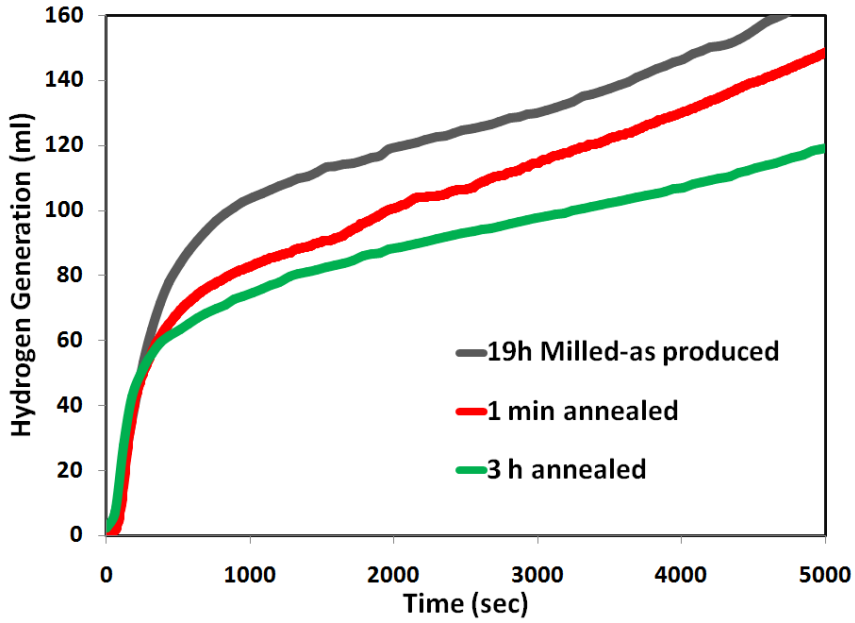

Fig. 6.6 The raw data on which Eq. 6.24 was fitted: hydrogen production of a fresh 19 h milled sample and samples annealed for 1 min and 3 h.

Fitting of Eq. 6.24 on data presented in was performed with R squares of 0.994, 0.987 and 0.995 for the fresh 19 h milled sample and samples annealed for 1 min and 3 h, respectively. A and k values were obtained from the fitting and J was calculated based on Eq. 6.25. Fig. 6.7 shows the calculated diffusion flux of water in the hydroxide layer of the samples that their hydrogen production was presented in Fig. 6.6.

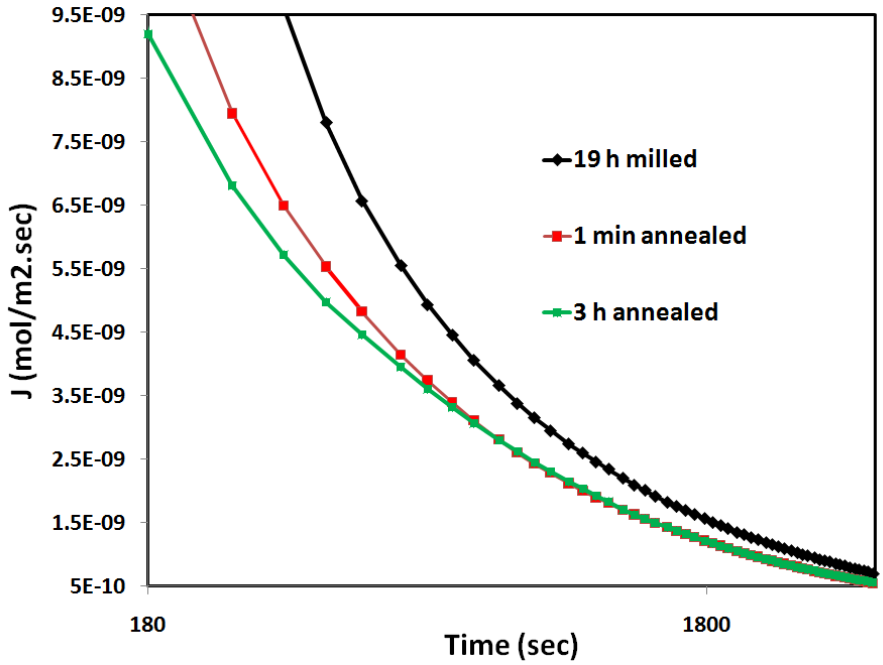

Fig. 6.7 The calculated diffusion flux of water in the hydroxide layer of the fresh 19 h milled sample and samples annealed for 1 min and 3 h.

One can see that at the beginning of the reaction, there is a significant difference between the flux of water molecules in the hydroxide layer for different samples. However as the reaction continues, the difference becomes negligible. This implies that at the beginning of the reaction where the hydroxide layer is thin, the microstructure determines flux of water molecules. As the reaction continues, the effect of the grown hydroxide layer prevails over the microstructure and all samples have similar values of the flux. This result obtained from the model is consistent with our latest electrochemical findings [229].

6.7. Conclusion

All steps of the reaction were evaluated and the diffusion of ion species/water molecules was determined as the rate controlling step. The model was developed based on the core-shell structure and considering that the overall size of the particles and the diffusion coefficient of ion species in the hydroxide layer change with time. The developed model was fitted with R-square of 0.99, compared to 0.82 for the traditional core-shell model. The model was further developed based on the Fick's law to calculate the flux of water molecules in the hydroxide layer. The results showed that at the beginning of the reaction, microstructure of the aluminum particles have a significant effect on the flux. However, the difference between the fluxes of different aluminum particles becomes negligible as the hydroxide layer thickens.

CHAPTER 7

EFFECT OF ADDITION OF WATER-SOLUBLE SALT POWDERS ON THE HYDROGEN GENERATION RATE OF ALUMINUM-WATER REACTION

7.1. Overview of Chapter 7

Previous chapters explained the mechanism of reaction of aluminum with water and the effect of ball milling on the reaction. A model also was provided to explain the kinetics of the reaction. Although so far a deep insight to different aspects of the reaction of ball milled aluminum particles with water has been provided, no solution has been suggested to increase the rate of hydrogen generation. The highest hydrogen production rate we obtained for the pure ball milled aluminum powder was for the 7 h milled sample (about 200 ml/h for 1 gram of aluminum). This rate means even if the reaction does not slow down, it takes at least 6-7 h for 1 gram of aluminum to fully react with water and produce 1270 ml of hydrogen.

This chapter explains that addition of water soluble salt powders to aluminum powder during ball milling is an affordable way to increase the reaction rate, and suggests a mechanism to explain the effect. As we explained in the first chapter, other methods of increasing the reaction rate (the use of LMPs, high pH solutions, ceramic particles) are not considered because of some practical issues regarding their usage in the future sustainable technologies.

This chapter is presented as manuscript #6 (Effect of Addition of Water-Soluble Salt Powders on the Hydrogen Generation Rate of Aluminum-Water Reaction). The PhD candidate's

contributions to the manuscript are: a) Powder preparation and hydrogen measurement tests. b) SEM and EDS analyses. c) Reviewing the relevant literature and preparing the manuscript.

The manuscript is to be submitted to the journal of Power Sources.

The references for this chapter along with references from other chapters are provided at the end of the thesis.

Effect of Addition of Water-Soluble Salt Powders on the Hydrogen Generation Rate of Aluminum-Water Reaction

S.S. Razavi-Tousi, J.A. Szpunar

Department of Mechanical Engineering, University of Saskatchewan, S7N 5A9 Saskatoon, Saskatchewan, Canada

7.2. Abstract

Aluminum powder was ball milled with different weight percentages of salt and potash. Scanning electron microscopy (SEM) was used to investigate the microstructure of the produced mixtures. The produced mixture was added to water and hydrogen generation rate was measured. The results showed that presence of salt or potash in the microstructure of aluminum can considerably increase the hydrogen generation rate. SEM results showed that a higher hydrogen generation rate of the mixtures milled for longer periods is correlated to a finer distribution of the second phase in the aluminum matrix. A higher percentage of the second phase can significantly decrease the milling time needed for activation of the aluminum particles.

Keywords: *Salt, Potash, Milling, Hydrogen, Microstructure*

7.3. Introduction

There are many works in which water soluble salt particles were added to enhance the reaction between aluminum and water [28, 76-78, 127, 230-232]. One can categorize the effect of presence of salt to chemical and structural effects. It is proven that presence of Cl^- in the solution promotes the corrosion of aluminum sheets by deteriorating the protective oxide/hydroxide layer [123-124, 233]. In the case of effect of addition of salt particles to promote hydrogen production, M.Q. Fan ascribed the effect of salt to the role of Cl^- in facilitating the corrosion [74].

On the other hand, B. Alinejad et al. considered that salt particles modify the structure of aluminum particles by providing more surfaces for the reaction. They suggested a schematic

model to illustrate how a presence of salt particles promotes the reaction [76]. In their model, they assumed that salt particles cover the aluminum particles during ball milling. As the mixture is exposed to water, salt particles are dissolved and a fresh surface of aluminum is exposed to water.

In spite of the number of works that used water-soluble salts to activate aluminum, no study was performed to distinguish whether the effect of addition of water-soluble salts is mainly a chemical or structural effect. The structural and chemical effects can be distinguished by introducing the same amount of a salt as either ball milled by aluminum powder or added to the hot water, and measuring the hydrogen production rate for the either case. Moreover, milling time, which changes the microstructure but does change the chemistry of the mixture, can also indicate the effect of presence of the salt. The above mentioned approaches in addition to changing the percentage and type of the water-soluble salts are considered in this work to evaluate the effect of presence of water-soluble salt.

7.4. Experimental Procedure

7.4.1. Ball Milling

Aluminum powder of 99.8% purity (MFCD00134029) was provided by Alfa Aeasar Company. 50 wt% of sodium chloride (purity: +99%) was mixed to the aluminum powder and the mixture ball milled. High energy ball milling was done in a planetary ball mill (Torrey Hills-ND2L) with stainless steel cups (285 ml capacity) and balls (28 of 16 mm and 6 of 18 mm diameter) in an argon atmosphere. Ball to powder weight ratio was 30:1 and mill speed was maintained at 200 RPM for durations of 0.25, 0.5, 1, 2, 4, 7, 11 and 19 hours. In order to evaluate the effect of weight percentage and type of salts, mixtures of 25 wt% NaCl- 75 wt% Al, 25 wt% NaCl- 75 wt% Al and 50 wt% KCl- 50 wt% Al were also ball milled for durations of 2, 7 and 19 hours. The KCl powder with a commercial purity was refined from the Saskatchewan potash (Potash Corp) products.

7.4.2. Hydrogen Measurement

The detail of hydrogen measurement procedure is similar to the manuscript #1.

7.4.3. Scanning Electron Microscopy

The detail of scanning electron microcopy (SEM) is similar to the manuscript #1.

7.5. Results and Discussion

7.5.1. Effect of Milling Time and Presence of Salt

In order to make the results comparable, the ball milling intervals for the mixture were chosen the same as the time intervals by which the pure aluminum powder was milled (chapter 2). All of the hydrogen generation tests for the mixtures were done in the same way as that of the pure aluminum powder. Fig. 7.1 shows the effect of ball milling of aluminum-salt mixture on the hydrogen generation through reaction with hot water.

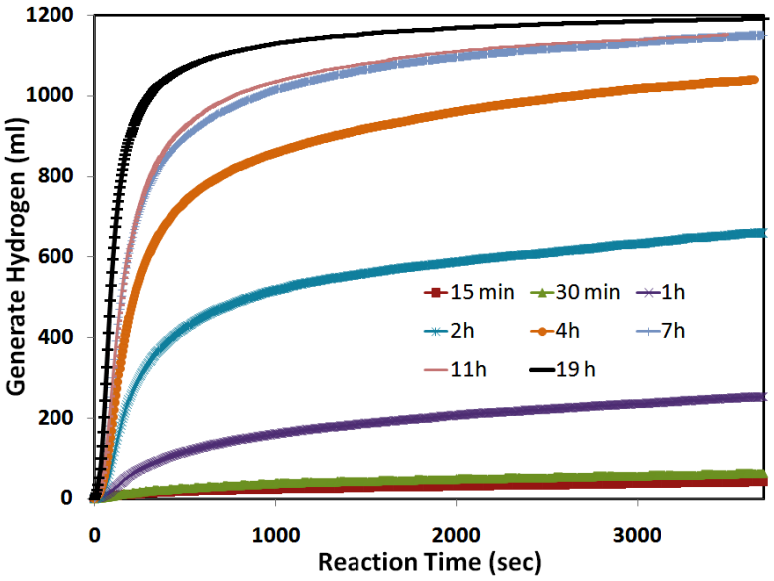

Fig. 7.1 Effect of milling time on hydrogen generation of 50-50 wt% ratio salt-aluminum powder mixture during first hour of the reaction.

Fig. 7.1 shows that longer ball milling times result in higher rates of hydrogen generation. The difference in hydrogen generation rate of the 7 h, 11 h and 19 h ball milled samples is not big, while prolonging ball milling from 15 min to 7 h results in a significant increase in hydrogen generation rate. Comparison of Fig. 7.1 with hydrogen generation from the pure aluminum (Fig. 2.7) reveals that presence of salt increases the hydrogen generation rate for all of the milling

durations. For example, the hydrogen generation of the 19 h milled sample during the first hour of the reaction increased from 100 ml to 1200 ml, which is considerable improvement.

In order to understand effect of presence of salt on the morphology of the particles, the ball milled mixtures were studied by SEM. Fig. 7.2 shows morphology of (a) the as received aluminum particles, and the mixture ball milled for (b) 0.25 h, (c) 0.5 h, (d) 1 h, (e) 2 h, (f) 4 h, (g) 7 h, (h) 11 h and (i) 19 h.

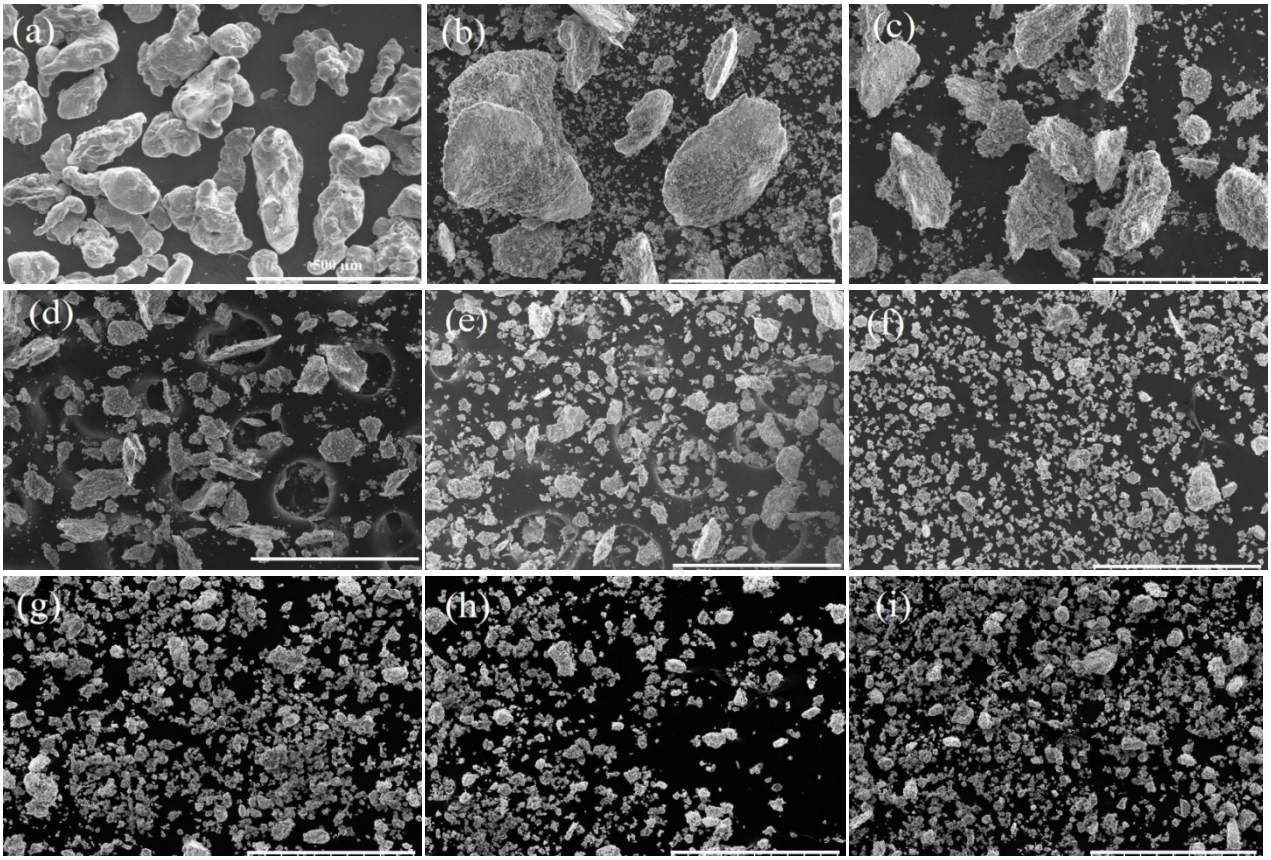

Fig. 7.2 SEM images of (a) the as received aluminum particles and the mixture (salt-aluminum) ball milled for (b) 0.25 h, (c) 0.5 h, (d) 1 h, (e) 2 h, (f) 4 h, (g) 7 h, (h) 11 h and (i) 19 h. The scale bar is 500 um and is the same for all of the images (Magnification ×100.).

The aluminum particles milled for 15 min and 30 min experienced no fracture but they are covered by salt particles. Beside aluminum particles, there are many very smaller salt particles that have no interaction with aluminum particles. Ball milling for 1 h and 2 h results in fracture of aluminum particles. The aluminum particles after 2 h are obviously smaller than the as

received particles. One can see that between 2 h to 4 h of milling, the particle size reaches to a steady state where more milling has no significant effect on the particle size.

Comparing the results in Fig. 7.2 with the morphology of the pure aluminum milled for the same durations (Fig. 2.4) reveals the effect of presence of salt particles. The overall trend in the change in the morphology of the aluminum is similar to that of the mixture. However, the particle size of the pure aluminum continuously decreases up to 19 h milling, while for the mixture (Fig. 7.2) there is no significant change in morphology after 4 h milling. Therefore, the presence of salt particles made the reduction in particle size faster so that steady state was reached at a shorter period of milling. A similar effect of presence of brittle particles on improvement of milling efficiency has been reported in the literature [39-41, 57].

A thorough understanding of the effect of salt particles on the reaction mechanism requires investigation of microstructural changes inside the particles. For that purpose, the ball milled mixture of the powders were hot mounted in a carbon resin, cross sectioned, polished and examined by SEM and electron dispersive X ray spectroscopy (EDS). Fig. 7.3 shows the EDS results for mixture powders milled for a) 0.25 h, (b) 0.5 h, (c) 1 h, (d) 2 h and (e) 4 h.

The very left images show the SEM of the particle, the next ones from left to right show the distribution of aluminum element, distribution of chlorine or sodium that represents salt, and distribution of carbon that comes from the carbon mount that holds particles, respectively. One can see that at the beginning of the ball milling (Fig. 7.3 (a)), the distribution of salt and aluminum particles is similar to what suggested by B. Alinejad et al. [76], i.e. the aluminum particle is covered by salt. However, their schematic model[76] is no longer accurate for the longer milling times where salt and aluminum make composite particles.

Fig. 7.4 shows high magnification images (×4000) from particles milled for 30 min and 4 h that their low magnification images (×100) were presented in Fig. 7.1(c) & (f). In spite of the big difference between size of the particles presented in Fig. 7.4, both are covered with small crystallite of salt. Therefore, in the case of surface properties, there is no much difference between the particles milled for short and long time.

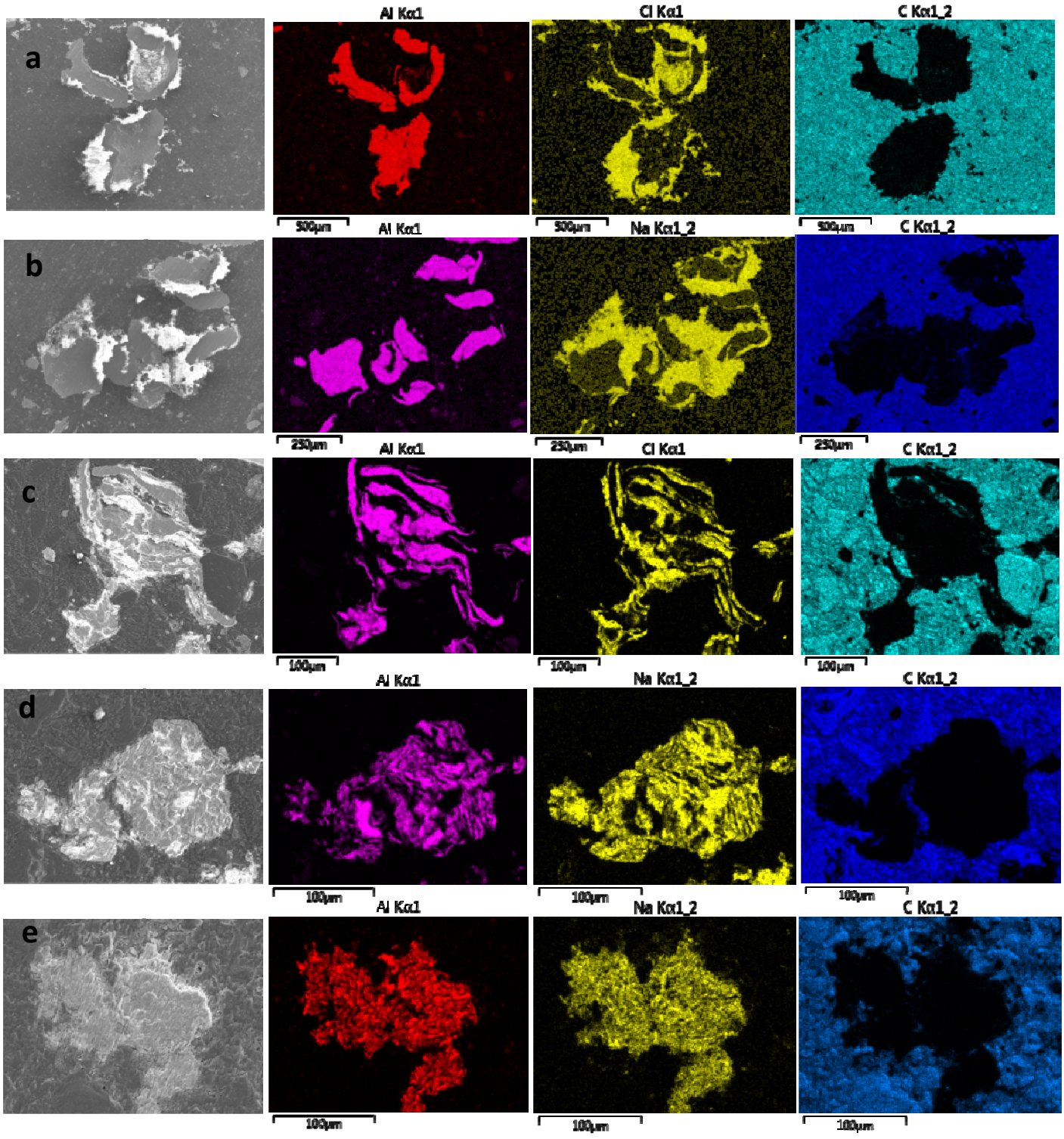

Fig. 7.3 EDS maps of the mixture milled for (a) 15 min, (b) 30 min, (c) 1 h, (d) 2 h and (e) 4 h. Note the change in the scale bar.

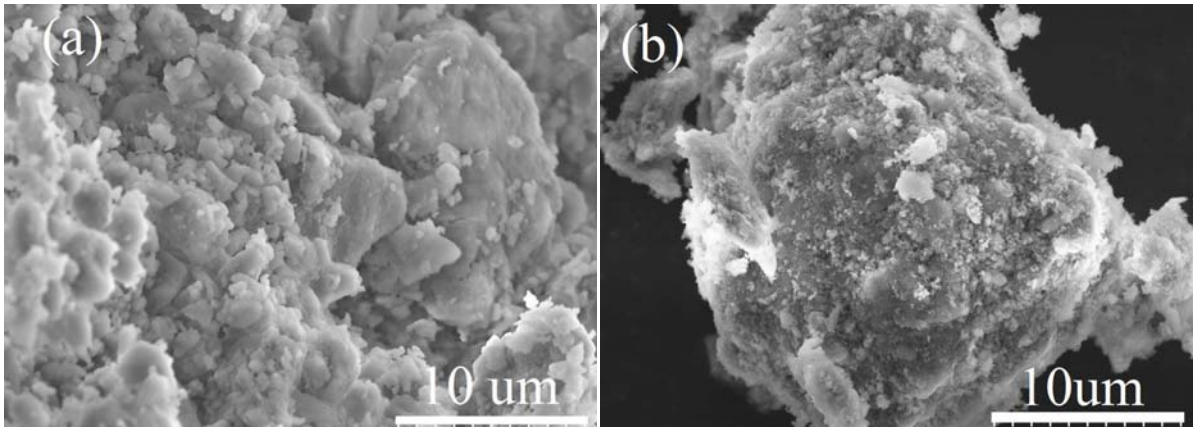

Fig. 7.4 Presence of salt particles on the surface of aluminum particles milled for 30 min and 4 h. Magnification of both images is ×4000.

For the mixtures milled for longer times, not only salt covers the surface of aluminum particles, but also salt particles are embedded inside aluminum particles (Fig. 7.3). The presence of salt particle inside aluminum particles is explained by the cold welding process during ball milling. Aluminum particles that are covered by salt are cold welded together, thus the salt particles are trapped inside new aluminum particles. Such a mechanism produces aluminum-salt composite particles. A similar mechanism for interaction of hard second phase particles with the metallic particles has been discussed in the literature [39, 41].

The longer the mixture is ball milled, the smaller is the distance between salt layers inside the aluminum particles. For the 4 h and longer milled mixtures, the salt particles are finely distributed inside aluminum particles in a way that the map resolution cannot anymore distinguish between salt and aluminum. Thus, a rather uniform distribution is detected for both elements (Al and Cl or Na). The results for 7 h, 11 h and 19 h were similar to 4 h, thus they are not reported in Fig. 7.3.

In order to better understand the effect of milling time on distribution of salt and aluminum particles inside the produced composite particles, the cross section of the particles was studied by the line scan EDS. Fig. 7.5 shows the line scan EDS analyses for the particles milled for (a) 15 min, (b) 30 min, (c) 1 h, (d) 2 h, (e) 4 h, (f) 7 h and (g) 11 h.

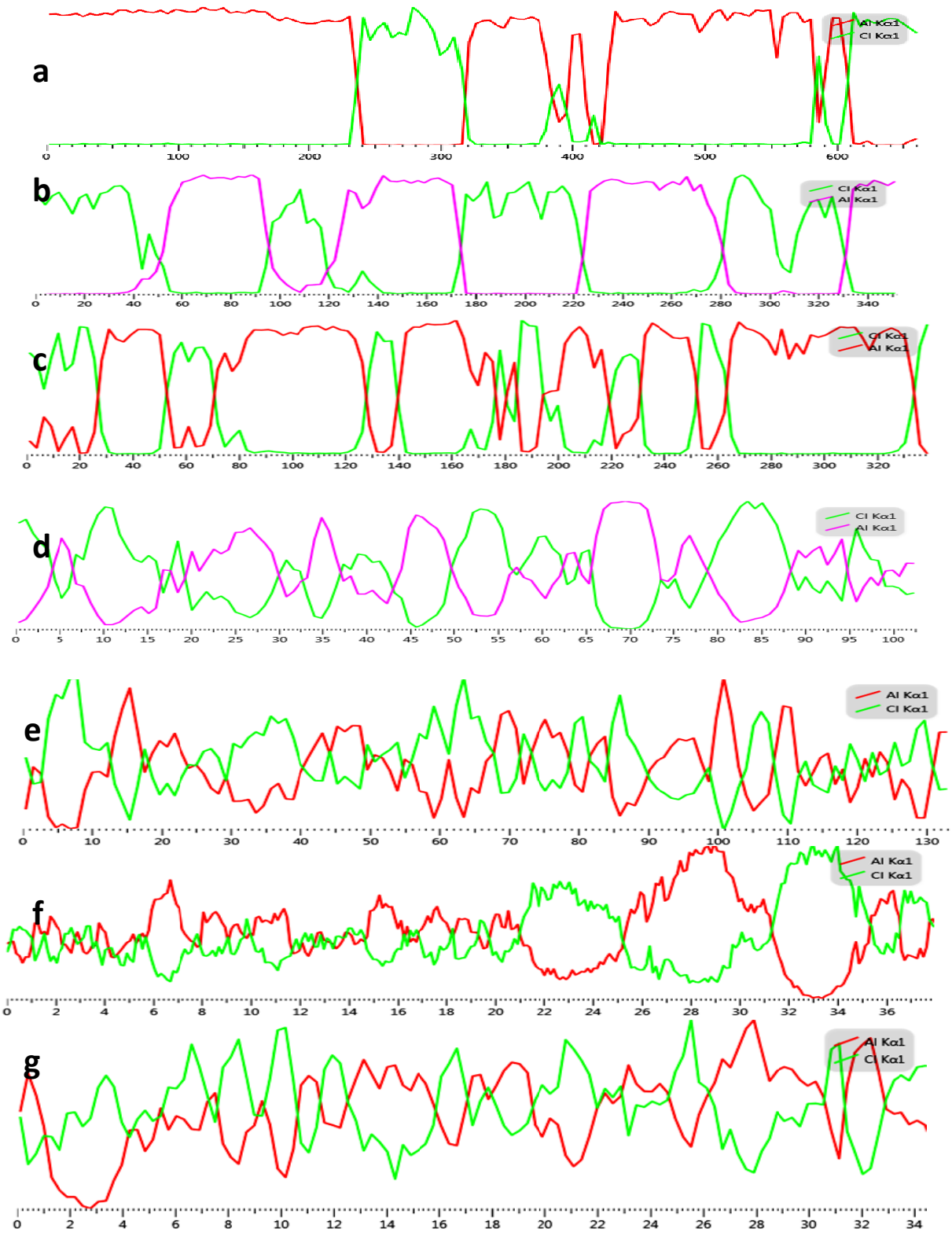

Fig. 7.5 Line scan EDS of the particles milled for (a) 15 min, (b) 30 min, (c) 1 h, (d) 2 h, (e) 4 h, (f) 7 h and (g) 11 h. The Y axis is normalized intensity, X axis length (μm), the green line represents Cl and the red represents Al.

Fig. 7.5 shows that for the short time milled mixtures, the salt-aluminum distances are in order of few ten to hundred micrometers (Fig. 7.5(a), (b) & (c)), while the distance changes to few micrometers for the longer milled mixtures (Fig. 7.5(f) & (g)). The important result from Fig. 7.5 is that the frequency of the presence of salt and aluminum inside the composite particles changes by time. Note that the X axis length is reducing from (a) to (h); implying that the salt particles inside the aluminum matrix becomes more and more finely distributed.

Considering Fig. 7.3 and Fig. 7.5, one can understand the mechanism of improvement of the reaction by the presence of salt particles. Ball milling produces composite particles composed of salt and aluminum. When the composite particles are immersed in hot water, the salt phase is immediately dissolved and leaves many fresh surfaces on and inside the aluminum particles. That means dissolving the salt results in porous aluminum particles with many voids/tunnels inside that provide space for penetration of water. The longer milling time, the better distribution of voids/tunnels is provided inside aluminum particles, which promotes access of water to spaces inside the particles. Accordingly, as Fig. 7.1 shows, the longer ball milling results in a higher hydrogen generation rate. Moreover, as the aluminum-salt ratio was fixed for all the powders, the chemical effect of presence of Cl^- is the same for all, while the structural effect of salt changes by milling time. This implies that the chemical effect of the presence of salt is negligible compared to the structural effect.

7.5.2. Effect of the Type of the Water-Soluble Salt

Potash powder (KCl) with a ratio of 50:50 was added to aluminum during ball milling, and the hydrogen generation of the mixture in reaction with hot water was measured. Fig. 7.6 shows the hydrogen generation of the aluminum-potash mixture milled for 2, 7 and 19 h. One can see that 7 h of milling is enough to make the reaction to complete in few minutes, and ball milling over 7 h has no effect on hydrogen generation rate. Comparing with Fig. 7.1, one can see that ball milling of the salt-aluminum mixture with same ratio of the second phase has a different result: ball milling over 7 h up to 11 h and 19 h still increases the hydrogen generation rate. Moreover, even for the 19 h milled mixture of aluminum-salt, it takes over one hour for the reaction to complete (Fig. 7.1). However, it takes a few minutes for the mixture of aluminum-potash milled for 7 h or 19 h to complete the reaction. Accordingly, potash has a markedly better effect compared to salt on improving the kinetics of the reaction.

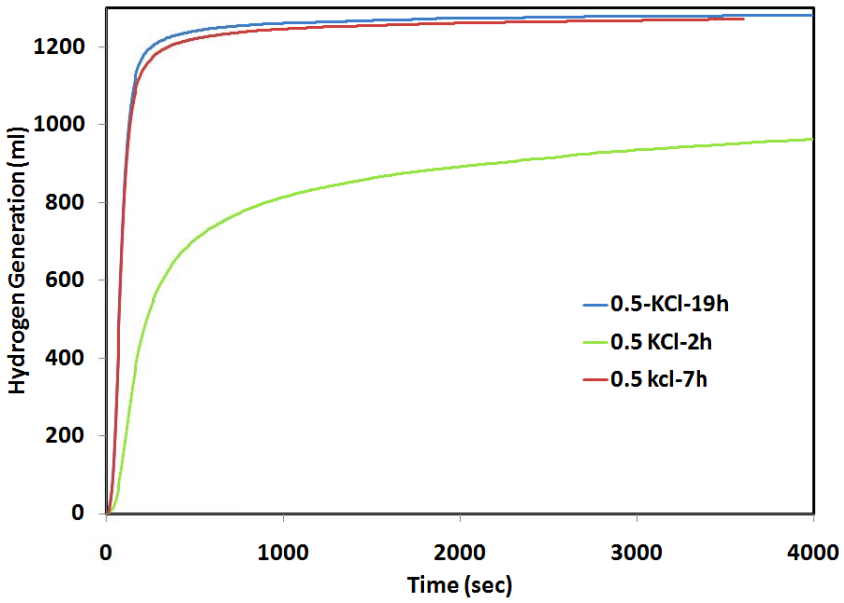

Fig. 7.6 Hydrogen generation of the aluminum-potash mixture (50:50) milled in argon for 2, 7 and 19 h.

7.5.3. Effect of Weight Percentage

Fig. 7.7 and Fig. 7.8 show the hydrogen generation of the 25 wt% and 75 wt% salt-aluminum mixtures milled for 2, 7 and 19 h, respectively. One can see that the hydrogen generation of the 75 wt% salt-aluminum mixture is similar to that of the 50 wt% potash-aluminum mixture. However, the 25 wt% salt-aluminum mixture reacts with water slower in a way that in one hour just around half of the reaction (650 ml compared to the 1270 ml for the full reaction) is completed. This suggests that the higher amount of the salt in the aluminum matrix promotes the reaction significantly. The effect of a higher amount of salt in improving the reaction is explained by considering that salt is dissolved in hot water and leaves fresh aluminum surfaces for the reaction, and that the smaller distance between salt layers in the aluminum matrix results in a higher hydrogen generation (section 7.5.1).

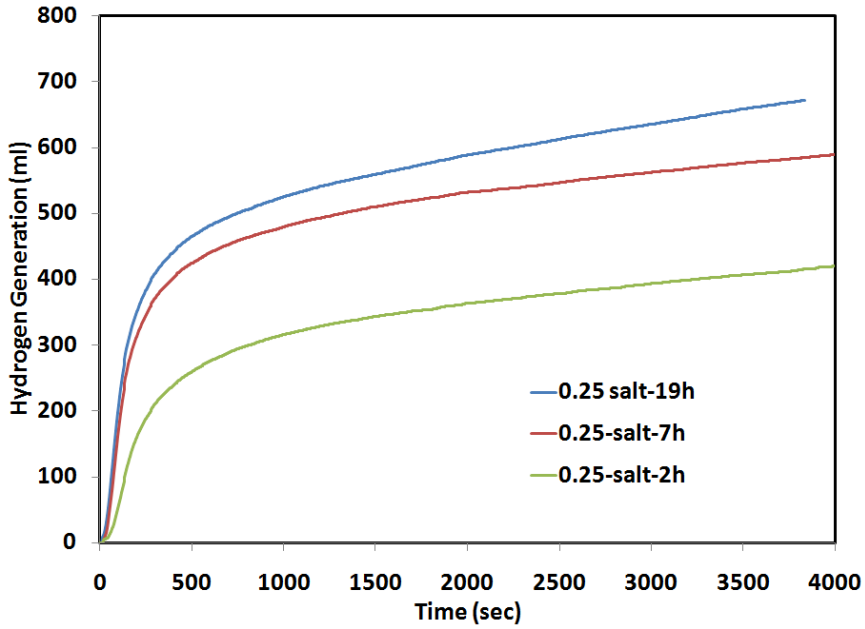

Fig. 7.7 Hydrogen generation of the 25 wt% salt-aluminum mixtures milled for 2, 7 and 19 h.

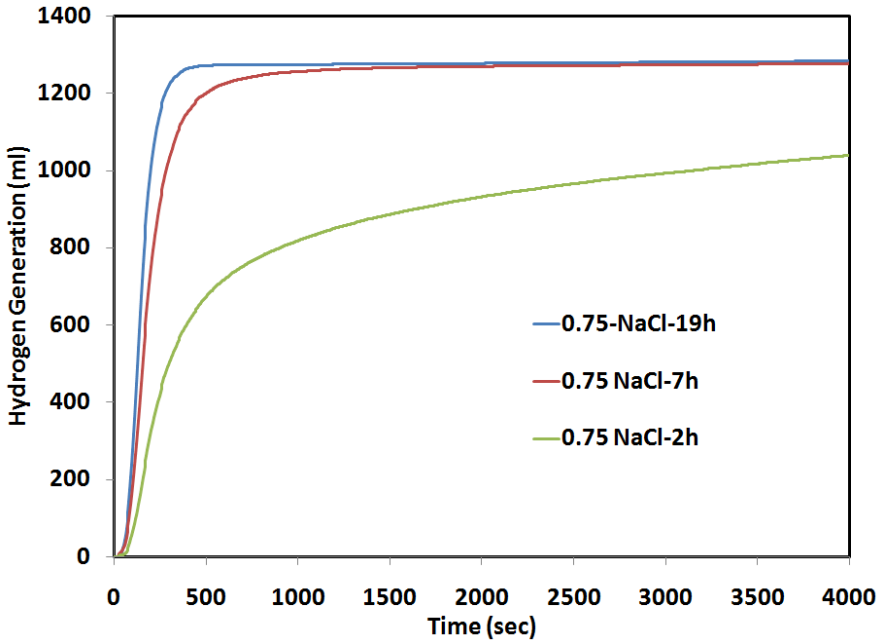

Fig. 7.8 Hydrogen generation of the 75 wt% salt-aluminum mixtures milled for 2, 7 and 19 h.

7.6. Conclusion

The presence of salt particles during ball milling has a significant impact on hydrogen generation rate of aluminum in reaction with hot water. Morphological analyses by SEM, elemental map distribution and line scan by EDS were performed to evaluate the effect of salt particles. SEM studies showed that the refinement process of the powder is improved at the presence of salt particles. Moreover, the surface of the particles is covered by salt. Considering the zero hydrogen production of the aluminum-salt mixture without ball milling, the effect of salt is explained by modifying the microstructure rather than a chemical effect. EDS results proved that salt particles are embedded inside aluminum particles. Salt particles are dissolved upon immersing in hot water, leaving many voids/tunnels for water to penetrate inside aluminum particles, which consequently improves the hydrogen generation rate. This explanation is supported by the fact that a higher weight percentage of the salt in aluminum matrix results in a higher hydrogen generation rate. Finally, it was found that potash powder has a better effect on improving the reaction compared to salt.

CHAPTER 8

CONCLUSION AND FUTURE WORKS

8.1. CONCLUSION

Activation of aluminum particles by ball milling with and without addition of water-soluble salts was studied. The purpose of activation was to use the aluminum powder as an agent to react with water and produce hydrogen. The refinement of aluminum microstructure by ball milling and its effect on the rate of reaction were evaluated. Hydrogen generation was considered as the main criterion by which the progress of the reaction was measured. Moreover, the electrochemistry and kinetics of the reaction were studied. Finally, the effect of addition of water-soluble salts to aluminum on the hydrogen generation rate was evaluated.

The first objective of this research was to evaluate and optimize the microstructural evolution of aluminum particles during ball milling and its effect on hydrogen production rate. The results showed that the particle size of aluminum powder significantly decreases during ball milling. The particle size of the as received sample was ~200 μm, which reduced to ~50 μm after 19 h ball milling. The particle size of the milled powder is important because it to a certain degree determines the available surface area of the particles for the reaction. However, the hydrogen measurement tests revealed that the highest hydrogen generation rate does not correspond to the finest powder (19 h milled powder), but to a powder that was milled for a shorter period of time (7 h). The examination of cross section of the milled particles revealed that the highest hydrogen generation rate is for the particles with a laminated microstructure. In other words, not only the

surface of the particles contributes to the reaction, but also the internal surfaces that can act as reaction sites. The EDS results confirmed penetration of water into aluminum particles milled for 7 h, which caused a higher hydrogen generation rate.

In addition to increasing the specific surface area of the powder that is correlated to the decrease in particles size, ball milling was found to promote the reaction of aluminum with water in two other ways. The first one was that ball milling breaks the native oxide layer on the surface of the particles. This oxide layer delays the hydrogen generation; this delay is so called "incubation time". This represents the time needed for the oxide layer to be hydrated or dissolved by water, so that the reaction between aluminum and water can be initiated. Comparison of the milled powders that were kept in argon or air revealed that the longer storage of the powders in air results in a longer incubation time, while the powders that were kept in argon started the reaction much faster. The XPS results showed that the native oxide film on the surface of the milled powder grows thicker by time, which confirms that the storage in air increases the incubation time.

The other contribution to improving the reaction was formation of grain boundaries and dislocations (crystallographic imperfections) in the microstructure of the particles. These imperfections make the microstructure unstable, therefore, the affinity of the aluminum to react with water increases. The effect of the mentioned lattice imperfections (grain boundaries and dislocations) on the hydrogen generation rate was studied by room temperature aging and high temperature annealing of the milled particles. The room temperature aging decreased the microstrain of the lattice. The high temperature annealing decreased the microstrain of the lattice and increased the grain size. In both cases, a decrease in hydrogen generation rate was observed, which suggested that the presence of grain boundaries and dislocations increases the affinity of the particles for the reaction.

Electrochemical tests also were performed to determine the effect of ball milling on corrosion potential and Tafel curves of the powders and consequently on the reaction rate. Corrosion potential tests showed that OCP decreases at the beginning of the reaction and then slightly increases. The changes in OCP were explained by effect of reaction time on Evans diagram. Tafel tests showed that the corrosion current is rather high at the beginning of the reaction and then significantly decreases. The decrease in corrosion current was ascribed to the effect of

growing hydroxide layer on the surface of particles. Moreover, the corrosion potential tests also confirmed that milled particles have a more negative potential value, which suggests that ball milling caused thermodynamical instability of the particles.

The importance of microstructural refinement on the reaction rate was the motivation for investigating the grain refinement mechanism of aluminum particles during ball milling. The EBSD studies showed that there are four major mechanisms that contribute to grain refinement during ball milling. 1) deformation banding, 2) cold welding of the particles, 3) increase in aspect ratio of the grains, and 4) lattice rotation induced during dynamic recrystallization. It was found that two critical steps are involved in the refinement process. The first step is formation of a network of low angle grain boundaries by dynamic recovery at the beginning of milling, which produces subgrains. The second step was rotation of the subgrains formed in the previous step to higher misorientations and consequently formation of new smaller grains.

The last objective regarding the reaction of the activated aluminum particles with hot water was to provide a model that defines the kinetics of the reaction. This was done by modifying the shrinking-core model. Two main assumptions in the traditional model were revised and changed to reflect the more realistic reaction of an aluminum particle with water. The first correction was introduced to describe that the hydroxide layer (shell) has a bigger thickness than the consumed aluminum (core). The second illustrated the fact that the diffusion coefficient of the hydroxide layer changes during the reaction. Applying these two modifications to the traditional shrinking-core model, the R-square of fitting of the model to the experimental data changed from 0.82 to 0.99.

After different aspects of the reaction of activation of aluminum particles with hot water for the purpose of hydrogen generation were evaluated, some experiments were performed to further improve the reaction rate. Salt and potash powders were added to aluminum during ball milling and the hydrogen production of the mixtures was measured. The results showed a significant improvement because of addition of water-soluble salts to aluminum. EDS and SEM results suggested that the main reason for improving the reaction rate is the structural modification of the particles by providing higher surface area (correlated to a smaller particles size and presence of salt layers inside particles) for the reaction. The additional surfaces were provided by

dissolution of the salts in hot water. It was found that chemical effect of presence of salts is negligible compared to their microstructural effects.

8.2. FUTURE WORKS

- In chapter 3, different contributions of milling to improvement of the reaction rate were discussed. It was found that both the decrease in particle size and increase in crystallographic imperfections have contributed significantly to enhancement of the hydrogen generation. However, the contribution of each effect was not quantified. It would be of interest to determine how much each effect is weighted regarding the hydrogen generation. Moreover, BET test can be used to measure the specific surface area of the milled powders and the results should be compared to the SEM observations.
- The effect of presence of contamination in water and aluminum can be considered as a factor determining the hydrogen generation rate. It would be of interest to perform some experiments to evaluate the effect of purity of reactant. Moreover, TGA analyses can be used to determine the progress of the reaction based on study of the hydroxide layer formed on the surface of particles.
- In chapter 4, the electrochemistry of the reaction of aluminum and water at 80^{o}C was studied. The temperature was chosen based on the optimum temperature of PEM fuel cells. Considering the effect of temperature on the type of the hydroxide layer formed on the surface of aluminum, investigation of the effect of temperature on the reaction mechanism would be of interest.
- In chapter 6, a model was proposed for reaction of a circular particle with water. This model can be further developed to consider effect of presence of water-soluble salt in the aluminum matrix
- In chapter 7, it was shown that potash has better effect on improving the reaction compared to salt. A future work can consider testing other water-soluble salts and investigating why different salts have different effects.

REFERENCES

1. Schlapbach, L. and A. Züttel, *Hydrogen-storage materials for mobile applications.* NATURE, 2001. **414** p. 353-358.
2. Larminie, J. and A. Dicks, *Fuel Cell Systems Explained*. 2003, Oxford Oxford Brookes University, UK.
3. Steele, B.C.H. and A. Heinzel, *Materials for fuel-cell technologies.* NATURE, 2001. **414**(6861): p. 345-352.
4. Mehta, V. and J.S. Cooper, *Review and analysis of PEM fuel cell design and manufacturing.* Journal of Power Sources, 2003. **114**(1): p. 32-53.
5. Litster, S. and G. McLean, *PEM fuel cell electrodes.* Journal of Power Sources, 2004. **130**(1-2): p. 61-76.
6. Faur Ghenciu, A., *Review of fuel processing catalysts for hydrogen production in PEM fuel cell systems.* Current Opinion in Solid State and Materials Science, 2002. **6**(5): p. 389-399.
7. Funke, H.H., et al., *Hydrogen generation by hydrolysis of zinc powder aerosol.* International Journal of Hydrogen Energy, 2008. **33**(4): p. 1127-1134.
8. Berman, A. and M. Epstein, *The kinetics of hydrogen production in the oxidation of liquid zinc with water vapor.* International Journal of Hydrogen Energy, 2000. **25**(10): p. 957-967.
9. Weiss, R.J., et al., *H2 production by Zn hydrolysis in a hot-wall aerosol reactor.* AIChE Journal, 2005. **51**(7): p. 1966-1970.
10. Grosjean, M.H., M. Zidoune, and L. Roue, *Hydrogen production from highly corroding Mg-based materials elaborated by ball milling.* Journal of Alloys and Compounds, 2005. **404**: p. 712-715.
11. Zidoune, M., et al., *Comparative study on the corrosion behavior of milled and unmilled magnesium by electrochemical impedance spectroscopy.* Corrosion Science, 2004. **46**(12): p. 3041-3055.
12. Grosjean, M.H., et al., *Effect of ball milling on the corrosion resistance of magnesium in aqueous media.* Electrochimica Acta, 2004. **49**(15): p. 2461-2470.
13. Grosjean, M.H., et al., *Hydrogen production via hydrolysis reaction from ball-milled Mg-based materials.* International Journal of Hydrogen Energy, 2006. **31**(1): p. 109-119.
14. Grosjean, M.-H. and L. Roué, *Hydrolysis of Mg–salt and MgH2–salt mixtures prepared by ball milling for hydrogen production.* Journal of Alloys and Compounds, 2006. **416**(1–2): p. 296-302.

15. Uan, J.-Y., et al., *Producing hydrogen in an aqueous NaCl solution by the hydrolysis of metallic couples of low-grade magnesium scrap and noble metal net.* International Journal of Hydrogen Energy, 2009. **34**(4): p. 1677-1687.

16. Yu, S.-H., J.-Y. Uan, and T.-L. Hsu, *Effects of concentrations of NaCl and organic acid on generation of hydrogen from magnesium metal scrap.* International Journal of Hydrogen Energy, 2012. **37**(4): p. 3033-3040.

17. Kojima, Y., K.I. Suzuki, and Y. Kawai, *Hydrogen generation by hydrolysis reaction of magnesium hydride.* Journal of Materials Science, 2004. **39**(6): p. 2227-2229.

18. Tayeh, T., et al., *Production of hydrogen from magnesium hydrides hydrolysis.* International Journal of Hydrogen Energy, 2014. **39**(7): p. 3109-3117.

19. Hiraki, T., et al., *Chemical equilibrium analysis for hydrolysis of magnesium hydride to generate hydrogen.* International Journal of Hydrogen Energy, 2012. **37**(17): p. 12114-12119.

20. Hong, S.-H., H.-J. Kim, and M.Y. Song, *Rate enhancement of hydrogen generation through the reaction of magnesium hydride with water by MgO addition and ball milling.* Journal of Industrial and Engineering Chemistry, 2012. **18**(1): p. 405-408.

21. Vlaskin, M.S., et al., *Computational and experimental investigation on thermodynamics of the reactor of aluminum oxidation in saturated wet steam.* International Journal of Hydrogen Energy, 2010. **35**(5): p. 1888-1894.

22. Petrovic, J. and G. Thomas, *Reaction of aluminum with water to produce hydrogen. A study of issues related to the use of aluminum for on-board vehicular hydrogen storage.* U. S. Department of Energy Report, 2008: p. 1-26.

23. Yang, S.H. and H. Knickle, *Design and analysis of aluminum/air battery system for electric vehicles.* Journal of Power Sources, 2002. **112**(1): p. 162-173.

24. Wang, H., et al., *Modeling of Parasitic Hydrogen Evolution Effects in an Aluminum−Air Cell†.* Energy & Fuels, 2010. **24**(7): p. 3748-3753.

25. Doche, M.L., et al., *Characterization of different grades of aluminum anodes for aluminum/air batteries.* Journal of Power Sources, 1997. **65**(1-2): p. 197-205.

26. Tang, Y.G., et al., *The effect of zinc on the aluminum anode of the aluminum-air battery.* Journal of Power Sources, 2004. **138**(1-2): p. 313-318.

27. Macdonald, D.D., S. Real, and M. Urquidimacdonald, *Evaluation of Alloy Anodes for Aluminum-Air Batteries .3. Mechanisms of Activation, Passivation, and Hydrogen Evolution.* Journal of The Electrochemical Society, 1988. **135**(10): p. 2397-2409.

28. Soler, L., et al., *Aluminum and aluminum alloys as sources of hydrogen for fuel cell applications.* Journal of Power Sources, 2007. **169**(1): p. 144-149.

29. Parmuzina, A.V. and O.V. Kravchenko, *Activation of aluminium metal to evolve hydrogen from water.* International Journal of Hydrogen Energy, 2008. **33**(12): p. 3073-3076.

30. Kravchenko, O.V., et al., *Activation of aluminum metal and its reaction with water.* Journal of Alloys and Compounds, 2005. **397**(1-2): p. 58-62.

31. Bunker, C.E. and M.J. Smith, *Nanoparticles for hydrogen generation.* Journal of Materials Chemistry, 2011. **21**(33): p. 12173-12180.

32. Benjamin, J.S. and M.J. Bamford, *Dispersion strengthened aluminum made by mechanical alloying.* Metal Trans A, 1977. **8**: p. 1301-1305.

33. Benjamin, J.S. and T.E. Volin, *Mechanism of Mechanical Alloying.* Metallurgical Transactions, 1974. **5**(8): p. 1929-1934.

34. Suryanarayana, C., *Mechanical alloying and milling.* Progress in Materials Science, 2001. **46**: p. 1-184.

35. Takacs, L., *Self-sustaining reactions induced by ball milling.* Progress in Materials Science, 2002. **47**: p. 355-414.

36. Ward, T.S., et al., *A study of mechanical alloying processes using reactive milling and discrete element modeling.* Acta Materialia, 2005. **53**(10): p. 2909-2918.

37. Kudaka, K., et al., *Effect of milling media on the reaction kinetics of the mechanochemical synthesis of pentatitanium trisilicide.* Journal of the American Ceramic Society, 2000. **83**(11): p. 2887-2889.

38. Delogu, F., R. Orru, and G. Cao, *A novel macrokinetic approach for mechanochemical reactions.* Chemical Engineering Science, 2003. **58**(3-6): p. 815-821.

39. Fogagnolo, J.B., M.H. Robert, and J.M. Torralba, *Mechanically alloyed AlN particle-reinforced Al-6061 matrix composites: Powder processing, consolidation and mechanical strength and hardness of the as-extruded materials.* Materials Science and Engineering a-Structural Materials Properties Microstructure and Processing, 2006. **426**(1-2): p. 85-94.

40. Fogognolo, J.B., et al., *Effect of mechanical alloying on the morphology, microstructure and properties of aluminum matrix composite powder.* Mat Sci Eng A, 2003. **342**: p. 131-143.

41. Razavi Tousi, S.S., et al., *Production of Al–20 wt.% Al2O3 composite powder using high energy milling.* Powder. Technol, 2009. **192** p. 346-351.

42. Amador, D.R. and J.M. Toualba, *Morphological and microstructural characterisation of low-alloying Fe powder obtained by mechanical attrition.* Journal of Materials Processing Technology, 2003. **143**: p. 776-780.

43. Mio, H., et al., *Effects of rotational direction and rotation-to-revolution speed ratio in planetary ball milling.* Materials Science and Engineering a-Structural Materials Properties Microstructure and Processing, 2002. **332**(1-2): p. 75-80.

44. Mio, H., et al., *Optimum revolution and rotational directions and their speeds in planetary ball milling.* International Journal of Mineral Processing, 2004. **74**: p. S85-S92.

45. Sato, A., J. Kano, and F. Saito, *Analysis of abrasion mechanism of grinding media in a planetary mill with DEM simulation.* Advanced Powder Technology, 2010. **21**(2): p. 212-216.

46. Ma, J., et al., *Application of back-propagation neural network technique to high-energy planetary ball milling process for synthesizing nanocomposite WC-MgO powders.* Materials & Design, 2009. **30**(8): p. 2867-2874.

47. Kano, J. and F. Saito, *Correlation of powder characteristics of talc during planetary ball milling with the impact energy of the balls simulated by the Particle Element Method.* Powder Technology, 1998. **98**(2): p. 166-170.

48. Watanabe, R., H. Hashimoto, and G.G. Lee, *Computer-Simulation of Milling Ball Motion in Mechanical Alloying.* Materials Transactions Jim, 1995. **36**(2): p. 102-109.

49. Ashrafizadeh, H. and M. Ashrafizaadeh, *Influence of processing parameters on grinding mechanism in planetary mill by employing discrete element method.* Advanced Powder Technology, 2012. **23**(6): p. 708-716.

50. Magini, M., et al., *Power measurements during mechanical milling—II. The case of "single path cumulative" solid state reaction.* Acta Materialia, 1998. **46**(8): p. 2841-2850.

51. Iasonna, A. and M. Magini, *Power measurements during mechanical milling. An experimental way to investigate the energy transfer phenomena.* Acta Materialia, 1996. **44**(3): p. 1109-1117.

52. Dallimore, M.P. and P.G. McCormick, *Dynamics of planetary ball milling: A comparison of computer simulated processing parameters with CuO/Ni displacement reaction milling kinetics.* Materials Transactions Jim, 1996. **37**(5): p. 1091-1098.

53. Magini, M. and A. Iasonna, *Energy-Transfer in Mechanical Alloying.* Materials Transactions Jim, 1995. **36**(2): p. 123-133.

54. Rosenkranz, S., S. Breitung-Faes, and A. Kwade, *Experimental investigations and modelling of the ball motion in planetary ball mills.* Powder Technology, 2011. **212**(1): p. 224-230.

55. Jiang, X.J., et al., *Mechanical alloying and reactive milling in a high energy planetary mill.* Journal of Alloys and Compounds, 2009. **478**(1-2): p. 246-251.

56. Murty, B.S., M. Mohan Rao, and S. Ranganathan, *Milling maps and amorphization during mechanical alloying.* Acta Metallurgica et Materialia, 1995. **43**(6): p. 2443-2450.

57. Razavi Tousi, S.S., et al., *Effect of milling time and addition of alumina powder on the structural properties and fracture surface of nanocrystalline Al.* Mater. Sci. Pol, 2009. **27** p. 875-884.

58. Wang, H.Z., et al., *A review on hydrogen production using aluminum and aluminum alloys.* Renewable & Sustainable Energy Reviews, 2009. **13**(4): p. 845-853.

59. Shkolnikov, E.I., A.Z. Zhuk, and M.S. Vlaskin, *Aluminum as energy carrier: Feasibility analysis and current technologies overview.* Renewable and Sustainable Energy Reviews, 2011. **15**(9): p. 4611-4623.

60. Aleksandrov, Y.A., E.I. Tsyganova, and A.L. Pisarev, *Reaction of Aluminum with Dilute Aqueous NaOH Solutions.* Russian Journal of General Chemistry 2003. **73**: p. 689-694.

61. Soler, L., et al., *Synergistic hydrogen generation from aluminum, aluminum alloys and sodium borohydride in aqueous solutions.* International Journal of Hydrogen Energy, 2007. **32**(18): p. 4702-4710.

62. Soler, L., et al., *In situ generation of hydrogen from water by aluminum corrosion in solutions of sodium aluminate.* Journal of Power Sources, 2009. **192**(1): p. 21-26.

63. Soler, L., et al., *Hydrogen generation by aluminum corrosion in seawater promoted by suspensions of aluminum hydroxide.* International Journal of Hydrogen Energy, 2009. **34**(20): p. 8511-8518.

64. Emregul, K.C. and A.A. Aksut, *The behavior of aluminum in alkaline media.* Corrosion Science, 2000. **42**(12): p. 2051-2067.

65. Franzoni, F., et al., *Combined hydrogen production and power generation from aluminum combustion with water: Analysis of the concept.* International Journal of Hydrogen Energy, 2010. **35**(4): p. 1548-1559.

66. Vlaskin, M.S., et al., *An experimental aluminum-fueled power plant.* Journal of Power Sources, 2011. **196**(20): p. 8828-8835.

67. Bunker, C.E., et al., *Spontaneous Hydrogen Generation from Organic-Capped Al Nanoparticles and Water.* ACS Applied Materials & Interfaces, 2010. **2**(1): p. 11-14.

68. Park, J.H., et al., *Control of hydrolytic reaction of aluminum particles for aluminum oxide nanofibers.* Materials Science and Engineering a-Structural Materials Properties Microstructure and Processing, 2004. **375**: p. 1263-1268.

69. Ilyukhina, A.V., et al., *Mechanochemical activation of aluminum with gallams for hydrogen evolution from water.* International Journal of Hydrogen Energy, 2010. **35**(5): p. 1905-1910.

70. Fan, M.Q., F. Xu, and L.X. Sun, *Studies on hydrogen generation characteristics of hydrolysis of the ball milling Al-based materials in pure water.* International Journal of Hydrogen Energy, 2007. **32**(14): p. 2809-2815.

71. Fan, M.Q., L.X. Sun, and F. Xu, *Study of the controllable reactivity of aluminum alloys and their promising application for hydrogen generation.* Energy Conversion and Management, 2010. **51**(3): p. 594-599.

72. Parmuzina, A.V., et al., *Oxidation of activated aluminum with water as a method for hydrogen generation.* Russian Chemical Bulletin, 2009. **58**: p. 493-498.

73. Fan, M.-q., L.-x. Sun, and F. Xu, *Feasibility study of hydrogen production for micro fuel cell from activated Al–In mixture in water.* Energy, 2010. **35** p. 1333-1337.

74. Fan, M.Q., F. Xu, and L.X. Sun, *Hydrogen generation by hydrolysis reaction of ball-milled Al-Bi alloys.* Energy & Fuels, 2007. **21**(4): p. 2294-2298.

75. Luo, H., et al., *Hydrogen Generation from Highly Activated Al-Ce Composite Materials in Pure Water.* Journal of the American Ceramic Society, 2011. **94**(11): p. 3976-3982.

76. Alinejad, B. and K. Mahmoodi, *A novel method for generating hydrogen by hydrolysis of highly activated aluminum nanoparticles in pure water.* International Journal of Hydrogen Energy, 2009. **34**: p. 7934-7938.

77. Mahmoodi, K. and B. Alinejad, *Enhancement of hydrogen generation rate in reaction of aluminum with water.* International Journal of Hydrogen Energy, 2010. **35**(11): p. 5227-5232

78. Czech, E. and T. Troczynski, *Hydrogen generation through massive corrosion of deformed aluminum in water.* International Journal of Hydrogen Energy, 2010. **35**(3): p. 1029-1037.

79. Dupiano, P., D. Stamatis, and E.L. Dreizin, *Hydrogen production by reacting water with mechanically milled composite aluminum-metal oxide powders.* International Journal of Hydrogen Energy, 2011. **36**: p. 4781-4791.

80. Deng, Z.Y., et al., *Effect of different modification agents on hydrogen-generation by the reaction of Al with water.* International Journal of Hydrogen Energy, 2010. **35**(18): p. 9561-9568.

81. Deng, Z.Y., et al., *Physicochemical mechanism for the continuous reaction of gamma-Al2O3-modified aluminum powder with water.* Journal of the American Ceramic Society, 2007. **90**(5): p. 1521-1526.

82. Deng, Z.-Y., et al., *Modification of Al Particle Surfaces by c-Al2O3 and Its Effect on the Corrosion Behavior of Al.* Journal of American Ceramic Society, 2005. **88** p. 977-979.

83. Chaklader, A.C.D., *HYDROGEN GENERATION FROM WATER SPLIT REACTION.* U.S. Patent, 2003. **6,582,676 B2**.

84. Streletskii, A.N., et al., *Mechanochemical activation of aluminum: 3. Kinetics of interaction between aluminum and water.* Colloid Journal, 2005. **67**(5): p. 631-637.

85. Wang, H.W., et al., *Generation of hydrogen from aluminum and water - Effect of metal oxide nanocrystals and water quality.* International Journal of Hydrogen Energy, 2011. **36**(23): p. 15136-15144.

86. Huang, X.-N., et al., *Hydrogen generation from hydrolysis of aluminum/graphite composites with a core–shell structure.* International Journal of Hydrogen Energy, 2012. **37**(9): p. 7457-7463.

87. Razavi-Tousi, S.S., R. Yazdani-Rad, and M.S. Abdi, *Impurity tracing in nanostructured Al and Al/Al 2O 3 composite prepared by high energy milling.* Advanced Composite Materials, 2010. **19**(4): p. 393-402.

88. Rodiguez, A., J.M. Gallardo, and E.J. Herrera, *Structure and properties of attrition-milled aluminum powder.* J Mater Sci, 1997. **32**: p. 3535-3539.

89. Fogognolo, J.B., M.H. Robert, and J.M. Torralba, *Mechanical alloyed AlN partic le-reinforced Al-6061 matrix composite: Powder processing, consolidation and mechanical strength and hardness of the as-extruded materials.* Mater Sci Eng A, 2006. **426**: p. 85-94.

90. Razavi Hesabi, Z., A. Simchi, and S.M. Seyed Reihani, *Structural evolution during mechanical milling of nanometric and micrometric Al2O3 reinforced Al matrix composite.* Mater Sci Eng A, 2006. **428**: p. 159-168.

91. Razavi-Tousi, S.S., R. Yazdani-Rad, and S.A. Manafi, *Structural evaluation of Al-4Mn-5Al2O3 (wt-%) nanocomposite produced by mechanical-thermal synthesis and powder technology methods* Materials Science and Technology, 2011 **27**: p. 755-760.

92. Zawrah, M.F., H. Abdel-Kader, and N.E. Elbaly, *Fabrication of Al2O3-20 vol.% Al nanocomposite powders using high energy milling and their sinterability.* Materials Research Bulletin, 2012. **47**(3): p. 655-661.

93. Khadem, S.A., S. Nategh, and H. Yoozbashizadeh, *Structural and morphological evaluation of Al-5 vol.%SiC nanocomposite powder produced by mechanical milling.* Journal of Alloys and Compounds, 2011. **509**(5): p. 2221-2226.

94. Prabhu, B., et al., *Synthesis and characterization of high volume fraction Al-Al2O3 nanocomposite powders by high-energy milling.* Materials Science and Engineering a-Structural Materials Properties Microstructure and Processing, 2006. **425**(1-2): p. 192-200.

95. Alizadeh, M. and M.M. Aliabadi, *Synthesis behavior of nanocrystalline Al-Al2O3 composite during low time mechanical milling process.* Journal of Alloys and Compounds, 2011. **509**(15): p. 4978-4986.

96. RACHINGER, W.A., *A correction for the α1 : α2 doublet in the measurement of widths of X-ray diffraction lines.* J. Sci. Instrum, 1948. **25**: p. 254 - 259.

97. Williamson, G.K. and W.H. Hall, *X-ray Line Broadening from Filed Al and W.* Acta Metall 1953. **1**: p. 22-31.

98. Rodriguez, J.A., J.M. Gallardo, and E.J. Herrera, *Structure and properties of attrition-milled aluminium powder.* Journal of Materials Science, 1997. **32**(13): p. 3535-3539.

99. Karagedov, G.R. and N.Z. Lyakhov, *Mechanochemical grinding of inorganic oxides.* KONA, 2003 **21**: p. 76-86.

100. Antunes, M.L.P., H.D. Santos, and P.D. Santos, *Characterization of the aluminum hydroxide microcrystals formed in some alcohol-water solutions.* Materials Chemistry and Physics, 2002. **76**(3): p. 243-249.

101. Iler, R.K., *Fibrillar Colloidal Boehmite - Progressive Conversion to Gamma, Theta, and Alpha Aluminas.* Journal of the American Ceramic Society, 1961. **44**(12): p. 618-624.

102. Thiruchitrambalam, M., V.R. Palkar, and V. Gopinathan, *Hydrolysis of aluminium metal and sol–gel processing of nano alumina.* Materials Letters, 2004. **58**(24): p. 3063-3066.

103. Sweegers, C., et al., *Morphology, evolution and other characteristics of gibbsite crystals grown from pure and impure aqueous sodium aluminate solutions.* Journal of Crystal Growth, 2001. **233**(3): p. 567-582.

104. Lloyd, S., et al., *Atomic force microscopy of gibbsite.* Applied Surface Science, 1998. **135**(1-4): p. 178-182.

105. Prestidge, C.A. and I. Ametov, *Cation effects during aggregation and agglomeration of gibbsite particles under synthetic Bayer crystallisation conditions.* Journal of Crystal Growth, 2000. **209**(4): p. 924-933.

106. Zhou, Q.S., et al., *Agglomeration of gibbsite particles from carbonation process of sodium aluminate solution.* Hydrometallurgy, 2009. **99**(3-4): p. 163-169.

107. Tait, J.M., A. Violante, and P. Violante, *Co-Crystallization of Gibbsite and Bayerite with Nordstrandite.* Clay Minerals, 1983. **18**(1): p. 95-99.

108. Aikin, B.J.M. and T.H. Courtney, *The Kinetics of Composite Particle Formation during Mechanical Alloying.* Metallurgical Transactions a-Physical Metallurgy and Materials Science, 1993. **24**(3): p. 647-657.

109. Sun, C.Q., *Size dependence of nanostructures: Impact of bond order deficiency.* Progress in Solid State Chemistry, 2007. **35**(1): p. 1-159.

110. Tjong, S.C. and H. Chen, *Nanocrystalline materials and coatings.* Materials Science and Engineering: R: Reports, 2004. **45**(1–2): p. 1-88.

111. Wang, W., D.M. Chen, and K. Yang, *Investigation on microstructure and hydrogen generation performance of Al-rich alloys.* International journal of hydrogen energy, 2010. **35** p. 12011-12019.

112. Leth-Olsen, H., J.H. Nordlien, and K. Nisancioglu, *Filiform corrosion of aluminium sheet. III. Microstructure of reactive surfaces.* Corrosion Science, 1998. **40**(12): p. 2051-2063.

113. Vedder, W. and Vermilye.Da, *Aluminum+Water Reaction.* Transactions of the Faraday Society, 1969. **65**(554P): p. 561-&.

114. David, E. and J. Kopac, *Hydrolysis of aluminum dross material to achieve zero hazardous waste.* Journal of Hazardous Materials, 2012. **209**: p. 501-509.

115. Watanabe, M., *Chemical reactions in cracks of aluminum crystals: Generation of hydrogen from water.* Journal of Physics and Chemistry of Solids, 2010. **71**(9): p. 1251-1258.

116. Razavi-Tousi, S.S., et al., *Modifying aluminum–water reaction to generate nano-sized aluminum hydroxide particles beside hydrogen.* Powder Technology, 2013. **241**(0): p. 166-173.

117. Razavi-Tousi, S.S. and J.A. Szpunar, *Effect of structural evolution of aluminum powder during ball milling on hydrogen generation in aluminum–water reaction.* International Journal of Hydrogen Energy, 2013. **38**(2): p. 795-806.

118. Zhao, Z.W., X.Y. Chen, and M.M. Hao, *Hydrogen generation by splitting water with Al-Ca alloy.* Energy, 2011. **36**(5): p. 2782-2787.

119. Huang, X.N., et al., *Hydrogen generation from hydrolysis of aluminum/graphite composites with a core-shell structure.* International Journal of Hydrogen Energy, 2012. **37**(9): p. 7457-7463.

120. Flamini, D.O., S.B. Saidman, and J.B. Bessone, *Aluminium activation produced by gallium.* Corrosion Science, 2006. **48**(6): p. 1413-1425.

121. Huang, X.N., et al., *Effects of amalgam on hydrogen generation by hydrolysis of aluminum with water.* International Journal of Hydrogen Energy, 2011. **36**(23): p. 15119-15124.

122. Mahmoodi, K. and B. Alinejad, *Enhancement of hydrogen generation rate in reaction of aluminum with water.* International Journal of Hydrogen Energy, 2010. **35**(11): p. 5227-5232.

123. Van Gheem, E., J. Vereecken, and C. Le Pen, *Influence of different anions on the behaviour of aluminium in aqueous solutions.* Journal of Applied Electrochemistry, 2002. **32**(11): p. 1193-1200.

124. McCafferty, E., *Sequence of steps in the pitting of aluminum by chloride ions.* Corrosion Science, 2003. **45**(7): p. 1421-1438.

125. R.A.Young, ed. *The Rietveld Method*. ed. R.A.Young. 1996, Oxford University, Press: Washington, DC. 1-38.

126. Strohmeier, B.R., *An ESCA method for determining the oxide thickness on aluminum alloys.* Surf. Interface Anal, 1990. **15**: p. 51.

127. Fan, M.-Q., et al., *Hydrolysis of ball milling Al–Bi–hydride and Al–Bi–salt mixture for hydrogen generation.* Journal of Alloys and Compounds, 2008. **460**(1–2): p. 125-129.

128. Hart, R.K., *The Formation of Films on Aluminium Immersed in Water.* Transactions of the Faraday Society, 1957. **53**(7): p. 1020-&.

129. Gurses, E., H. Wafai, and T. El Sayed, *Constitutive modeling of stress-driven grain growth in nanocrystalline metals.* Modelling and Simulation in Materials Science and Engineering, 2013. **21**(2).

130. Saldana, C., et al., *Stabilizing nanostructured materials by coherent nanotwins and their grain boundary triple junction drag.* Applied Physics Letters, 2009. **94**(2).

131. Haber, J.A. and W.E. Buhro, *Kinetic instability of nanocrystalline aluminum prepared by chemical synthesis; Facile room-temperature grain growth.* Journal of the American Chemical Society, 1998. **120**(42): p. 10847-10855.

132. Zhang, K., J.R. Weertman, and J.A. Eastman, *The influence of time, temperature, and grain size on indentation creep in high-purity nanocrystalline and ultrafine grain copper.* Applied Physics Letters, 2004. **85**(22): p. 5197-5199.

133. Ralston, K.D. and N. Birbilis, *Effect of Grain Size on Corrosion: A Review.* Corrosion, 2010. **66**(7): p. 075005-075005-13.

134. Song, D., et al., *Corrosion behavior of ultra-fine grained industrial pure Al fabricated by ECAP.* Transactions of Nonferrous Metals Society of China, 2009. **19**(5): p. 1065-1070.

135. Sikora, E., X.J. Wei, and B.A. Shaw, *Corrosion Behavior of Nanocrystalline Bulk Al-Mg-Based Alloys.* Corrosion, 2004. **60**(4): p. 387-398.

136. Kus, E., et al., *A Comparison of the Corrosion Behavior of Nanocrystalline and Conventional Al 5083 Samples.* Corrosion, 2006. **62**(2): p. 152-161.

137. Chung, M.-K., et al., *Effect of the number of ECAP pass time on the electrochemical properties of 1050 Al alloys.* Materials Science and Engineering: A, 2004. **366**(2): p. 282-291.

138. Tsai, T.C. and T.H. Chuang, *Role of grain size on the stress corrosion cracking of 7475 aluminum alloys.* Materials Science and Engineering: A, 1997. **225**(1–2): p. 135-144.

139. Mahmoud, T.S., *Effect of friction stir processing on electrical conductivity and corrosion resistance of AA6063-T6 Al alloy.* Proceedings of the Institution of Mechanical Engineers, Part C: Journal of Mechanical Engineering Science, 2008. **222**(7): p. 1117-1123.

140. Osório, W.R., C.M. Freire, and A. Garcia, *The role of macrostructural morphology and grain size on the corrosion resistance of Zn and Al castings.* Materials Science and Engineering: A, 2005. **402**(1–2): p. 22-32.

141. Ralston, K.D., N. Birbilis, and C.H.J. Davies, *Revealing the relationship between grain size and corrosion rate of metals.* Scripta Materialia, 2010. **63**(12): p. 1201-1204.

142. Bunker, B.C., et al., *Hydration of passive oxide films on aluminum.* Journal of Physical Chemistry B, 2002. **106**(18): p. 4705-4713.

143. Pyun, S.I. and S.M. Moon, *Corrosion mechanism of pure aluminium in aqueous alkaline solution.* Journal of Solid State Electrochemistry, 2000. **4**(5): p. 267-272.

144. Bernard, W.J. and J.J. Randall, *An Investigation of the Reaction between Aluminum and Water.* Journal of the Electrochemical Society, 1960. **107**(6): p. 483-487.

145. Stralin, A. and T. Hjertberg, *Influence of Surface-Composition on Initial Hydration of Aluminum in Boiling Water.* Applied Surface Science, 1994. **74**(3): p. 263-275.

146. Alwitt, R.S., *The Growth of Hydrous Oxide Films on Aluminum.* Journal of The Electrochemical Society, 1974. **121**(10): p. 1322-1328.

147. Vermilyea, D.A. and W. Vedder, *Inhibition of the aluminum+water reaction.* Transactions of the Faraday Society, 1970. **66**(0): p. 2644-2654.

148. Hasnaoui, A., et al., *Molecular dynamics simulations of the nano-scale room-temperature oxidation of aluminum single crystals.* Surface Science, 2005. **579**(1): p. 47-57.

149. Jeurgens, L.P.H., et al., *Determination of thickness and composition of aluminium-oxide overlayers on aluminium substrates.* Applied Surface Science, 1999. **144-45**: p. 11-15.

150. Reichel, F., L.P.H. Jeurgens, and E.J. Mittemeijer, *The role of the initial oxide-film microstructure on the passivation behavior of Al metal surfaces.* Surface and Interface Analysis, 2008. **40**(3-4): p. 281-284.

151. Jeurgens, L.P.H., et al., *Growth kinetics and mechanisms of aluminum-oxide films formed by thermal oxidation of aluminum.* Journal of Applied Physics, 2002. **92**(3): p. 1649-1656.

152. Farrell, K., *5.07 - Performance of Aluminum in Research Reactors*, in *Comprehensive Nuclear Materials*, J.M.K. Editor-in-Chief: Rudy, Editor. 2012, Elsevier: Oxford. p. 143-175.

153. Gholizadeh Aghoyeh, R. and H. Khalafi, *Corrosion monitoring and determination of aluminium fuel clad of Tehran Research Reactor (TRR).* Progress in Nuclear Energy, 2010. **52**(2): p. 225-228.

154. *Corrosion of Research Reactor Aluminium Clad Spent Fuel in Water*, in *Technical Reports Series No.418*. 2003, INTERNATIONAL ATOMIC ENERGY AGENCY: Vienna, Austria.

155. Pawel, R.E., et al., *The corrosion of 6061 aluminum under heat transfer conditions in the ANS corrosion test loop.* Oxidation of Metals, 1991. **36**(1-2): p. 175-194.

156. Draley, J.E., S. Mori, and R.E. Loess, *The Corrosion of 1100 Aluminum in Oxygen-Saturated Water at 70°C.* J. Electrochem. Soc., 1963. **110**: p. 622-627

157. Mori, S. and J.E. Draley, *Oxide Dissolution and Its Effect on the Corrosion of 1100 Aluminum in Water at 70°C.* Journal of The Electrochemical Society, 1967. **114**(4): p. 352-353.

158. Rider, A.N., *The influence of porosity and morphology of hydrated oxide films on epoxy-aluminium bond durability.* Journal of Adhesion Science and Technology, 2001. **15**(4): p. 395-422.

159. Underhill, P.R. and A.N. Rider, *Hydrated oxide film growth on aluminium alloys immersed in warm water.* Surface and Coatings Technology, 2005. **192**(2–3): p. 199-207.

160. Rider, A.N. and D.R. Arnott, *Boiling water and silane pre-treatment of aluminium alloys for durable adhesive bonding.* International Journal of Adhesion and Adhesives, 2000. **20**(3): p. 209-220.

161. Altenpohl, D. and W. Post, *Hydrated Oxide Films on Aluminum - Their Growth and Their Importance in Electrolytic Capacitors.* Journal of The Electrochemical Society, 1961. **108**(7): p. 628-631.

162. Baker, B.R. and J.D. Balser, *Formation of films on aluminum by reaction with water.* Aluminum 1976. **52** p. 197-200.

163. Moon, S.M. and S.I. Pyun, *Effects of applied anodic potential and pH on the repassivation kinetics of pure aluminium in aqueous alkaline solution.* Journal of Solid State Electrochemistry, 1999. **3**(2): p. 104-110.

164. Liang, L.B., et al., *Effect of hydration pretreatment on tunnel etching behaviour of aluminium foil.* Corrosion Science, 2013. **70**: p. 180-187.

165. Ambat, R. and E.S. Dwarakadasa, *Studies on the influence of chloride ion and pH on the electrochemical behaviour of aluminium alloys 8090 and 2014.* Journal of Applied Electrochemistry, 1994. **24**(9): p. 911-916.

166. Birss, V.I. and D.R. Truax, *An effective approach to teaching electrochemistry.* Journal of Chemical Education, 1990. **67**(5): p. 403.

167. MURALIDHARAN, V.S., *AN INSIGHT INTO THE ORIGIN OF CORROSION POTENTIAL: A CRITICAL REVIEW*. Bulletin of Electrochemistry, 2002. **18** p. 179-186.

168. Geiculescu, A.C. and T. F. Strange, *A microstructural investigation of low-temperature crystalline alumina films grown on aluminum.* Thin Solid Films, 2003. **426**(1–2): p. 160-171.

169. Geiculescu, A.C. and T.F. Strange, *Aluminum oxide thin dielectric film formation under elevated gravity conditions.* Thin Solid Films, 2006. **503**(1–2): p. 45-54.

170. Chen, C., et al., *Measurement of oxide film growth on Mg and Al surfaces over extended periods using XPS.* Surface Science, 1997. **382**(1-3): p. L652-L657.

171. Ambat, R., et al., *Effect of iron-containing intermetallic particles on the corrosion behaviour of aluminium.* Corrosion Science, 2006. **48**(11): p. 3455-3471.

172. Zhang, D.L., *Processing of advanced materials using high-energy mechanical milling.* Progress in Materials Science, 2004. **49**(3-4): p. 537-560.

173. Witkin, D.B. and E.J. Lavernia, *Synthesis and mechanical behavior of nanostructured materials via cryomilling.* Progress in Materials Science, 2006. **51**(1): p. 1-60.

174. Courtney, T.H., *Process Modeling of Mechanical Alloying.* Materials Transactions Jim, 1995. **36**(2): p. 110-122.

175. Huang, J.Y., Y.K. Wu, and H.Q. Ye, *Ball-Milling of Ductile Metals.* Materials Science and Engineering a-Structural Materials Properties Microstructure and Processing, 1995. **199**(2): p. 165-172.

176. Fecht, H.J., *Nanostructure formation by mechanical attrition.* Nanostructured Materials, 1995. **6**(1-4): p. 33-42.

177. Fecht, H.J., et al., *Nanocrystalline Metals Prepared by High-Energy Ball Milling.* Metallurgical Transactions a-Physical Metallurgy and Materials Science, 1990. **21**(9): p. 2333-2337.

178. He, J.H. and E.J. Lavernia, *Development of nanocrystalline structure during cryomilling of Inconel 625.* Journal of Materials Research, 2001. **16**(9): p. 2724-2732.

179. Zhang, X., et al., *Evidence for the formation mechanism of nanoscale microstructures in cryomilled Zn powder.* Acta Materialia, 2001. **49**(8): p. 1319-1326.

180. Han, B.Q., et al., *Processing and behavior of nanostructured metallic alloys and composites by cryomilling.* Journal of Materials Science, 2007. **42**(5): p. 1660-1672.

181. Xun, Y.W., E.J. Lavernia, and F.A. Mohamed, *Synthesis of nanocrystalline Zn-22 pct Al using cryomilling.* Metallurgical and Materials Transactions a-Physical Metallurgy and Materials Science, 2004. **35A**(2): p. 573-581.

182. Huang, J.Y., et al., *Grain boundary structure of nanocrystalline Cu processed by cryomilling.* Philosophical Magazine, 2003. **83**(12): p. 1407-1419.

183. Liao, X.Z., et al., *Nanostructures and deformation mechanisms in a cryogenically ball-milled Al-Mg alloy.* Philosophical Magazine, 2003. **83**(26): p. 3065-3075.

184. Ye, J.C., et al., *Cryomilling for the fabrication of a particulate B4C reinforced Al nanocomposite: Part II. Mechanisms for microstructural evolution.* Metallurgical and Materials Transactions a-Physical Metallurgy and Materials Science, 2006. **37A**(10): p. 3111-3117.

185. Zheng, B.L., et al., *Twinning in cryomilled nanocrystalline Mg powder.* Philosophical Magazine Letters, 2013. **93**(8): p. 457-464.

186. Huang, J.Y., Y.K. Wu, and H.Q. Ye, *Deformation structures in ball milled copper.* Acta Materialia, 1996. **44**(3): p. 1211-1221.

187. Zhou, F., et al., *Formation of nanostructure in Al produced by a low-energy ball milling at cryogenic temperature.* Materials Science and Engineering a-Structural Materials Properties Microstructure and Processing, 2004. **375**: p. 917-921.

188. Eckert, J., et al., *Structural and thermodynamic properties of nanocrystalline fcc metals prepared by mechanical attrition.* Journal of Materials Research, 1992. **7**(07): p. 1751-1761.

189. Guo, B., et al., *Crystalline phase of Y2O3:Eu particles generated in a substrate-free flame process.* Particuology, 2011. **9**(1): p. 24-31.

190. Small, J.A. and J.R. Michael, *Phase identification of individual crystalline particles by electron backscatter diffraction.* Journal of Microscopy-Oxford, 2001. **201**: p. 59-69.

191. Godec, A., D. Nolan, and M. Jenko, *Characterisation of crystallisation in amorphous soft magnetic Fe74Si11B14Ni1 powders by EBSD method.* Materials Science and Engineering B-Solid State Materials for Advanced Technology, 2006. **129**(1-3): p. 31-38.

192. Hedberg, Y., et al., *Ultrafine 316 L stainless steel particles with frozen-in magnetic structures characterized by means of electron backscattered diffraction.* Materials Letters, 2011. **65**(14): p. 2089-2092.

193. Hughes, D.A. and N. Hansen, *High angle boundaries formed by grain subdivision mechanisms.* Acta Materialia, 1997. **45**(9): p. 3871-3886.

194. Bor, T.C., et al., *Analysis of ball-milled Mo powder using X-ray diffraction.* Philosophical Magazine, 2003. **83**(29): p. 3327-3373.

195. Lin, Y., et al., *Strain Energy During Mechanical Milling: Part I. Mathematical Modeling.* Metallurgical and Materials Transactions A, 2012. **43**(11): p. 4247-4257.

196. Zhang, Z.H., et al., *Critical grain size for nanocrystalline-to-amorphous phase transition in Al solid solution.* Philosophical Magazine Letters, 2012. **92**(5): p. 235-244.

197. Feng, Y.T., K. Han, and D.R.J. Owen, *Discrete element simulation of the dynamics of high energy planetary ball milling processes.* Materials Science and Engineering a-Structural Materials Properties Microstructure and Processing, 2004. **375**: p. 815-819.

198. Rydin, R.W., D. Maurice, and T.H. Courtney, *Milling Dynamics .1. Attritor Dynamics - Results of a Cinematographic Study.* Metallurgical Transactions a-Physical Metallurgy and Materials Science, 1993. **24**(1): p. 175-185.

199. Zahid, G.H., Y. Huang, and P.B. Prangnell, *Microstructure and texture evolution during annealing a cryogenic-SPD processed Al-alloy with a nanoscale lamellar HAGB grain structure.* Acta Materialia, 2009. **57**(12): p. 3509-3521.

200. Apps, P.J., J.R. Bowen, and P.B. Prangnell, *The effect of coarse second-phase particles on the rate of grain refinement during severe deformation processing.* Acta Materialia, 2003. **51**(10): p. 2811-2822.

201. Apps, P.J., M. Berta, and P.B. Prangnell, *The effect of dispersoids on the grain refinement mechanisms during deformation of aluminium alloys to ultra-high strains.* Acta Materialia, 2005. **53**(2): p. 499-511.

202. Jazaeri, H. and F.J. Humphreys, *The transition from discontinuous to continuous recrystallization in some aluminium alloys I - the deformed state.* Acta Materialia, 2004. **52**(11): p. 3239-3250.

203. Toth, L.S., et al., *Effect of grain refinement by severe plastic deformation on the next-neighbor misorientation distribution.* Acta Materialia, 2010. **58**(20): p. 6706-6716.

204. Mei, Q.S., K. Tsuchiya, and H. Gao, *Different stages in the continuous microstructural evolution of copper deformed to ultrahigh plastic strains.* Scripta Materialia, 2012. **67**(12): p. 1003-1006.

205. Snyder, D., et al., *Deformation Characteristics and Recrystallization Response of a 9310 Steel Alloy.* Metallurgical and Materials Transactions a-Physical Metallurgy and Materials Science, 2013. **44A**(1): p. 479-493.

206. Sun, L., et al., *The effect of strain path reversal on high-angle boundary formation by grain subdivision in a model austenitic steel.* Scripta Materialia, 2011. **64**(3): p. 280-283.

207. Hansen, N. and D.J. Jensen, *Development of microstructure in FCC metals during cold work.* Philosophical Transactions of the Royal Society a-Mathematical Physical and Engineering Sciences, 1999. **357**(1756): p. 1447-1469.

208. Hughes, D.A. and N. Hansen, *Deformation structures developing on fine scales.* Philosophical Magazine, 2003. **83**(31-34): p. 3871-3893.

209. Kuhlmann-Wilsdorf, D., et al., *Deformation bands, the LEDS theory, and their importance in texture development: Part I. Previous evidence and new observations.* Metallurgical and Materials Transactions a-Physical Metallurgy and Materials Science, 1999. **30**(9): p. 2491-2501.

210. Ferrasse, S., et al., *Microstructure and properties of copper and aluminum alloy 3003 heavily worked by equal channel angular extrusion.* Metallurgical and Materials Transactions a-Physical Metallurgy and Materials Science, 1997. **28**(4): p. 1047-1057.

211. Kuhlmanwilsdorf, D. and N. Hansen, *Geometrically Necessary, Incidental and Subgrain Boundaries.* Scripta Metallurgica Et Materialia, 1991. **25**(7): p. 1557-1562.

212. Humphreys, F.J. and M. Hatherly, *Recrystallization and Related Annealing Phenomena (Second Edition)*, ed. F.J. Humphreys and M. Hatherly. 2004, Oxford: Elsevier. 1-574.

213. Huang, Y. and P.B. Prangnell, *The effect of cryogenic temperature and change in deformation mode on the limiting grain size in a severely deformed dilute aluminium alloy.* Acta Materialia, 2008. **56**(7): p. 1619-1632.

214. Cizek, P., *Dislocation boundaries and disclinations formed within the cube-oriented grains during tensile deformation of aluminium.* Acta Materialia, 2010. **58**(17): p. 5820-5833.

215. Liu, Q. and N. Hansen, *Geometrically Necessary Boundaries and Incidental Dislocation Boundaries Formed during Cold Deformation.* Scripta Metallurgica Et Materialia, 1995. **32**(8): p. 1289-1295.

216. Wu, X., et al., *Microstructure and evolution of mechanically-induced ultrafine grain in surface layer of AL-alloy subjected to USSP.* Acta Materialia, 2002. **50**(8): p. 2075-2084.

217. Hughes, D.A., *Microstructure evolution, slip patterns and flow stress.* Materials Science and Engineering a-Structural Materials Properties Microstructure and Processing, 2001. **319**: p. 46-54.

218. Chae, J.Y., R.S. Qin, and H.K.D.H. Bhadeshia, *Topology of the Deformation of a Non-uniform Grain Structure.* Isij International, 2009. **49**(1): p. 115-118.

219. Bate, P.S. and W.B. Hutchinson, *Grain boundary area and deformation.* Scripta Materialia, 2005. **52**(3): p. 199-203.

220. Canova, G.R., et al., *Effect of rate sensitivity on slip system activity and lattice rotation.* Acta Metallurgica, 1988. **36**(8): p. 1961-1970.

221. Chang, C.P., P.L. Sun, and P.W. Kao, *Deformation induced grain boundaries in commercially pure aluminium.* Acta Materialia, 2000. **48**(13): p. 3377-3385.

222. Doherty, R.D., et al., *Current issues in recrystallization: a review.* Materials Science and Engineering a-Structural Materials Properties Microstructure and Processing, 1997. **238**(2): p. 219-274.

223. Soler, L., et al., *Hydrogen generation from water and aluminum promoted by sodium stannate.* International Journal of Hydrogen Energy, 2010. **35**(3): p. 1038-1048.

224. Tikhov, S., et al., *Kinetics of aluminum powder oxidation by water at 100°C.* Reaction Kinetics and Catalysis Letters, 2007. **92**(1): p. 83-88.

225. Chambon, M., S. Abanades, and G. Flamant, *Kinetic investigation of hydrogen generation from hydrolysis of SnO and Zn solar nanopowders.* International Journal of Hydrogen Energy, 2009. **34**(13): p. 5326-5336.

226. Rat'ko, A.I., et al., *Hydrothermal Synthesis of Porous Al2O3/Al Metal Ceramics: II. Mechanism of Formation of a Porous Al(OH)3/Al Composite.* Kinetics and Catalysis, 2004. **45**(1): p. 149-155.

227. Nie, H., M. Schoenitz, and E.L. Dreizin, *Calorimetric investigation of the aluminum–water reaction.* International Journal of Hydrogen Energy, 2012. **37**(15): p. 11035-11045.

228. Levenspiel, O., *Chemical Reaction Engineering*. 1999, New York John Wiley & Sons

229. Razavi-Tousi, S.S. and J.A. Szpunar, *Mechanism of Corrosion of Activated Aluminum Particles by Hot Water.* Electrochimica Acta, 2014. **127**(0): p. 95-105.

230. Skrovan, J., A. Alfantazi, and T. Troczynski, *Enhancing aluminum corrosion in water.* Journal of Applied Electrochemistry, 2009. **39**(10): p. 1695-1702.

231. Alinejad, B., K. Mahmoodi, and K. Ahmadi, *A new route to mass production of metal hydroxide/oxide hydroxide nanoparticles.* Materials Chemistry and Physics, 2009. **118**(2-3): p. 473-476.

232. Mahmoodi, K. and B. Alinejad, *Fast and facile synthesis of boehmite nanofibers.* Powder Technology, 2010. **199**(3): p. 289-292.

233. Szklarska-Smialowska, Z., *Pitting corrosion of aluminum.* Corrosion Science, 1999. **41**(9): p. 1743-1767.

APPENDIX

COPYRIGHT PERMISSIONS

For previously published manuscripts that form a part of a thesis, written permission from the publisher (copyright holder) is required by the College of Graduate Studies and Research (CGSR). This appendix includes the copyright permissions from the publishers for the manuscripts that were published or are under review, and used in the thesis.

Copyright Permission for Manuscript #1

T. Nejat Veziroglu <veziroglu@iahe.org> Fri, May 9, 2014 at 7:28 AM
To: Salman Razavi <ser105@mail.usask.ca>
Cc: "Emre A. Veziroglu" <emrev1@cox.net>

Subject: Copyright permission
Dear Salman:
In accordance with your request, we are happy to give you permission to use the following article in your Ph.D. thesis:
S.S. Razavi-Tousi, J.A. Szpunar, Effect of structural evolution of aluminum powder during ball milling on hydrogen generation in aluminum–water reaction, International Journal of Hydrogen Energy, Volume 38, Issue 2, 24 January 2013, Pages 795-806
Wishing you all the best in your endeavours, I remain
Sincerely yours,

T. Nejat Veziroglu
Founding Editor-in-Chief

International Journal of Hydrogen Energy (IJHE)

Copyright Permission for Manuscript #2

01_03 PERMISSION LETTER

October 30, 2014
Springer reference
Metallurgical and Materials Transactions EMaterials for Energy Systems

10.1007/s40553-014-0024-7
Role of Ball Milling of Aluminum Powders in Promotion of Aluminum-Water Reaction to Generate Hydrogen

Journal no. 40553	Salman Razavi	**Hydrogen**
Your project Requestor:	Department of Mechanical Engineering University of Saskatchewan 57 Campus Drive Saskatoon, Saskatchewan, S7N 5A9, Canada +1 (306) 290 9084	S. S. Razavi-Tousi1 and J. A. Szpunar1 DOI: 10.1007/s40553-014-0024-7 Print ISSN: 2196-2936 Online ISSN: 2196-2944
University:	University of Saskatchewan	
Purpose:	Dissertation/Thesis	

With reference to your request to reuse material in which Springer Science+Business Media controls the copyright, our permission is granted free of charge under the following conditions:

Springer material

 represents original material which does not carry references to other sources (if material in question refers with a credit to another source, authorization from that source is required as well);

 requires full credit (Springer and the original publisher, book/journal title, chapter/article title, volume, year of publication, page, name(s) of author(s), original copyright notice) to the publication in which the material was originally published by adding: "With kind permission of Springer Science+Business Media";

 may not be altered in any manner. Abbreviations, additions, deletions and/or any other alterations shall be made only with prior written authorization of the author and/or Springer Science+Business Media;

 Springer does not supply original artwork or content.

This permission

 is non-exclusive;

 is valid for one-time use only for the purpose of defending your thesis and with a maximum of 100 extra copies in paper. If the thesis is going to be published, permission needs to be reobtained.
 includes use in an electronic form, provided it is an author-created version of the thesis on his/her own website and his/her university's repository, including UMI (according to the definition on the Sherpa website: http://www.sherpa.ac.uk/romeo/);
 is subject to courtesy information to the co-author or corresponding author;
 is personal to you and may not be sublicensed, assigned, or transferred by you to any other person without Springer's written permission.

This license is valid only when the conditions noted above are met.

Permission free of charge does not prejudice any rights we might have to charge for reproduction of our copyrighted material in the future.
Rights and Permissions
Springer Science+Business Media
Tiergartenstr. 17
69121 Heidelberg
Germany

Copyright Permission for Manuscript #3

ELSEVIER LICENSE
TERMS AND CONDITIONS
Jun 10, 2014

This is a License Agreement between Salman Razavi ("You") and Elsevier ("Elsevier") provided by Copyright Clearance Center ("CCC"). The license consists of your order details, the terms and conditions provided by Elsevier, and the payment terms and conditions.

All payments must be made in full to CCC. For payment instructions, please see information listed at the bottom of this form.

Supplier	Elsevier Limited The Boulevard,Langford Lane Kidlington,Oxford,OX5 1GB,UK
Registered Company Number	1982084
Customer name	Salman Razavi
Customer address	57 Campus Dr Saskatoon, SK S7N 5A9
License number	3405660695077

License date	Jun 10, 2014
Licensed content publisher	Elsevier
Licensed content publication	Electrochimica Acta
Licensed content title	Mechanism of Corrosion of Activated Aluminum Particles by Hot Water
Licensed content author	S.S. Razavi-Tousi,J.A. Szpunar
Licensed content date	1 May 2014
Licensed content volume number	127
Licensed content issue number	None
Number of pages	11
Start Page	95
End Page	105
Type of Use	reuse in a thesis/dissertation
Intended publisher of new work	other
Portion	full article
Format	both print and electronic
Are you the author of this Elsevier article?	Yes
Will you be translating?	No
Title of your thesis/dissertation	Mechanism of reaction of Activated Aluminum Particles by Hot Water
Expected completion date	Sep 2014
Estimated size (number of pages)	250
Elsevier VAT number	GB 494 6272 12
Permissions price	0.00 USD
VAT/Local Sales Tax	0.00 USD / 0.00 GBP
Total	0.00 USD
Terms and Conditions	

INTRODUCTION

1. The publisher for this copyrighted material is Elsevier. By clicking "accept" in connection with completing this licensing transaction, you agree that the following terms and conditions apply to this transaction (along with the Billing and Payment terms and conditions established by Copyright Clearance Center, Inc. ("CCC"), at the time that you opened your Rightslink account and that are available at any time at http://myaccount.copyright.com).

GENERAL TERMS

2. Elsevier hereby grants you permission to reproduce the aforementioned material subject

to the terms and conditions indicated.

3. Acknowledgement: If any part of the material to be used (for example, figures) has appeared in our publication with credit or acknowledgement to another source, permission must also be sought from that source. If such permission is not obtained then that material may not be included in your publication/copies. Suitable acknowledgement to the source must be made, either as a footnote or in a reference list at the end of your publication, as follows:

"Reprinted from Publication title, Vol /edition number, Author(s), Title of article / title of chapter, Pages No., Copyright (Year), with permission from Elsevier [OR APPLICABLE SOCIETY COPYRIGHT OWNER]." Also Lancet special credit - "Reprinted from The Lancet, Vol. number, Author(s), Title of article, Pages No., Copyright (Year), with permission from Elsevier."

4. Reproduction of this material is confined to the purpose and/or media for which permission is hereby given.

5. Altering/Modifying Material: Not Permitted. However figures and illustrations may be altered/adapted minimally to serve your work. Any other abbreviations, additions, deletions and/or any other alterations shall be made only with prior written authorization of Elsevier Ltd. (Please contact Elsevier at permissions@elsevier.com)

6. If the permission fee for the requested use of our material is waived in this instance, please be advised that your future requests for Elsevier materials may attract a fee.

7. Reservation of Rights: Publisher reserves all rights not specifically granted in the combination of (i) the license details provided by you and accepted in the course of this licensing transaction, (ii) these terms and conditions and (iii) CCC's Billing and Payment terms and conditions.

8. License Contingent Upon Payment: While you may exercise the rights licensed immediately upon issuance of the license at the end of the licensing process for the transaction, provided that you have disclosed complete and accurate details of your proposed use, no license is finally effective unless and until full payment is received from you (either by publisher or by CCC) as provided in CCC's Billing and Payment terms and conditions. If full payment is not received on a timely basis, then any license preliminarily granted shall be deemed automatically revoked and shall be void as if never granted. Further, in the event that you breach any of these terms and conditions or any of CCC's Billing and Payment terms and conditions, the license is automatically revoked and shall be void as if never granted. Use of materials as described in a revoked license, as well as any use of the materials beyond the scope of an unrevoked license, may constitute copyright infringement and publisher reserves the right to take any and all action to protect its copyright in the materials.

9. Warranties: Publisher makes no representations or warranties with respect to the licensed

material.

10. Indemnity: You hereby indemnify and agree to hold harmless publisher and CCC, and their respective officers, directors, employees and agents, from and against any and all claims arising out of your use of the licensed material other than as specifically authorized pursuant to this license.

11. No Transfer of License: This license is personal to you and may not be sublicensed, assigned, or transferred by you to any other person without publisher's written permission.

12. No Amendment Except in Writing: This license may not be amended except in a writing signed by both parties (or, in the case of publisher, by CCC on publisher's behalf).

13. Objection to Contrary Terms: Publisher hereby objects to any terms contained in any purchase order, acknowledgment, check endorsement or other writing prepared by you, which terms are inconsistent with these terms and conditions or CCC's Billing and Payment terms and conditions. These terms and conditions, together with CCC's Billing and Payment terms and conditions (which are incorporated herein), comprise the entire agreement between you and publisher (and CCC) concerning this licensing transaction. In the event of any conflict between your obligations established by these terms and conditions and those established by CCC's Billing and Payment terms and conditions, these terms and conditions shall control.

14. Revocation: Elsevier or Copyright Clearance Center may deny the permissions described in this License at their sole discretion, for any reason or no reason, with a full refund payable to you. Notice of such denial will be made using the contact information provided by you. Failure to receive such notice will not alter or invalidate the denial. In no event will Elsevier or Copyright Clearance Center be responsible or liable for any costs, expenses or damage incurred by you as a result of a denial of your permission request, other than a refund of the amount(s) paid by you to Elsevier and/or Copyright Clearance Center for denied permissions.

LIMITED LICENSE

The following terms and conditions apply only to specific license types:

15. **Translation**: This permission is granted for non-exclusive world **English** rights only unless your license was granted for translation rights. If you licensed translation rights you may only translate this content into the languages you requested. A professional translator must perform all translations and reproduce the content word for word preserving the integrity of the article. If this license is to re-use 1 or 2 figures then permission is granted for non-exclusive world rights in all languages.

16. **Posting licensed content on any Website**: The following terms and conditions apply as follows: Licensing material from an Elsevier journal: All content posted to the web site must maintain the copyright information line on the bottom of each image; A hyper-text

must be included to the Homepage of the journal from which you are licensing at http://www.sciencedirect.com/science/journal/xxxxx or the Elsevier homepage for books at http://www.elsevier.com; Central Storage: This license does not include permission for a scanned version of the material to be stored in a central repository such as that provided by Heron/XanEdu.

Licensing material from an Elsevier book: A hyper-text link must be included to the Elsevier homepage at http://www.elsevier.com . All content posted to the web site must maintain the copyright information line on the bottom of each image.

Posting licensed content on Electronic reserve: In addition to the above the following clauses are applicable: The web site must be password-protected and made available only to bona fide students registered on a relevant course. This permission is granted for 1 year only. You may obtain a new license for future website posting.

For journal authors: the following clauses are applicable in addition to the above: Permission granted is limited to the author accepted manuscript version* of your paper.

*Accepted Author Manuscript (AAM) Definition: An accepted author manuscript (AAM) is the author's version of the manuscript of an article that has been accepted for publication and which may include any author-incorporated changes suggested through the processes of submission processing, peer review, and editor-author communications. AAMs do not include other publisher value-added contributions such as copy-editing, formatting, technical enhancements and (if relevant) pagination.

You are not allowed to download and post the published journal article (whether PDF or HTML, proof or final version), nor may you scan the printed edition to create an electronic version. A hyper-text must be included to the Homepage of the journal from which you are licensing at http://www.sciencedirect.com/science/journal/xxxxx. As part of our normal production process, you will receive an e-mail notice when your article appears on Elsevier's online service ScienceDirect (www.sciencedirect.com). That e-mail will include the article's Digital Object Identifier (DOI). This number provides the electronic link to the published article and should be included in the posting of your personal version. We ask that you wait until you receive this e-mail and have the DOI to do any posting.

Posting to a repository: Authors may post their AAM immediately to their employer's institutional repository for internal use only and may make their manuscript publically available after the journal-specific embargo period has ended.

Please also refer to Elsevier's Article Posting Policy for further information.

18. **For book authors the following clauses are applicable in addition to the above:** Authors are permitted to place a brief summary of their work online only.. You are not allowed to download and post the published electronic version of your chapter, nor may you scan the printed edition to create an electronic version. Posting to a repository:

Authors are permitted to post a summary of their chapter only in their institution's repository.

20. **Thesis/Dissertation**: If your license is for use in a thesis/dissertation your thesis may be submitted to your institution in either print or electronic form. Should your thesis be published commercially, please reapply for permission. These requirements include permission for the Library and Archives of Canada to supply single copies, on demand, of the complete thesis and include permission for UMI to supply single copies, on demand, of the complete thesis. Should your thesis be published commercially, please reapply for permission.

Elsevier Open Access Terms and Conditions

Elsevier publishes Open Access articles in both its Open Access journals and via its Open Access articles option in subscription journals.

Authors publishing in an Open Access journal or who choose to make their article Open Access in an Elsevier subscription journal select one of the following Creative Commons user licenses, which define how a reader may reuse their work: Creative Commons Attribution License (CC BY), Creative Commons Attribution – Non Commercial - ShareAlike (CC BY NC SA) and Creative Commons Attribution – Non Commercial – No Derivatives (CC BY NC ND)

Terms & Conditions applicable to all Elsevier Open Access articles:

Any reuse of the article must not represent the author as endorsing the adaptation of the article nor should the article be modified in such a way as to damage the author's honour or reputation.

The author(s) must be appropriately credited.

If any part of the material to be used (for example, figures) has appeared in our publication with credit or acknowledgement to another source it is the responsibility of the user to ensure their reuse complies with the terms and conditions determined by the rights holder.

Additional Terms & Conditions applicable to each Creative Commons user license:

CC BY: You may distribute and copy the article, create extracts, abstracts, and other revised versions, adaptations or derivative works of or from an article (such as a translation), to include in a collective work (such as an anthology), to text or data mine the article, including for commercial purposes without permission from Elsevier

CC BY NC SA: For non-commercial purposes you may distribute and copy the article, create extracts, abstracts and other revised versions, adaptations or derivative works of or

from an article (such as a translation), to include in a collective work (such as an anthology), to text and data mine the article and license new adaptations or creations under identical terms without permission from Elsevier

CC BY NC ND: For non-commercial purposes you may distribute and copy the article and include it in a collective work (such as an anthology), provided you do not alter or modify the article, without permission from Elsevier

Any commercial reuse of Open Access articles published with a CC BY NC SA or CC BY NC ND license requires permission from Elsevier and will be subject to a fee.

Commercial reuse includes:

- Promotional purposes (advertising or marketing)
- Commercial exploitation (e.g. a product for sale or loan)
- Systematic distribution (for a fee or free of charge)

Please refer to Elsevier's Open Access Policy for further information.

21. **Other Conditions**:

v1.7

If you would like to pay for this license now, please remit this license along with your payment made payable to "COPYRIGHT CLEARANCE CENTER" otherwise you will be invoiced within 48 hours of the license date. Payment should be in the form of a check or money order referencing your account number and this invoice number 501325060.
Once you receive your invoice for this order, you may pay your invoice by credit card. Please follow instructions provided at that time.

Make Payment To:
Copyright Clearance Center
Dept 001
P.O. Box 843006
Boston, MA 02284-3006

For suggestions or comments regarding this order, contact RightsLink Customer Support: customercare@copyright.com or +1-877-622-5543 (toll free in the US) or +1-978-646-2777.

Gratis licenses (referencing $0 in the Total field) are free. Please retain this printable license for your reference. No payment is required.

Copyright Permission for Manuscript #4

For manuscripts that are under review or published by Elsevier, the authors retain the right to include their work in a thesis without requesting a written permission:

"As an author, you retain rights for a large number of author uses, including use by your employing institute or company. These rights are retained and permitted without the need to obtain specific permission from Elsevier. These include:

- The right to make copies of the article for your own personal use, including for your own classroom teaching use.
- The right to make copies and distribute copies (including through e-mail) of the article to research colleagues, for the personal use by such colleagues (but not commercially or systematically, e.g. via an e-mail list or list serve).
- The right to post a pre-print version of the article on Internet web sites including electronic pre-print servers, and to retain indefinitely such version on such servers or sites (see also our information on electronic preprints for a more detailed discussion on these points.).
- The right to post a revised personal version of the text of the final article (to reflect changes made in the peer review process) on the author's personal or institutional web site or server, with a link to the journal home page (on elsevier.com).
- The right to present the article at a meeting or conference and to distribute copies of such paper or article to the delegates attending the meeting.
- For the author's employer, if the article is a 'work for hire', made within the scope of the author's employment, the right to use all or part of the information in (any version of) the article for other intra-company use (e.g. training).
- Patent and trademark rights and rights to any process or procedure described in the article.

- The right to include the article in full or in part in a thesis or dissertation (provided that this is not to be published commercially).
- The right to use the article or any part there of in a printed compilation of works of the author, such as collected writings or lecture notes (subsequent to publication of the article in the journal).
- The right to prepare other derivative works, to extend the article into book-length form, or to otherwise re-use portions or excerpts in other works, with full acknowledgement of its original publication in the journal."

The above quotation was copied in June 2014 from:

http://support.elsevier.com/app/answers/detail/a_id/565/session/L3RpbWUv

Copyright Permission for Manuscript #5 and #6

Because the manuscript #5 and #6 are to be submitted, and are not published or under consideration for publication in any journal at the time, no copyright permission is needed for them. However, for unpublished manuscripts, written permission from co-authors is required by CGSR to include the manuscripts in a thesis.

Copyright Permission Request Form

I am preparing the publication of manuscripts titled:

Modifying the Shrinking-Core Model to Evaluate the Kinetics of the Reaction between Aluminum Particles and Hot Water

and

Effect of Addition of Water-Soluble Salt Powders on the Hydrogen Generation Rate of Aluminum-Water Reaction

to be published as the sixth and seventh chapters of my Ph.D. thesis, and to be submitted to the Department of Mechanical Engineering at the University of Saskatchewan. The authors contributing in the completion of this manuscript are as follows:

S.S. Razavi-Tousi and J.A. Szpunar

I am requesting permission to use the materials described in aforementioned manuscripts in my Ph.D. thesis and all subsequent editions that may be prepared at the University of Saskatchewan. Please indicate agreement by signing below:

Yours sincerely,

Salman Razavi

June 11, 2014

Permission granted by: J.A. Szpunar

Signature:

Date:

Copyright Permissions for Figure. 1.1, 1.2, 1.3, 1.4 and 1.5

Figure. 1.1:

NATURE PUBLISHING GROUP LICENSE

TERMS AND CONDITIONS

Oct 22, 2014

This is a License Agreement between Salman Razavi ("You") and Nature Publishing Group ("Nature Publishing Group") provided by Copyright Clearance Center ("CCC"). The license consists of your order details, the terms and conditions provided by Nature Publishing Group, and the payment terms and conditions.

All payments must be made in full to CCC. For payment instructions, please see information listed at the bottom of this form.

License Number 3494290692865

License date Oct 22, 2014

Licensed content publisher Nature Publishing Group

Licensed content publication Nature

Licensed content title Materials for fuel-cell technologies

Licensed content author Brian C. H. Steele and Angelika Heinzel

Licensed content date Nov 15, 2001

Volume number 414

Issue number 6861

Type of Use reuse in a dissertation / thesis

Requestor type academic/educational

Format print and electronic

Portion figures/tables/illustrations

Number of figures/tables

/illustrations 1

Figures Figure 1

Author of this NPG article no

Your reference number None

Title of your thesis / dissertation

ACTIVATION OF ALUMINUM PARTICLES TO REACT WITH WATER FOR

THE PURPOSE OF HYDROGEN GENERATION

Expected completion date Oct 2014

Estimated size (number of pages) 200

Total 0.00 USD

Terms and Conditions

Terms and Conditions for Permissions

Nature Publishing Group hereby grants you a non-exclusive license to reproduce this

material for this purpose, and for no other use,subject to the conditions below:

NPG warrants that it has, to the best of its knowledge, the rights to license reuse of this material. However, you should ensure that the material you are requesting is original to

1.

Nature Publishing Group and does not carry the copyright of another entity (as credited in the published version). If the credit line on any part of the material you have requested indicates that it was reprinted or adapted by NPG with permission from another source, then you should also seek permission from that source to reuse the material.

Permission granted free of charge for material in print is also usually granted for any electronic version of that work, provided that the material is incidental to the work as a whole and that the electronic version is essentially equivalent to, or substitutes for, the print version.Where print permission has been granted for a fee, separate permission must be obtained for any additional, electronic re-use (unless, as in the case of a full paper, this has already been accounted for during your initial request in the calculation of a print run).NB: In all cases, web-based use of full-text articles must be authorized separately through the 'Use on a Web Site' option when requesting permission.

2. Permission granted for a first edition does not apply to second and subsequent editions and for editions in other languages (except for signatories to the STM Permissions Guidelines, or where the first edition permission was granted for free).

3. Nature Publishing Group's permission must be acknowledged next to the figure, table or abstract in print. In electronic form, this acknowledgement must be visible at the same

time as the figure/table/abstract, and must be hyperlinked to the journal's homepage.

4. The credit line should read:

Reprinted by permission from Macmillan Publishers Ltd: [JOURNAL NAME] (reference citation), copyright (year of publication)

For AOP papers, the credit line should read:

Reprinted by permission from Macmillan Publishers Ltd: [JOURNAL NAME], advance online publication, day month year (doi: 10.1038/sj.[JOURNAL ACRONYM].XXXXX)

Note: For republication from the *British Journal of Cancer,* the following credit lines apply.

Reprinted by permission from Macmillan Publishers Ltd on behalf of Cancer Research UK: [JOURNAL NAME] (reference citation), copyright (year of publication)For AOP papers, the credit line should read:

Reprinted by permission from Macmillan Publishers Ltd on behalf of Cancer Research UK: [JOURNAL NAME], advance online publication, day month year (doi: 10.1038/sj.[JOURNAL ACRONYM].XXXXX)

5. Adaptations of single figures do not require NPG approval. However, the adaptation should be credited as follows:

Adapted by permission from Macmillan Publishers Ltd: [JOURNAL NAME] (reference citation), copyright (year of publication)

Note: For adaptation from the *British Journal of Cancer,* the following credit line applies.

Adapted by permission from Macmillan Publishers Ltd on behalf of Cancer Research UK: [JOURNAL NAME] (reference citation), copyright (year of publication)

6. Translations of 401 words up to a whole article require NPG approval. Please visit

http://www.macmillanmedicalcommunications.com for more information.Translations of up to a 400 words do not require NPG approval. The translation should be credited as follows: Translated by permission from Macmillan Publishers Ltd: [JOURNAL NAME] (reference citation), copyright (year of publication).

Note: For translation from the *British Journal of Cancer,* the following credit line applies.

Translated by permission from Macmillan Publishers Ltd on behalf of Cancer Research UK: [JOURNAL NAME] (reference citation), copyright (year of publication)

7.We are certain that all parties will benefit from this agreement and wish you the best in the

Rightslink Printable License
https://s100.copyright.com/App/PrintableLicenseFrame.jsp?publisherID...

2 of 3 10/22/2014 10:22 AM

use of this material. Thank you.

Special Terms: v1.1

Questions? customercare@copyright.com or +1-855-239-3415 (toll free in the US) or +1-978-646-2777.

Gratis licenses (referencing $0 in the Total field) are free. Please retain this printable license for your reference. No payment is required.

Rightslink Printable License
https://s100.copyright.com/App/PrintableLicenseFrame.jsp?publisherID...

3 of 3 10/22/2014 10:22 AM

Figure. 1.2:

ELSEVIER LICENSE

TERMS AND CONDITIONS

Oct 22, 2014

This is a License Agreement between Salman Razavi ("You") and Elsevier ("Elsevier") provided by Copyright Clearance Center ("CCC"). The license consists of your order details, the terms and conditions provided by Elsevier, and the payment terms and conditions.

All payments must be made in full to CCC. For payment instructions, please see information listed at the bottom of this form.

Supplier Elsevier Limited

The Boulevard,Langford Lane

Kidlington,Oxford,OX5 1GB,UK

Registered Company

Number 1982084

Customer name Salman Razavi

Customer address 57 Campus Dr

Saskatoon, SK S7N 5A9

License number 3494000794798

License date Oct 22, 2014

Licensed content publisher Elsevier

Licensed content publication Journal of Power Sources

Licensed content title PEM fuel cell electrodes

Licensed content author S. Litster,G. McLean

Licensed content date 3 May 2004

Licensed content volume

Number 130

Licensed content issue

Number 1-2

Number of pages 16

Start Page 61

End Page 76

Type of Use reuse in a thesis/dissertation

Portion figures/tables/illustrations

Number of figures/tables

/illustrations 1

Format both print and electronic

Are you the author of this Elsevier article?

No

Will you be translating? No

Title of your thesis/dissertation

ACTIVATION OF ALUMINUM PARTICLES TO REACT WITH WATER FOR THE PURPOSE OF HYDROGEN GENERATION

Expected completion date Oct 2014

Rightslink Printable License
https://s100.copyright.com/App/PrintableLicenseFrame.jsp?publisherID...

1 of 6 10/21/2014 10:13 PM

Estimated size (number of pages) 200

Elsevier VAT number GB 494 6272 12

Permissions price 0.00 USD

VAT/Local Sales Tax 0.00 USD / 0.00 GBP

Total 0.00 USD

Terms and Conditions

INTRODUCTION

1. The publisher for this copyrighted material is Elsevier. By clicking "accept" in connection with completing this licensing transaction, you agree that the following terms and conditions apply to this transaction (along with the Billing and Payment terms and conditions established by Copyright Clearance Center, Inc. ("CCC"), at the time that you opened your Rightslink account and that are available at any time at http://myaccount.copyright.com).

GENERAL TERMS

2. Elsevier hereby grants you permission to reproduce the aforementioned material subject to the terms and conditions indicated.

3. Acknowledgement: If any part of the material to be used (for example, figures) has appeared in our publication with credit or acknowledgement to another source, permission must also be sought from that source. If such permission is not obtained then that material may not be included in your publication/copies. Suitable acknowledgement to the source must be made, either as a footnote or in a reference list at the end of your publication, as follows:

“Reprinted from Publication title, Vol /edition number, Author(s), Title of article / title of chapter, Pages No., Copyright (Year), with permission from Elsevier [OR APPLICABLE SOCIETY COPYRIGHT OWNER].” Also Lancet special credit - “Reprinted from The Lancet, Vol. number, Author(s), Title of article, Pages No., Copyright (Year), with permission from Elsevier.”

4. Reproduction of this material is confined to the purpose and/or media for which permission is hereby given.

5. Altering/Modifying Material: Not Permitted. However figures and illustrations may be altered/adapted minimally to serve your work. Any other abbreviations, additions, deletions

and/or any other alterations shall be made only with prior written authorization of Elsevier Ltd. (Please contact Elsevier at permissions@elsevier.com)

6. If the permission fee for the requested use of our material is waived in this instance, please be advised that your future requests for Elsevier materials may attract a fee.

7. Reservation of Rights: Publisher reserves all rights not specifically granted in the combination of (i) the license details provided by you and accepted in the course of this licensing transaction, (ii) these terms and conditions and (iii) CCC's Billing and Payment terms and conditions.

8. License Contingent Upon Payment: While you may exercise the rights licensed

immediately upon issuance of the license at the end of the licensing process for the transaction, provided that you have disclosed complete and accurate details of your proposed use, no license is finally effective unless and until full payment is received from you (either by publisher or by CCC) as provided in CCC's Billing and Payment terms and conditions. If full payment is not received on a timely basis, then any license preliminarily granted shall be deemed automatically revoked and shall be void as if never granted. Further, in the event that you breach any of these terms and conditions or any of CCC's Billing and Payment terms and conditions, the license is automatically revoked and shall be void as if never granted. Use of materials as described in a revoked license, as well as any use of the materials beyond the scope of an unrevoked license, may constitute copyright infringement and publisher reserves the right to take any and all action to protect its copyright in the materials.

9. Warranties: Publisher makes no representations or warranties with respect to the licensed material.

10. Indemnity: You hereby indemnify and agree to hold harmless publisher and CCC, and their respective officers, directors, employees and agents, from and against any and all claims arising out of your use of the licensed material other than as specifically authorized pursuant to this license.

11. No Transfer of License: This license is personal to you and may not be sublicensed, assigned, or transferred by you to any other person without publisher's written permission.

12. No Amendment Except in Writing: This license may not be amended except in a writing signed by both parties (or, in the case of publisher, by CCC on publisher's behalf).

13. Objection to Contrary Terms: Publisher hereby objects to any terms contained in any purchase order, acknowledgment, check endorsement or other writing prepared by you, which terms are inconsistent with these terms and conditions or CCC's Billing and Payment terms and conditions. These terms and conditions, together with CCC's Billing and Payment terms and conditions (which are incorporated herein), comprise the entire agreement between you and publisher (and CCC) concerning this licensing transaction. In the event of any conflict between your obligations established by these terms and conditions and those established by CCC's Billing and Payment terms and conditions, these terms and conditions shall control.

14. Revocation: Elsevier or Copyright Clearance Center may deny the permissions described in this License at their sole discretion, for any reason or no reason, with a full refund payable to you. Notice of such denial will be made using the contact information provided by you. Failure to receive such notice will not alter or invalidate the denial. In no event will Elsevier or Copyright Clearance Center be responsible or liable for any costs, expenses or damage

incurred by you as a result of a denial of your permission request, other than a refund of the amount(s) paid by you to Elsevier and/or Copyright Clearance Center for denied permissions.

LIMITED LICENSE

The following terms and conditions apply only to specific license types:

15. **Translation**: This permission is granted for non-exclusive world **English** rights only unless your license was granted for translation rights. If you licensed translation rights you

may only translate this content into the languages you requested. A professional translator must perform all translations and reproduce the content word for word preserving the integrity of the article. If this license is to re-use 1 or 2 figures then permission is granted for non-exclusive world rights in all languages.

16. **Posting licensed content on any Website**: The following terms and conditions apply as follows: Licensing material from an Elsevier journal: All content posted to the web site must maintain the copyright information line on the bottom of each image; A hyper-text must be included to the Homepage of the journal from which you are licensing at http://www.sciencedirect.com/science/journal/xxxxx or the Elsevier homepage for books at http://www.elsevier.com; Central Storage: This license does not include permission for a scanned version of the material to be stored in a central repository such as that provided by Heron/XanEdu.

Licensing material from an Elsevier book: A hyper-text link must be included to the Elsevier homepage at http://www.elsevier.com . All content posted to the web site must maintain the

copyright information line on the bottom of each image.

Posting licensed content on Electronic reserve: In addition to the above the following clauses are applicable: The web site must be password-protected and made available only to bona fide students registered on a relevant course. This permission is granted for 1 year only. You may obtain a new license for future website posting.

For journal authors: the following clauses are applicable in addition to the above:

Permission granted is limited to the author accepted manuscript version* of your paper.

***Accepted Author Manuscript (AAM) Definition:** An accepted author manuscript (AAM) is the author's version of the manuscript of an article that has been accepted for publication and which may include any author-incorporated changes suggested through the processes of submission processing, peer review, and editor-author communications. AAMs do not include other publisher value-added contributions such as copy-editing, formatting, technical enhancements and (if relevant) pagination.

You are not allowed to download and post the published journal article (whether PDF or HTML, proof or final version), nor may you scan the printed edition to create an electronic version. A hyper-text must be included to the Homepage of the journal from which you are licensing at http://www.sciencedirect.com/science/journal/xxxxx. As part of our normal production process, you will receive an e-mail notice when your article appears on Elsevier's online service ScienceDirect (www.sciencedirect.com). That e-mail will include the article's Digital Object Identifier (DOI). This number provides the electronic link to the published article and should be included in the posting of your personal version. We ask that you wait until you receive this e-mail and have the DOI to do any posting.

Posting to a repository: Authors may post their AAM immediately to their employer's institutional repository for internal use only and may make their manuscript publically

available after the journal-specific embargo period has ended.

Please also refer to Elsevier's Article Posting Policy for further information.

18. **For book authors** the following clauses are applicable in addition to the above:

Authors are permitted to place a brief summary of their work online only.. You are not allowed to download and post the published electronic version of your chapter, nor may you

scan the printed edition to create an electronic version. **Posting to a repository:** Authors are permitted to post a summary of their chapter only in their institution's repository.

20. **Thesis/Dissertation**: If your license is for use in a thesis/dissertation your thesis may be submitted to your institution in either print or electronic form. Should your thesis be published commercially, please reapply for permission. These requirements include permission for the Library and Archives of Canada to supply single copies, on demand, of the complete thesis and include permission for UMI to supply single copies, on demand, of the complete thesis. Should your thesis be published commercially, please reapply for permission.

Elsevier Open Access Terms and Conditions

Elsevier publishes Open Access articles in both its Open Access journals and via its Open Access articles option in subscription journals.

Authors publishing in an Open Access journal or who choose to make their article Open Access in an Elsevier subscription journal select one of the following Creative Commons user licenses, which define how a reader may reuse their work: Creative Commons Attribution License (CC BY), Creative Commons Attribution – Non Commercial -

5 of 6 10/21/2014 10:13 PM

the article, without permission from Elsevier

Any commercial reuse of Open Access articles published with a CC BY NC SA or CC BY NC ND license requires permission from Elsevier and will be subject to a fee.

Commercial reuse includes:

· Promotional purposes (advertising or marketing)

· Commercial exploitation (e.g. a product for sale or loan)

· Systematic distribution (for a fee or free of charge)

Please refer to Elsevier's Open Access Policy for further information.

21. **Other Conditions**: v1.6

Questions? customercare@copyright.com or +1-855-239-3415 (toll free in the US) or +1-978-646-2777.

Gratis licenses (referencing $0 in the Total field) are free. Please retain this printable license for your reference. No payment is required.

Rightslink Printable License
https://s100.copyright.com/App/PrintableLicenseFrame.jsp?publisherID...

6 of 6 10/21/2014 10:13 PM

Figure. 1.3:

ELSEVIER LICENSE

TERMS AND CONDITIONS

Oct 22, 2014

This is a License Agreement between Salman Razavi ("You") and Elsevier ("Elsevier") provided by Copyright Clearance Center ("CCC"). The license consists of your order details,

the terms and conditions provided by Elsevier, and the payment terms and conditions.

All payments must be made in full to CCC. For payment instructions, please see information listed at the bottom of this form.

Supplier Elsevier Limited

The Boulevard,Langford Lane

Kidlington,Oxford,OX5 1GB,UK

Registered Company

Number 1982084

Customer name Salman Razavi

Customer address 57 Campus Dr

Saskatoon, SK S7N 5A9

License number 3494000975802

License date Oct 22, 2014

Licensed content publisher Elsevier

Licensed content publication Journal of Power Sources

Licensed content title Design and analysis of aluminum/air battery system for electric vehicles

Licensed content author Shaohua Yang,Harold Knickle

Licensed content date 24 October 2002

Licensed content volume

Number 112

Licensed content issue

Number 1

Number of pages 12

Start Page 162

End Page 173

Type of Use reuse in a thesis/dissertation

Intended publisher of new work other

Portion figures/tables/illustrations

Number of figures/tables

/illustrations 1

Format both print and electronic

Are you the author of this Elsevier article? No

Will you be translating? No

Rightslink Printable License
https://s100.copyright.com/App/PrintableLicenseFrame.jsp?publisherID...

1 of 6 10/21/2014 10:16 PM

Title of your thesis/dissertation

ACTIVATION OF ALUMINUM PARTICLES TO REACT WITH WATER FOR

THE PURPOSE OF HYDROGEN GENERATION

Expected completion date Oct 2014

Estimated size (number of pages) 200

Elsevier VAT number GB 494 6272 12

Permissions price 0.00 USD

VAT/Local Sales Tax 0.00 USD / 0.00 GBP

Total 0.00 USD

Terms and Conditions

INTRODUCTION

1. The publisher for this copyrighted material is Elsevier. By clicking "accept" in connection

with completing this licensing transaction, you agree that the following terms and conditions apply to this transaction (along with the Billing and Payment terms and conditions established by Copyright Clearance Center, Inc. ("CCC"), at the time that you opened your Rightslink account and that are available at any time at http://myaccount.copyright.com).

GENERAL TERMS

2. Elsevier hereby grants you permission to reproduce the aforementioned material subject to the terms and conditions indicated.

3. Acknowledgement: If any part of the material to be used (for example, figures) has appeared in our publication with credit or acknowledgement to another source, permission must also be sought from that source. If such permission is not obtained then that material may not be included in your publication/copies. Suitable acknowledgement to the source must be made, either as a footnote or in a reference list at the end of your publication, as follows:

“Reprinted from Publication title, Vol /edition number, Author(s), Title of article / title of chapter, Pages No., Copyright (Year), with permission from Elsevier [OR APPLICABLE SOCIETY COPYRIGHT OWNER].” Also Lancet special credit - “Reprinted from The Lancet, Vol. number, Author(s), Title of article, Pages No., Copyright (Year), with permission from Elsevier.”

4. Reproduction of this material is confined to the purpose and/or media for which permission is hereby given.

5. Altering/Modifying Material: Not Permitted. However figures and illustrations may be altered/adapted minimally to serve your work. Any other abbreviations, additions, deletions and/or any other alterations shall be made only with prior written authorization of Elsevier Ltd. (Please contact Elsevier at permissions@elsevier.com)

6. If the permission fee for the requested use of our material is waived in this instance, please be advised that your future requests for Elsevier materials may attract a fee.

7. Reservation of Rights: Publisher reserves all rights not specifically granted in the combination of (i) the license details provided by you and accepted in the course of this

licensing transaction, (ii) these terms and conditions and (iii) CCC's Billing and Payment terms and conditions.

8. License Contingent Upon Payment: While you may exercise the rights licensed immediately upon issuance of the license at the end of the licensing process for the transaction, provided that you have disclosed complete and accurate details of your proposed use, no license is finally effective unless and until full payment is received from you (either by publisher or by CCC) as provided in CCC's Billing and Payment terms and conditions. If full payment is not received on a timely basis, then any license preliminarily granted shall be deemed automatically revoked and shall be void as if never granted. Further, in the event that you breach any of these terms and conditions or any of CCC's Billing and Payment terms and conditions, the license is automatically revoked and shall be void as if never granted. Use of materials as described in a revoked license, as well as any use of the materials beyond the scope of an unrevoked license, may constitute copyright infringement and publisher reserves the right to take any and all action to protect its copyright in the materials.

9. Warranties: Publisher makes no representations or warranties with respect to the licensed material.

10. Indemnity: You hereby indemnify and agree to hold harmless publisher and CCC, and their respective officers, directors, employees and agents, from and against any and all claims arising out of your use of the licensed material other than as specifically authorized pursuant to this license.

11. No Transfer of License: This license is personal to you and may not be sublicensed, assigned, or transferred by you to any other person without publisher's written permission.

12. No Amendment Except in Writing: This license may not be amended except in a writing signed by both parties (or, in the case of publisher, by CCC on publisher's behalf).

13. Objection to Contrary Terms: Publisher hereby objects to any terms contained in any purchase order, acknowledgment, check endorsement or other writing prepared by you, which terms are inconsistent with these terms and conditions or CCC's Billing and Payment terms and conditions. These terms and conditions, together with CCC's Billing and Payment terms and conditions (which are incorporated herein), comprise the entire agreement between you and publisher (and CCC) concerning this licensing transaction. In the event of any conflict between your obligations established by these terms and conditions and those established by CCC's Billing and Payment terms and conditions, these terms and conditions shall control.

14. Revocation: Elsevier or Copyright Clearance Center may deny the permissions described in this License at their sole discretion, for any reason or no reason, with a full refund payable to you. Notice of such denial will be made using the contact information provided by you. Failure to receive such notice will not alter or invalidate the denial. In no event will Elsevier or Copyright Clearance Center be responsible or liable for any costs, expenses or damage incurred by you as a result of a denial of your permission request, other than a refund of the amount(s) paid by you to Elsevier and/or Copyright Clearance Center for denied

permissions.

LIMITED LICENSE

Rightslink Printable License
https://s100.copyright.com/App/PrintableLicenseFrame.jsp?publisherID...

3 of 6 10/21/2014 10:16 PM

The following terms and conditions apply only to specific license types:

15. **Translation**: This permission is granted for non-exclusive world **English** rights only unless your license was granted for translation rights. If you licensed translation rights you may only translate this content into the languages you requested. A professional translator must perform all translations and reproduce the content word for word preserving the integrity of the article. If this license is to re-use 1 or 2 figures then permission is granted for non-exclusive world rights in all languages.

16. **Posting licensed content on any Website**: The following terms and conditions apply as follows: Licensing material from an Elsevier journal: All content posted to the web site must maintain the copyright information line on the bottom of each image; A hyper-text must be included to the Homepage of the journal from which you are licensing at http://www.sciencedirect.com/science/journal/xxxxx or the Elsevier homepage for books at http://www.elsevier.com; Central Storage: This license does not include permission for a scanned version of the material to be stored in a central repository such as that provided by Heron/XanEdu.

Licensing material from an Elsevier book: A hyper-text link must be included to the Elsevier homepage at http://www.elsevier.com . All content posted to the web site must maintain the copyright information line on the bottom of each image.

Posting licensed content on Electronic reserve: In addition to the above the following

clauses are applicable: The web site must be password-protected and made available only to bona fide students registered on a relevant course. This permission is granted for 1 year only. You may obtain a new license for future website posting.

For journal authors: the following clauses are applicable in addition to the above:

Permission granted is limited to the author accepted manuscript version* of your paper.

***Accepted Author Manuscript (AAM) Definition:** An accepted author manuscript (AAM) is the author's version of the manuscript of an article that has been accepted for publication and which may include any author-incorporated changes suggested through the processes of submission processing, peer review, and editor-author communications. AAMs do not include other publisher value-added contributions such as copy-editing, formatting, technical enhancements and (if relevant) pagination.

You are not allowed to download and post the published journal article (whether PDF or HTML, proof or final version), nor may you scan the printed edition to create an electronic version. A hyper-text must be included to the Homepage of the journal from which you are licensing at http://www.sciencedirect.com/science/journal/xxxxx. As part of our normal production process, you will receive an e-mail notice when your article appears on Elsevier's online service ScienceDirect (www.sciencedirect.com). That e-mail will include the article's Digital Object Identifier (DOI). This number provides the electronic link to the published article and should be included in the posting of your personal version. We ask that you wait until you receive this e-mail and have the DOI to do any posting.

Posting to a repository: Authors may post their AAM immediately to their employer's institutional repository for internal use only and may make their manuscript publically available after the journal-specific embargo period has ended.

Please also refer to Elsevier's Article Posting Policy for further information.

18. **For book authors** the following clauses are applicable in addition to the above:
Authors are permitted to place a brief summary of their work online only.. You are not allowed to download and post the published electronic version of your chapter, nor may you scan the printed edition to create an electronic version. **Posting to a repository:** Authors are permitted to post a summary of their chapter only in their institution's repository.

20. **Thesis/Dissertation**: If your license is for use in a thesis/dissertation your thesis may be submitted to your institution in either print or electronic form. Should your thesis be published commercially, please reapply for permission. These requirements include permission for the Library and Archives of Canada to supply single copies, on demand, of the complete thesis and include permission for UMI to supply single copies, on demand, of the complete thesis. Should your thesis be published commercially, please reapply for permission.

Elsevier Open Access Terms and Conditions

Elsevier publishes Open Access articles in both its Open Access journals and via its Open Access articles option in subscription journals.

Authors publishing in an Open Access journal or who choose to make their article Open Access in an Elsevier subscription journal select one of the following Creative Commons user licenses, which define how a reader may reuse their work: Creative Commons Attribution License (CC BY), Creative Commons Attribution – Non Commercial - ShareAlike (CC BY NC SA) and Creative Commons Attribution – Non Commercial – No Derivatives (CC BY NC ND)

Terms & Conditions applicable to all Elsevier Open Access articles:

Any reuse of the article must not represent the author as endorsing the adaptation of the article nor should the article be modified in such a way as to damage the author's honour or reputation.

The author(s) must be appropriately credited.

If any part of the material to be used (for example, figures) has appeared in our publication with credit or acknowledgement to another source it is the responsibility of the user to ensure their reuse complies with the terms and conditions determined by the rights holder.

Additional Terms & Conditions applicable to each Creative Commons user license:

CC BY: You may distribute and copy the article, create extracts, abstracts, and other revised versions, adaptations or derivative works of or from an article (such as a translation), to include in a collective work (such as an anthology), to text or data mine the article, including for commercial purposes without permission from Elsevier

CC BY NC SA: For non-commercial purposes you may distribute and copy the article, create extracts, abstracts and other revised versions, adaptations or derivative works of or from an article (such as a translation), to include in a collective work (such as an anthology), to text and data mine the article and license new adaptations or creations under identical terms without permission from Elsevier

Rightslink Printable License
https://s100.copyright.com/App/PrintableLicenseFrame.jsp?publisherID...
5 of 6 10/21/2014 10:16 PM

CC BY NC ND: For non-commercial purposes you may distribute and copy the article and include it in a collective work (such as an anthology), provided you do not alter or modify the article, without permission from Elsevier

Any commercial reuse of Open Access articles published with a CC BY NC SA or CC BY NC ND license requires permission from Elsevier and will be subject to a fee.

Commercial reuse includes:

· Promotional purposes (advertising or marketing)

· Commercial exploitation (e.g. a product for sale or loan)

· Systematic distribution (for a fee or free of charge)

Please refer to Elsevier's Open Access Policy for further information.

21. **Other Conditions**: v1.6

Questions? customercare@copyright.com or +1-855-239-3415 (toll free in the US) or +1-978-646-2777.

Gratis licenses (referencing $0 in the Total field) are free. Please retain this printable license for your reference. No payment is required.

Rightslink Printable License
https://s100.copyright.com/App/PrintableLicenseFrame.jsp?publisherID...

6 of 6 10/21/2014 10:16 PM

Figure. 1.4 and 1.5 :

ELSEVIER LICENSE

TERMS AND CONDITIONS

Oct 22, 2014

This is a License Agreement between Salman Razavi ("You") and Elsevier ("Elsevier") provided by Copyright Clearance Center ("CCC"). The license consists of your order details, the terms and conditions provided by Elsevier, and the payment terms and conditions.

All payments must be made in full to CCC. For payment instructions, please see

information listed at the bottom of this form.

Supplier Elsevier Limited

The Boulevard,Langford Lane

Kidlington,Oxford,OX5 1GB,UK

Registered Company

Number 1982084

Customer name Salman Razavi

Customer address 57 Campus Dr

Saskatoon, SK S7N 5A9

License number 3494001146669

License date Oct 22, 2014

Licensed content publisher Elsevier

Licensed content publication Progress in Materials Science

Licensed content title Mechanical alloying and milling

Licensed content author C. Suryanarayana

Licensed content date January 2001

Licensed content volume

Number 46

Licensed content issue number 1-2

Number of pages 184

Start Page 1

End Page 184

Type of Use reuse in a thesis/dissertation

Intended publisher of new work other

Portion figures/tables/illustrations

Number of figures/tables /illustrations 2

Format both print and electronic

Are you the author of this Elsevier article? No

Will you be translating? No

Title of your thesis/dissertation

ACTIVATION OF ALUMINUM PARTICLES TO REACT WITH WATER FOR

THE PURPOSE OF HYDROGEN GENERATION

Rightslink Printable License
https://s100.copyright.com/App/PrintableLicenseFrame.jsp?publisherID...

1 of 6 10/21/2014 10:19 PM

Expected completion date Oct 2014

Estimated size (number of pages) 200

Elsevier VAT number GB 494 6272 12

Permissions price 0.00 USD

VAT/Local Sales Tax 0.00 USD / 0.00 GBP

Total 0.00 USD

Terms and Conditions

INTRODUCTION

1. The publisher for this copyrighted material is Elsevier. By clicking "accept" in connection with completing this licensing transaction, you agree that the following terms and conditions apply to this transaction (along with the Billing and Payment terms and conditions established by Copyright Clearance Center, Inc. ("CCC"), at the time that you opened your Rightslink account and that are available at any time at http://myaccount.copyright.com).

GENERAL TERMS

2. Elsevier hereby grants you permission to reproduce the aforementioned material subject to the terms and conditions indicated.

3. Acknowledgement: If any part of the material to be used (for example, figures) has appeared in our publication with credit or acknowledgement to another source, permission must also be sought from that source. If such permission is not obtained then that material may not be included in your publication/copies. Suitable acknowledgement to the source must be made, either as a footnote or in a reference list at the end of your publication, as follows:

"Reprinted from Publication title, Vol /edition number, Author(s), Title of article / title of chapter, Pages No., Copyright (Year), with permission from Elsevier [OR APPLICABLE SOCIETY COPYRIGHT OWNER]." Also Lancet special credit - "Reprinted from The Lancet, Vol. number, Author(s), Title of article, Pages No., Copyright (Year), with permission from Elsevier."

4. Reproduction of this material is confined to the purpose and/or media for which permission is hereby given.

5. Altering/Modifying Material: Not Permitted. However figures and illustrations may be altered/adapted minimally to serve your work. Any other abbreviations, additions, deletions and/or any other alterations shall be made only with prior written authorization of Elsevier Ltd. (Please contact Elsevier at permissions@elsevier.com)

6. If the permission fee for the requested use of our material is waived in this instance, please be advised that your future requests for Elsevier materials may attract a fee.

7. Reservation of Rights: Publisher reserves all rights not specifically granted in the combination of (i) the license details provided by you and accepted in the course of this

licensing transaction, (ii) these terms and conditions and (iii) CCC's Billing and Payment terms and conditions.

8. License Contingent Upon Payment: While you may exercise the rights licensed immediately upon issuance of the license at the end of the licensing process for the transaction, provided that you have disclosed complete and accurate details of your proposed use, no license is finally effective unless and until full payment is received from you (either by publisher or by CCC) as provided in CCC's Billing and Payment terms and conditions. If full payment is not received on a timely basis, then any license preliminarily granted shall be deemed automatically revoked and shall be void as if never granted. Further, in the event that you breach any of these terms and conditions or any of CCC's Billing and Payment terms and conditions, the license is automatically revoked and shall be void as if never granted. Use of materials as described in a revoked license, as well as any use of the materials beyond the scope of an unrevoked license, may constitute copyright infringement and publisher reserves the right to take any and all action to protect its copyright in the materials.

9. Warranties: Publisher makes no representations or warranties with respect to the licensed material.

10. Indemnity: You hereby indemnify and agree to hold harmless publisher and CCC, and their respective officers, directors, employees and agents, from and against any and all claims arising out of your use of the licensed material other than as specifically authorized pursuant to this license.

11. No Transfer of License: This license is personal to you and may not be sublicensed, assigned, or transferred by you to any other person without publisher's written permission.
12. No Amendment Except in Writing: This license may not be amended except in a writing signed by both parties (or, in the case of publisher, by CCC on publisher's behalf).
13. Objection to Contrary Terms: Publisher hereby objects to any terms contained in any purchase order, acknowledgment, check endorsement or other writing prepared by you, which terms are inconsistent with these terms and conditions or CCC's Billing and Payment terms and conditions. These terms and conditions, together with CCC's Billing and Payment terms and conditions (which are incorporated herein), comprise the entire agreement between you and publisher (and CCC) concerning this licensing transaction. In the event of any conflict between your obligations established by these terms and conditions and those established by CCC's Billing and Payment terms and conditions, these terms and conditions shall control.
14. Revocation: Elsevier or Copyright Clearance Center may deny the permissions described in this License at their sole discretion, for any reason or no reason, with a full refund payable to you. Notice of such denial will be made using the contact information provided by you. Failure to receive such notice will not alter or invalidate the denial. In no event will Elsevier or Copyright Clearance Center be responsible or liable for any costs, expenses or damage incurred by you as a result of a denial of your permission request, other than a refund of the amount(s) paid by you to Elsevier and/or Copyright Clearance Center for denied permissions.

LIMITED LICENSE

The following terms and conditions apply only to specific license types:
15. **Translation**: This permission is granted for non-exclusive world **English** rights only

unless your license was granted for translation rights. If you licensed translation rights you may only translate this content into the languages you requested. A professional translator must perform all translations and reproduce the content word for word preserving the integrity of the article. If this license is to re-use 1 or 2 figures then permission is granted for non-exclusive world rights in all languages.

16. **Posting licensed content on any Website**: The following terms and conditions apply as follows: Licensing material from an Elsevier journal: All content posted to the web site must maintain the copyright information line on the bottom of each image; A hyper-text must be included to the Homepage of the journal from which you are licensing at http://www.sciencedirect.com/science/journal/xxxxx or the Elsevier homepage for books at http://www.elsevier.com; Central Storage: This license does not include permission for a scanned version of the material to be stored in a central repository such as that provided by Heron/XanEdu.

Licensing material from an Elsevier book: A hyper-text link must be included to the Elsevier homepage at http://www.elsevier.com . All content posted to the web site must maintain the copyright information line on the bottom of each image.

Posting licensed content on Electronic reserve: In addition to the above the following clauses are applicable: The web site must be password-protected and made available only to bona fide students registered on a relevant course. This permission is granted for 1 year only. You may obtain a new license for future website posting.

For journal authors: the following clauses are applicable in addition to the above:

Permission granted is limited to the author accepted manuscript version* of your paper.

***Accepted Author Manuscript (AAM) Definition:** An accepted author manuscript (AAM) is the author's version of the manuscript of an article that has been accepted for publication and which may include any author-incorporated changes suggested through the processes of submission processing, peer review, and editor-author communications. AAMs do not include other publisher value-added contributions such as copy-editing, formatting, technical enhancements and (if relevant) pagination.

You are not allowed to download and post the published journal article (whether PDF or HTML, proof or final version), nor may you scan the printed edition to create an electronic version. A hyper-text must be included to the Homepage of the journal from which you are licensing at http://www.sciencedirect.com/science/journal/xxxxx. As part of our normal production process, you will receive an e-mail notice when your article appears on Elsevier's online service ScienceDirect (www.sciencedirect.com). That e-mail will include the article's Digital Object Identifier (DOI). This number provides the electronic link to the published article and should be included in the posting of your personal version. We ask that you wait until you receive this e-mail and have the DOI to do any posting.

Posting to a repository: Authors may post their AAM immediately to their employer's institutional repository for internal use only and may make their manuscript publically available after the journal-specific embargo period has ended.

Please also refer to Elsevier's Article Posting Policy for further information.

18. **For book authors** the following clauses are applicable in addition to the above:

Authors are permitted to place a brief summary of their work online only.. You are not

allowed to download and post the published electronic version of your chapter, nor may you scan the printed edition to create an electronic version. **Posting to a repository:** Authors are permitted to post a summary of their chapter only in their institution's repository.

20. **Thesis/Dissertation**: If your license is for use in a thesis/dissertation your thesis may be submitted to your institution in either print or electronic form. Should your thesis be published commercially, please reapply for permission. These requirements include permission for the Library and Archives of Canada to supply single copies, on demand, of the complete thesis and include permission for UMI to supply single copies, on demand, of the complete thesis. Should your thesis be published commercially, please reapply for permission.

Elsevier Open Access Terms and Conditions

Elsevier publishes Open Access articles in both its Open Access journals and via its Open Access articles option in subscription journals.

Authors publishing in an Open Access journal or who choose to make their article Open Access in an Elsevier subscription journal select one of the following Creative Commons user licenses, which define how a reader may reuse their work: Creative Commons Attribution License (CC BY), Creative Commons Attribution – Non Commercial - ShareAlike (CC BY NC SA) and Creative Commons Attribution – Non Commercial – No Derivatives (CC BY NC ND)

Terms & Conditions applicable to all Elsevier Open Access articles:

Any reuse of the article must not represent the author as endorsing the adaptation of the article nor should the article be modified in such a way as to damage the author's honour or reputation.

The author(s) must be appropriately credited.

If any part of the material to be used (for example, figures) has appeared in our publication with credit or acknowledgement to another source it is the responsibility of the user to ensure their reuse complies with the terms and conditions determined by the rights holder.

Additional Terms & Conditions applicable to each Creative Commons user license:

CC BY: You may distribute and copy the article, create extracts, abstracts, and other revised versions, adaptations or derivative works of or from an article (such as a translation), to include in a collective work (such as an anthology), to text or data mine the article, including for commercial purposes without permission from Elsevier

CC BY NC SA: For non-commercial purposes you may distribute and copy the article, create extracts, abstracts and other revised versions, adaptations or derivative works of or from an article (such as a translation), to include in a collective work (such as an anthology), to text and data mine the article and license new adaptations or creations under identical terms without permission from Elsevier

CC BY NC ND: For non-commercial purposes you may distribute and copy the article and

include it in a collective work (such as an anthology), provided you do not alter or modify the article, without permission from Elsevier

Any commercial reuse of Open Access articles published with a CC BY NC SA or CC BY NC ND license requires permission from Elsevier and will be subject to a fee.

Commercial reuse includes:

· Promotional purposes (advertising or marketing)

· Commercial exploitation (e.g. a product for sale or loan)

· Systematic distribution (for a fee or free of charge)

Please refer to Elsevier's Open Access Policy for further information.

21. **Other Conditions**:

v1.6

Questions? customercare@copyright.com or +1-855-239-3415 (toll free in the US) or +1-978-646-2777.

Gratis licenses (referencing $0 in the Total field) are free. Please retain this printable license for your reference. No payment is required.